OPTIMIZATION OF PATHS AND LOCATIONS OF WATER QUALITY MONITORING SYSTEMS IN SURFACE WATER ENVIRONMENTS

A Thesis
Presented to
The Academic Faculty

by

Kijin Nam

In Partial Fulfillment
of the Requirements for the Degree
Doctor of Philosophy in the
School of Civil and Environmental Engineering

Georgia Institute of Technology
August 2008

OPTIMIZATION OF PATHS AND LOCATIONS OF WATER QUALITY MONITORING SYSTEMS IN SURFACE WATER ENVIRONMENTS

Approved by:

Dr. Mustafa M. Aral, Advisor
School of Civil and Environmental Engineering
Georgia Institute of Technology

Dr. Seong-Hee Kim
School of Industrial and Systems Engineering
Georgia Institute of Technology

Dr. Philip J. Roberts
School of Civil and Environmental Engineering
Georgia Institute of Technology

Dr. Turgay Uzer
School of Physics
Georgia Institute of Technology

Dr. Jiabao Guan
School of Civil and Environmental Engineering
Georgia Institute of Technology

Date Approved: JUNE 30 2008

To my family

ACKNOWLEDGEMENTS

I would like to appreciate Dr. Mustafa M. Aral for his guidance, encouragement, and support through my graduate studies. His advice and support were invaluable, and this research would have not been possible without these.

I want to thank my committee members: Dr. Philip J. Roberts, Dr. Jiabao Guan, Dr. Turgay Uzer, and, Dr. Seong-Hee Kim for their comments and suggestions.

Also, I am grateful and lucky for working with the members of MESL. The experience with them was enjoyable and inspiring.

I also have to express my gratitude to my parents and wife for their love, understanding, and support during my Ph.D. program.

TABLE OF CONTENTS

Pages

LIST OF TABLES

LIST OF FIGURES

LIST OF SYMBOLS

A_x, A_y, A_z	Eddy viscosity coefficients of fluid *x*-,*y*- and ,*z*-directions [$ML^{-1}T^{-1}$]
A_H	Horizontal eddy viscosity coefficient [$ML^{-1}T^{-1}$]
A_D	Dissipation parameter for a horizontal eddy viscosity coefficient [$ML^{-1}T^{-1}$]
C	Concentration of a contaminant [ML^{-3}]
$\hat{C}$	Chézy coefficient
c_b	Bottom friction coefficient
c_s	Wind friction coefficient
D_L, D_T	Longitudinal and transverse dispersion coefficient of a contaminant [L^2T^{-1}]
$D_{xx}, D_{xy}, D_{xz}, D_{yx}, D_{yy}, D_{yz}, D_{zx}, D_{zy}, D_{zz}$	Dispersion coefficients of a contaminant [L^2T^{-1}]
$D_{Hxx}, D_{Hxy}, D_{Hyx}, D_{Hyy}$	Horizontal dispersion coefficients of a contaminant [L^2T^{-1}]
e	Base of the natural logarithm
F_x, F_y, F_z	Body forces on fluid in *x*-,*y*-, and *z*-direction [MLT^{-2}]
f	The Coriolis parameter [LT^{-2}]
$f(\cdot)$	Objective function
$\hat{f}$	Darcy-Weisbach friction factor
g	The gravitational acceleration coefficient [LT^{-2}]

H	Bottom depth from a mean water level [L]
H_0	Depth of a channel [L]
h	Total water column depth [L]
J_α	Bessel function of the first kind for order of α
L	the length scale or length of a channel [L]
M	Mass of an injected contaminant [M]
N	Number of monitoring locations
N_s	Number of scenarios
n	Manning's roughness coefficient
p	Pressure of fluid [$ML^{-1}T^{-2}$]
q_x, q_y	Flow rate of fluid in *x*- and *y*-directions [L^2T^{-1}]
R	Linearized bottom friction coefficient [T^{-1}]
R_H	Hydraulic radius [L]
s	Slope of a channel
$t_{d,s}$	Detection time (time elapsed from the time of a contaminant release to the time of detection) for a scenario *s* [T]
$t_{d,s,j}$	Detection time of *j*-th deployment of a scenarios *s* [T]
$\mathbf{U}$	Vector of vertically-averaged velocity of fluid [LT^{-1}]
U, V, W	Mean values of velocities of fluid in *x*-,*y*-, and *z*-directions [LT^{-1}]
$\bar{U}, \bar{V}$	Vertically-averaged velocities of fluid in *x*- and *y*-directions [LT^{-1}]
U_w, V_w	Wind velocities at 10 m above the water surface in *x*- and *y*-directions [LT^{-1}]

u, v, w	Velocities of fluid in x-,y-, and z-direction [LT^{-1}]
u', v', w'	Fluctuations of velocities of fluid in x-,y-, and z-directions [LT^{-1}]
W	Sum of weight of all scenarios
Y_α	Bessel function of the second find for order of α
δ_s	Detection flag of a scenarios s
$\delta_{s,j}$	Detection flag of j-th deployment of a scenarios s
ϕ	Latitude
Γ	Boundary of a domain
η	Water level from a mean water level [L]
η_0	Water level from a mean water level at an end of a channel [L]
μ	Viscosity coefficient of fluid [$ML^{-1}T^{-1}$]
ρ	Density of fluid [ML^{-3}]
ρ_a	Density of air [ML^{-3}]
τ_{bx}, τ_{by}	Bottom shear stress in x- and y-directions [$ML^{-1}T^{-2}$]
τ_{sx}, τ_{sy}	Wind shear stress in x- and y-directions [$ML^{-1}T^{-2}$]
θ	Angle of flow
Ω	Domain of interest
$\hat{\Omega}$	The rotation rate of the Earth [T^{-1}]
ω	Frequency of a tidal forcing function [T]
∇	Gradient operator or Divergence operator

SUMMARY

Even though the necessity of water quality monitoring systems is increasing due to the degradation of surface water quality and concerns on health risk outcome, research on the design of water quality monitoring systems for surface water environments is limited. Also, mobile watery quality monitoring systems using the combination of automatic measuring devices and autonomous vehicles is becoming available, but research on effective deployment of such systems is almost non-existent.

Since a water quality monitoring program is a costly endeavor, it must be implemented carefully to maximize its performance. Among various goals of water quality monitoring systems, early and reliable detection of possible contaminations are important ones, especially for early warning systems. To maximize these performance measures, many design factors of a water quality monitoring system can be adjusted, but locations or paths to take the measurement are one of the most important design factors which have not been fully investigated. Designing locations and paths in a two-dimensional space to maximize two objectives is a complex multi-objective spatial optimization problem.

To solve these optimization problems, multi-objective genetic algorithms based on NSGA-II (Non-dominated Sorting Genetic Algorithm-II) are proposed. Also, because water quality monitoring systems should respond to various conditions effectively, many possible scenarios were assumed and simulated to provide the background data of the optimization models. The simulation procedures consisted of hydrodynamics and contaminant transport models. These simulations of the physical models require great

amount of computational power so that parallel computational routines based on MPI (Message Passing Interface) were built to reduce computational time.

The proposed optimization procedures were tested on hypothetical circular lakes with wind or tide and Lake Pontchartrain in order to obtain optimal monitoring locations, straight monitoring paths, and higher-order monitoring paths under various conditions. The effect of various parameters such as the number of monitoring locations, the speed of a monitoring vessels, the effect of weights, and *etc*. were also investigated.

The results show that the distribution of possible spill locations is the most important factor that affects optimal solutions. Assuming most possible spill locations were located on the shore of closed water bodies, all of the optimal monitoring locations, monitoring lines and paths were placed close to the shore as well because wind-generated longshore currents, which transports contaminants, prevailed along the shorelines. Also, the performance of optimal monitoring locations was degraded under transient and realistic flow conditions. Optimal monitoring lines did not perform very well due to their incapability to cover the irregular boundaries of water bodies. Higher-order optimal monitoring paths overcame this difficulty and performed well even under transient realistic flow conditions. However, a monitoring vessel could cover only a part of a large domain so that one vessel was not enough to monitor a large domain effectively, even though one monitoring vessel performed comparably to several stationary monitoring locations.

CHAPTER 1

INTRODUCTION

1.1. Surface water contamination and health risk

Surface water environment plays a vital role in human lives as fresh water source, transportation media, and recreation location. Also coastal waters and freshwater coasts are home of natural resources and are rich with diverse species. Hence, surface water environment has been attracting people since the human history began. As of 1998, over half the population of the planet – about 3.2 billion – lives and works in a coastal strip just 200 km wide (Hinrichsen, 1999). In the United States, estimated 153 million people lived in coastal counties in 2003, which is more than 50 percent of the nation's population (Crossett, Culliton*, et al.*, 2004). The Great Lakes in the North America is home to more than one-tenth of the population of the United States and one-quarter of the population of Canada, and the world's largest concentrations of industrial capacity are located in the region (Government of Canada and United States Environmental Protection Agency, 1995). Coastal tourism and recreation in the U.S. constitute some of the fasted growing business sectors, and they generated 1.67 million jobs and annual economic output of $29.5 billion in 2000 (Natural Resources Defense Council (NRDC), 2006). Simply put, human beings cannot survive without adequate access to clean water. However, surface ecosystems and their water quality are pressured by population growth and various human activities. In 2001, 44 percent of the U.S.'s estuarine areas were characterized by impaired human use or impaired aquatic life use (USEPA, 2001). Due to continuing increase in global population and socioeconomic development, the

degradation of water quality is one of the main problems among the environmental concerns. The degradation of water quality reduces the amount of water available for potable, agricultural, and industrial use, and causes human health risks. Despite efforts of world organization such as United Nations and international banks, human health due to water quality problems is substantial in many areas of the world (World Resources Institute (WRI), 2000).

The contaminants that pollute surface water are as follows: Excess nutrients such as nitrogen and phosphorous are the most widespread pollution. They originate as runoff from agricultural land, animal feeding operation, and urban areas, discharges from wastewater treatment plan, storm sewer, and *etc*. These nutrients themselves are not toxic, but they cause oxygen depletion, toxic algal blooms, and so on. Oil is another major source of contaminant. In the U.S., more than 28 million gallons of oil from human activities enter North American waters and land-based runoff accounts for well over half of this (National Research Council (U.S.), 2003). Harmful human pathogens are a big concern as well. Pharmaceuticals and personal-care product (PPCPs), endocrine disrupters, and toxic substances such as pesticides and chlorinated hydrocarbons are getting more attentions recently. Some PPCPs are already being detected in water environment (Boyd, Palmen, *et al.*, 2004). The Great Lakes in the United States has been experiencing pathogen problems, eutrophication, oxygen depletion, and threat from toxic contaminants such as pesticides (Government of Canada and United States Environmental Protection Agency, 1995).

Contamination of surface water causes many human health risks. Across the globe, marine toxins afflict more than 90,000 people annually and are responsible for an

estimated 62 percent of all seafood related illnesses (U.S. Commission on Ocean Policy, 2004). Because of pollution of the Great Lakes by PCBs (polychlorinated biphenyls), and DDT (dichlorodiphenyltrichloroethane), *etc.*, consumption advisories for sport-caught fish were first issued by the Great Lakes states during the 1970s (Imm, Knobeloch*, et al.*, 2005), and breast cancer risk related to the contaminants from the fish of the Great Lakes was shown (McElroy, Kanarek*, et al.*, 2004).

Waterside activity is one of the most popular outdoor activities. In a survey of over 200 million people in the U.S., 1999, more than 97 million people over 16 years of age reported swimming in natural waters such as streams, lakes, ponds and oceans (USDA Forest Service and the University of Tennessee, 2000). Due to degraded water quality, human health is endangered by recreational use of surface water as well. Risk related to recreational water activities in coastal waters is increasing over the world (Corbett, Rubin*, et al.*, 1993; Fleisher, Kay*, et al.*, 1998; Pruss, 1998). During 2001-2002 in the United States, a total of 65 waterborne-disease outbreaks associated with recreational water were reported by 23 states, and they caused illness among an estimated 2,536 persons; 61 persons were hospitalized, eight of whom died (Yoder, Blackburn*, et al.*, 2004).

200 designated swimming beaches did not meet the public health standards at least 25 percent of the time, and, due to such health risks, the number of closing and advisory days at ocean, bay, and Great Lakes beaches in the U.S. topped 20,000. Some 45 percent of U.S. waters assessed by state agencies were not clean enough for fishing or swimming, according to U.S. Environmental Protection Agency (USEPA) data from 2000. Based on information for the 2002 swim season of the U.S., almost every coastal

and Great Lakes state reported having at least one beach where stormwater, runoff, and/or sewage is known source of pollution at or near bathing waters (Natural Resources Defense Council (NRDC), 2006). Eventually, degraded coastal waters are threatening not only human health but business sectors related to tourism and recreation as well,

In response, researchers and public health managers have been seeking better ways to monitor and/or predict water quality to minimize health risk and maximize usage of surface water environment at the same time. These efforts include informing the public of any risk from adverse water quality clearly and promptly. In the U.S., through Beaches Environmental Assessment and Coastal Health (BEACH) Act of 2000 (2000), every coastal and Great Lakes state has a monitoring and public notification program in place (Natural Resources Defense Council (NRDC), 2006), and still the BEACH programs is on-going as of 2007. The roles of water quality monitoring are more than just for public health. Better technical information on status and trends in the aquatic environment is necessary to guide management and regulatory decision, verify the efficacy of existing programs, and help shape national policy. Modeling and monitoring share a close interdependence. Modeling enables one to synthesize the results of observation programs. As such, models provide important assistance for the development of monitoring arrays. On the other hand, modeling needs the initial conditions, boundary conditions, and forcing function from observations. Modeling also needs to be calibrated and verified with observations (National Research Council (U.S.). Committee on the Causes and Management of Coastal Eutrophication, 2000).

1.2. Water quality monitoring and its design

Traditional way of water quality monitoring is spot (bottle or grab) sampling and is built around fixed devices and sampling schemes, which is not effective enough to obtain a good representative picture of water quality across a wide area over time. To overcome this shortcoming, many alternative methods are being developed and becoming available. There are three categories of the alternative tools for water quality monitoring, and they are *in-situ*, on-line and off-line methods (Greenwood, Mills*, et al.*, 2007). Especially, recent advances in communication and sensor technology has expedited the progress of real time monitoring capabilities for water quality, and a few real-time remote monitoring programs over the world are already running (Glasgow, Burkholder*, et al.*, 2004). It is expected that these new methods improve water quality monitoring significantly in terms of temporal and spatial scales. For example, *in-situ* chemical sensor to measure dissolved gases such as oxygen, carbon dioxide, methane, pH, and *etc*. were developed and used for sustained and autonomous observations (Johnson, Needoba*, et al.*, 2007), and rapid water-quality indicators to predict gastrointestinal illness are being developed (Wade, Calderon*, et al.*, 2006).

With the development of alternative measuring methods, autonomous water vehicles are being developed concurrently, and they are being adopted to measure various constituents of water quality. An autonomous underwater vehicles (AUV) equipped with an optical phytoplankton discriminator (OPD) was developed to monitor and track harmful algal blooms (HABs) along the Florida coast. It overcame the shortcoming of satellite monitoring and improved the ability to investigate in small scales in conjunction with multiple parameters of the surrounding water column (Robbins, Kirkpatrick*, et al.*,

2006). A sensor network and a mobile robotic boat for real-time in-situ measurements and analysis of chemical, physical and biologically phenomena governing microorganisms was tried (Dhariwal, Bin*, et al.*, 2006). For example, MERHAB Autonomous Research Vessel for In-Situ Sampling, or MARVIN was developed for Monitoring and Event Response for Harmful Algal Blooms. Its equipment to monitor is solar powered and controlled by a computer program (Florida Fish and Wildlife Conservation Commission: Fish and Wildlife Research Institute, 2005). Even though the movement of the vehicle is not yet remotely controlled, it clearly shows the capability of this type of monitoring water vessels. In the near future, it is certain that autonomous vessels with measuring equipment will provide valuable quasi-continuous and/or real-time information on water quality and environment. Eventually, it will be used to monitor water quality in order to respond to any health hazards in various surface environments. Even though the importance of water quality monitoring is well understood, and some of water quality monitoring systems is already running, designing monitoring programs is hard and still being studied. The technical design of monitoring programs refers to the process of deciding what to measure; how, where, and when to take the measurements; and how to analyze and interpret the resulting data (National Research Council (U.S.). Committee on a Systems Assessment of Marine Environmental Monitoring, 1990). Among them, locations of measurements are one of the important factors, especially when an area to be monitored is large.

1.3. Scope of this study and organization of the thesis

Even though many rapid and *in-situ* or on-line methods are being developed and researched, how to design monitoring network or paths in a two-dimensional space of

surface water has not been studied despite its importance. Until now, monitoring locations or paths are decided by expertise rather than by a systematic approach. Hence, the goal of this research is developing systematic ways of designing water quality monitoring systems.

The two main objectives of this study are developing methods to find the best locations and paths to monitor in 2-dimensional surface water environment. To achieve these goals, a numerical approach was used to simulate a range of hydrodynamics and contaminant transport. Genetic algorithms were adopted to find the optimized locations and paths to monitor using the simulation results. This process require enormous amount of computation, so parallel simulation routines were developed as a way to reduce computational time.

Chapter 2 reviews literatures related to research topics of this study such as current water quality monitoring systems and design of them. In Chapter 3, an overall proposed procedure of the optimization of monitoring locations and paths is proposed. In Chapter 4, numerical simulations for hydrodynamics and contaminant transport are developed. In Chapter 5, an optimization model for monitoring locations is developed and tested. In Chapter 6 and 7, an optimization models for monitoring paths are developed and tested. Chapter 8 concludes the study and suggests the future direction of research.

CHAPTER 2

Literature Review

2.1. Introduction

The ultimate goal of environmental monitoring including water quality monitoring is to protect the environment, living resources, and finally human health. Monitoring will be beneficial to achieving the goal once it turns into more effective management decisions. For example, monitoring data can trigger shutting down water treatment plants, giving out advisories or beach closures if necessary. In addition to direct management decisions, monitoring can provide valuable data for setting standards, verifying predictive models, and checking compliance with regulations, as well as enhancing our understanding and knowledge about ecosystems. Failure to obtain the information necessary for proper monitoring may cause environmental damage, human health effect, and eventually social and political damage. Hence, designing and running a monitoring program properly is extremely important.

Traditional ways of water quality evaluation are based on costly, time- and labor-intensive on-site sampling and data collection, and transport to land-based or shipboard laboratories for evaluation. Even though intensive efforts are applied to these traditional ways, results are typically limited on temporal and spatial scales. Much effort has been put into developing fast and reliable methods to measure contaminants in real-time and/or remotely (Glasgow, Burkholder, *et al.*, 2004) such as pathogens from water (Wade, Calderon, *et al.*, 2006). These new methods make continuous remote monitoring possible, which is very important for the public health sectors to react within an appropriate time

scale. However, some of them may not be fast enough to catch and react to rapid change of water quality.

Another way is a predictive water quality simulation to estimate water quality change and it has been shown to be useful (Liu, Phanikumar*, et al.*, 2006). However, systematic monitoring of water quality is still important since numerical models need input and calibration data and numerical simulations cannot replace actual monitoring.

Regardless of the type of water quality monitoring, it is highly complex due to uncertainties in the nature of water quality and difficulties in the specification of the purpose of monitoring. The reasons of uncertainties in the nature of water quality are natural hydrologic cycle and man made effects. Difficulties in the specification of monitoring purposes are the social, economic, and legal constraints. These complexities make the designing process very challenging. Hence, a good designing procedure must encompass these complexities well.

What needs to be considered in traditional water quality monitoring program design was well reviewed by Dixon *et al* (1996). The design factors from Dixon *et al*. are spatial distribution of sampling sites, sampling frequency, cost-effectiveness, *etc.* Similar topics were discussed in National Research Council (U.S.) (1990; National Research Council (U.S.). Committee on the Causes and Management of Coastal Eutrophication., 2000) including a planning procedure. Many of those procedures and criteria can be used for the optimization of any types of water monitoring systems.

Monitoring and detecting the spatial and temporal extent of contamination in surface water environment requires a scientifically designed monitoring network to perform up to its requirement. Also, setting up and running such monitoring systems are

very costly endeavor. The cost of monitoring system includes monitoring devices, labors, sample analysis cost, data collection and distribution cost, maintenance, and so on. Hence, a plan for water quality monitoring must be well-engineered to maximize the performance and to minimize the cost at the same time. This planning procedure is an optimal design problem with uncertainties as well. Sometimes, there are multiple objectives in the monitoring system design that conflict one another. Furthermore, the design of a monitoring network needs to accommodate for periodic modifications to reflect any change in physics and goals. Hence, developing a solid strategy to design a better monitoring network is very crucial, and at the end it must help decision makers to select a sound plan that will protect environment and human health.

Despite its importance, not much research has been done on how to design and optimize a monitoring network in surface water environment. On the other hand, good amount of research for the optimization of monitoring networks in a river system and long-term monitoring (LTM) of contaminant groundwater site has been done. Also, due to recently-heightened security concerns as the risk of terrorism increased, the optimization of monitoring networks for water distribution networks became a hot issue. Even though the optimizations for different fields are not directly applicable to the optimization of monitoring locations or paths in surface water, all of them have many common concepts. Hence, useful methods and procedures from the optimization of monitoring in river, groundwater, and water distribution network may be adopted for the optimization of monitoring in surface water.

2.2. Studies on monitoring network for rivers and watersheds

The real applications of river water quality monitoring systems are not very common yet even in developed countries despite many related researches available. One of those real applications of such online and continuous river water quality monitoring systems is reported by Drage, Upton, *et al.* (1998). The system is not an extensive network, but it clearly shows what is possible with water quality monitoring and how much it costs. Trent River in the United Kingdom was planned to be used as drinking water source, and there was a need of a safeguard system because the river contained the treated sewage effluent making the river water quality highly variable. Hence, the automated monitoring system that can measure multi-parameter as indicators of gross changes was set up at the river. The indicators included pH, ammonia, dissolved oxygen (DO), conductivity, turbidity, temperature and nitrate. The system also has automated liquid chromatography and gas chromatography to measure more than 40 risk compounds such as herbicides. Capital costs were approximately £500,000 with annual revenue costs estimated at £250,000. Another example of river water quality monitoring systems is Nation Long-term Surveillance of Swiss Rivers (NADUF) (Jakob, Binderheim-Bankay, *et al.*, 2002). It has 19 stations continuously measuring water level, temperature, pH, electrical conductivity, and oxygen concentration. Other chemicals are measured over 14-day periods.

Many researches were done on the optimization of river system monitoring with various methods. Early studies such as Sharp (1971) focused on the best sampling locations to find out possible contaminant sources with less cost. The cost of the study was the length of rivers to search source locations based on what is found from

monitoring. At that time, the methods were mathematical theories rather than computational practices due to lack of available data and computational capacity. In 1990s, computational optimizations including heuristic methods were adopted widely for optimization problems in water resources fields as the computers advanced enough to handle heuristic methods with low cost. Dixon *et al.* (1999) adopted simulated annealing to optimize sampling sites in a river system. The objective was the expected cost of obtaining information subsequent of detection of a problem at a sample site. Their objective was rather simple, but real geographical data from a geographical information system (GIS) was used. Some of the recent studies used the genetic algorithms. Ning and Chang (2002) designed optimal expansion and relocation strategies of a water quality monitoring network in Kao-Ping River Basin, Taiwan. They used pre-emptive goal programming model and multi-objective optimization at the same time. They later expanded their work with the fuzzy logics (Ning and Chang, 2004). Icaga (2005) designed water quality network in Gediz river basin in Turkey using a genetic algorithm for a single objective. Park *et al.* (2006) applied the genetic algorithm to optimize water quality monitoring network for Nakdong River in South Korea with multiple objectives. They proposed 5 objectives; representativeness of a river basin, compliance with water quality standards, supervision of water use, surveillance of pollution sources, and examination of water quality change. Through their study, they suggested that only 35 of 110 stations in the watershed coincide with their optimal solutions. Others used the fuzzy logic to select critical sampling points (Strobl, Robillard, *et al.*, 2006; Strobl, Robillard, *et al.*, 2006) as well. Strobl *et al*.'s objective was to develop a designing methodology within small agricultural-forested watersheds with minimal data. They considered many

factors such as slope, curvature, and sediment transport as well as some other components. Even though many researches are available, most of them do not consider river hydrology in depth, which may play an important role in terms of contaminant transport.

2.3. Studies on monitoring network for a groundwater monitoring network

For contaminated groundwater sites, long-term monitoring (LTM) is an important environmental issue. The attention to LTM has increased recently as the use of monitored natural attenuation has increased. However, LTM is costly due to the large number of sampling locations and number of constituents monitored. U.S. Department of Energy (DOE) estimated that the total coast may be up to $100 million per year for the sites where DOE has been mandated to conduct long-term stewardship (U.S. Department of Energy, 2001). Therefore, the optimization of LTM systems may save significant amount of money, and it has been a topic of many researches.

Early works related to this topic was about selecting observation locations to minimize kriging variance (Carrera, Usunoff*, et al.*, 1984; Hughes and Lettenmaier, 1981; Loaiciga, 1989). Later studies in 1980s and early 1990s were focused on contaminant detection for landfill designs (McKinney and Loucks, 1992; Meyer and Brill, 1988; Meyer, Valocchi*, et al.*, 1994) considering uncertainties from the characterization of the subsurface and the nature of the contaminant source. For example, Meyer, *et al*. (1994) used Monte Carlo simulation and integer programming to optimize three objectives. Optimization of monitoring network for source-identification was also tried (Mahar and Datta, 1997).

In late 1990s, computational capacities grew enough to manage heuristic optimization methods that requires great amount of computation. Monte Carlo methods, genetic algorithms, simulated annealing, and *etc.* were adopted widely for the optimization. For examples, Reed, *et al.* (2000) used a genetic algorithm (GA) to reduce global mass estimates that were calculated using several plume interpolation methods. Li and Hilton (2007) used an ant colony optimization to reduce the number of monitoring wells. Dhar and Datta (2007) proposed a multi-objective nonlinear optimization models for dynamic ground water pollution monitoring using chance-constrained optimization model.

Many different objectives for groundwater quality monitoring were suggested throughout the studies, and the most common ones were: minimizing the number of monitoring wells, maximizing the probability of detecting a contaminant, and minimizing the expected area of contamination at the time of detection. These objectives can be applied for water quality monitoring systems in different domains including the optimization of surface water monitoring.

On the other hand, the major difference between groundwater and surface water is the time scales of the hydrodynamics. The hydraulics of groundwater is rather slow and is expressed in Darcy's law, which is a linear system whereas the hydraulics of surface water changes rather fast and is highly nonlinear.

2.4. Studies on monitoring network for a water distribution network

After the tragic events of September 11 at New York City, the risk of terrorism changed the meaning of uncertainty and security in many areas over the World. Even before September 11, the Safe Drinking Water Act of the U.S. (US Congress, 1974)

required that the water quality in water distribution systems is to be sampled at locations that are representative of the system. Since drinking water is a crucial element in maintaining public health, it can be a target of intentional and malicious attacks. Traditionally, application of the optimization related to water distribution network has mainly been about the structural and quantitative aspects of water network such as network capacity. However, the recent changes of the circumstances mentioned above boosted research related to this topic.

One of the early works on this topic was done by Lee and Deininger (1992) using integer programming. They combined pathway analysis, coverage matrices, and integer programming to maximize the demand covered by monitoring stations. Kessler *et al.* (1998) used all shortest paths algorithms to detect contamination within the maximum volume of contaminated water that is consumed prior to detection. Their works have been expanded extensively after the event on September 11 (Ostfeld, Kessler*, et al.*, 2004; Ostfeld and Salomons, 2005).

Other researches poured out at the same time (Berry, Hart*, et al.*, 2006; Berry, Fleischer*, et al.*, 2005; Carr, Greenberg*, et al.*, 2006; Cozzolino, Mucherino*, et al.*, 2006; Guan, Aral*, et al.*, 2006; Kumar, Kansal*, et al.*, 1999; Shastri and Diwekar, 2006) after the heightened concern about water security. The common objectives for the studies were minimization of detection time, minimization of consumed water volume before detection, and maximization of detection likelihood. Each research used different methods such as integer programming, combinatorial heuristics, stochastic programming, and genetic algorithms. Main difficulty in the optimization of water sensor networks has

been managing variable flow conditions, vast amount of candidate locations and possible contaminant source locations.

Just like the other monitoring systems mentioned in the previous sections, even though the hydrodynamics of water distribution networks are different from that of surface water, many of the objectives and solving algorithms may be applicable for the optimization of water quality monitoring systems in surface water environments.

2.5. Mobile water quality monitoring

Due to recent advances in robotics, mobile water quality monitoring, which means measuring water quality constituents by a mobile vehicle on or in a water body, is becoming more available. A mobile water quality monitoring has a few merits over a fixed monitoring network. For example, a path to monitor can be adjusted easily whenever it is required. Also, one mobile unit may cover a wider area than a fixed monitoring unit. This means there is a possibility of cost reduction as well. Especially when a mobile unit is operated autonomously without manual control, it can monitor a wide area continuously with a fraction of cost required for a manned monitoring system.

The most recent example of mobile monitoring in surface water environment by Li, Weeks, *et al.* (2007) clearly shows what is possible in water quality monitoring currently and in the near future. They developed an unmanned automated boat, which was preprogrammed to follow a certain path repeatedly and measures flow velocity, salinity, and temperature in a tidal channel continuously. The course was adjusted by itself using a high-resolution GPS (0.2m accuracy). This equipment can make continuous monitoring through a path with a fraction of the cost compared to those with a manned

boat. The same type of equipment can be adopted to monitor water quality easily, and it will open a whole new chapter in water quality monitoring.

In oceanographic fields, autonomous underwater vehicles (AUV) are being adopted to replace expensive and possibly dangerous manned underwater vehicles. Many experiments, observing microbial activities, are being done successfully. (Dhariwal, Bin*, et al.*, 2006; Robbins, Kirkpatrick*, et al.*, 2006; Thomas, Sibenac*, et al.*, 2003). For example, Robbins, *et al*. (2006) attached an optical phytoplankton discriminator (OPD) on REMUS (Remote Environmental Monitoring UnitS), which is a commercially available, about 3 meter-long rocket-shaped propulsion-driven AUV to study harmful algal blooms in the Gulf of Mexico. It traveled underwater in the west coast of Florida for about 2 hours for twice and collected temperature, salinity, and plankton index. These AUVs will be promising tools to measure water quality as well, especially when the difference of water quality over the depth is an important factor.

As discussed in water quality monitoring with a fixed network in various environments, designing a monitoring path is important to make a monitoring program successful. Since the mobile water quality monitoring is not yet common, the designing of the monitoring plan is not well established to the best of the author's knowledge. However, the path optimization has been studied in robotics, and some of the concepts from the robotics may be applied for the optimization of a path for water quality monitoring.

2.5.1. Path optimization

The optimization of paths has been the subject of great interests in many engineering fields. The most-well known problem of a path optimization is travel-

salesman problem, often shortened to TSP. Even though the statement of the problem is simple – what is the shortest (or cheapest) round-trip route that visits each city exactly once, – the problem is known to be very hard to solve. It is a combinatorial optimization, which is shown to be nondeterministic polynomial-time hard. The problem is of importance in many real problems such as logistics so that is has been studied extensively (Applegate, 2007; Gutin and Punnen, 2002; Lawler, 1985).

In mobile robotics, path planning has great importance so that it has been researched very thoroughly. Many of the studies focused on wheeled robots moving on surfaces. Recently, unmanned aerial vehicle (UAV) is being used in various fields including military, and path planning for this system is becoming a popular topic. Many of these studies are dynamic real-time optimizations by collecting information while a vehicle is moving. Also, most of objectives in these researches are avoiding obstacles under certain constraints (Kunchev, Jain*, et al.*, 2006). Hence, some of them are not compatible for path optimization in a steady or non-real time environment, but the basis of the optimization from these studies can be adopted for path optimization for water quality monitoring as well.

In one example of path optimization in underwater environment, Peter *at al.* (2007) proposed an efficient path-planning algorithms for autonomous underwater vehicles. Their objective was planning a path to avoid obstacles under influence of currents in 2-D trajectory solutions using Fast Marching (FM)-based approach.

2.6. Summary

It is crucial to set up and run a water quality monitoring system in many water environments to protect environment and public health. Without well-engineered

monitoring programs, water quality monitoring systems cannot meet the requirements and perform successfully. Designing an effective water quality monitoring in many environment is a challenging task due to its complexity of physics and many uncertainties. Hence, enormous amount of efforts has been put in to develop robust methods to plan water quality monitoring programs in various fields such as river, groundwater and water distribution system. The recent water quality degradation and increased concerns about security necessitate better water quality monitoring systems more than ever. However, designing water quality monitoring system in two-dimensional surface water environment has not been studied well despite its importance.

One of most recent types of monitoring systems is mobile monitoring that often uses autonomous vehicles. A mobile monitoring system may reduce cost of monitoring while covering a wide area over a short time period. In the future, it will be common for water quality monitoring in two- and three- dimensional water environment. A mobile monitoring system requires a path to monitor that is subject to be designed in a scientific way, but it has not been studied much.

The literature review showed that many different optimization methodologies were applied for different problems, but many of problem objectives and optimization methods are common. The common objectives of water quality monitoring programs are: fast detection of any adverse change of water quality, less failure in detection of change of water quality, less cost of monitoring, less consumption or exposure before detection, better representation of whole problem domain, and so on.

Major difficulties in water quality monitoring systems are complexity and uncertainty in physics of the problems, which leads to simplification and stochastic

methods. Many of the reviewed problems were reduced into integer programming or combinatorial problems to make the problems more manageable. Popular methods in the optimization of water quality monitoring systems are heuristic methods that require intensive computation such as Genetic algorithms, Monte Carlo simulation, simulated annealing, and *etc*. To manage uncertainties, fuzzy methods are also quite commonly being used now. Recent advances in computer science greatly accelerate the utilization of computational methods. Among the various optimization methods, the genetic algorithms are very popular due to their flexibility and robustness. The genetic algorithms well manage multi-objective problems as shown in many studies. After some modifications, these methodologies can be adopted for two- and three-dimensional water environments.

CHAPTER 3

THE DESIGN OF THE OPTIMIZATION PROBLEMS

3.1. Introduction

The technical design of water quality monitoring programs is a decision making process determining what to measure, how, where, and when to take the measurement, as well as how to analyze and interpret the resulting data. An appropriate technical design is critical to the success of monitoring program because it will provide meaningful information that will be useful to decision makers and eventually address public concerns, as some of the design factors rather belong to the area of public policies such as laws, regulations, and public expectations.

The first step of monitoring programs is setting up their objectives. There are various goals of monitoring programs, for examples, early detection of water quality change, tracking the change of water quality over time, and better reconstruction of concentration contours.

What to measure and how to take the measurements are decided based on the ultimate goal of a monitoring program and the available technologies. Where and when to take the measurements are decided by the combination of the physical transport phenomena and the goal of a monitoring program. In fact, all the factors are related so that it is not possible to separate them completely. For example, where to take the measurement may depend on what to measure.

Among the various decision factors of a water quality monitoring system, deciding where to take the measurement is still a challenge because monitoring the entire

area is simply not possible most of the time. Recent adaptation of remote sensing such as satellite imaginary overcomes some of the spatial limitations, but they are still very limited. The placement of monitoring sites are often dictated by ease of access, or decided subjectively based on experience and expertise. However, in order to determine the best spatial distribution of monitoring sites or paths, it should be based on the goal of the program. Hence, the optimal design depends on the program goals. The most general goal of monitoring is to produce information that is useful in managing a problem. For example, a monitoring within a site concentrates on specific questions about the dispersal of disposed material to trigger a management action if the material spread beyond site boundary. The goal of a monitoring may not be very clear when a question is comprehensive. For instance, monitoring any change of indicators to study how they are impacted by human activities, and what will be adverse effect of them.

Among various objectives and factors mentioned above, the goal of the monitoring program for this thesis is the earliest detection with highest reliability for an early water quality warning system because an early detection of change in water quality can maximize the utilization of water body while minimizing adverse human health effects and environmental damages. Secondly, where to take the measurement is the designing factor of an early-warning system in this study.

To make monitoring designs successful in meeting the goals mentioned above, they must reflect cause-effect relationships while accounting for variability and uncertainty of the nature. In other words, a good design needs to be supporter by what happens in the area of interest such as physical and statistical studies.

3.2. Design of scenarios

As mentioned in the previous section, a monitoring program must reflect cause-effect relationship. Hence, where to take measurement also must reflect cause-effect relationship well. The major cause of spatial and temporal change of the water quality is governed mainly by transport phenomena based on which harmful chemicals and/or pathogens are spread. The contaminants travel from one place to another by two transport mechanisms called advection and dispersion: Advection is the transport of a property such as contaminant and heat by a moving mass of fluid, and dispersion is scattering of a property by random molecular motion and mechanical mixing by turbulence of fluid. In many cases when there is flow of the water, advection is the major mechanism of transport. The motion of fluid by these two phenomena is referred as hydrodynamics, and it is decided by many physical factors. For shallow water such as lakes and oceans, wind, tides and inflow/outflow are the major forces of hydrodynamics.

Another cause of change in the water quality is the reactions of contaminants, but it is not considered in this study for simplicity. The time scale of an early warning system is relatively short, for example, less than one day so that reactions may not be very important in this time scale. However, some water quality constituents such as coliforms may involve fast change of concentration in a relatively short time period. In that case, additional consideration may be required.

The other factor that affects the early warning system is where and how much a contaminant was released and spilled. If some sources at specific locations are more likely to happen than some others, then a monitoring system needs to reflect that. The effect of sediment as source and sink is ignored for simplicity. Thus, the causes that need

to be reflected in the design of an early warning system in this study are simplified into hydrodynamics and possible contaminant sources.

In the real world, there are numerous possibilities of contaminant sources and transport since the conditions of natures are never constant over time, and the sources of pollution are random. The best way to consider the random nature of the problem would be to use a statistical method such as Monte Carlo simulation based on the probability. However, it is computationally infeasible, and also it is hard to know the probability distribution of pollutions. An alternative way is where representative or more likely cases of hydrodynamics and sources are selected and designed. If representative cases of hydrodynamics and transport are set up, an optimized solution of monitoring programs can be calculated with the cases. For convenience, a combination of hydrodynamics and/or contaminant spill will be referred as a 'scenario' from now on.

A hydrodynamic scenario consists mainly of a combination of different wind and tidal conditions. For example, a spring tide and constant wind from east over the domain can be a hydrodynamics scenario. If necessary, other physical parameters such as bottom frictions can be changed and another scenario can be set up. Setting up a various possible scenarios, the optimization model can include uncertainties as well. Each scenario has its own weight that represents relative likeliness to happen. By adjusting the weight, a collection of scenarios can act like samples from some distributions.

A contaminant scenario consists mainly of a location of contaminant release and corresponding hydrodynamics scenario. For instance, a contaminant can be released under easterly wind condition at the east corner of a lake because there is a factory. Generally, the more scenarios are included, the more comprehensive the optimization can

be. However, many scenarios will not necessarily give better solutions, and too many of them will increase computational time. If necessary, other physical parameters such as dispersion coefficient can be modified and another new scenario can be added. A contaminant scenario has also weight to adjust the likeliness.

3.3. Simulation of hydrodynamics and contaminant transport

After scenarios are designed using the knowledge on a problem domain, they need to be simulated numerically, and the result of the simulations is stored and used for the optimization of the monitoring program in the next step. The simulation can be divided into two steps: hydrodynamics and contaminant transport. The first step solves the hydrodynamics that determines advections of a contaminant. The second step solves the movement of a contaminant, which gives temporal and spatial concentration profiles in a problem domain.

It is assumed that the contaminant transport is not density-driven for this research so that hydrodynamics and contaminant transport can be simulated separately. This approach can save computational burden because one result of hydrodynamics can be used several times for different contaminant settings. The details of simulations will be discussed in Chapter IV.

3.4. Optimization of water quality monitoring systems

The final step of the procedure is the optimization for water quality monitoring systems. To optimize a monitoring system mathematically, the objectives of the optimizations should be stated clearly in mathematical formulae. For example, to minimize the time between the time of contaminant release and that of detection is an objective that can be defined and calculated mathematically or numerically. Other factors

such as minimizing contaminated area, maximizing reliability, and minimizing cost to find a source location inversely are other possibilities that can be used as objectives for optimization. The objectives can be virtually anything depending on what researchers and decision makers need, and often the objectives should be optimized at the same time. Therefore, the objectives often conflict one other, which makes the problem a multi-objective optimization. Since the main goal of this study is an early warning system, the minimization of the average detection time and the maximization of detection reliability are selected as two major objectives. The method of the optimization was genetic algorithms due to its flexibility and robustness.

3.4.1. Two types of water quality monitoring systems

Traditionally, water quality is monitored at fixed sampling or monitoring locations. Once locations for measurement are decided and/or devices are set up, they are used for a time period and adjusted afterward if necessary. This method is straightforward and measurements are taken continuously at given locations. In addition, determining monitoring locations is relatively easy. However, because the coverage by one monitoring location is limited, a system may require many monitoring locations to cover a large area, and the increased number of monitoring locations to set up means increased cost. Furthermore, sending out personnel to measure in many locations can be very costly. Relocation of continuous monitoring stations to respond to the changes in circumstances may be costly as well, making relocation difficult, in turn causing the flexibility to be low.

The new method of mobile monitoring opens another possibility of monitoring. The major advantage of the mobile monitoring system against traditional fixed-location monitoring is the possibility of covering a wide area with flexibility. The path to monitor

can be easily adjusted to adapt changing situations. Whenever physical conditions and/or objectives change, a path can be designed and applied without paying major cost, whereas a monitoring network with immovable stations will cost much for relocations.

Monitoring water quality using a manned research vessel has been used, but it is not very cost effective. Implementing a regular or continuous water quality monitoring using a manned monitoring vessel is even more prohibitive. These difficulties can be solved by adopting the autonomous monitoring vessel or vehicle. An autonomous vessel can be smaller and it can also be controlled by a person or a preprogrammed computer. Furthermore, it can be used continuously with a fraction of cost of a manned monitoring vessel. The fact that the size of an autonomous monitoring vessel can be much smaller than a manned one, also gives some advantage over manned vessel in terms of operations. Early trials on autonomous water vehicles are already being studied. For example, Li and *et al.* (2007) manufactured and ran a 10-ft long unmanned boat controlled by an onboard computer with ADCP (Acoustic Doppler Current Profiler). Their vehicle was set to run round-the-clock repeatedly.

The comparison of schematics from the two monitoring systems is presented in Figure 3.1. The main objectives for both monitoring systems are essentially the same, but some operational objectives may differ. For an instance, the path optimization may include different design factors such as the length of a path, and speed of the boat.

The optimization procedures of fixed locations and paths are different because of different natures of the two systems. To evaluate a set of fixed monitoring locations one needs to consider only when a contaminant is detected at one of the monitoring locations, whereas to evaluate a monitoring path one needs to consider the location and the time of

a vehicle in the middle of a path at the same time. This makes the optimization of a path harder than that of a network of fixed monitoring locations. The detail of the two different types of optimization procedures will be discussed in Chapter 5, 6, and 7.

3.5. Summary

As described in the previous sections, the whole procedure of the optimization involves four major steps as presented in Figure 3.2: (1) Designing the contamination scenarios; (2) Simulating scenarios of hydrodynamics; (3) Simulating scenarios of contaminant transport; and, (4) determination of optimal monitoring locations or optimal monitoring path. Among these four steps, the second and third steps generally require most of computational time. The details of each step will be discussed in the following chapters.

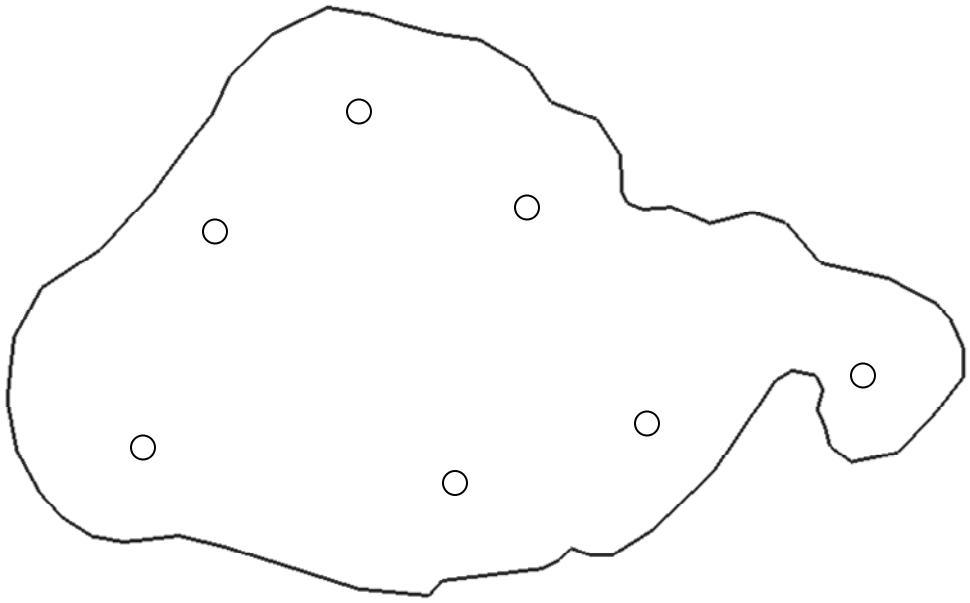

(a)

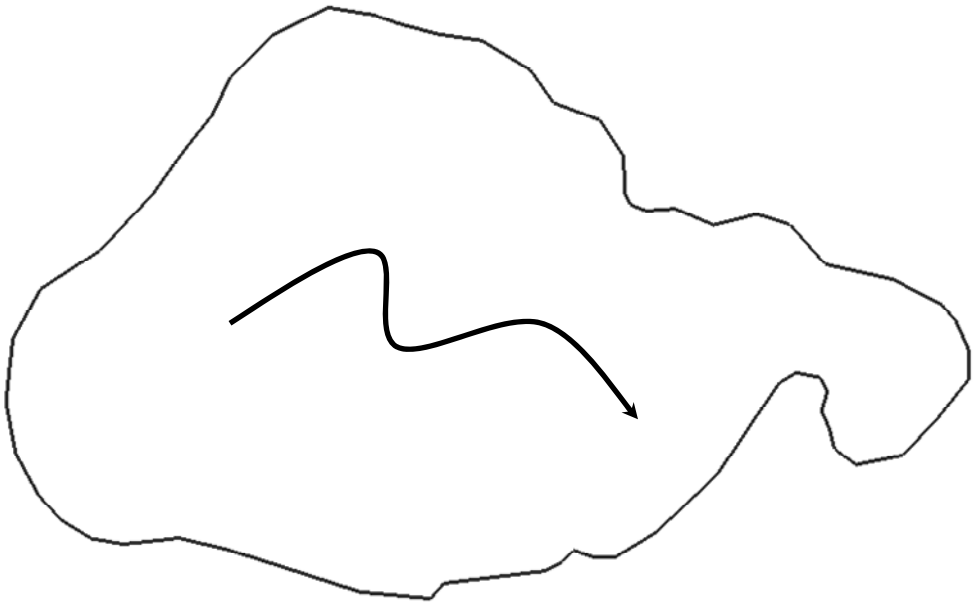

(b)

Figure 3.1 Examples of Conceptual Schematics of Water Quality Monitoring Systems (a) Stationary monitoring locations, and (b) Continuous path monitoring systems

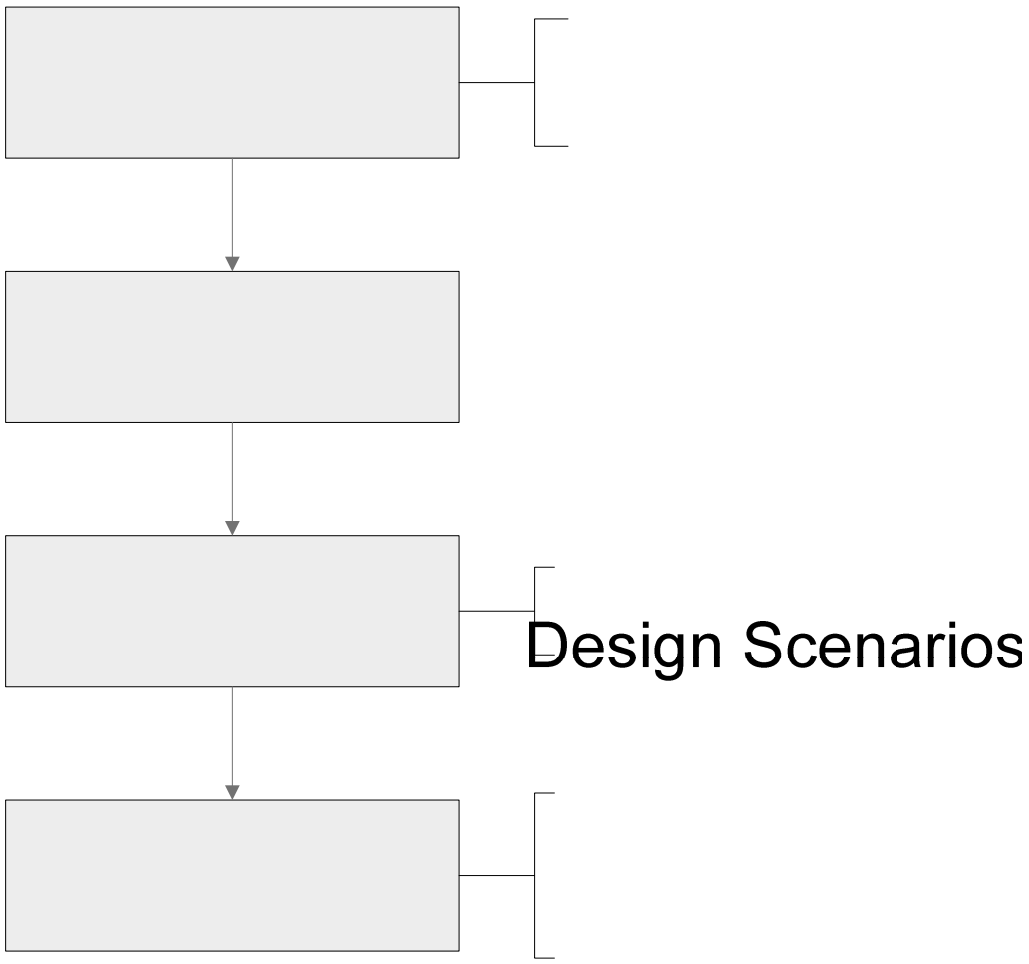

Figure 3.2 Overall design procedure for water quality monitoring system

Simulate Hydrodynamics Scenarios

CHAPTER 4

HYDRODYNAMICS AND CONTAMINANT TRANSPORT

To design a water quality monitoring system efficiently, a good understanding on hydrodynamics and contaminant transport is crucial, and a numerical simulation can be a good tool for it. Numerical simulation can manage many different hydrodynamic and contaminant transport cases within feasible computational time and cost limits.

4.1. Simulation of hydrodynamics

4.1.1. Governing equations

Navier-Stokes equations are a set of equations that describe the motion of fluid based on the balance of forces acting at any given region of the fluid such as liquids and gases (Batchelor, 1973). Numerous phenomena in nature involve certain forms of fluids so that a set of Navier-Stokes equations are the most important and useful sets of equations that explain physics of processes in the nature such as weather phenomena and ocean currents. This means that solving the Navier-Stokes equations of a given physical problem is the first step to understand the problem and seek an answer for it.

The continuity equation in rectangular coordinate of three dimensions is:

$$\frac{\partial \rho}{\partial t} + \frac{\partial (\rho u)}{\partial x} + \frac{\partial (\rho v)}{\partial y} + \frac{\partial (\rho w)}{\partial z} = 0 \tag{4.1}$$

where ρ is the density of fluid and u, v, and w are the velocity components in x, y, and z coordinates.

The equation of motion for Newtonian fluid with a constant viscosity in rectangular coordinate where z direction corresponds to gravity is:

$$\begin{aligned}
&\frac{\partial(\rho u)}{\partial t}+\frac{\partial(\rho uu)}{\partial x}+\frac{\partial(\rho uv)}{\partial y}+\frac{\partial(\rho uw)}{\partial z}=-\frac{\partial p}{\partial x}+\rho F_x \\
&\frac{\partial(\rho v)}{\partial t}+\frac{\partial(\rho vu)}{\partial x}+\frac{\partial(\rho vv)}{\partial y}+\frac{\partial(\rho vw)}{\partial z}=-\frac{\partial p}{\partial y}+\rho F_y \\
&\frac{\partial(\rho w)}{\partial t}+\frac{\partial(\rho wu)}{\partial x}+\frac{\partial(\rho wv)}{\partial y}+\frac{\partial(\rho ww)}{\partial z}=-\frac{\partial p}{\partial z}+\rho F_z-\rho g
\end{aligned} \tag{4.2}$$

where p is the pressure, g is the gravitational acceleration coefficient, F_x, F_y, and F_z are the *x*, *y*, and *z* components of friction forces per unit mass. The first terms on the left hand side are change of momentum over time, and the second to fourth terms are momentum transfers by the flow. For a Newtonian fluid with constant density and constant viscosity, the friction forces from viscosity on the right hand side take the forms:

$$\begin{aligned}
F_x &= \mu\left(\frac{\partial^2 u}{\partial x^2}+\frac{\partial^2 u}{\partial y^2}+\frac{\partial^2 u}{\partial z^2}\right) \\
F_y &= \mu\left(\frac{\partial^2 v}{\partial x^2}+\frac{\partial^2 v}{\partial y^2}+\frac{\partial^2 v}{\partial z^2}\right) \\
F_z &= \mu\left(\frac{\partial^2 w}{\partial x^2}+\frac{\partial^2 w}{\partial y^2}+\frac{\partial^2 w}{\partial z^2}\right)
\end{aligned} \tag{4.3}$$

where μ is the viscosity coefficient (Panton, 1996). These forces are called shear stresses and are very small, especially in a large water body.

Another mechanism of momentum transfer is turbulence. Turbulence arises from the non-linear terms in the momentum equations due to small fluctuation of flow velocity. In a large scale simulation, however, average values are more of interest, not small

fluctuations of velocities. Through the derivation based on mean value over time or space, the transfer of the momentum due to turbulence, so called 'Reynolds Stresses,' can be derived, and they are given:

$$\begin{aligned} F_x &= -\frac{\partial}{\partial x}\langle u'u'\rangle - \frac{\partial}{\partial y}\langle u'v'\rangle - \frac{\partial}{\partial z}\langle u'w'\rangle \\ F_y &= -\frac{\partial}{\partial x}\langle v'u'\rangle - \frac{\partial}{\partial y}\langle v'v'\rangle - \frac{\partial}{\partial z}\langle v'w'\rangle \\ F_z &= -\frac{\partial}{\partial x}\langle w'u'\rangle - \frac{\partial}{\partial y}\langle w'v'\rangle - \frac{\partial}{\partial z}\langle w'w'\rangle \end{aligned} \tag{4.4}$$

where

$$\begin{aligned} &u = U + u';\ v = V + v';\ w = W + w' \\ &U = \langle u\rangle = \frac{1}{T}\int_0^T u(t)dt \quad \text{or} \quad U = \langle u\rangle = \frac{1}{X}\int_0^X u(x)dx \\ &U, V, W = \text{ mean values of velocity components} \\ &u', v', w' = \text{ fluctuations of velocity components.} \end{aligned} \tag{4.5}$$

It is known that the Reynolds stresses act as viscous terms in the equation of motions, and are given such as:

$$\langle u'v'\rangle = -A_y \frac{\partial U}{\partial y} \tag{4.6}$$

where A_y is an eddy viscosity or eddy diffusivity. Generally, friction forces from viscosity and turbulence are combined, and the eddy diffusivity includes both of them. Under the assumption that the eddy viscosities are constant or vary slowly, Eqs. (4.2) can be written with average velocities as:

$$
\begin{aligned}
&\frac{\partial(\rho U)}{\partial t}+\frac{\partial(\rho UU)}{\partial x}+\frac{\partial(\rho UV)}{\partial y}+\frac{\partial(\rho UW)}{\partial z}\\
&\qquad=-\frac{\partial p}{\partial x}+\rho\left[A_x\frac{\partial^2 U}{\partial x^2}+A_y\frac{\partial^2 U}{\partial y^2}+A_z\frac{\partial^2 U}{\partial z^2}\right]\\
&\frac{\partial(\rho V)}{\partial t}+\frac{\partial(\rho VU)}{\partial x}+\frac{\partial(\rho VV)}{\partial y}+\frac{\partial(\rho VW)}{\partial z}\\
&\qquad=-\frac{\partial p}{\partial y}+\rho\left[A_x\frac{\partial^2 V}{\partial x^2}+A_y\frac{\partial^2 V}{\partial y^2}+A_z\frac{\partial^2 V}{\partial z^2}\right]\\
&\frac{\partial(\rho W)}{\partial t}+\frac{\partial(\rho WU)}{\partial x}+\frac{\partial(\rho WV)}{\partial y}+\frac{\partial(\rho WW)}{\partial z}\\
&\qquad=-\frac{\partial p}{\partial z}+\rho\left[A_x\frac{\partial^2 W}{\partial x^2}+A_y\frac{\partial^2 W}{\partial y^2}+A_z\frac{\partial^2 W}{\partial z^2}\right]-\rho g
\end{aligned}
\tag{4.7}
$$

and they are called as ‘Reynolds-averaged Navier-Stokes equations’.

Solving Eqs (4.7) in three dimensions numerically, however, is not feasible over a large scale of a water body due to enormous computational requirement. In addition, the scale in depth direction in shallow water is much smaller than one in horizontal directions, and the horizontal scale of the flow is more important relatively to small vertical flow. Secondly, the body force by the gravity balances closely against pressure gradient in the vertical direction, implying that vertical accelerations are negligible. In other words, the weight of the fluid balances the pressure so that the vertical velocity is negligible, and this is called as hydrostatic assumption.

Considering these factors, the set of Reynolds-averaged Navier-Stokes equations can be vertically integrated and cab be averaged in order to simplify the equations into two dimensions. The result of the vertical averaging is often called ‘shallow water equation’ in two dimensions and is given as:

$$\frac{\partial h}{\partial t}+\frac{\partial\left(h\bar{U}\right)}{\partial x}+\frac{\partial\left(h\bar{V}\right)}{\partial y}=0 \tag{4.8}$$

$$\begin{aligned}
&\frac{\partial\left(h\bar{U}\right)}{\partial t}+\frac{\partial\left(h\bar{U}\bar{U}\right)}{\partial x}+\frac{\partial\left(h\bar{U}\bar{V}\right)}{\partial y}=A_H\left[\frac{\partial^2(h\bar{U})}{\partial x^2}+\frac{\partial^2(h\bar{U})}{\partial y^2}\right]-gh\frac{\partial(h-H)}{\partial x}\\
&\frac{\partial\left(h\bar{V}\right)}{\partial t}+\frac{\partial\left(h\bar{V}\bar{U}\right)}{\partial x}+\frac{\partial\left(h\bar{V}\bar{V}\right)}{\partial y}=A_H\left[\frac{\partial^2(h\bar{V})}{\partial x^2}+\frac{\partial^2(h\bar{V})}{\partial y^2}\right]-gh\frac{\partial(h-H)}{\partial y}
\end{aligned} \tag{4.9}$$

where $\bar{U}$, and $\bar{V}$ are the vertically averaged horizontal velocities in x and y coordinates, h is the total water column depth, H is the bottom depth from a mean water level, A_H is the horizontal eddy viscosity coefficients. The pressure terms disappear due to the hydrostatic assumption. This form of shallow water equation is widely used for numerous studies in ocean and lake simulations and contaminant transport simulations as well. (Form now on, all the bars on the vertically averaged horizontal velocities will be dropped for notational convenience.) With the growth of computational capacity, three-dimensional numerical simulation becomes popular. However, even in three-dimensional simulations, the set of shallow water equations are solved as part of simulations to reduce computational burden by separating a three-dimensional simulation into two separate modes, called as internal and external modes (Blumberg and Mellor, 1987). The governing equations are often written in vector form for simplicity as follows:

$$\frac{\partial(h\mathbf{U})}{\partial t}+\nabla\cdot(h\mathbf{U}\mathbf{U})=A_H\nabla^2(h\mathbf{U})-gh\nabla(h-H) \tag{4.10}$$

where

$$\mathbf{U}=\begin{Bmatrix}U\\V\end{Bmatrix}=\text{The vector of velocities.}$$

The horizontal eddy viscosity, A_H, in open water is related to eddy spectrums. Generally, the order of the coefficient in lake is 10^2~10^4 m/sec (Lam and Jaquet, 1976). The value of the horizontal eddy viscosity for a numerical simulation is usually decided by the length scale of a mesh or grid in the model. The empirical formula between the length scale and the horizontal dispersion coefficient is given as:

$$A_H = A_D L^{4/3} \tag{4.11}$$

where L is the length scale in centimeter and A_D is the dissipation parameter of the order 0.005 with A_H in cm^2/sec (Bowie, Mills, *et al.*, 1985).

In the nature, wind friction, bottom friction, and Coriolis force act as major external body forces on a large water body. After adding external body forces into equations above, they become very common shallow water equation:

$$\begin{aligned}
&\frac{\partial(hU)}{\partial t}+\frac{\partial(hUU)}{\partial x}+\frac{\partial(hUV)}{\partial y}\\
&\quad=A_H\left[\frac{\partial^2(hU)}{\partial x^2}+\frac{\partial^2(hU)}{\partial y^2}\right]-gh\frac{\partial(h-H)}{\partial x}+hfV-\frac{\tau_{bx}}{\rho}+\frac{\tau_{sx}}{\rho}\\
&\frac{\partial(hV)}{\partial t}+\frac{\partial(hVU)}{\partial x}+\frac{\partial(hVV)}{\partial y}\\
&\quad=A_H\left[\frac{\partial^2(hV)}{\partial x^2}+\frac{\partial^2(hV)}{\partial y^2}\right]-gh\frac{\partial(h-H)}{\partial y}-hfU-\frac{\tau_{by}}{\rho}+\frac{\tau_{sy}}{\rho}
\end{aligned} \tag{4.12}$$

where τ_{bx} and τ_{by} are bottom shear stress in *x*- and *y*-direction, and τ_{sx} and τ_{sy} are surface shear stress in *x*- and *y*-directions.

The Coriolis Effect is an inertial force of moving objects in a rotating system. Usually, the effect of the Coriolis force is very small, but it is responsible for many large circulation phenomena on the Earth. The Coriolis parameter, *f*, is defined by:

$$f = 2\hat{\Omega}\sin\phi \tag{4.13}$$

where $\hat{\Omega}$ is the rotation rate of the Earth (or angular speed of the Earth), and ϕ is latitude. The spatial difference of atmospheric pressure can be ignored when an area of interest is not too large, but it may be important in specific conditions such as a storm surge that involves a very low pressure. In this study, the effect from atmospheric pressure was ignored.

There are many available forms of wind and bottom friction equations. Commonly used form is a quadratic relationship to the velocity. The bottom shear equation with a quadratic form can be written as:

$$\tau_{bx} = c_b\sqrt{U^2+V^2}U;\ \ \tau_{by} = c_b\sqrt{U^2+V^2}V \tag{4.14}$$

where c_b is dimensionless friction coefficient, which depends on many different factors, but mainly on the bottom roughness, and the velocity of the water. The bottom friction coefficient, c_b, can be expressed with the Chézy coefficient, $\hat{C}$. The bottom shear equation with the Chézy coefficient is given as:

$$\tau_{xb} = \frac{\rho g|\mathbf{U}|U}{\hat{C}^2};\ \ \tau_{xb} = \frac{\rho g|\mathbf{U}|V}{\hat{C}^2} \tag{4.15}$$

where $\mathbf{U} = (U,V)$ (Ramming and Kowalik, 1980).

The relationship between the Manning coefficient and the Chézy coefficient is derived from the Manning's equation, which is given as:

$$\hat{C} = \frac{h^{1/6}}{n} \tag{4.16}$$

where n is the Manning's roughness coefficient, which is a dimensionless parameter only depending on the material of a bottom. The range of the value n varies widely from 0.02 and 0.1 in natural main streams according to the material of the bottom and roughness (Chow, 1959).

Sometimes a linearized bottom stress is used to simplify the equation and obtain analytic solutions. The linearized equations of the bottom stress are given as:

$$\tau_{xb} = RU; \quad \tau_{xy} = RV \tag{4.17}$$

where R is the friction coefficient. The value of R is in the range of 10^{-5} to 10^{-6} in CGS units (Ramming and Kowalik, 1980). If R is derived from the velocity of the flow, the equation of the friction becomes quadratic as in Eqn (4.14). Some analytic solutions with linearized bottom friction were presented by Lynch and Gray (1978) and have been used for the evaluation of many numerical models.

Wind stress is a major hydrodynamics forcing in a shallow water body such as a lake. For the wind stress on the water surface, a quadratic relationship is often used as well. The equations of the wind stress are given by:

$$\tau_{sx} = \rho_a c_s \sqrt{U_w^2 + V_w^2} U_w; \ \tau_{sy} = \rho_a c_s \sqrt{U_w^2 + V_w^2} V_w \tag{4.18}$$

where c_s is wind friction coefficient or drag coefficient, ρ_a and U_w and V_w are x and y components of the wind velocity at 10 m above the surface. Many empirical equations for the wind friction coefficient are derived. One of equations is given by Garratt (1977) as:

$$c_s = 0.001(0.75 + 0.067\sqrt{U_w^2 + V_w^2}) . \quad (4.19)$$

The coefficient equations for the wind friction equations are different from researches. The factors in the coefficients are the density of winds, temperature, *etc*.

4.1.2. Implementation of the numerical model for hydrodynamics

Finite Element Method is efficient numerical method for solving partial differential equations. Also, it can handle irregular boundaries and heterogeneity of domain properties better than finite difference methods. Due to such advantage, the finite element method is widely used in many scientific and engineering researches including simulation of surface water hydrodynamics. In the finite element method, a solution domain is discretized into a set of irregularly shaped element cells. Then, a given set of partial differential equations is transformed into algebraic equations based on the discretization (Zienkiewicz and Taylor, 1989).

The methods to handle irregular boundaries in the surface water modeling should be chosen carefully to ensure overall satisfaction of mass conservation. Straight sided elements are often used for the finite element method due to its simplicity, but they have limitation for surface water simulation. It is impossible to specify parallel flow conditions at all locations on the boundary of an irregular system without leakage of water mass into or out of the system. In this method, to maintain the mass balance of water, the sum of the leakage is adjusted to be zero (Engelman, Sani, *et al.*, 1982). However, it will not

solve the mass conservation issue of contaminants due to the leakage. The alternative to overcome the described difficulty with straight sided elements is adopting isoparametric elements which have continuous edges at inter-elemental boundary connections. The isoparameteric elements can be designed so that the flow on the boundary can be maintained without loss of continuity (King and Norton, 1978). For this study, the isoparametric elements on the boundary were designed using Bézier curves, which guaranteed smooth continuous edges. Once a mesh was designed to have unique normal direction on the boundary, appropriate rotating procedure and Dirichlet boundary conditions were imposed. The details of the procedure followed as described in Pinder and Gray (1977).

The time derivatives were approximated by a finite difference technique, which uses the weighted average of the time derivatives of two consecutive time steps (Reddy, 1984). Hence, the scheme becomes implicit or partially implicit depending on the coefficient of implicity. The three hydrodynamics equations – Continuity and Navier-Stokes equations – were solved simultaneously. The linear solver is based on a Krylov solver from PETSc library (Balay, Buschelman, *et al.*, 2004). Because the governing equations of hydrodynamics are nonlinear, a numerical method to manage the non-linearity is necessary. To resolve non-linearity, Picard iterative method (Zienkiewicz and Taylor, 1989) was selected due to its simplicity.

This numerical procedure required significant computational time depending on the degree of mesh refinement and complexity of the equations. Also, the optimization for the water quality monitoring problem requires numerous results from the simulations. In result, the overall procedure required great amount of computational capacity. Hence,

reducing computational time became crucial to finish simulations in feasible time scale. One way to overcome the computational burden without sacrificing the quality of solutions is adopting high performance computing. Parallel computing becomes common recently because using a large number of moderately fast processors is less expensive than using an expensive and fast single processor to achieve the same speed. There are various architectures of parallel computing (Parhami, 1999), and among them Message Passing Interface (MPI) (Message Passing Interface Forum, 2003) is getting popular due to its flexibility and ease of expansion.

The definition of MPI is point-to-point message passing and collective operation over cluster of computers connected by network. MPI was introduced in early 1990s, and the second standard, MPI-2 was established in 1998. MPI itself is a language-independent communication protocol so that MPI is implemented into different computational languages by several groups. Since MPI works on computers connected by a network, memories of computers are not shared at all. This type of parallel computing is called a distributed memory system, and it requires data transactions among computers to synchronize data. This is a key role of MPI: several computers are connected over a network, and jobs are distributed, run, and collected to reduce computational time. MPI can be used also on computers with multiple CPUs often called multicore CPUs, which are very common and affordable now. MPI has become so popular that it is the de facto standard for communication for parallel programs on a distributed memory system. In fact, many of today's supercomputers such as IBM's BlueGene use MPI structure (Gara, Blumrich*, et al.*, 2005) with very fast network connections. The schematic of MPI computing is shown in Figure 4.1.

The finite element method routines to solve the hydrodynamics and contaminant transport based on the parallel computing was written using libMesh (Kirk, Peterson, *et al.*, 2006), which is a C++ library based on MPI and PETSc (Balay, Buschelman, *et al.*, 2001). The library, libMesh, has key components of FEM such as mesh handling and solvers. The platform for development was Linux RedHat with Intel-family multi-core processors, and the code was compiled with G++ (Free Software Foundation, 2006) since general Linux distributions and G++ are mature, stable, and freely available.

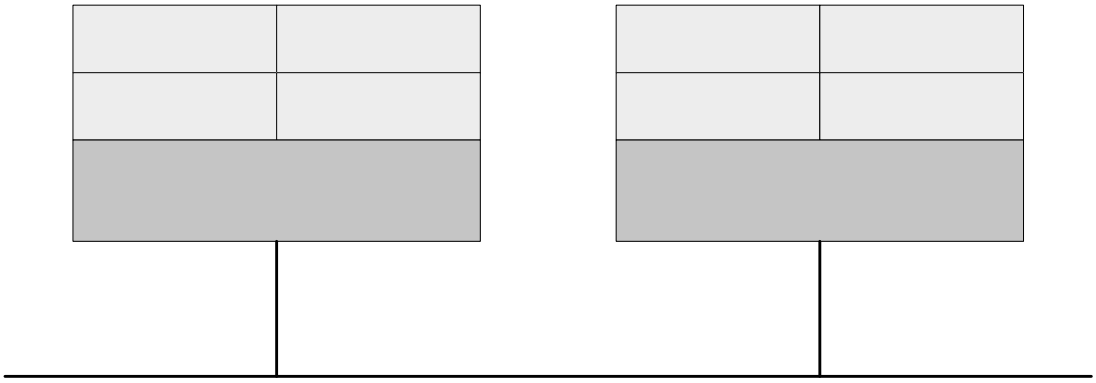

Figure 4.1 Schematic of parallel computing with MPI (Message Passing Interface) on multi-core computers

4.1.3. Verification of the hydrodynamics model

The hydrodynamics model was tested and compared with known analytical solutions to be evaluated.

4.1.3.1. Wind setup in a rectangular basin

When a wind blows steadily over a water body, the water level is sloped due to the stress from wind, which is often called wind setup or wind surge. Since the wind is a major factor of hydrodynamics of closed or semi-closed water body, this type of test is

done often for verification of hydrodynamics for a closed water body. When a wind setup is applied to a flat-bottomed, rectangular domain using 2-dimensional hydrodynamics equations, the hydrodynamics reaches a stationary state since the wind stress and water and hydrostatic force generated by a water surface slope are balanced out, and it is given mathematically as:

$$\tau_{sx} = \rho g h \frac{\partial \eta}{\partial x} \tag{4.20}$$

where the water level, $\eta = h - H$. An analytical solution of Eqn (4.20) is obtained by integration by part and it is given as:

$$\eta = \sqrt{\frac{2\tau_{sx} x}{g\rho} + (H + \eta_0)^2} - H \tag{4.21}$$

where η_0 is the water level at $x = 0$. If the change of the water level is small relatively to water depth, i.e. $\eta \ll H$, the slope is almost linear. The water level does not depend on the bottom stress since the mass transport is equal to zero at the stationary state

The numerical model for the wind setup was tested to check if the effect of the wind stress is applied correctly. The parameters used in the analytical and numerical solutions were: initial water depth, $h_0 = 5$ m ; domain length, $l = 10,000$ m ; the density of air, $\rho_a = 1.168$ kg/m^3 ; the density of water, $\rho_0 = 998$ kg/m^3 ; wind speed, $u = 10$ m/s from left to right. The initial condition of the numerical simulation was stagnant water body, which had no flow, flat water level. The numerical model reached a sloped water surface less than half a day of the simulation time. The numerical result was extracted on the center line of the basin, and it is presented in Figure 4.2 with the analytical solutions.

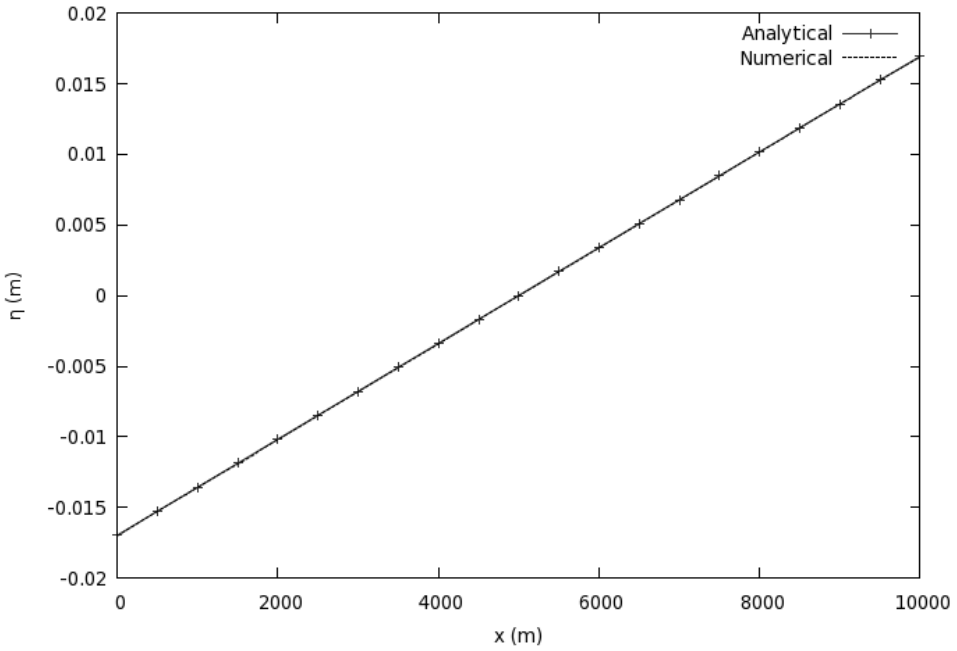

Figure 4.2 Comparison of numerical model results with the analytical solution of wind setup for a rectangular, flat-bottomed basin subject to a constant wind of 10 m/s

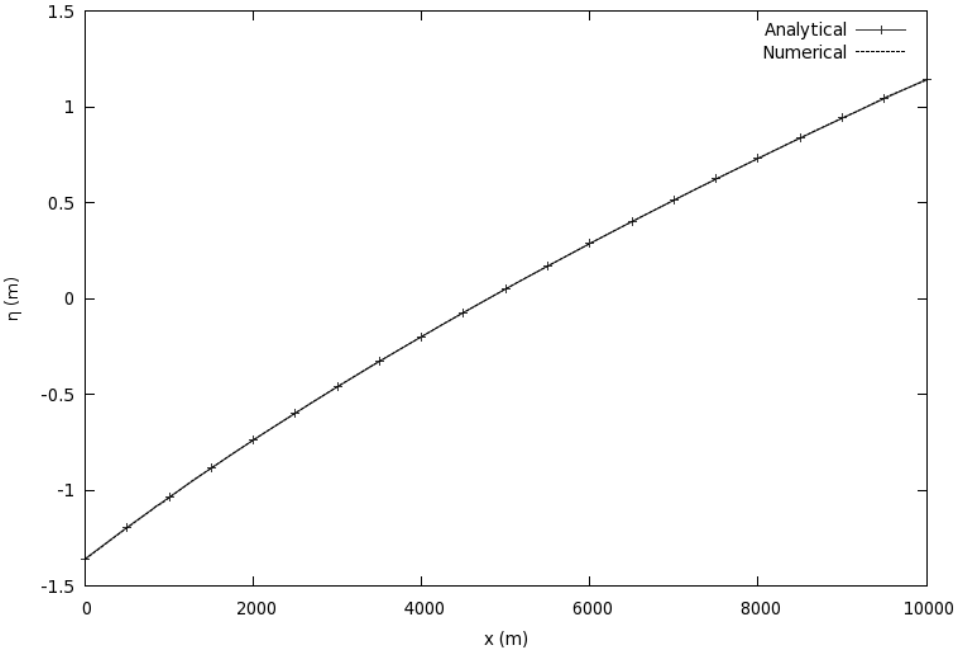

Figure 4.3 Comparison of numerical model results with the analytical solution of wind setup for a rectangular, flat-bottomed basin subject to a constant wind of 50 m/s

Both lines coincide so that they are indistinguishable. The surface slope was almost linear, and no flow was observed. Figure 4.3 shows a result with the same parameters but higher wind speed, 50 m/s. The analytical and numerical solutions are almost identical again, and this time the surface levels show the curvature of the square root function as in Eqn. (4.21). The winds of 10 m/s and 50 m/s are categorized as 4 and 12, or descriptively fresh breeze and hurricane respectively according to Beaufort scale.

4.1.3.2. Tides in a canal

A canal closed at one end and communicating at the other with an open sea under a periodic oscillation is tested to validate the model. The analytical solutions of the shallow water equations with a liniearized bottom friction in a rectangular geometry were provided by Lynch and Gray (1978). Although, the solutions by Lynch and Gray are based on the linearized version of the bottom frictions, they have been widely used to test models. The linearized bottom friction terms is given as:

$$\tau_{bx} = RU, \ \tau_{bx} = RV \tag{4.22}$$

where R is the linearized bed friction parameter. Eqn (4.22) is substituted for Eqn (4.15) in Navier-Stokes equations.

The solutions of a canal with a flat bed under a tidal forcing at an right open end are given as:

$$\eta(x,t) = \mathrm{Re}\left\{\eta_0 e^{i\omega t}\,\frac{\cos[\beta x]}{\cos[\beta L]}\right\} \tag{4.23}$$

$$U(x,t) = \mathrm{Re}\left\{-\frac{i\omega\eta_0}{\beta H_0} e^{i\omega t}\,\frac{\sin[\beta x]}{\cos[\beta L]}\right\} \tag{4.24}$$

under boundary conditions, which is a sinusoidal wave in Euler form:

$$\eta(L,t) = \mathrm{Re}\{\eta_0 e^{i\omega t}\} \tag{4.25}$$

where

ω = the frequency of the tidal forcing function
η_0 = the tidal amplitude
L = the length of the channel
H_0 = the depth of the channel
$\beta = \sqrt{\dfrac{\omega^2 - i\omega R}{gH_0}}$
$i = \sqrt{-1}$.

To compare with this analytical solution, the numerical model was tested with linearized bottom friction terms. The numerical simulation started from a flat surface, stagnant state. Comparisons between the numerical and analytical solutions are presented in Figure 4.4 through Figure 4.7. The numerical solutions were taken at the center line of the canal. The parameters used were: the length of the channel, 10 km; depth of the channel, 5 m; the bottom friction parameter, 2.3×10^{-3} m/s ; the tidal amplitude, 0.1 m; and the frequency of the tide, 30 min at the right end of the canal. The mesh used for the simulation had 756 nodes and 334 elements. The size of the time step was 30 seconds.

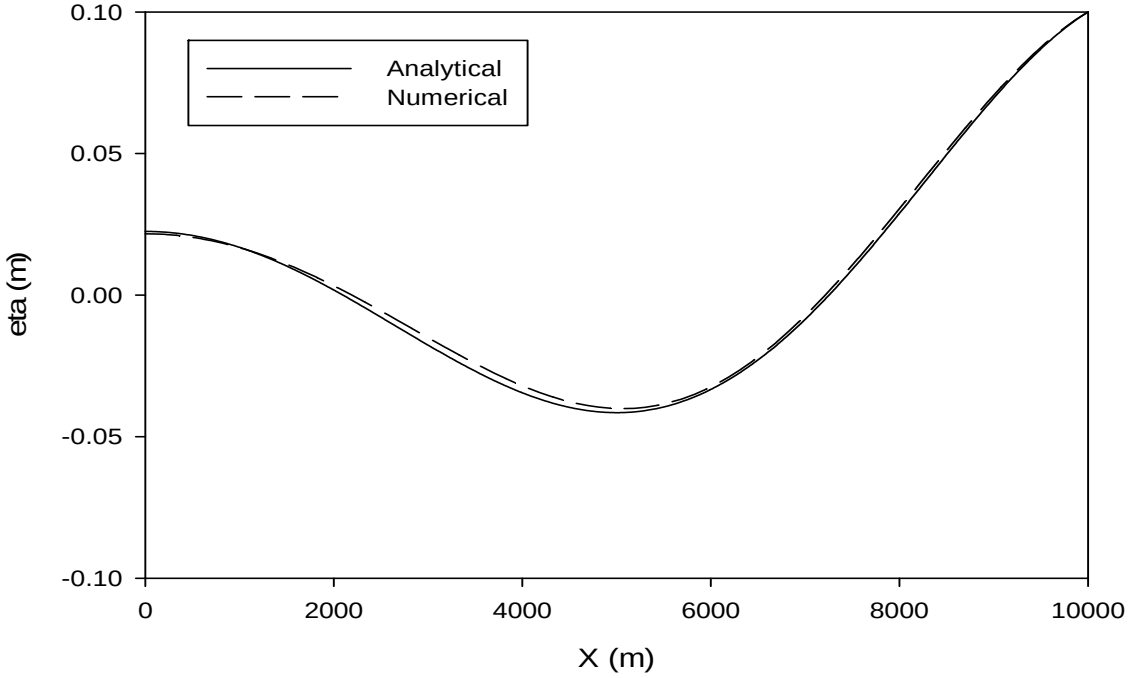

Figure 4.4 Surface level in a rectangular flat-bottom channel due to periodic forcing, $t = n\omega, \omega = 30\,\text{min}, \eta_0 = 0.1\text{m}, H_0 = 5\text{m}$

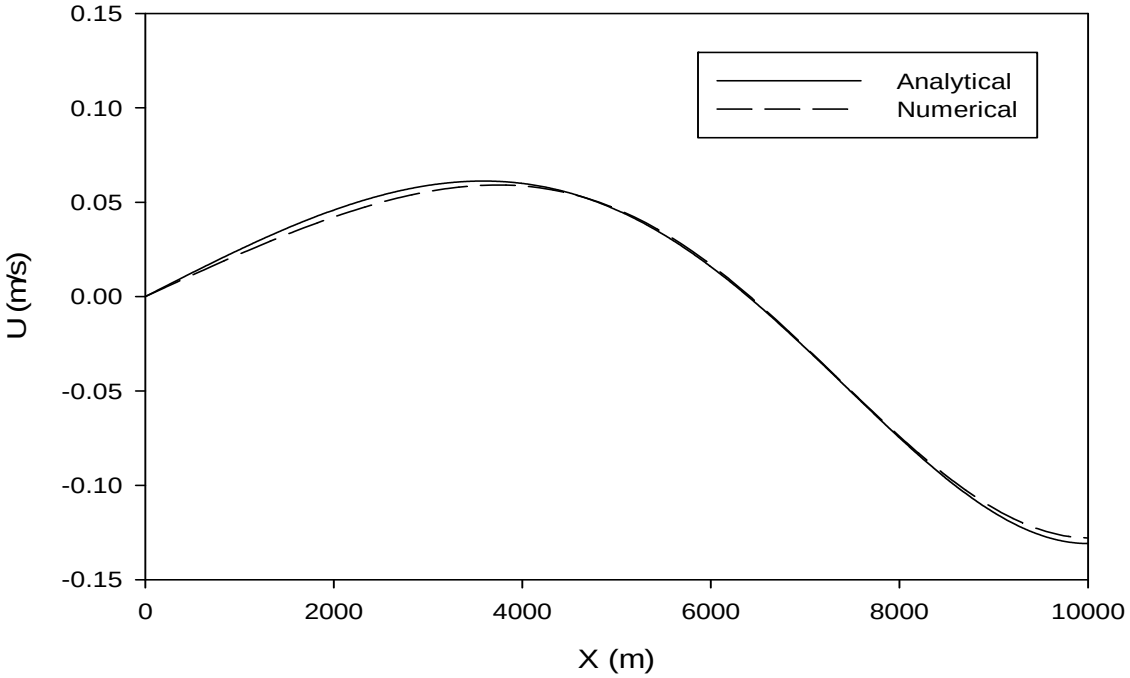

Figure 4.5 Velocity in a rectangular flat-bottom channel due to periodic forcing, $t = n\omega, \omega = 30\,\text{min}, \eta_0 = 0.1\text{m}, H_0 = 5\text{m}$

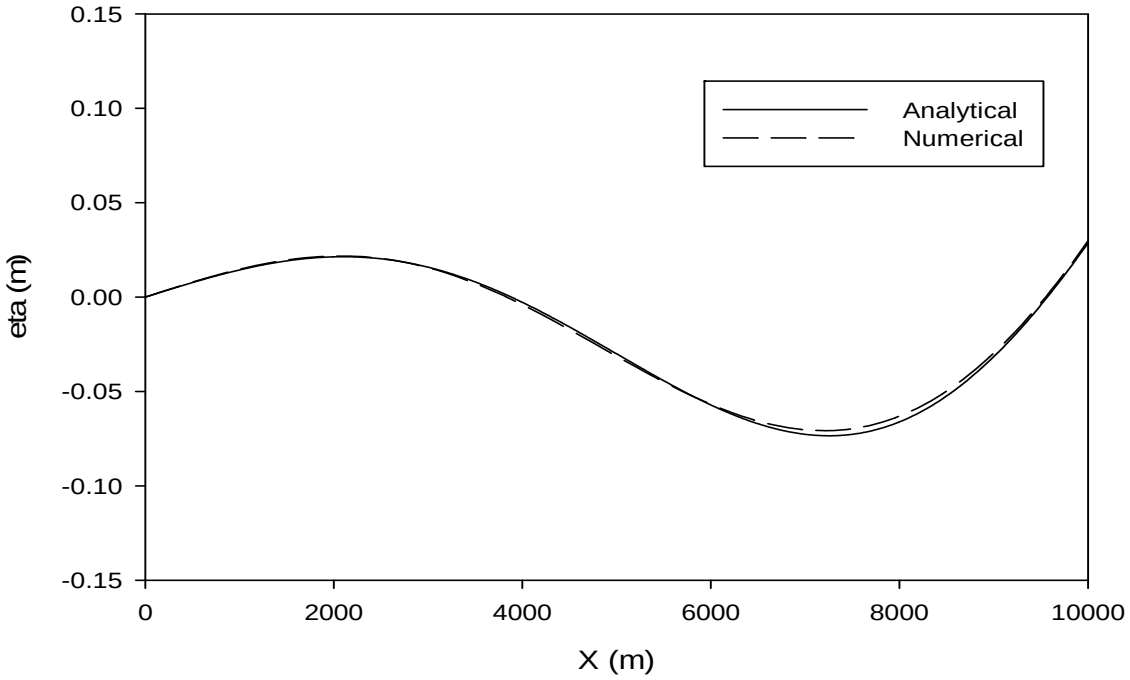

Figure 4.6 Surface level in a rectangular flat-bottom channel due to periodic forcing, $t = (n+1/4)\omega, \omega = 30\,\text{min}, \eta_0 = 0.1\text{m}, H_0 = 5\text{m}$

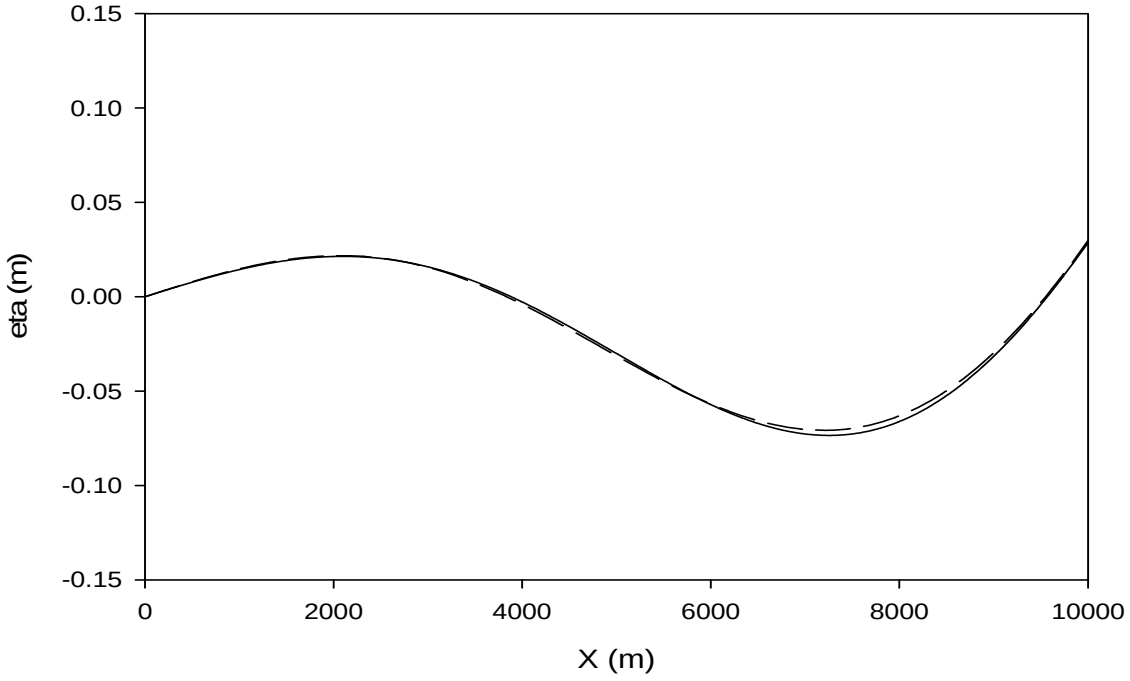

Figure 4.7 Velocity in a rectangular flat-bottom channel due to periodic forcing, $t = (n+1/4)\omega, \omega = 30\,\text{min}, \eta_0 = 0.1\text{m}, H_0 = 5\text{m}$

The numerical solutions for comparison were picked after 40 cycles of tides. The numerical solutions agreed well to the analytical solutions, and it verified the model's ability for the bottom friction and tidal inputs.

The same problem was solved with a linear bottom slope to check the effect of variable bottom elevation. The shape of the canal bottom is presented in Figure 4.8. The analytical solutions were also provided by Lynch and Gray(1978) as follows:

$$\eta(x,t) = \mathrm{Re}\{[AJ_0(2\beta\sqrt{x} + BY_0(2\beta\sqrt{x})]e^{i\omega t}\} \tag{4.26}$$

$$U(x,t) = \mathrm{Re}\left\{\frac{1}{\sqrt{x}}[-AJ_1(2\beta\sqrt{x}) - BY_1(2\beta\sqrt{x})]\frac{i\omega}{\beta H_0}e^{i\omega t}\right\} \tag{4.27}$$

where

$$A = \eta_0 Y_1(2\beta\sqrt{x_1})/[J_0(2\beta\sqrt{x_2})Y_1(2\beta\sqrt{x_1}) - Y_0(2\beta\sqrt{x_2})J_1(2\beta\sqrt{x_1})]$$

$$B = -\eta_0 J_1(2\beta\sqrt{x_1})/[J_0(2\beta\sqrt{x_2})Y_1(2\beta\sqrt{x_1}) - Y_0(2\beta\sqrt{x_2})J_1(2\beta\sqrt{x_1})]$$

J_α = the Bessel function of the first kind for order of α

Y_α = the Bessel function of the second kind for order of α

s = the slope of the channel

x_1 = the left end of the channel

x_2 = the right end of the channel

$$\beta = \sqrt{\frac{\omega^2 - i\omega R}{gs}}.$$

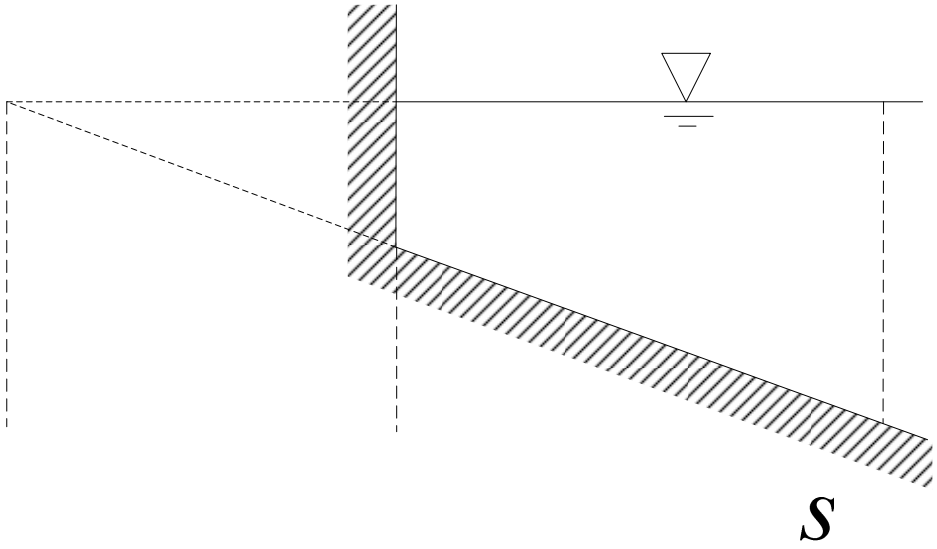

Figure 4.8 Shape of the sloped canal for the analytical solution

The numerical settings including the initial and boundary conditions were the same as the previous flat bottom case. The length of the canal was 10 km, the slope was set 0.0002, and x_1 and x_2 were 15,000 and 25,000 m respectively. Then, the depths at the left end and right end of the canal become 3 and 5 m respectively. The results from the numerical solutions after 40 tidal periods are compared with the analytical ones in Figure 4.9 through Figure 4.12. The numerical solutions agreed with the analytical solutions. It can be noticed that the wave was delayed and the water surface elevation at the left end of the sloped-bottom canal was higher than that of the flat-bottom canal. This was caused by the slowdown of the wave speed by the sloped bottom.

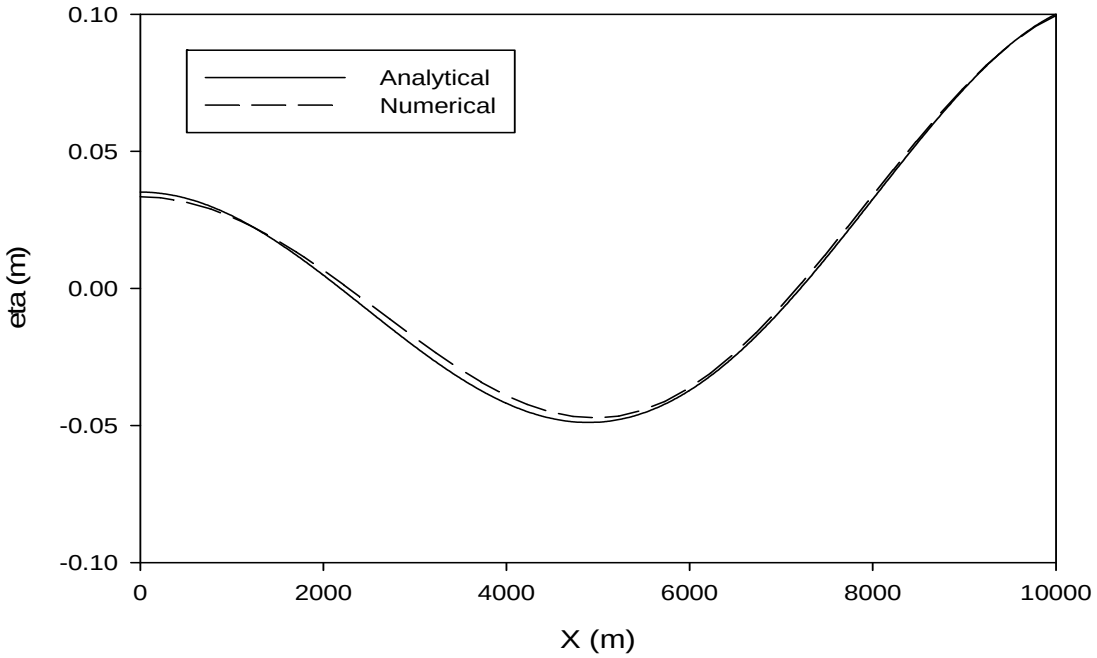

Figure 4.9 Surface elevation in a rectangular sloped-bottom channel due to periodic forcing, $t = n\omega, \omega = 30\,\text{min}, \eta_0 = 0.1\text{m}, s = 2\times10^{-4}$

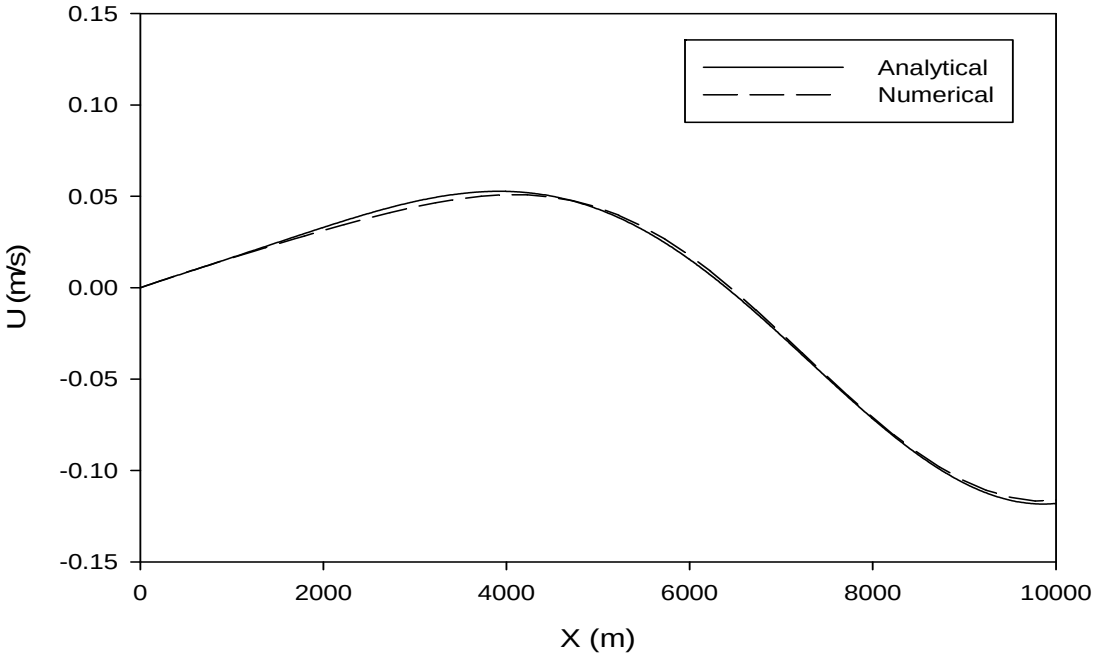

Figure 4.10 Velocity in a rectangular sloped-bottom channel due to periodic forcing, $t = n\omega, \omega = 30\,\text{min}, \eta_0 = 0.1\text{m}, s = 2\times10^{-4}$

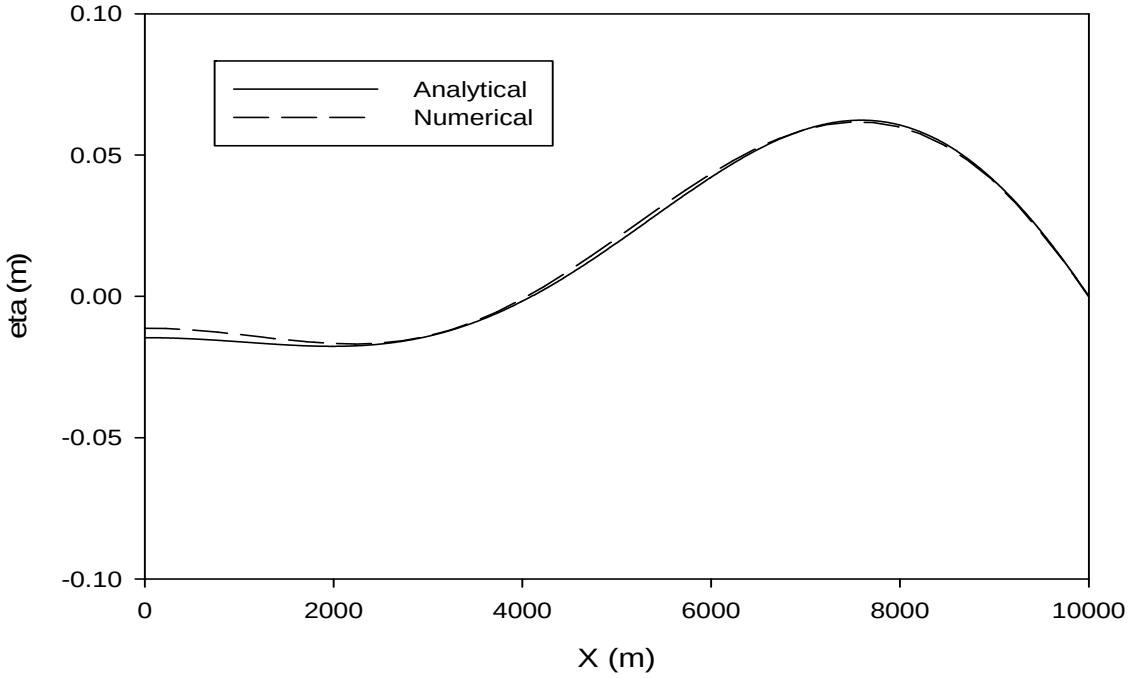

Figure 4.11 Surface elevation in a rectangular sloped-bottom channel due to periodic forcing, $t = (n+1/4)\omega, \omega = 30\,\text{min}, \eta_0 = 0.1\text{m}, s = 2\times10^{-4}$

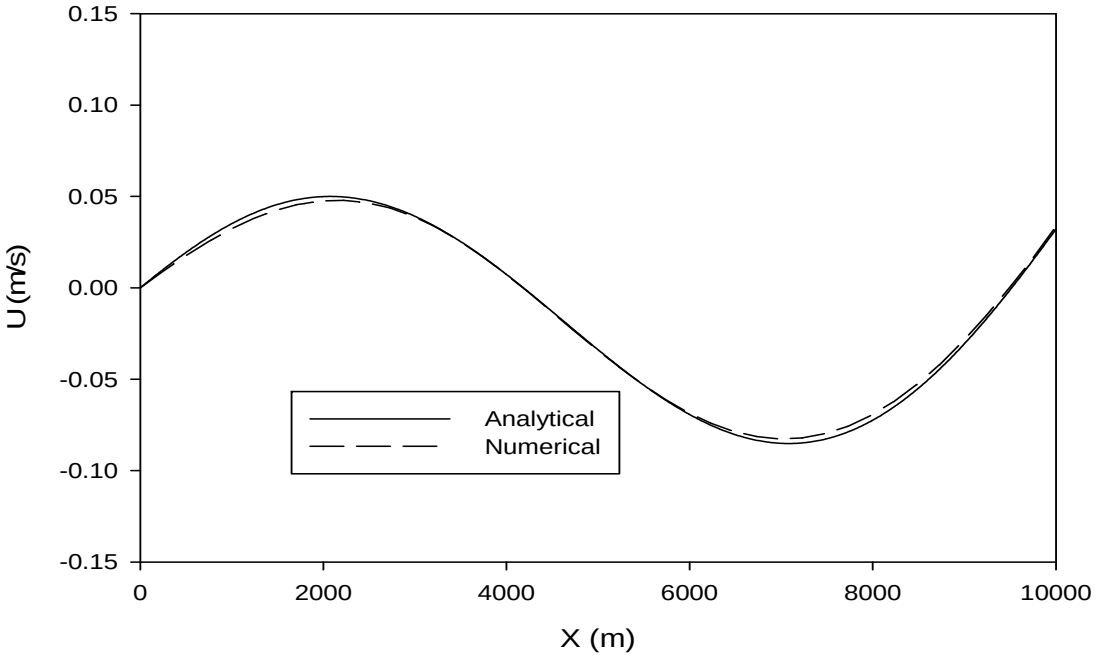

Figure 4.12 Velocity in a rectangular sloped-bottom channel due to periodic forcing, $t = (n+1/4)\omega, \omega = 30\,\text{min}, \eta_0 = 0.1\text{m}, s = 2\times10^{-4}$

4.1.3.3. The effectiveness of parallel computing

The purpose of introduction of parallel computing is to reduce computational time since the whole procedure of the optimization will require many simulations. Hence, the effectiveness of the parallel computing was evaluated.

Selected problem for the test was the same one in the previous subsection, 'tides in a canal' with the same mesh and parameters. When only one processor was used for the simulation of one day period, the total running time was 12 minutes and 32 seconds. When four processors on a computer were used simultaneously, the same simulation ended in 6 minutes 14 seconds. Figure 4.13 shows the trend of normalized running time and normalized apparent computational capacity versus the number of processors used for the simulation. As it shows, the run time decreased as the number of processors increased. However, the run time did not follow the reciprocal of the number of processors. The reasons why it did not are mainly the overhead of data transactions and computational cost for input/output routines of a mater node. When multiple processors are used, a job must be distributed and collected at each iteration of a simulation, and the data passing for distribution and collection causes extra load. In addition, some of jobs cannot be distributed. For example, only one master computational node can collect data and write the result into files if necessary. While a master computational node is executing input/output routines, which are relatively slow, other computational nodes have to wait for next jobs. Hence, the overall speed of calculation does not increased linear-proportionally to the number of processors used. In this test with a coarse mesh, the improvement of overall speed with four processors was less than two fold as shown in Figure 4.13.

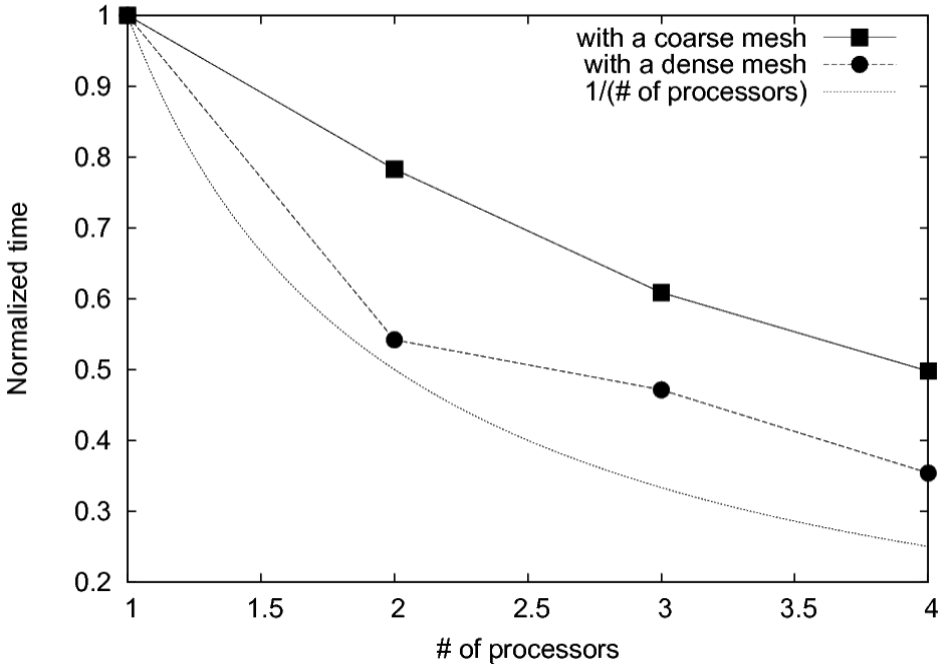

(a)

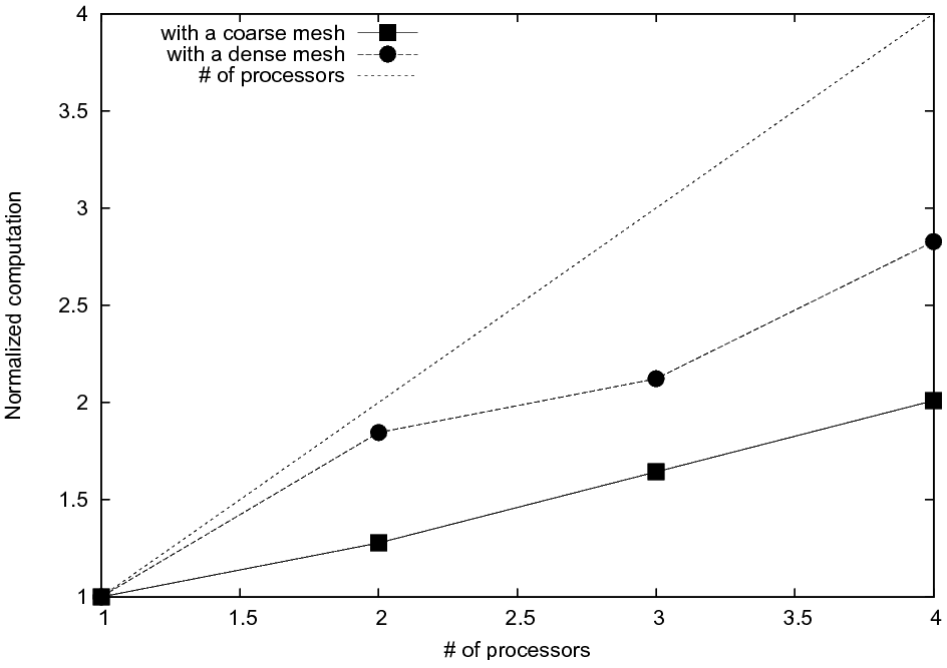

(b)

Figure 4.13 Normalized running time and capability according to the number of processors on a computer
(a) Normalized running time, and (b) normalized computational power for the test simulation

To check the effect of the overhead, the same problem was solved with a denser mesh, which has 3,349 nodes and 1,586 elements. With one processor, it took about 55 minutes for the simulation to finish. However, because the dense mesh has 3 times more elements, the relative overhead from transaction and input/output to the calculation load for the dense mesh case became smaller than those from the coarse mesh case. In result, the running time of the dense mesh case with two processors almost halved that with one processor, whereas only 20% of the running time was reduced by two processors in the coarse mesh case as shown in Figure 4.13. Thus, this tells that the parallel computing with MPI will be more efficient with large and complex problems.

4.1.4. Hydrodynamics of Lake Pontchartrain

4.1.4.1. Introduction to Lake Pontchartrain

Lake Pontchartrain is rather an estuary, not a lake, located in southeastern Louisiana, the United Sates. It covers 1,632 square km with an average depth of about 4~5 meters. The shape of the lake is roughly oval, 64 km wide and 29 km from south to north. It has provided with a means of transportation, commerce and sources of food so that it has been important for New Orleans and surrounding communities. The lake is connected to Gulf of Mexico via the Rigolets strait and Chef Menteur Pass into Lake Borgne, which is a lagoon rather than a lake. Hence, Lake Pontchartrain communicates with an open sea, and it is under tidal changes. The Inner Harbor Navigation Canal (IHNC), which is referred to the 'Industrial Canal,' also connects the Mississippi River with the lake. Bonnet Carré Spillway sometimes diverts water from Mississippi River to the Lake Pontchartrain. The lake is partly blackish due to the ocean salinity. Salinity

varies almost zero at the west end of the lake to about half of the sea salinity at the east end (U.S. Geological Survey, 2002).

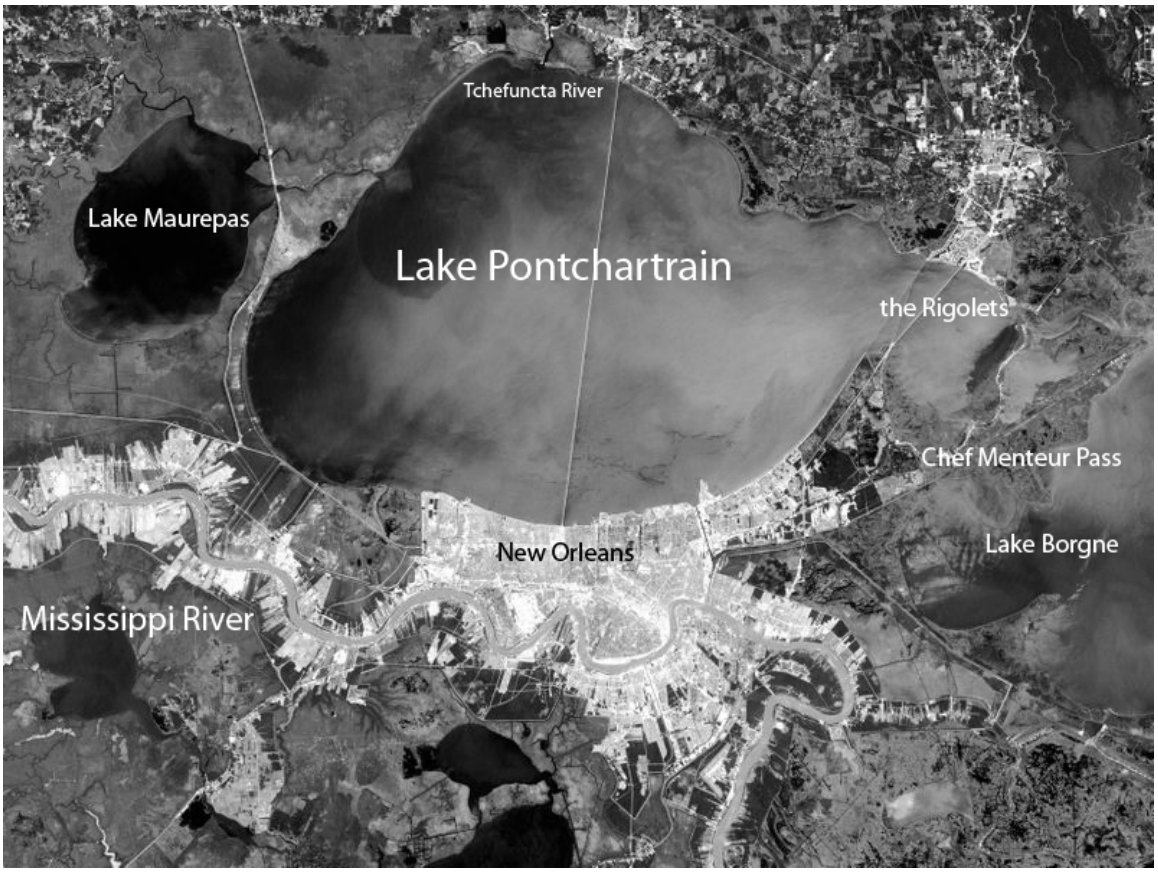

Figure 4.14 Satellite Image of Lake Pontchartrain Area
(Modified from NASA Landsat image)

Lake Pontchartrain is known by many environmental concerns. It suffers from loss of coastal wetlands, and pollution from runoff and sewage. Bacteria and viruses (pathogens) from animal and human wastes are a major source of pollution that prohibits from recreational use of the part of the lake. Heavy metals has been known another

pollutants in Lake Pontchartrain, especially in sediments (Manheim, 1998). In 2005, Hurricane Katrina hit New Orleans area and the city was flooded by the water from Lake Pontchartrain and Mississippi River. This event raised concerns about the pollution by the flooded water (EPA, 2006).

The water quality of Lake Pontchartrain is monitored under EPA program in coordination with the Louisiana Department of Environmental Quality. Most recent water qualities are available online (Lake Pontchartrain Basin Foundation).

4.1.4.2. Data preparation

The outline and the bathymetry data of Lake Pontchartrain were obtained from GeoCommunity (MindSites Group. LLC) and a USGS report (Manheim and Hayes, 2002) respectively, most of which are freely available. These geographical data were imported into geographical information system (GIS) software and their coordinates were converted into the states plane system. The bathymetry data is presented in Figure 4.16. The shallow area of the lake was adjusted to prevent too shallow elements. Then, the data were imported into an automatic mesh generator, ArgusONE (Argus Holdings. Ltd., 1999), and irregular 6-node triangular meshes were generated as shown in Figure 4.15. The size of elements close to the boundary is smaller than that at the center of the lake to manage any effect of boundaries. The length scale of small elements was about 200m. The meshes were further modified in order to ensure smooth boundaries to conserve the mass well. The total number of nodes and elements in the mesh are 61,092 and 30,169 respectively. It is known that the water column is generally well mixed, showing only weak stratification near the passes at certain times (Sikora and Kjerfve, 1985) so that one layer, two-dimensional model can readily be applicable.

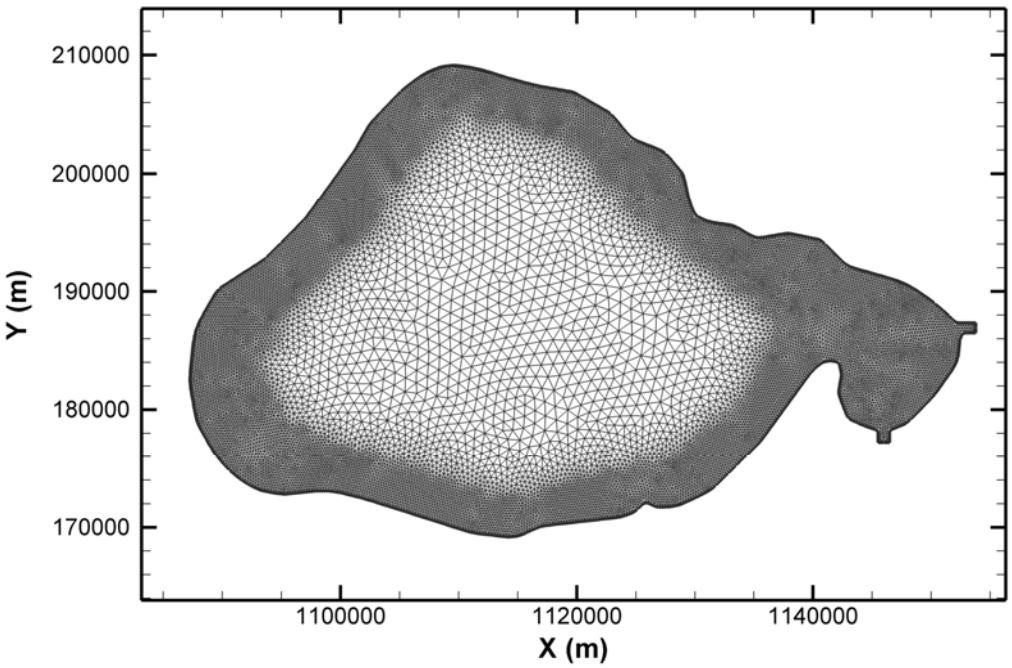

Figure 4.15 Discretized mesh of Lake Pontchartrain (in Louisiana south state plane coordinates)

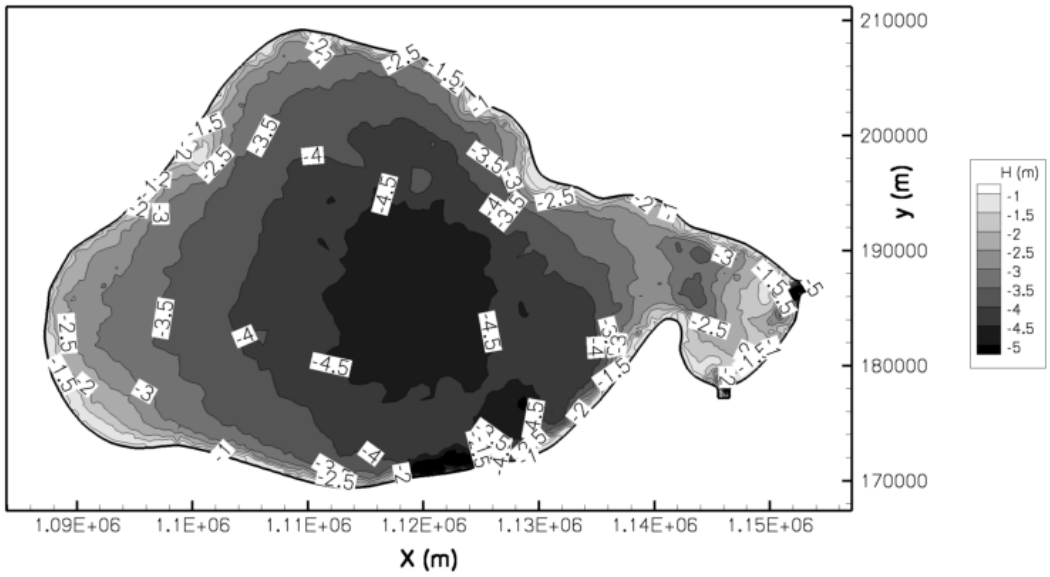

Figure 4.16 Bathymetry of Lake Pontchartrain for the model (grey scale color indicates bottom elevation)

For the boundary conditions at the two channel that communicates with Gulf of Mexico, the astronomical tidal prediction were obtained from NOAA web site (Center for Operational Oceanographic Products and Services, 2007) since no observation is available at the locations. Wind data for the simulation were obtained from NOAA web site (National Climate Data Center, 2007). The nearest station to Lake Pontchartrain that has wind observation is at Lakefront Airport, City of New Orleans. Fresh water input into the lake was ignored. The Manning's *n* of Lake Pontchartrain for the quadratic equations of bottom roughness was set as 0.02 uniformly. This is the same value used for background open-water area in post-Katrina study (Interagency Performance Evaluation Task Force (U.S.) and United States. Army. Corps of Engineers., 2006).

For all the following simulations, the size of time step was 10 seconds and the coefficient of implicity was 0.67. The Corilois Effect was also included by applying the latitude 30 degree for the simulation.

4.1.4.3. Constant wind-only Case

Since it is known that the wind is the major force over Lake Pontchartrain, the effect of the wind over the lake was tested following the similar simulation carried (Hamilton, Soileau, *et al.*, 1982) with wind speed 15 m/s. According to the historical wind data as shown in Figure 4.17, no dominant wind direction and speed exists. All the passes were blocked so that the lake was handled as a closed water body.

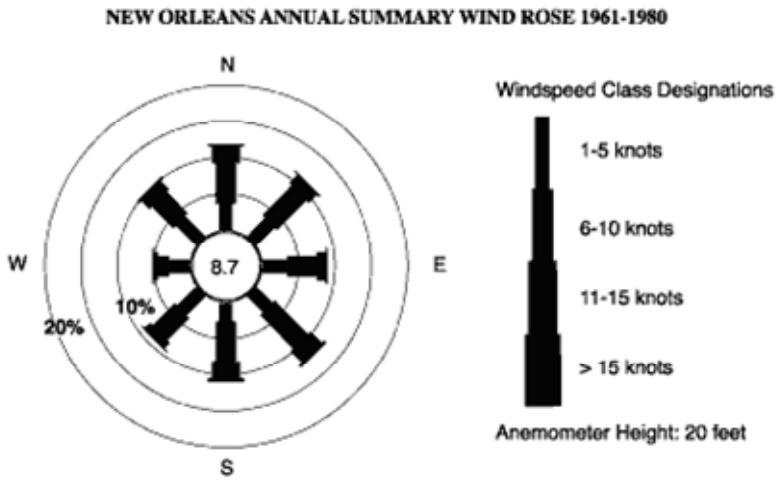

Figure 4.17 Rose diagram for the New Orleans area from years 1961~1980 (Adopted from U.S. Geological Survey, 2002)

The hydrodynamics reached to a steady state after about a day of the simulation as presented in Figure 4.18. The pattern of the flow had two-large gyres, which are typical in a closed water body under the wind drag. The flow along the shore was in the same direction to the wind, and the flow returned through the center of the lake. The velocities at the center and the shore of the lake were around 13 cm/s and 25 cm/s respectively. The surface setup by the wind was about 50 cm across the lake. The pattern of the flow was very similar to descriptions by other researchers (Hamilton, Soileau, *et al.*, 1982; U.S. Geological Survey, 2002). The amount of the surface setup by the simulation was predicted less than that of Hamilton *et al*. (1983), which was up to 70 cm, but the pattern of the setup and the velocities are comparable. The reasons of the difference are mainly from different wind friction, bottom friction equations and corresponding parameters, and the different viscosity handling in the numerical models.

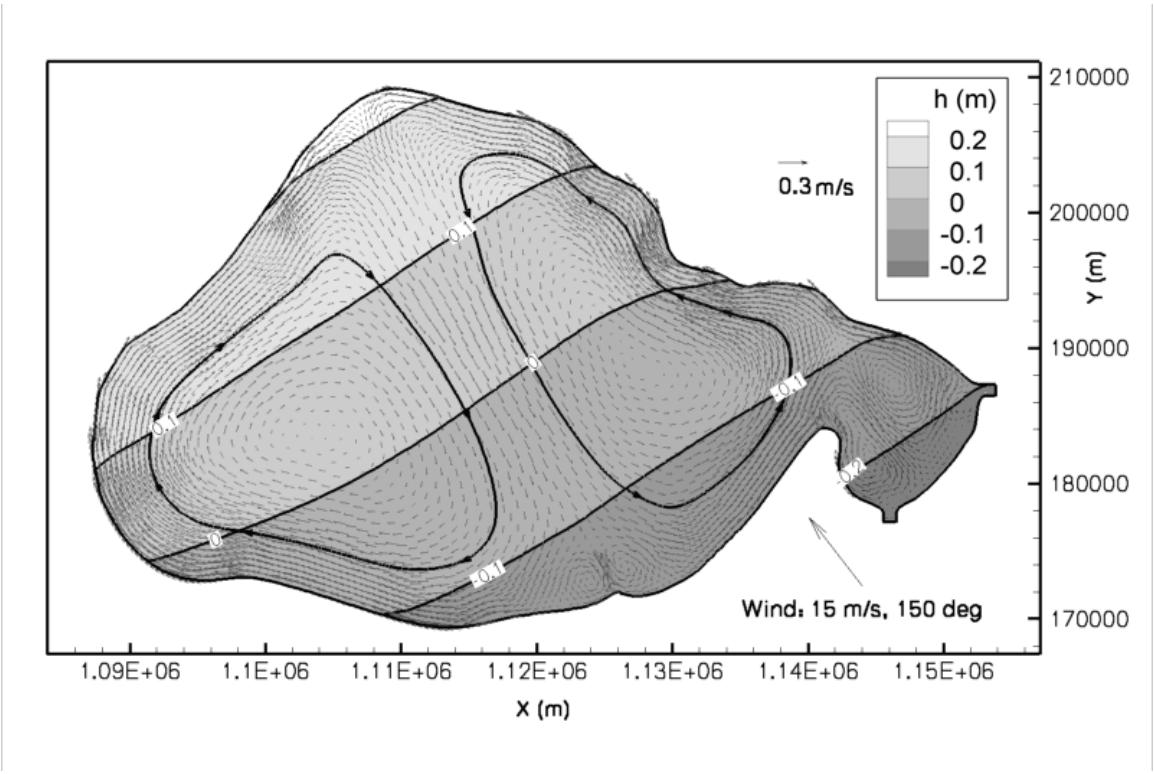

Figure 4.18 Circulation of Lake Pontchartrain by a constant wind, 15 m/s from southeast

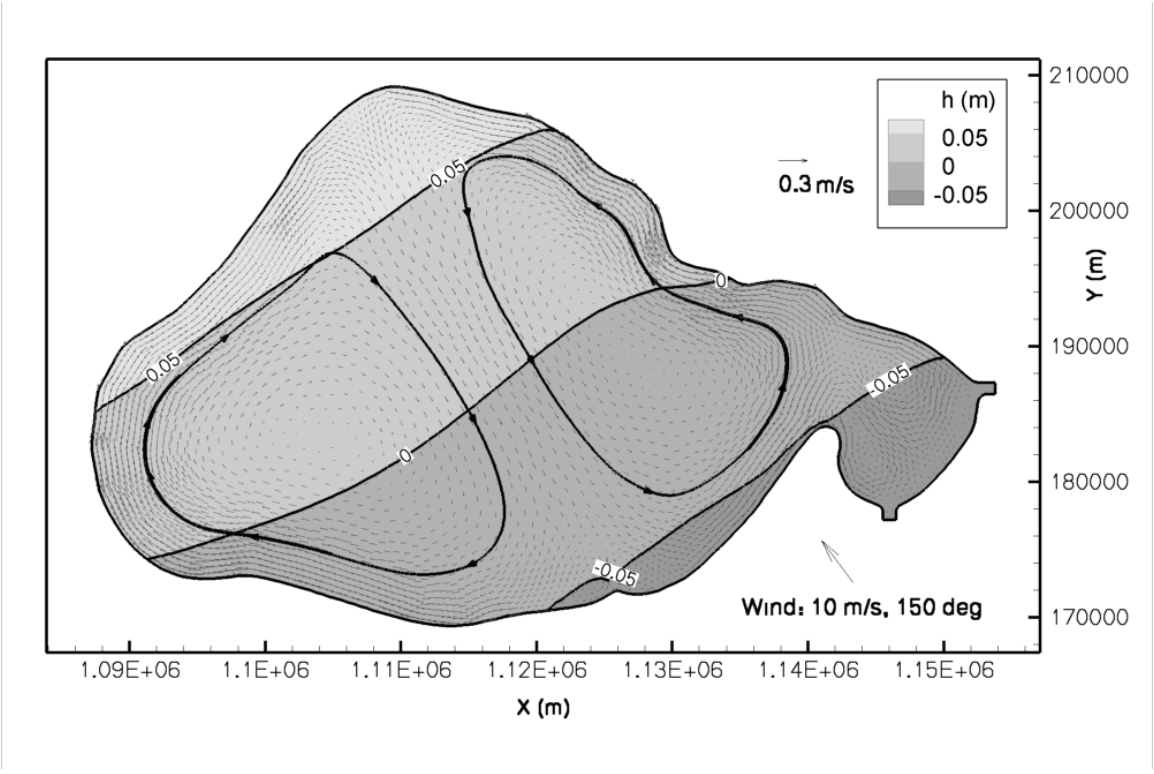

Figure 4.19 Circulation of Lake Pontchartrain by a constant wind, 10 m/s from southeast

The same simulation was tested with a slower wind speed to check the response to the different wind speed. The wind speed was set as 10 m/sec, and the wind direction was 150 degree, the same as the previous case. As shown in Figure 4.19, the pattern of the flow was the same as that with 15 m/sec wind, but the water surface slope was less than half of that with 15 m/sec wind. The water velocity at the center of the lake and on the shore was about 7 cm/sec and 13 cm/sec respectively, which were also about half of the previous case. Even though the wind speed was reduced by one third, the effect of the wind speed change was more than one third in the hydrodynamics, because the wind stress was calculated by the quadratic relationship to wind speed. Hence, the effect of the wind stress is more important especially when the wind blows strongly.

4.1.4.4. Real wind-only case

To investigate the effect of the changing wind condition, a set of observed wind data was applied to the simulation. The wind data at Lakefront airport from March 1st to 5th of 2008 were obtained from the NOAA website, and are presented in Figure 4.20. From 1st to 4th of March, the wind from southeast sustained. On March 5th, the wind direction changed from south to northwest gradually. The wind speed was over 10 m/s on March 4th. The initial condition of the model was stagnant.

Two snapshots of hydrodynamics were presented in Figure 4.21 and Figure 4.22. Similarly to the constant wind case, two wind-driven gyres according to the wind direction were observed, but the shapes of the circulation were not as well defined as in the constant wind case because of the transient wind condition. These results showed that the circulation by the wind is important even under variable real wind conditions. Also, these results justify adopting average constant wind speed and direction if necessary

because average wind conditions may produces very similar hydrodynamics to real situations.

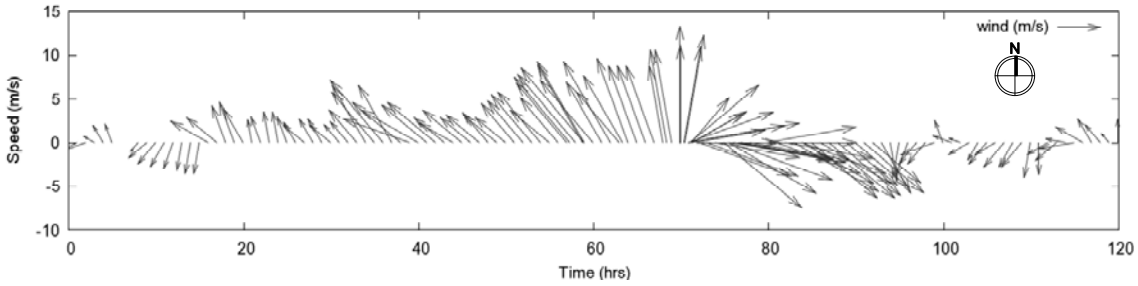

Figure 4.20 Wind speed and direction at Lakefront airport from March 1st, 2008 (NOAA)

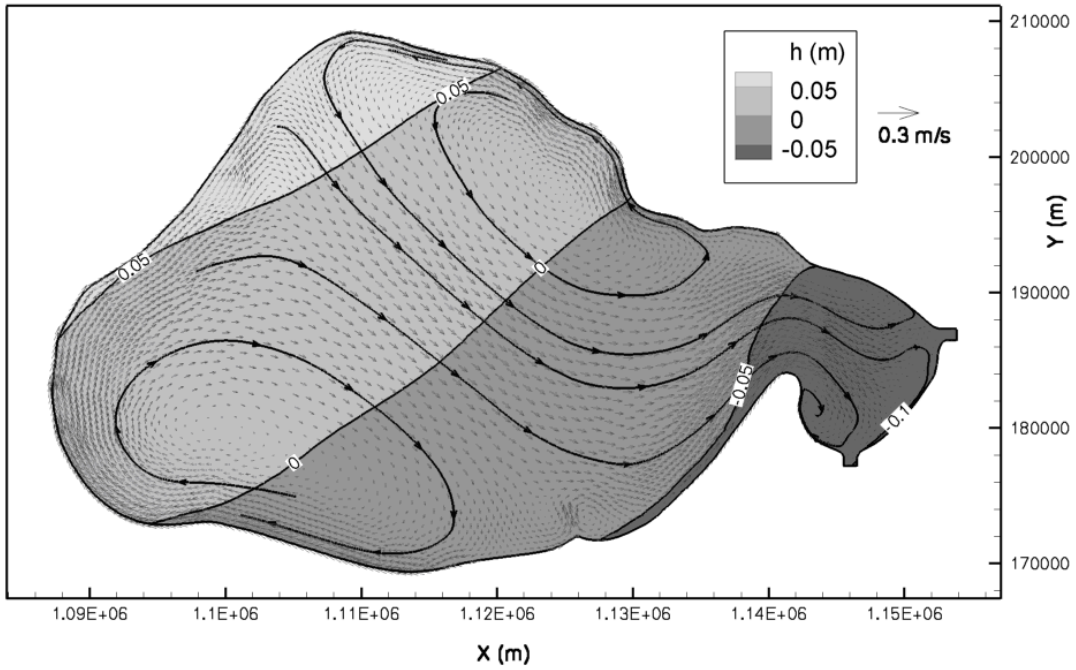

Figure 4.21 Circulation of Lake Pontchartrain by real wind condition at 12:00, March 3rd (after 60 hrs of the simulation)

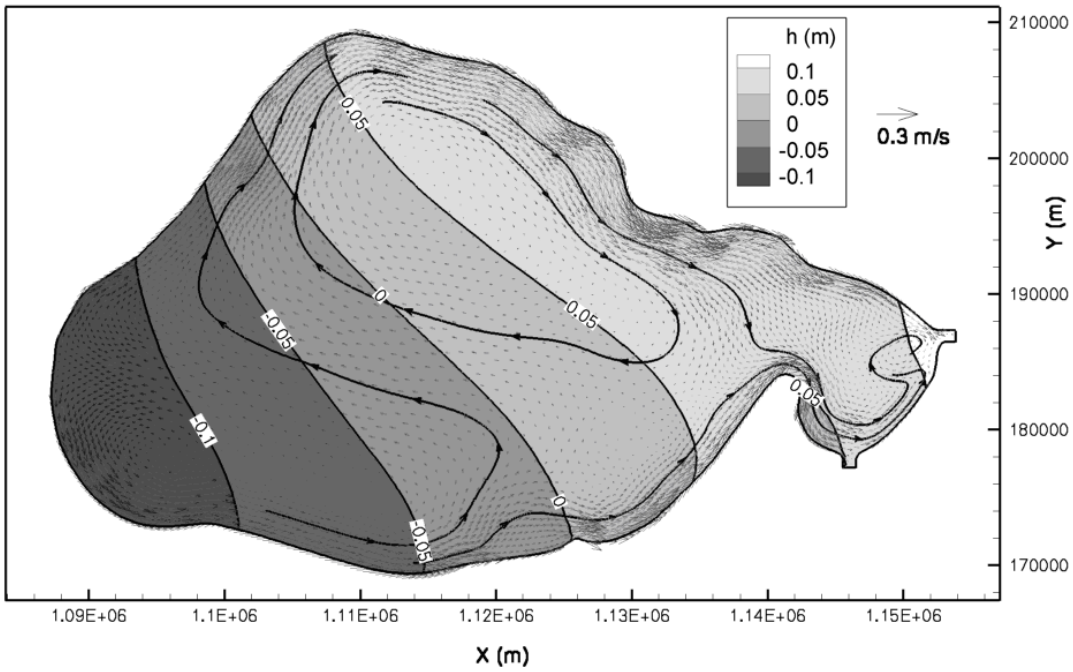

Figure 4.22 Circulation of Lake Pontchartrain by real wind condition at 04:00, March 5th (after 100 hrs of the simulation)

4.1.4.5. Tide-only case

To check if the model reflects the tidal forces correctly in the Lake Pontchartrain, only astronomical tides were imposed as hydrodynamics forcing. This way, the effect of the wind over the lake can be separated. Lake Pontchartrain has two major waterways, Chef Menteur Pass and the Rigolets strait that communicate with Lake Borgne which is actually a part of the Gulf of Mexico. Thus, the two channels were selected as locations of tidal boundary conditions in the simulation. NOAA provides the prediction of astronomical tides around the U.S. through its website, including Chef Menteur pass, New Canal, and Tchefuncta river in Lake Pontchartrain. The locations of the three stations are presented in Figure 4.23. The tide at the Rigolets was assumed the same as that of Chef Menteur. Since the NOAA prediction only provides high and low tide so that

the shape of the tide was reconstructed, and the result is presented in Figure 4.24. This tidal prediction was used for the value of tide input for the model at the two channels, Chef Menteur pass and the Rigolets. The dates selected for the simulation were from March 1 to March 6, 2008. This period was spring tide period, which showed the large fluctuation of the tides. The initial condition was stagnant. To calibrate the model, the datum of the bathymetry was adjusted slightly. Because the velocity of flow is important for the contaminant transport, the model was calibrated mainly to match tidal fluctuation. Fresh water inputs from rivers were not included in the simulation because: (1) It was hard to find inflow rates from all the rivers, and (2) the effect of fresh water input is known to be relatively small to the effect to the tides. The tidal prism, which is the change in the volume of water by the tides, is about 1.56×10^{8} m^3, and the tidal flows through the channels are about 20 times greater that the total river flow into the lake (Swenson and Chuang, 1983). The salinity from the tide was ignored.

The result of the numerical model was compared with the NOAA predictions at Tchefuncta river station and New Canal station as shown in Figure 4.25. At the New Canal station, the water level from the numerical model was adjusted to MLLW (mean lower low water) of the station. The amount of fluctuation was quite close, but the numerical model predicted about 3 cm lower water level. Considering possible error in the datum, it was reasonably close. The NAGD 29 datum at the Tchefuncta river station is not provided from NOAA, the only fluctuation was compared after adjusting the water level. The amount of the fluctuation was a little less than the prediction, but they are close. The times of high tide at both locations agreed with each other, but the low tide of the numerical prediction at the both locations showed some lags.

Figure 4.26 shows the hydrodynamics at March 3rd 23:54, which is about 3 days after the simulation time when the water level at Menteur Pass was highest during the tides. The flow direction is from east to west, and the effect of the tides was quickly attenuated in the right bulge of the Lake, and the velocity at the center was less than 5 cm/sec. The water level difference between the passes and the lake was less than 10 cm. Figure 4.27 shows the hydrodynamics at March 4th, 10:11 when the waver level at Menteur pass was lowest. The flow direction was west to east and the velocity at the center of the lake was again less than 5 cm/sec. According to the simulation, the effect of tide was mainly localized on the eastern part of the lake, but still the range of the tide fluctuation inside of the lake is about 20~30 cm especially at spring tides.

Comparing with the result of the constant wind cases, the velocity generated by the tides was generally smaller than the velocity generated by the wind. Especially, the velocity generated by the wind along the shore of the major part of the lake was 10 times faster than the velocity generated by the tide. Hence, the effect of the wind was dominant over that of the tide on the most part of the lake, and this agrees with the previous researches (Hamilton, Soileau*, et al.*, 1982; U.S. Geological Survey, 2002).

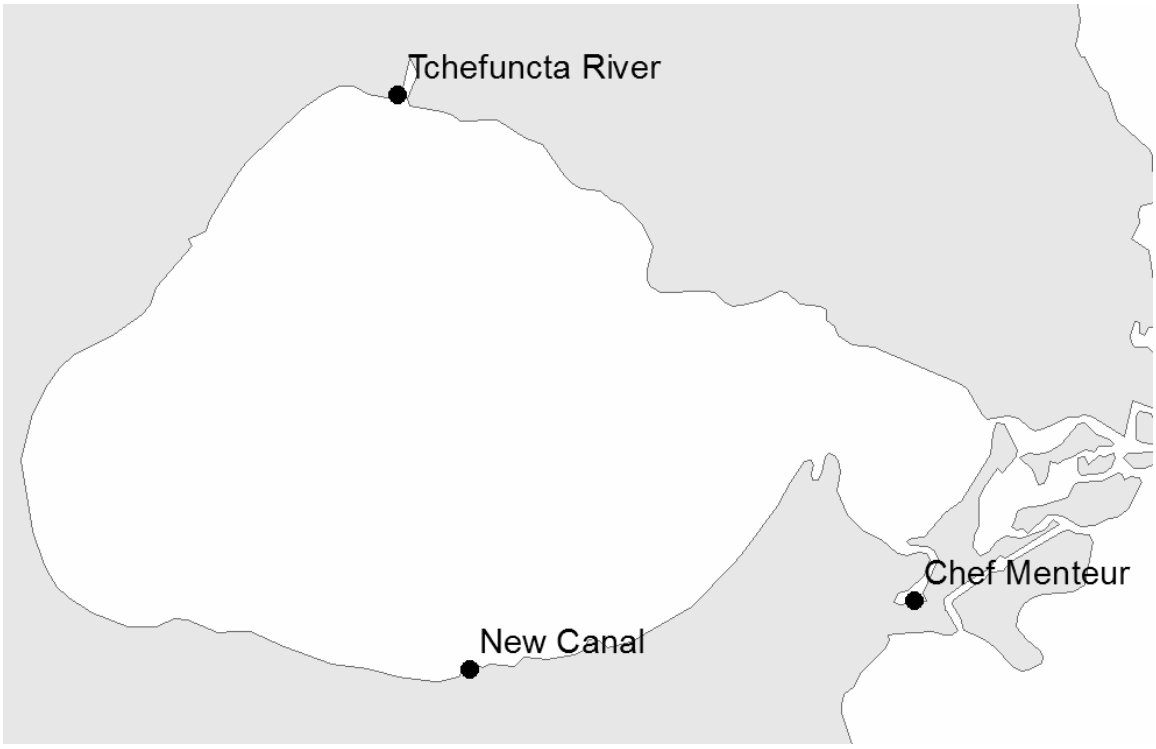

Figure 4.23 Locations of tide predictions from NOAA

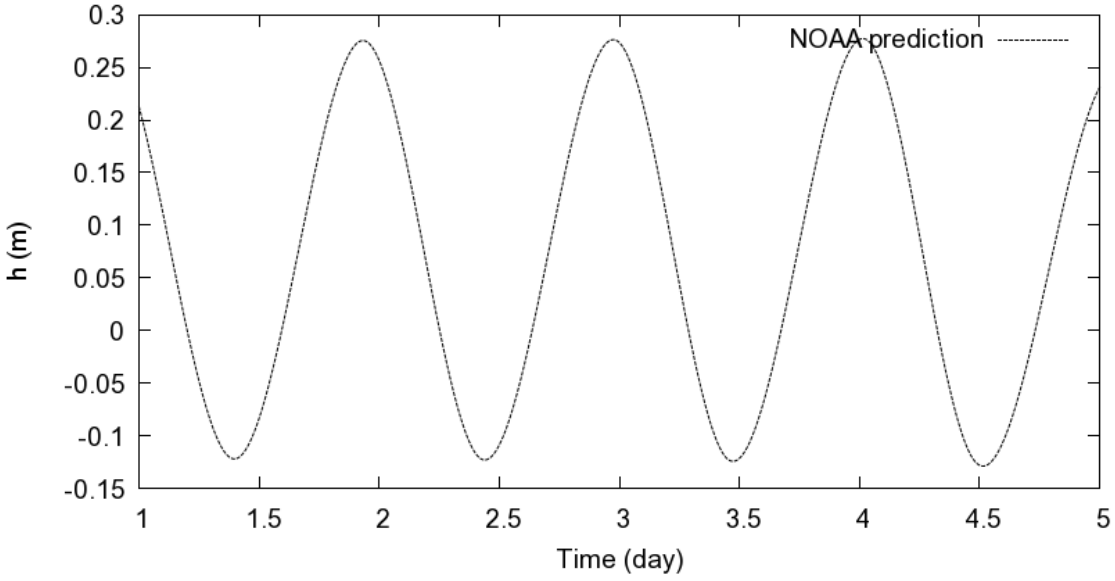

Figure 4.24 Astronomical tide prediction at Chef Mentuer pass from March 1st , 2008 (datum: MLLW)

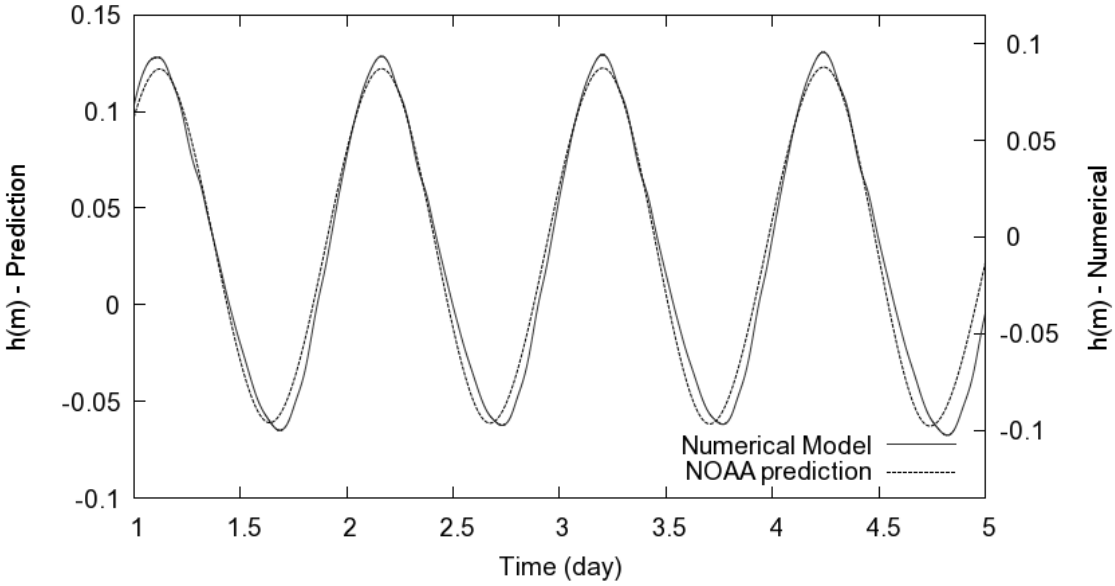

(a)

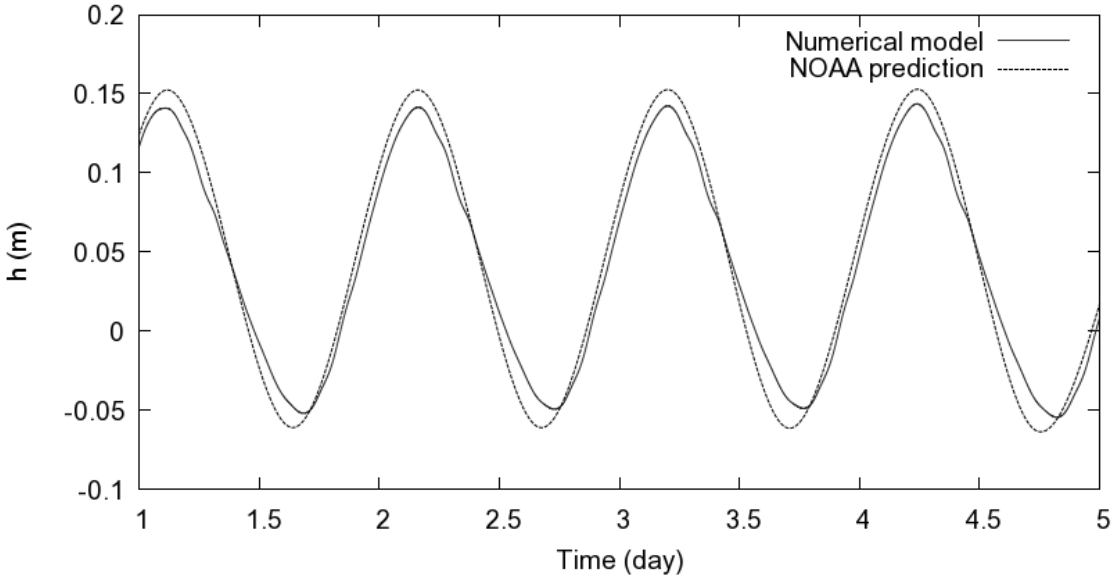

(b)

Figure 4.25 Comparison between the numerical model and prediction of Lake Pontchartrain
(a) at New Canal station, and (b) at Tchefuncta river station from March 1st, 2008

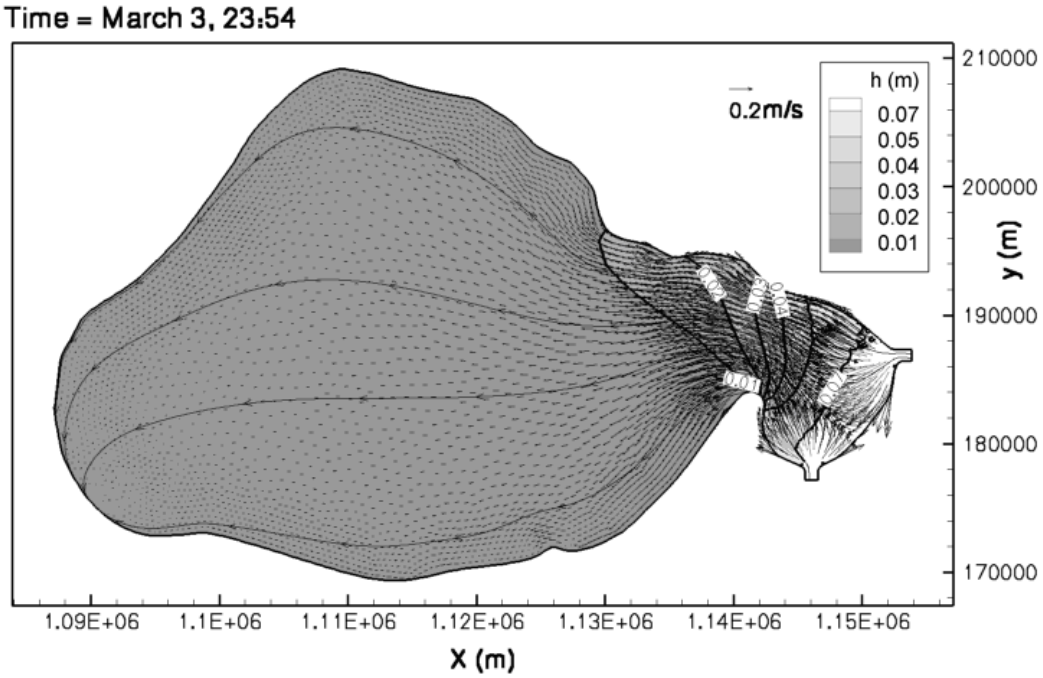

Figure 4.26 Hydrodynamics snapshot at 21:54, March 3rd only with the tides

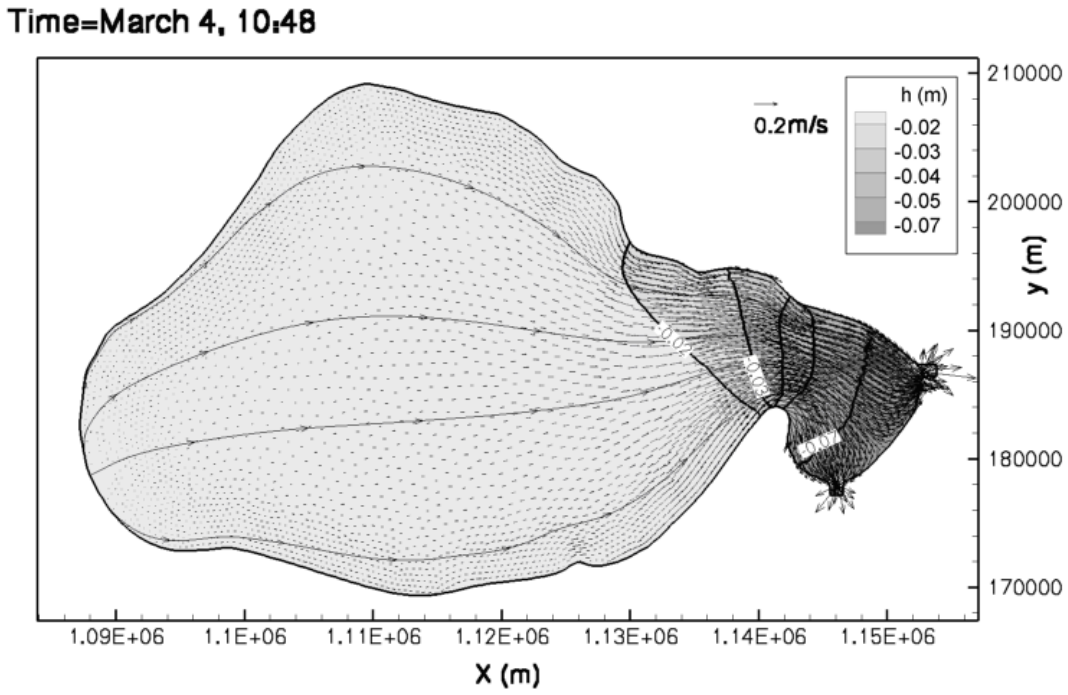

Figure 4.27 Hydrodynamics snapshot at 10:48, March 4th only with the tides

4.1.4.6. Tide with constant wind case

To check the effect of the combination of wind and tide, a simulation was designed and run with a constant wind and the predicted tides. The 10 m/sec constant wind from southeast (150º) was imposed. The overall pattern of flow was similar to the result under the wind-driven circulation, but distinctive two-gyre pattern was partly broken down because of the influence of the tides on the eastern part of the lake as shown in the streamlines of Figure 4.28 and Figure 4.29. The slope of the water surface also generally followed the water surface setup by the wind only cases. However, because the water mass can be supplied through the two channels at the east end, the water surface level was higher than that of the wind-only case as shown in Figure 4.29. Overall, the major part of the lake was mainly under the effect of the wind.

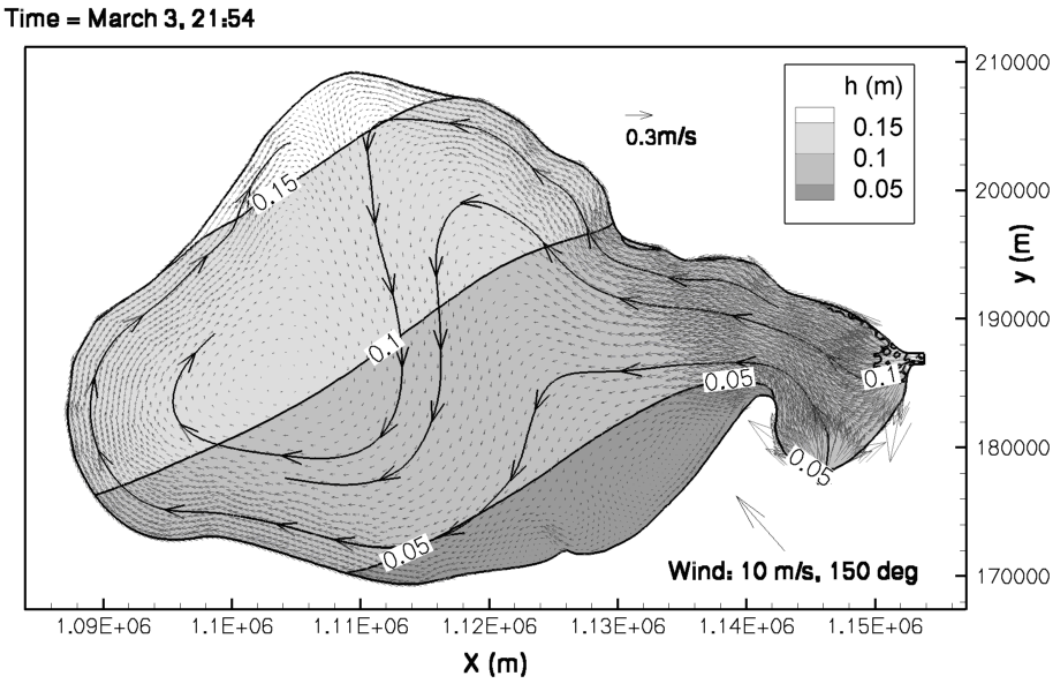

Figure 4.28 Hydrodynamics snapshot at 21:54, March 3rd with tides and constant wind

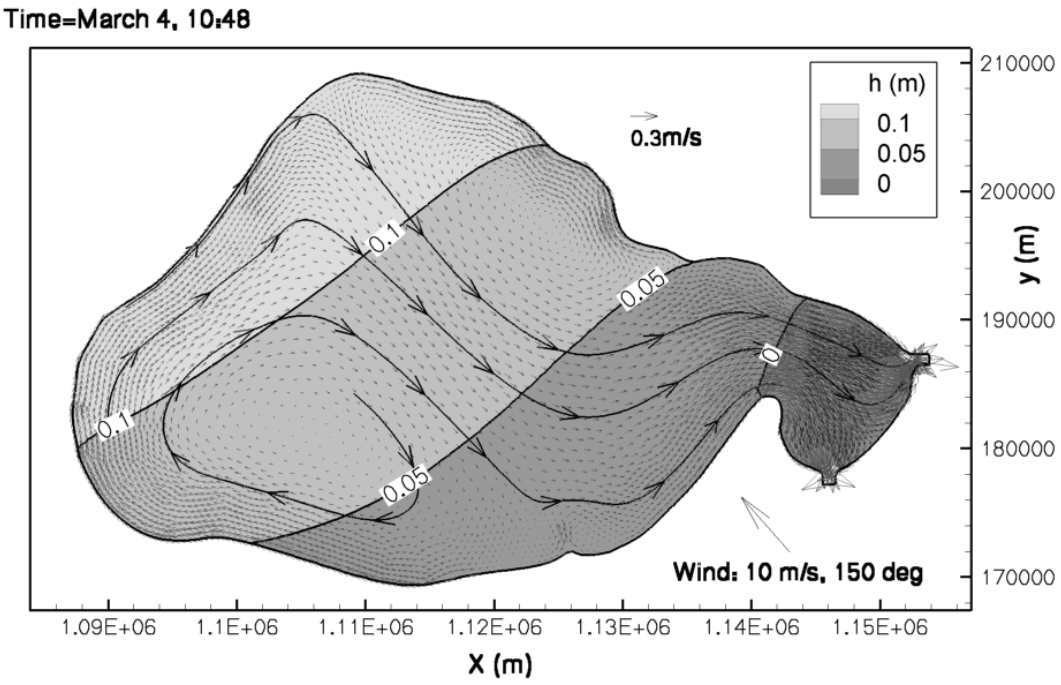

Figure 4.29 Hydrodynamics snapshot at 10:48, March 4th with the tides and constant wind

4.1.4.7. Tide with real wind case

For the last case, the tide prediction and the variable real wind data from March 1st to 5th, 2008 were applied for the simulation to model the real situation closely. Ideally, using the observed tidal values at the boundary is the best option to model the real case if they are available. However, the tidal observations at Chef Menteur pass and the Rigolets are not available, and the tidal prediction at Menteur pass was used for the boundary conditions.

Figure 4.30 shows the comparison of the observed and simulated water level at New Canal station in the lake. Due to the transient wind, the water surface did not change smoothly. The simulation result deviated from the observation from the beginning of day

2 of the simulation time, and the discrepancy sustained to the beginning of day 4 of the simulation. This was caused by a higher tide than the predicted one in Gulf of Mexico. Figure 4.31 is the comparison between the observed and predicted water level by NOAA at Bay Waveland Yacht Club on of coast the state of Mississippi, and it shows about 50 cm higher observed tide than the predicted one. A sudden rise of the water level in the lake around at 3 day simulation time was observed from both of observation and numerical results. This surge around at the New Canal station the midnight of March 4th was caused by the change of the wind direction from southeast wind to northwest wind at the same hours (70 ~ 80 hours) as shown in the wind chart, Figure 4.20.

The change of hydrodynamics from 10:11, March 3 to 10:48 March 4 is presented form Figure 4.32 and Figure 4.34. In this time period, the wind direction changed from southeast to east, and the effect of the change of the wind direction is well shown in the figures. Also, the figure shows the effect of the tides as well. The tides tended to control the water level all over the lake, and the wind controlled the circulation and surface slope.

Overall, the simulation missed the high water level in the lake because the predicted astronomical tidal level, which was lower than actually surface level, was used as boundary conditions, but the model followed fluctuation of water surface level. As shown this simulation, the effect of the tides can be important depending on the tides conditions, but the wind still plays important roles especially at the center of the lake.

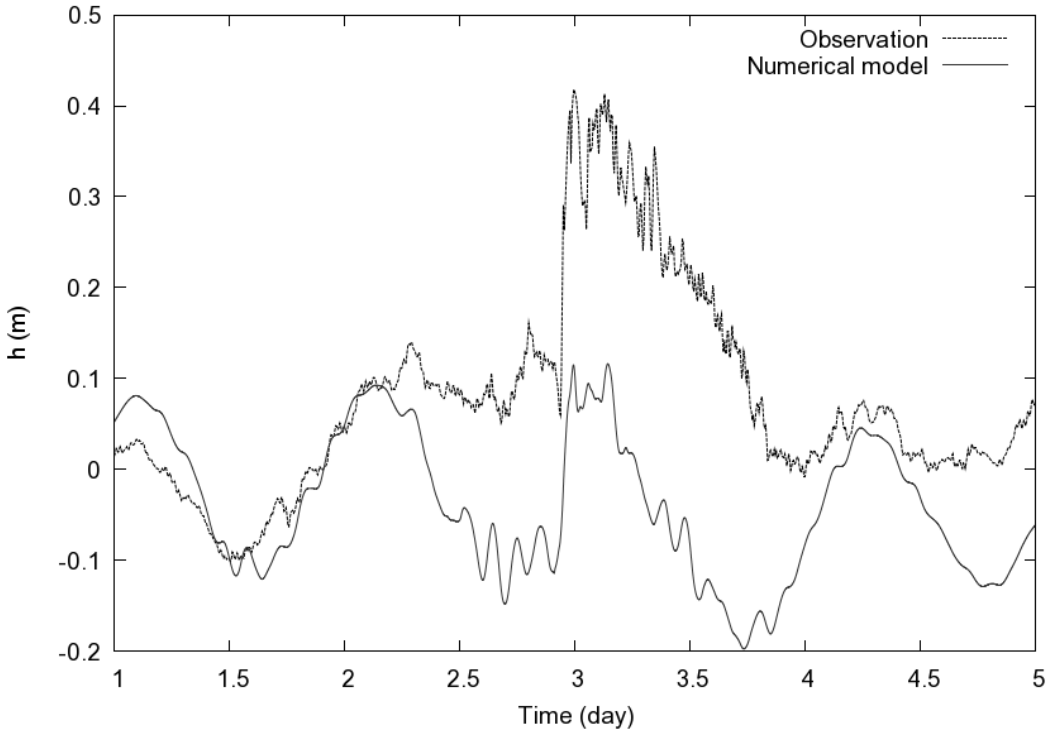

Figure 4.30 Comparison between the observed and simulated water level at New Canal station

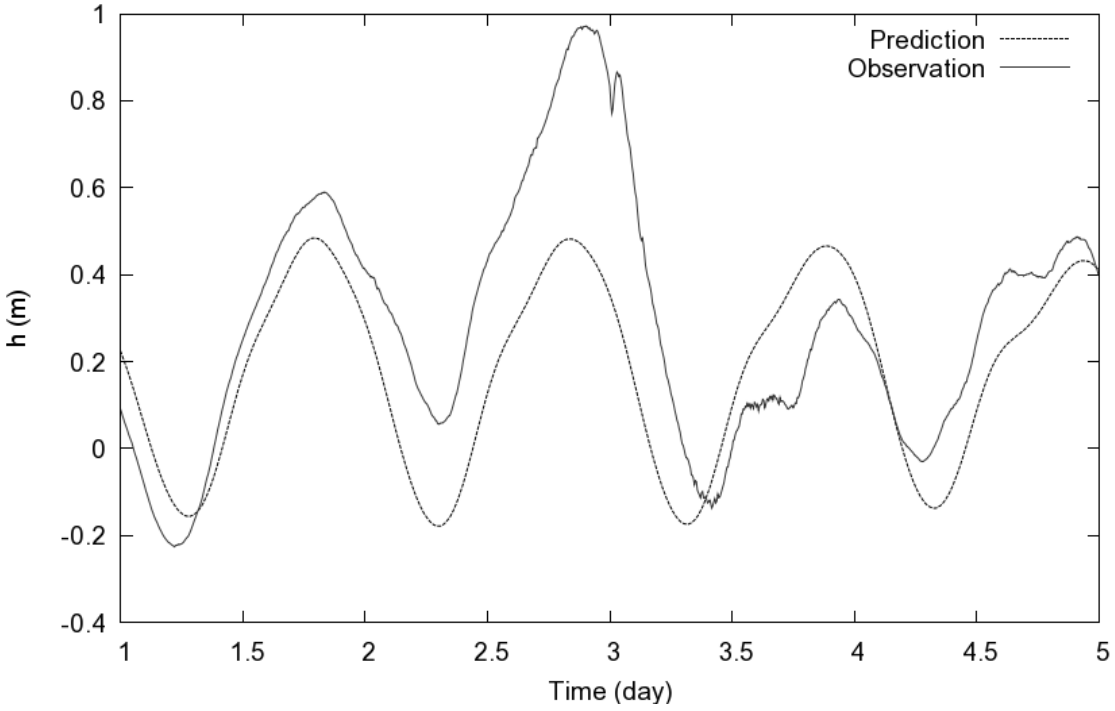

Figure 4.31 Comparison between the observed and predicted water level by NOAA at Bay Waveland Yacht Club, MS from March 2nd to March 5th

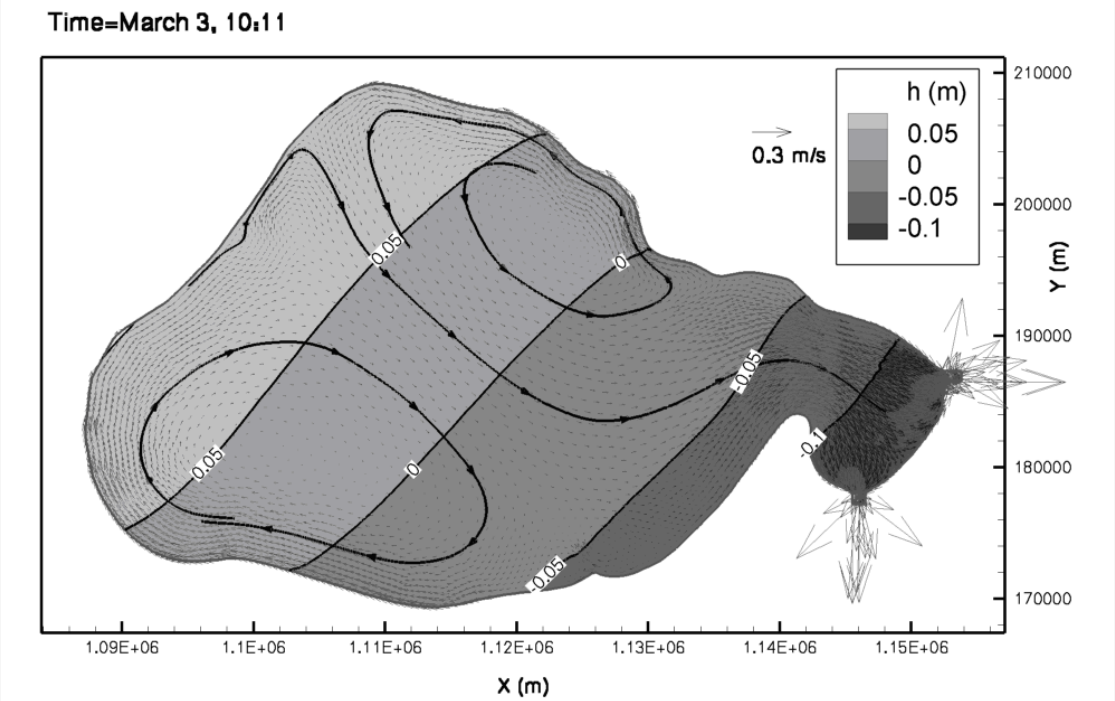

Figure 4.32 Hydrodynamics snapshot at 10:11, March 3rd with the tides and variable wind

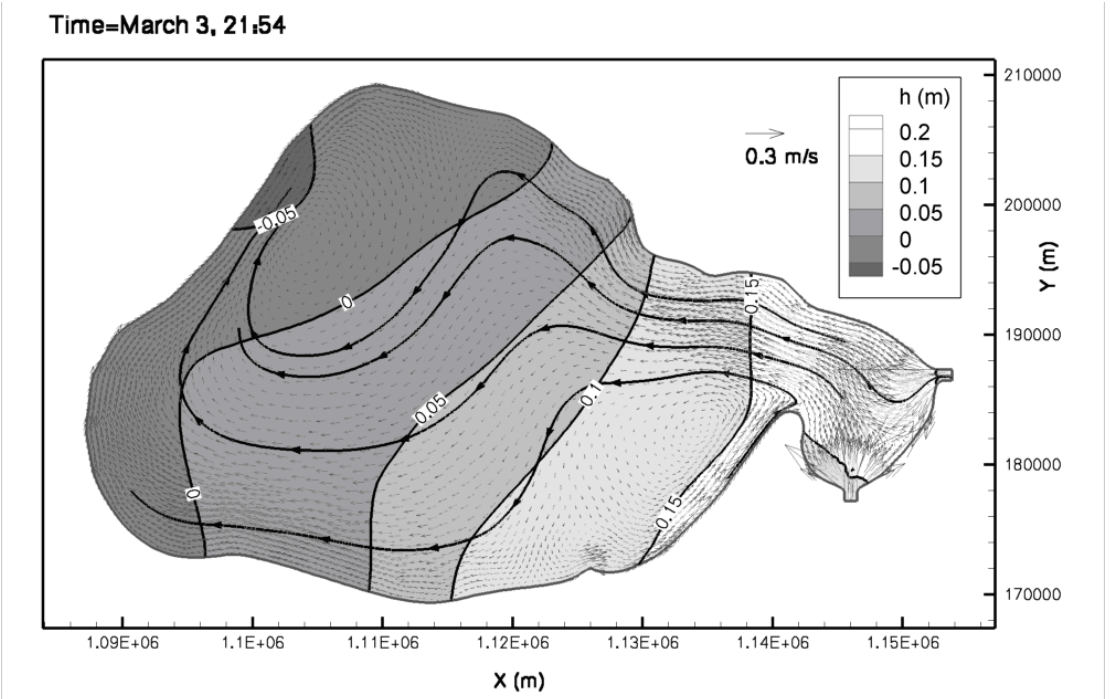

Figure 4.33 Hydrodynamics snapshot at 21:54, March 3rd with the tides and variable wind

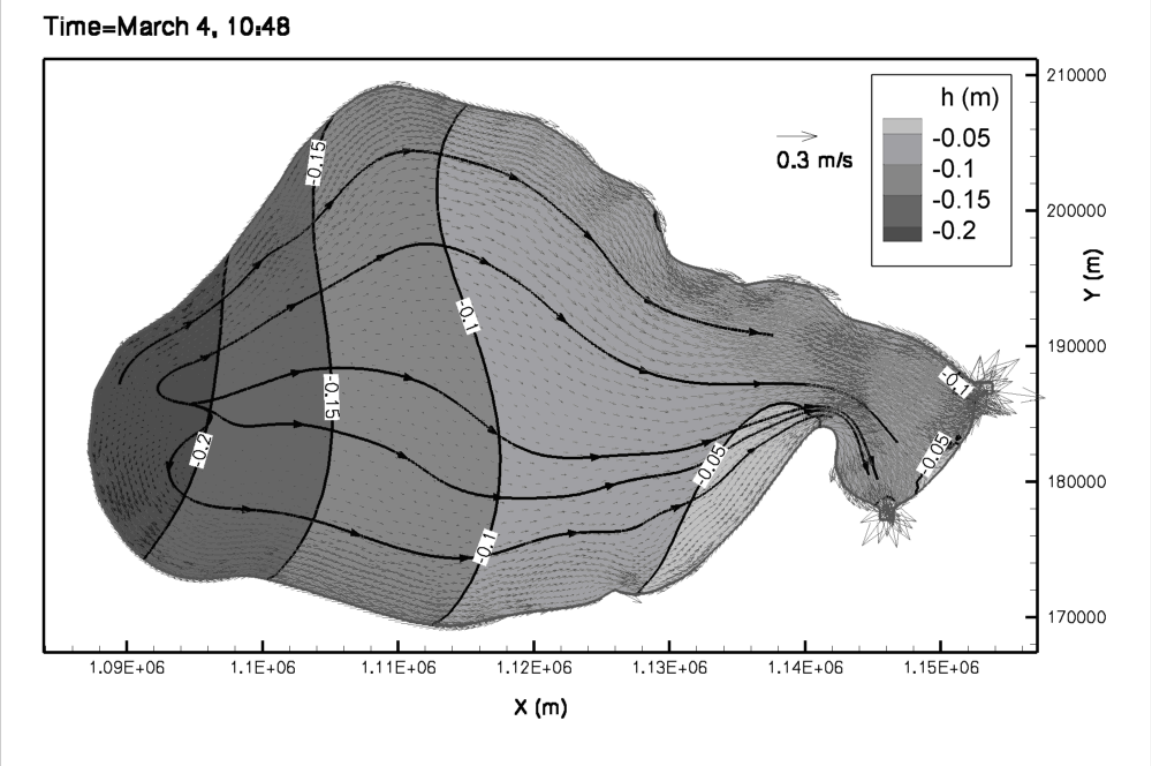

Figure 4.34 Hydrodynamics snapshot at 10:48, March 4th with the tides and variable wind

4.1.4.8. Summary

According to the numerical simulations with the various conditions, the wind was the major factor on the hydrodynamics as reported by other researches. Typically, the wind generates large circulations, water surface slope, and water level over Lake Pontchartrain. The water surface slope and water velocity mainly depended on the wind speed. The water velocity along the shore was higher than that at the center of the lake. When the wind speed was around 10 m/sec, the water velocity at the center was less than 10 cm/sec, and the water velocity along the shore was between 10 and 20 cm/sec generally. However, the tidal effect from the two channels on the east side of the lake affected the hydrodynamics over the eastern bulge of the lake, and changed the flow

pattern. The water velocity around the two channels was faster than that at the center of the lake. It increased more than 1 m/sec around the channels.

The numerical model predicted the trend of water surface fluctuation well, and the pattern of hydrodynamics was comparable to previous studies, even though it has some limitation to represent real cases due to limited boundary conditions.

4.2. Contaminant transport

4.2.1. Governing equation

Equation for contaminant transport can be derived in a similar way done for the hydrodynamics equations in the previous sections. The 3-dimensional form of contaminant transport equation without source/sink is given as:

$$\begin{aligned}&\frac{\partial c}{\partial t}+\frac{\partial (cu)}{\partial x}+\frac{\partial (cv)}{\partial y}+\frac{\partial (cw)}{\partial z}= \\ &\frac{\partial}{\partial x}\left(D_{xx}\frac{\partial c}{\partial x}\right)+\frac{\partial}{\partial x}\left(D_{xy}\frac{\partial c}{\partial y}\right)+\frac{\partial}{\partial x}\left(D_{xz}\frac{\partial c}{\partial z}\right) \\ &+\frac{\partial}{\partial y}\left(D_{yx}\frac{\partial c}{\partial x}\right)+\frac{\partial}{\partial y}\left(D_{yy}\frac{\partial c}{\partial y}\right)+\frac{\partial}{\partial y}\left(D_{yz}\frac{\partial c}{\partial z}\right) \\ &+\frac{\partial}{\partial z}\left(D_{zx}\frac{\partial c}{\partial x}\right)+\frac{\partial}{\partial z}\left(D_{zy}\frac{\partial c}{\partial y}\right)+\frac{\partial}{\partial z}\left(D_{zz}\frac{\partial c}{\partial z}\right)\end{aligned} \tag{4.28}$$

where D_{xx}, D_{xy}, D_{xz}, D_{yx}, D_{yy}, D_{yz}, D_{zx}, D_{zy}, and D_{zz} are dispersion coefficients. Equation (4.28) can be vertically integrated for shallow water in the same fashion done the hydrodynamics equations. The generic transport equation in shallow water for a non-reactive component is given as:

$$\frac{\partial(hC)}{\partial t}+\frac{\partial(hCU)}{\partial x}+\frac{\partial(hCV)}{\partial y}$$
$$=\frac{\partial}{\partial x}\left(D_{Hxx}h\frac{\partial C}{\partial x}\right)+\frac{\partial}{\partial x}\left(D_{Hxy}h\frac{\partial C}{\partial y}\right)+\frac{\partial}{\partial y}\left(D_{Hyx}h\frac{\partial C}{\partial x}\right)+\frac{\partial}{\partial y}\left(D_{Hyy}h\frac{\partial C}{\partial y}\right) \tag{4.29}$$

where C is the vertically averaged concentration and D_{Hxx}, D_{Hxy}, D_{Hyx}, and D_{Hyy} are horizontal dispersion coefficients. To simplify Eqn (4.29) further, the equation of water mass conservation, Eqn (4.8), can be substituted into Eqn (4.29). Then, Eqn (4.29) becomes:

$$\frac{\partial C}{\partial t}+hU\frac{\partial C}{\partial x}+hV\frac{\partial C}{\partial y}$$
$$=\frac{\partial}{\partial x}\left(D_{Hxs}h\frac{\partial C}{\partial x}\right)+\frac{\partial}{\partial x}\left(D_{Hxy}h\frac{\partial C}{\partial y}\right)+\frac{\partial}{\partial y}\left(D_{Hyx}h\frac{\partial C}{\partial x}\right)+\frac{\partial}{\partial y}\left(D_{Hyy}h\frac{\partial C}{\partial y}\right) \tag{4.30}$$

which is a non-conservative form of the contaminant transport equation in shallow water. Both forms are used in numerical simulation of contaminant transport often, and the first form was used for the simulation of this study.

In the surface water, the matrix of the dispersion coefficient is symmetric so that the longitudinal and transverse dispersion coefficients are used often instead of dispersion coefficient matrix, D_{Hxx}, D_{Hxy}, D_{Hyx}, and D_{Hyy}. The value of the dispersion coefficient depends on many physical factors such as the velocity of the flow, depth so on, and it is very hard to estimate an actual value. Many empirical equations for dispersion coefficients are suggested (Fischer, List*, et al.*, 1979) mainly for man-made or natural channels, but they cannot be applied for Lakes or wide two-dimensional domains directly. Typical range of dispersion coefficients are also compiled (Schnoor, 1996). For example

as shown in Table 4.1, the ranges of longitudinal and transverse dispersion in a large river are 10^0 to 10^2 and 10^{-4} to 10^{-3} m^2/s respectively.

Table 4.1 Typical range of dispersion coefficient (Schnoor, 1996)

Condition	Dispersion coefficient, m^2/s
Molecular diffusion	10^{-9}
Compacted sediment	10^{-11}~10^{-9}
Bioturbated sediment	10^{-9}~10^{-8}
Lakes – vertically	10^{-6}~10^{-3}
Large rivers – lateral	10^{-2}~10^{-1}
Large rivers – longitudinal	10^{0}~10^{2}
Estuaries – longitudinal	10^{2}~10^{3}

In a numerical study for contaminant transport, the dispersion coefficients are characteristic not only of the flow conditions to be simulated, but more significantly of how the process is modeled (Bowie, Mills*, et al.*, 1985). For example, the less detailed the flow field is modeled, the larger the dispersion coefficient of the model needs to be used for the spreading that would happen under actual circulation. Thus, the dispersion coefficients are actually model-dependent so that it is very hard to quantify in theoretical manner in general. In result, the best way to quantify the dispersion coefficients for a numerical model would be through the calibration started from estimation. However, concentration distribution in estuaries and streams are not sensitive to dispersion coefficients, and precise calibration usually is not critical (United States. Environmental Protection Agency. Office of Water., 1990).

Among many equations for dispersion coefficients, one set of expressions used for the dispersion coefficients in two-dimensional model was suggested as follows (Bowie, Mills, *et al.*, 1985):

$$
\begin{aligned}
D_{Hxx} &= \sqrt{\frac{\hat{f}}{8}(q_x^2 + q_y^2)}(5.9 - 5.7\sin^2\theta) \\
D_{Hxy} &= D_{Hyx} = 5.7\sqrt{\frac{\hat{f}}{8}(q_x^2 + q_y^2)}\sin\theta\cos\theta \\
D_{Hyy} &= \sqrt{\frac{\hat{f}}{8}(q_x^2 + q_y^2)}(5.9 - 5.7\cos^2\theta)
\end{aligned}
\tag{4.31}
$$

where

$$
\begin{aligned}
\theta &= \arctan(q_y / q_x) = \text{angle of flow} \\
q_x &= \text{flow in } x\text{-direction} \\
q_y &= \text{flow in } y\text{-direction} \\
\hat{f} &= \text{Darcy-Weisbach friction factor} \\
&= \frac{8gn^2}{R_H^{1/3}} \\
R_H &= \text{the hydraulic radius in units of meters,}
\end{aligned}
\tag{4.32}
$$

and this set of equations were used for the simulation with adjustment for calibration.

The contaminant interaction with sediment may be important for some contaminant such as hydrophobic components or bacteria, especially when a contaminant of interest is highly related to the sediment by deposition/re-suspension, but it is ignored in the simulation for the simplicity.

4.2.2. Implementation of the numerical model for contaminant transport

The numerical implementation of the contaminant transport was done by Taylor-Galerkin procedure, which is known to perform well for advection-dominated problems (Zienkiewicz and Taylor, 1989). Taylor-Galerkin method uses second-order expansion with respect to a time derivative term so that it achieves better results without too much increase of computational cost. In the study, the implicit Taylor-Galerkin method was adopted with the coefficient of implicity of 1/3, which is known to be optimal.

The contaminant transport equation is linear whereas those of hydrodynamics are nonlinear. Hence, the simulation of contaminant transport does not require iterations for nonlinear solutions. The linear solver is the same Krylov solver as used in hydrodynamics.

The velocity values for the advection terms were imported from the result of corresponding hydrodynamics simulation. The same mesh and the same time step size used for the hydrodynamics simulation were used in the contaminant transport model to avoid unnecessary interpolation of data. Hence, every time step of the contaminant transport read corresponding hydrodynamics simulation results: depths and velocities.

The source of a contaminant input was given as slug injection into an element. To reduce oscillation from sudden mass introduction, mass was injected over some time period.

4.2.3. Model verification

4.2.3.1. Slug injection

The contaminant transport model was tested with a slug injection case, which is a very similar case used for the optimization of this study. The analytical solution of slug injection of a tracer into a uniform flow with constant dispersion coefficients in two-

dimensional domain is available to compare (Fetter, 1999; Schnoor, 1996), and the solution is given as:

$$C(x,y,t) = \frac{M}{4\pi t\sqrt{D_L D_T}H}\exp\left[-\frac{((x-x_0)-v_x t)^2}{4D_L t} - \frac{(y-y_0)^2}{4D_T t}\right] \tag{4.33}$$

where

$$\begin{aligned} M &= \text{the mass of the injected tracer} \\ (x_0, y_0) &= \text{the coordinate of the injection} \\ D_L &= \text{the longitudinal dispersion coefficient} \\ D_T &= \text{the transverse dispersion coefficient} \end{aligned} \tag{4.34}$$

This solution is widely used to verify models in groundwater hydrology and contaminant transport.

A long rectangular domain was designed to simulate the slug injection test. Since the analytical solution is for a case that has a uniform flow with uniform depth, hydrodynamics conditions were adjusted accordingly. The depth and velocity was set as 1 m and 1 m/s respectively. The direction of the flow was from left to right of the domain. The longitudinal and lateral dispersion coefficients were set constant as 100 m^2/s and 1 m^2/s respectively. The contaminant was injected at (0, 0) of Cartesian coordinates, and the total mass was 1,000 kg. The size of the time step was 10 seconds. The results of the numerical simulation are presented in Figure 4.35. The analytical and numerical solutions were almost identical and not distinguishable, but the numerical solution shows small amount of oscillation at the tail of the plume.

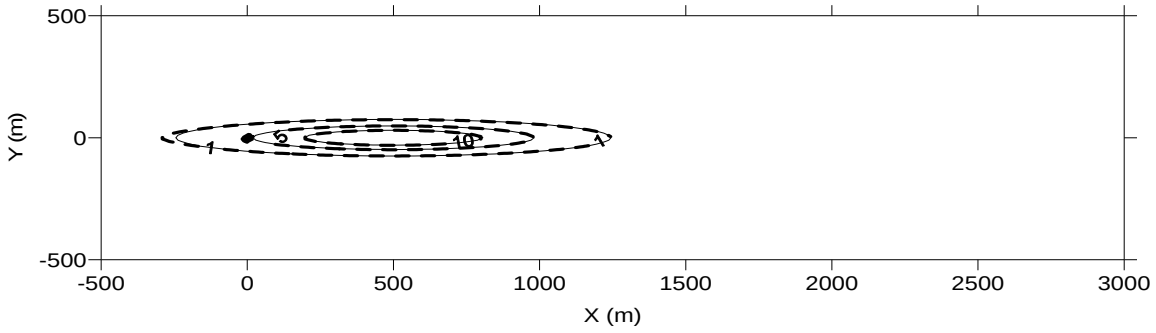

(a)

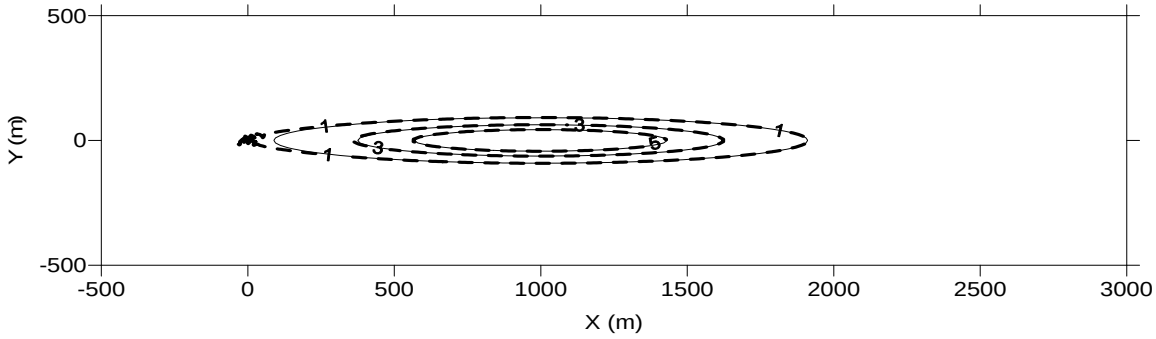

(b)

Figure 4.35. Comparison between analytical and numerical solutions of slug injection
(a) after 500 seconds, (b) after 1,000 seconds
(solid line: analytical, dashed line: numerical)

4.2.4. Contaminant transport in Lake Pontchartrain

The contaminant transport model was test with Lake Pontchartrain. For the simulation, the dispersion coefficients must be estimated first. A typical way to estimate dispersion coefficients for a model is adopting an empirical equation. Many empirical equations of horizontal dispersion coefficients for rivers were developed, but they are not directly applicable for lakes due to different physical processes of turbulence. The other way is experimental values that were measured directly at a domain of interest. Unfortunately, not many values of horizontal dispersion coefficients at Lake Pontchartrain are available. One set of the values was obtained from Jin *et al*. (2003) for

E. coli at the southwest part of Lake Pontchartrain, and the values are 0.85 and 0.88 m^2/s for *x* and *y* directions respectively. Based on these values, Eqns (4.31) were adjusted by multiplying by a constant number to obtain similar numbers at the area. Since observations of contaminant transport for calibration were not available, calibration on the parameters was not done. The size of the time step was 30 seconds.

4.2.4.1. Constant wind-only case

The contaminant was released in Lake Pontchartrain driven only by the 15 m/s wind from southeast, which was one of the hydrodynamics conditions in the previous section. Figure 4.1 shows an example of the change of contaminant concentration over time. The 1 ton of contaminant was injected over 1 hour period at the mouth of Tchefuncta river. Because the flow velocity was less than or around 15 cm/sec along the shore, and the dispersion coefficient was also small – the longitudinal dispersion coefficient was around 1 m^2/sec, – the contaminant did not travel far (relatively to the scale of the lake) from the source location. In this example, the contaminant plume traveled to the west from the source location in 12 hours. The flow developed along the shore of the lake, the contaminant was also transported along the shore. As shown in the figures, the contaminant only traveled into the lake when it met the circulation flow into the center of the lake. Since the limitation of the refinement in the mesh, some numerical oscillation was unavoidable, and the outline of the contaminant plume was not very smooth. However, the pattern and amount of the advection agreed with the hydrodynamics.

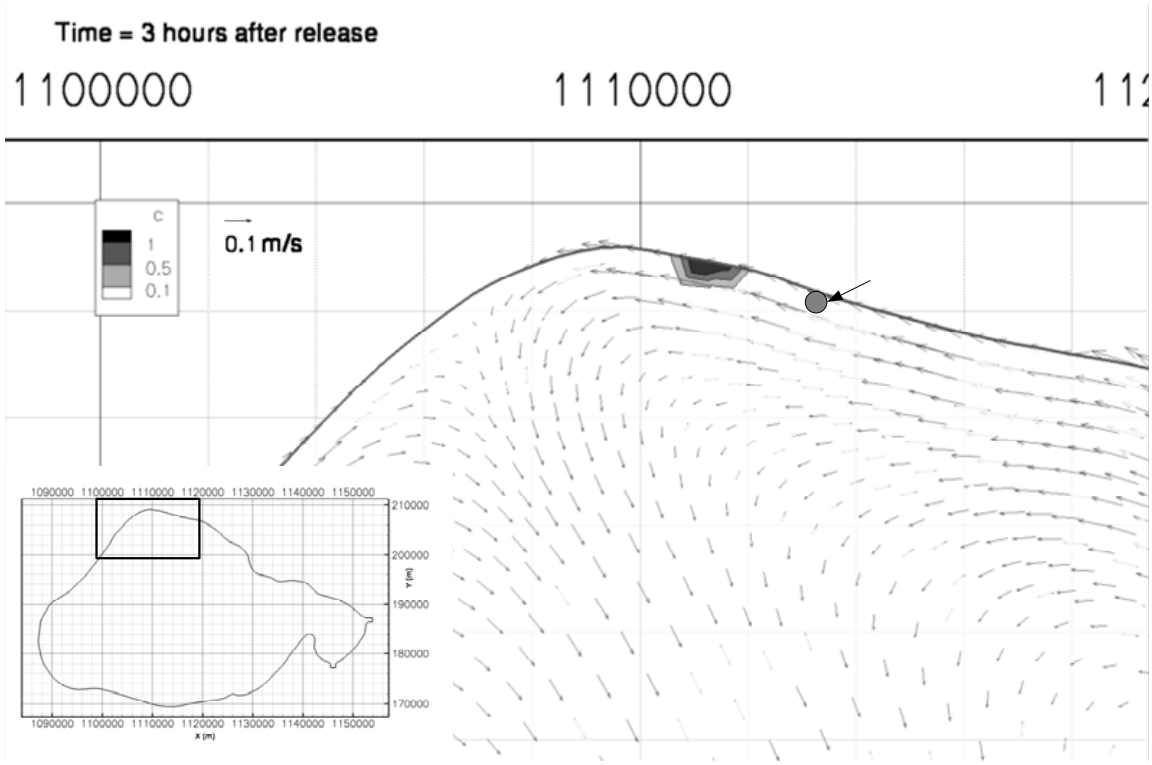
Time = 3 hours after release
1100000
1110000
C
1
0.5
0.1
0.1 m/s
1090000 1100000 1110000 1120000 1130000 1140000 1150000
210000
200000
190000
180000
170000
y (m)
x (m)

(a)

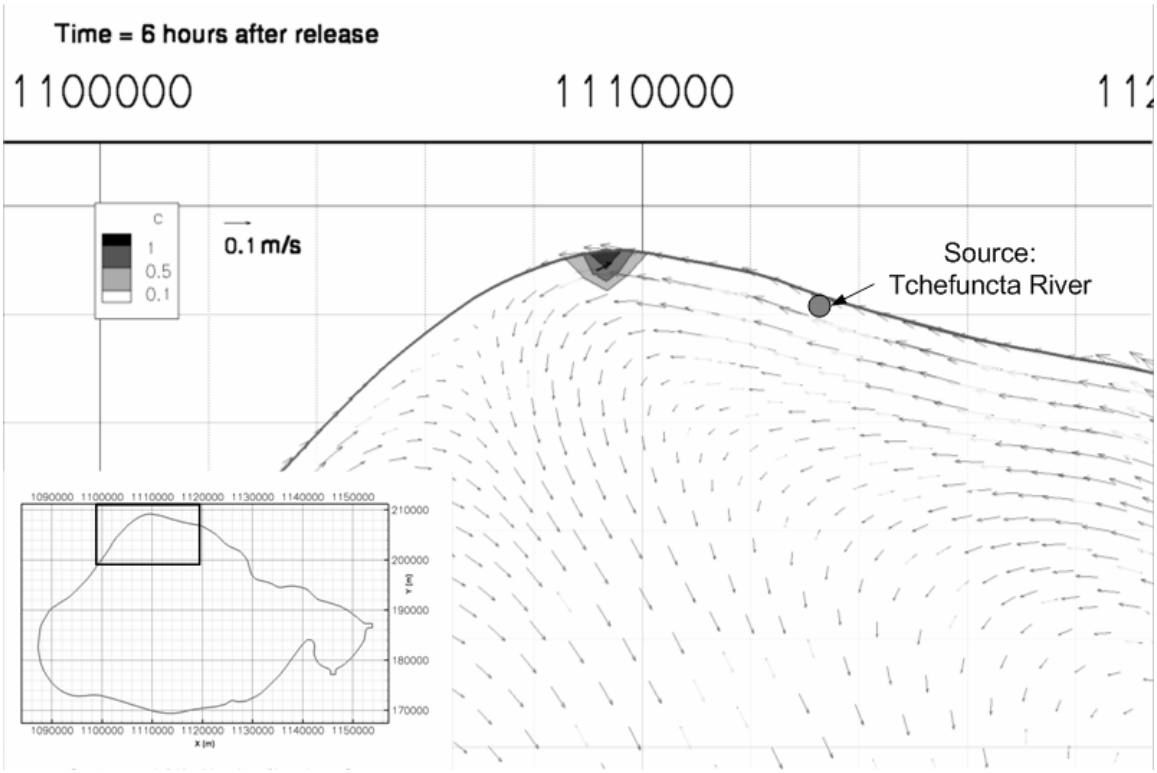
Time = 6 hours after release
1100000
1110000
C
1
0.5
0.1
0.1 m/s
Source:
Tchefuncta River
1090000 1100000 1110000 1120000 1130000 1140000 1150000
210000
200000
190000
180000
170000
y (m)
x (m)

(b)

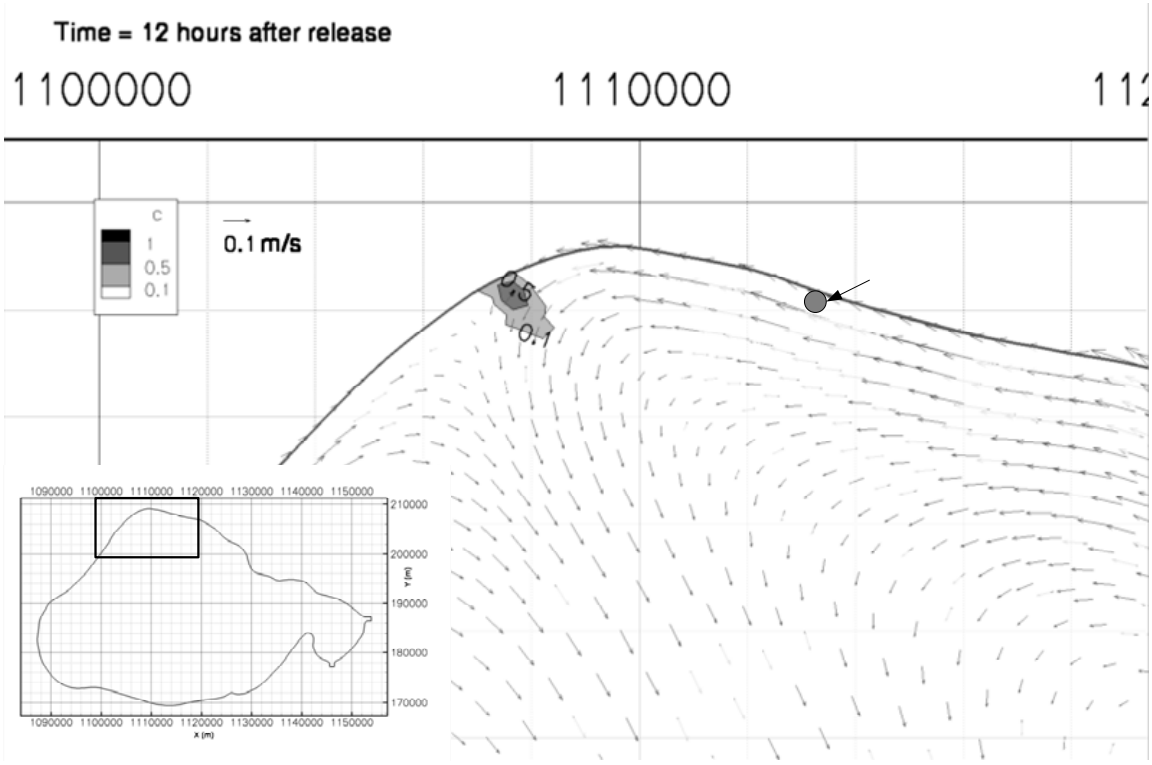

(c)

Figure 4.36 Contours of a contaminant concentration over time in Lake Pontchartrain driven by the wind
(a) 3 hours, (b) 6 hours, and (c) 12 hours after the spill at Tchefuncta River

4.2.4.2. Tide with real wind case

To see the effect of the tides and wind on the contaminant transport, a contaminant spill at Grand Lagoon, which is close to the tidal channels, was simulated under the combination of the predicted tides and observed wind as presented in the previous hydrodynamics sections. Unlike the case with the constant wind above, the hydrodynamics varied over time due to transient wind and tides. Hence, the time of a contaminant spill became a factor of a contaminant transport scenario even for the same location of spill. Figure 4.36 and Figure 4.37 show the two sets of series of concentration contours over time that were developed differently by two spill sceanrios with different spill times but at the same spill location. As it can be noticed, the contaminant in the

former case traveled into the lake as in Figure 4.36, but it in the latter case traveled to the tide channel, the Rigolets, as in Figure 4.37 because the former one was released at a flood tide period and the latter one was released at a ebb tide period.

The flow speed around the spill location varied from less than 10 cm/sec to more than 50 cm/sec due to the effect of the tides. In result, the contaminant traveled farther from the spill location and dispersed more than it did in the wind-only case. In some of the ebb tide cases, the contaminant exited out of the lake through the channels. If a contaminant did not reach to the channel, it moved back and forth around a spill location and dispersed away.

4.2.4.3. Summary

The contaminant transports in Lake Pontchartrain with constant wind and the combination of tides and wind were simulated. As expected from the circulation from the hydrodynamics in the previous sections, if a contaminant was released on the shore, it traveled and dispersed along the shore generally. If a spill occurred at a place under a strong tidal influence, a contaminant released on the shore moved back and forth according to the tidal conditions. In some cases, the contaminant exited out of the lake through the tidal channels. Due to the relatively large size of the lake, a spill could not travel far from a spill location in the time scale of a day, and it eventually dispersed away.

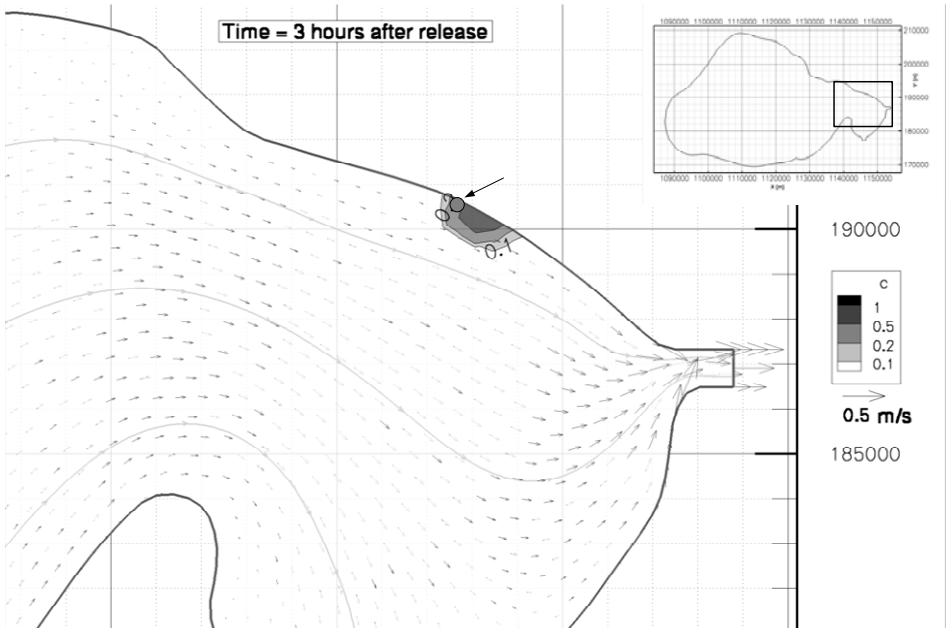
Time = 3 hours after release
0.5
0.1
190000
C
1
0.5
0.2
0.1
0.5 m/s
185000

(a)

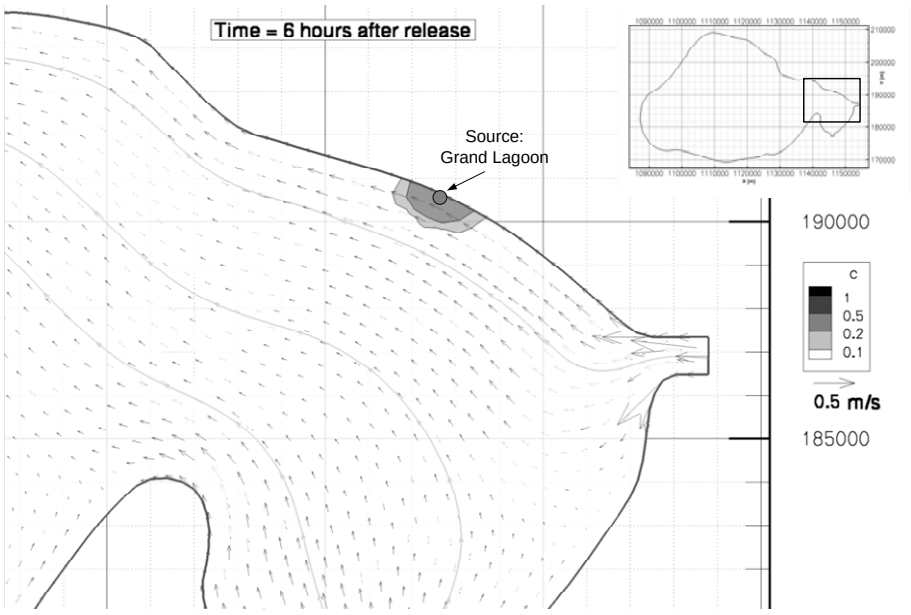
Time = 6 hours after release
Source:
Grand Lagoon
190000
C
1
0.5
0.2
0.1
0.5 m/s
185000

(b)

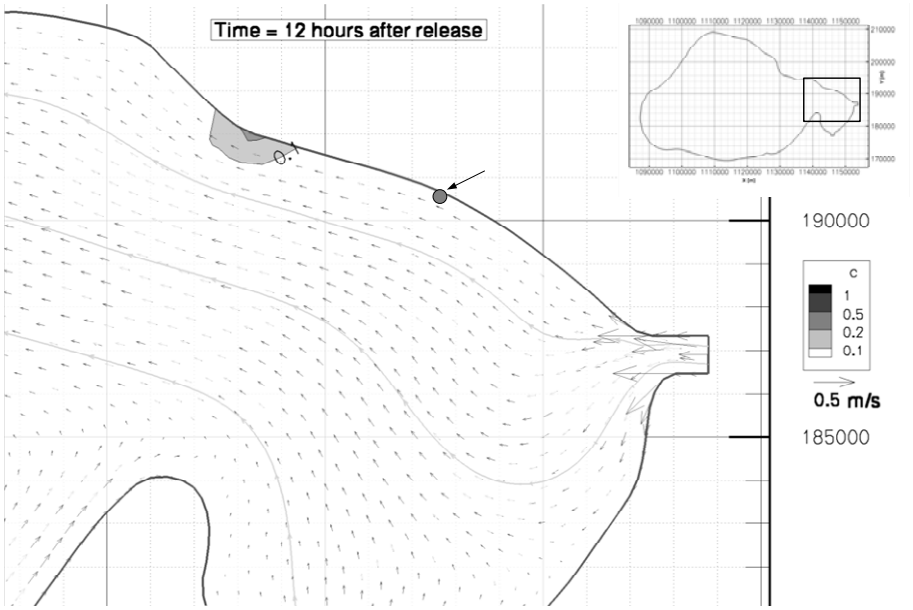

(c)

Figure 4.37 Contours of contaminant concentration over time in Lake Pontchartrain under tide and wind effects, released at 12:00, March 3rd
(a) 3 hours, (b) 6 hours, and (c) 12 hours after the spill at Grand Lagoon

(a)

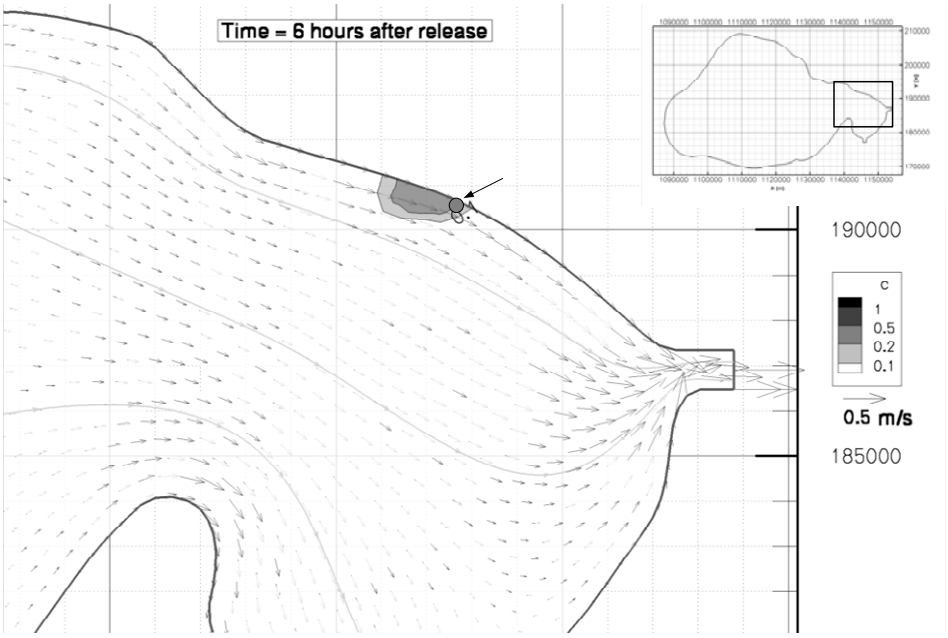

(b)

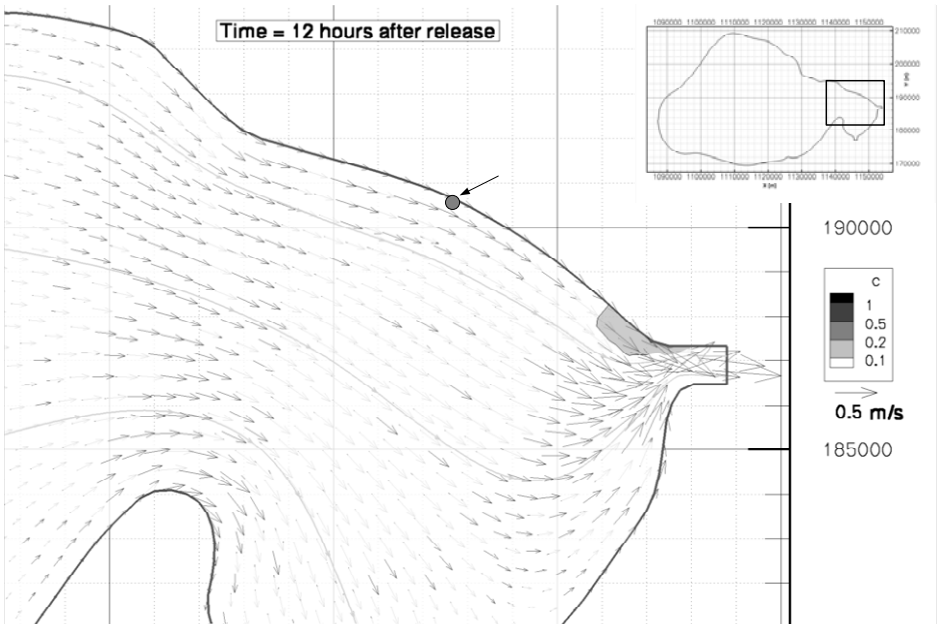

(c)

Figure 4.38 Contours of contaminant concentration over time in Lake Pontchartrain under tide and wind effects, released at 21:00, March 3rd
(a) 3 hours, (b) 6 hours, and (c) 12 hours after the spill at Grand Lagoon

CHAPTER 5

Optimal Design of Stationary Monitoring Locations

The first and traditional water quality monitoring system is based on sampling or stationary (immobile) water quality monitoring stations as described in Chapter 3. One of the most important factors in the design of water quality monitoring locations is its spatial distribution. In this chapter, the genetic algorithm and its implementation for the solution of the optimization problem for finding the locations of stationary monitoring systems.

5.1. Introduction on the genetic algorithms

The origin of the idea of genetic algorithms (GAs) is dated back to 1950 and 60s (Sarker, Mohammadian*, et al.*, 2002), and it was common among biologists in 60s and 70s (Fraser and Burnell, 1970). However, the idea of population in the genetic algorithms was introduced later (Schwefel, 1981), the computational genetic algorithm became well-known through Holland (1975), and current framework of GAs were established later. GAs started being widely adopted in 1980s in various fields because of the increase in computational power Hence, GAs are relatively new optimization techniques, and many improvement and modifications are still being made on this subject.

GAs are heuristic search techniques based on the mechanics of natural selection, sometimes called Darwinian evolution, which combines survival of the fittest with genetic operations. The GAs are different from other traditional optimization and search methods: (i) GAs work with a coding of parameter sets; (ii) GAs search from a population of points, not a single point; (iii) GAs use payoff (objective function) information, not derivatives or other auxiliary knowledge; and, (iv) GAs use probabilistic

transition rules, not deterministic rules (Goldberg, 1989). In result, GAs are simple but yet robust irrespective of the problem analyzed. Also, GAs do not require linearity, continuity, and gradient information based on the mathematical description of a problem. Thus they have become powerful algorithms for the optimization of complex nonlinear problems.

GAs have been widely used in various fields such as: machine learning, optimal control and general search problems in business. GAs are also adapted in the water resource management including surface water and groundwater optimization problems.

Assuming that a single-objective optimization problem that has only one objective value is described as:

$$\max \text{ (or min) } f(\mathbf{x}) \tag{5.1}$$

$$\mathbf{x} \in \Omega \tag{5.2}$$

where $\mathbf{x}$ is a vector with n unknown decision variables, which may be continuous or discrete variables, Ω is a solution space or domain, and $f(\mathbf{x})$ is a map from solution domain to a set of real number. The function $f(\mathbf{x})$ is often called as an objective function. The purpose of optimization is to search a solution $\mathbf{x}^* \in \Omega$ which maximizes or maximize the objective function.

The idea of GAs for searching the optimal solution of the optimization problem is very straightforward. As inspired by evolutionary processes, a group of candidate solutions, called a population, undergo through environmental pressures to drive candidate solutions (populations in GAs) to an optimized status. Each individual in a population corresponds to a solution in the solution space.

The initial population is generated first, which are done often randomly. In many cases, a candidate solution, called as an individual or a building block, is encoded as a binary string, as a biological chromosome consists of four kinds of DNAs (Deoxyribonucleic acids). Starting with the initial population, three operations, selection, crossover, and mutation are applied to generate an improved new generation. The general procedure of GAs is presented in Figure 5.1.

Generate the initial population $P(0)$ at random

Loop

Evaluate the fitness of each individual in $P(i)$

Select two parents from $P(i)$

Crossover and mutate the parents

Generate the next generation $P(i+1)$

Until the population converges or the maximum generation is reached

Figure 5.1 A general framework of genetic algorithms

5.2. Multi-objective optimization

Even though some real-world problems can be reduced to a single objective, it is often very hard to define many aspects of complex problems into a single objective. Also, defining multiple objectives gives a better idea of a problem, and multiple optimal solutions of multiple objectives may provide more information on relationship among different objectives. In result, decision makers can obtain better information without bias that may be involved in the reduction procedure to a single objective problem from a multi-objective one.

A general multi-objective optimization problem can be written in the form: minimize $[f_1(\mathbf{x}), f_2(\mathbf{x}),\ldots, f_n(\mathbf{x})]$ for k objective functions, $f_i : \mathbb{R}^n \to \mathbb{R}$ for $\mathbf{x} = [x_i, x_2,\ldots, x_n]$ subject to several equality and inequality constraints. The optimization is to determine the set F of all vectors which satisfy all the constraints and also yields the optimum values for all the objective functions.

A candidate solution could be better, worse or indifferent to another solutions with respect to the objective values. A better solution to another means a solution that is not worse in any of given objectives and at least better in one objective than another solution. This is expressed as 'a better solution dominates a worse solution' descriptively. Hence, the best solutions must not be dominated any other solutions, which means that the best solutions are not worse in any of objectives and at least better in one objective than any other candidate solutions. Such a solution is called Pareto-optimal, and the entire set of such optimal solutions is called a Pareto-optimal set. The mathematical definition of a Pareto solution for a minimization problem can be given as: A solution $\mathbf{x}^*$ is called a Pareto solution if and only if there is no other solution $\mathbf{x}$ such that $f_k(\mathbf{x}) \leq f_k(\mathbf{x}^*)$ for all k, where $f_k(\mathbf{x})$ is the k^{th} objective of solution $\mathbf{x}$. The concept of Pareto-optima with two objectives is shown in Figure 5.2 for example. What an optimization procedure does is to find the approximation of a Pareto-set as closely as to a true global Pareto set. In many cases, a Pareto-set contains multiple optimal solutions, and one or a few solutions among Pareto optimal solutions needs to be picked by decision makers for the final choice if necessary.

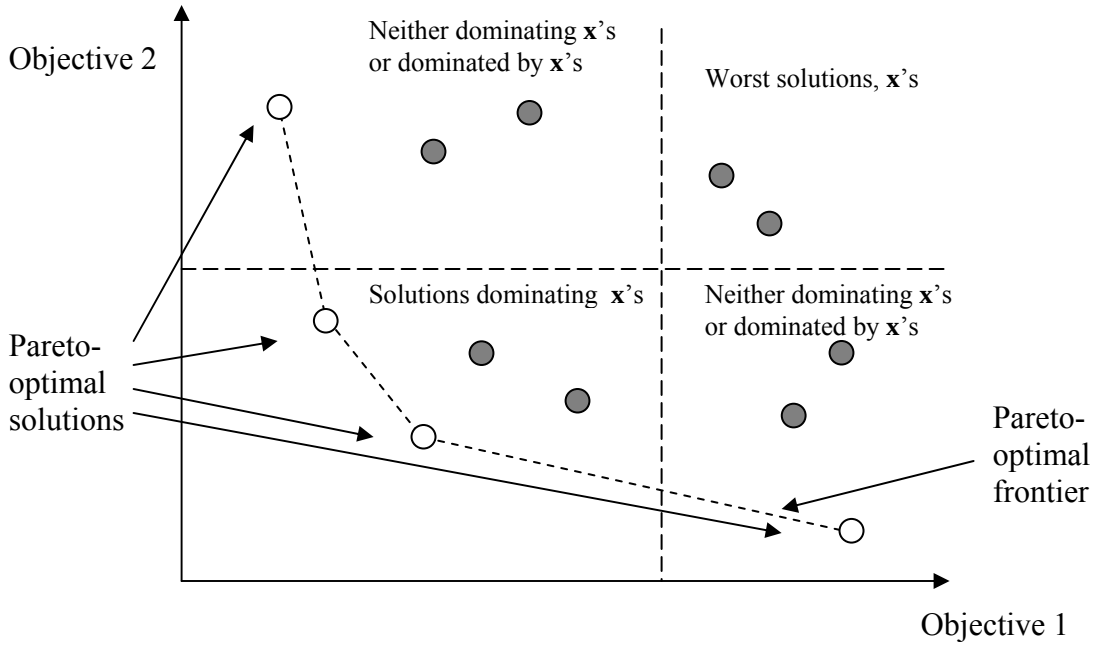

Figure 5.2 Concept of Pareto optimality for a problem minimizing two objectives

5.2.1. Multi-objective optimization with genetic algorithms

There are many multi-objective optimization techniques including stochastic methods such as simulated annealing, tabu search, ant colony optimization, and so on, which could be used to generate an approximation set of Pareto-optimal. Genetic algorithms also can solve multi-objective optimization problems well and are being studied widely.

GAs for multi-objective optimizations are often called multi-objective evolutionary algorithms (MOEA), and they are dated back to the mid-1980s (Schaffer, 1985). Because GAs use a population, GAs for multi-objective optimizations can find several members of the Pareto-optimal set in a single run instead of performing a series of separate runs, which is the case for some of the conventional stochastic processes

(Abraham, Jain, *et al.*, 2005). In addition, GAs for multi-objective optimizations also keep well-known properties of single-objective GAs such as avoiding local minima successfully.

Several genetic algorithms for multi-objective problems were proposed such as non-dominated sorting genetic algorithm page 117, niched-Pareto genetic algorithm (NPGA), strength Pareto evolutionary algorithm (SPEA) and so on. Among them, non-dominated sorting genetic algorithm–II (NSGA-II) is one of widely-used algorithms now. Initially, Non-dominated Sorting Genetic Algorithm (NSGA) was proposed by Srinivas and Deb (1994). In this approach, a population is ranked on the basis of non-domination, and the ranks are used as the fitness for the selection. The original NSGA was revised and called NSGA-II (Deb, Pratap, *et al.*, 2002), which is computationally more efficient and uses elitism and a crowded comparison operation that keeps diversity. The pseudo-code of NSGA-II is presented in Figure 5.3, and the concept of crowding distance for two-objective optimization is shown in Figure 5.4.

In the selection operation in NGSA-II, individuals in the best ranks are selected for mating. If individuals that are compared have the same rank, then the selection operation compares the crowding distances of individuals. For example in Figure 5.4, the crowding distance of individual i and j are the summations of the widths and heights of the cuboid constructed by individual i-1 and i+1, and j-1 and j+1 respectively. Since individual i and j are at the same rank, when two are compared for selection, individual j is selected due to its larger crowding distance. This way, NSGA-II obtains a well-spread Pareto optimal frontier, which is desirable.

```
for each p ∈ P
    S_p = ∅
    n_p = 0
    for each q ∈ P
        if (p ≺ q) then                 if p dominates q then
            S_p = S_p ∪ {q}             include q in S_p
        else if (q ≺ p) then            if p is dominated by q then
            n_p = n_p + 1               increment n_p
    if n_p = 0 then                     if no solution dominates p then
        p_rank = 1                      p is a member of the first front
        F_1 = F_1 ∪ {p}
i = 1
while F_i ≠ ∅
    H = ∅
    for each p ∈ F_i                    for each member p in F_i
        for each q ∈ S_p                modify each member from the set S_p
            n_q = n_q − 1               decrement n_q by one
            if n_q = 0 then             if n_q is zero, q is a member of a list H
                q_rank = i + 1
                H = H ∪ {q}             current front is formed with all member of H
    i = i + 1
    F_i = H

        where

            P = the population
            n_p = domination count
            S_p = a set of solution that the solution p dominates
            F_i = the population with rank i
            H = newly identified front
            ≺= domination comparison operator
```

(a)

$l = |I|$ number of solutions in I

for each i, set $I[i]_{\text{distance}} = 0$ initialize distance

for each objective m

$I = sort(I, m)$ sort using each objective value

$I[1]_{\text{distance}} = I[l]_{\text{distance}} = \infty$ so that boundary points are always selected

for $i = 2$ to $(l-1)$ for all other points

$$I[i]_{\text{distance}} = I[i]_{\text{distance}} + (I[i+1].m - I[i-1].m) / (f_m^{\max} - f_m^{\min})$$

where

$I[i]_{\text{distance}}$ = crowding-distance of the i-th indiviual in the set I

$I[i].m$ = m-th objective function value of the i-th individual in the set I

$f_m^{\max}$ and $f_m^{\min}$ = the maximum and minimum values of mth objective function

(b)

Figure 5.3 Pseudo-code of NSGA-II (Deb, Pratap, *et al.*, 2002)
(a) fast-non-dominated sort, and (b) crowding-distance-assignment

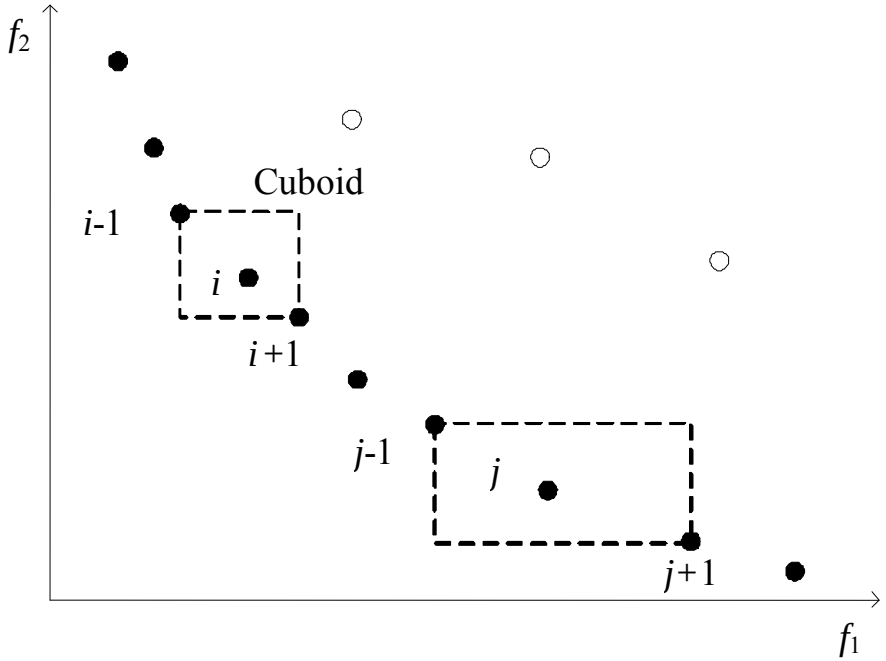

Figure 5.4 Comparison by the crowding-distance for two-objective optimization
(The black dots are on the Pareto frontier, i.e. with the best rank.)

5.3. Optimal model for a monitoring locations

5.3.1. Implementation of the genetic algorithm for monitoring locations

The first step of an optimization is to set up objective functions and constraints in mathematical forms. Because the main goal of the monitoring program in this study is for an early warning system, the selected main objectives of a monitoring network of stationary monitoring locations are: (1) detecting a contaminant in a water body as soon as possible in order to minimize the area affected by contamination till detection and to secure ample amount of time for appropriate response, and (2) maximizing detection likelihood, or reliability. In other words, the two objectives are stated as detecting as many contaminations as possible within the shortest time. The optimization problem with the given two objectives can be mathematically stated as:

$$\min f_1 = \frac{1}{W}\sum_{s=1}^{N_s} w_s t_{d,s}(X) \tag{5.3}$$

$$\max f_2 = \frac{1}{W}\sum_{s=1}^{N_s} w_s \delta_s(X) \tag{5.4}$$

such that

$$\begin{aligned} &X = \{x_1, \ldots, x_i, \ldots, x_N\},\ 0 < x_i \le x_{\max} \\ &n(X) = N \end{aligned} \tag{5.5}$$

where

X = the set of monitoring locations in nodal indices
x_i = a nodal index representing coordinate of a monitoring location
$x_{\max}$ = the maximum nodal index number
N = the number of monitoring locations
$t_{d,s}$ = the time elapsed from the time of a contaminant release
to the time of detection for a scenario s, if detected
otherwise, a penalty value (5.6)
δ_s = the detection flag of a scenario s
0 if not detect, 1 if detected
w_s = the weight of scenario s
$W = \sum_{s=1}^{N_s} w_s$ = the sum of weights of all scenarios
N_s = the number of scenarios.

Eqn (5.3) represents the weighted estimation of detection time, and Eqn (5.4) represents the weighted estimation of detection likelihood for a set of assumed scenarios. The range of the detection likelihood value, the value of the Eqn (5.4) is between zero and one. The detection time of a scenario s, $t_{d,s}$, is calculated by subtracting the simulation time when a contaminant is released from the earliest simulation time when the contaminant is detected at one of the monitoring locations. A contaminant is detected when the concentration of a contaminant at a candidate monitoring location reaches over a given concentration threshold of detection. However, not every scenario may be detected by a candidate monitoring network within a given detection time limit in which a monitoring system should detect a contaminant. For example, when a monitoring network is designed to detect contamination within 2 hours since a spill accident, the detection of water quality change after 4 hours of a spill may be considered as failure and as non-detected case. In such cases, the calculation of the estimation of detection time may be problematic because the detection time cannot be defined. To resolve this issue,

two options can be considered: The first one is to ignore non-detected cases in the estimation of detection time. The second one is to adopt a penalty value instead for the detection time of a non-detected case. The problem of using the former one in the optimization is that the optimization may obtain numerous practically-useless solutions that have very low estimations of detection time but very low detection likelihood at the same time by ignoring non-detected scenarios. The latter one gets rid of such meaningless solutions out of an optimal solution set by adding a fictitious penalty detection time for a non-detected case. In results, the number of optimal solutions will be reduced, and this narrows down the choices for the decision makers at the end. The final optimal solutions will consist only of solutions with high detection likelihood, which is necessary attribute for an early warning system. Hence, the method with the penalty value is selected to manage non-detected cases.

The decision variable X is a set of nodal indices of candidate monitoring locations in a discretized mesh instead of a set of coordinates of candidate monitoring locations. Using x- and y-coordinates for monitoring locations is straightforward, but it can be computationally expensive because this approach may require interpolation of values from the result of numerical simulations. An interpolation procedure must read the data from numerical simulations every time it is done. The amount of data from numerical simulations is vast in most of the cases, and eventually the computation burden to handle the data overwhelms the whole optimization procedure. An alternative approach that avoids such an interpolation is using nodal or grid values from numerical simulations directly without interpolation. The results of a numerical simulation are given as values on every node or point in a discretized mesh or grid. Hence, if candidate monitoring

locations are placed only on nodes or grid points in a mesh or a grid, interpolation is not necessary, and the values at nodes or grid points can be used directly for the optimization. Then, the earliest detection or arrival times – when the concentration reaches to detection threshold – at every node in a mesh for a numerical simulation can be calculated based on a given detection threshold in advance of a optimization procedure. The amount of these pre-calculated data of possible detection times at every node is much smaller than the whole results of numerical simulations. Furthermore, this set of possible detection times can be used in the optimization without any arithmetic. Because the heuristic optimizations typically involve many evaluation steps that calculate the quality of candidate solutions, such reduction of computational burden is crucial for heuristic optimization methods such as genetic algorithms

After the preliminary step, the optimization routine becomes an integer programming to find the best integer combination, which is similar to the well-known knapsack problem – the maximization problem of the best choice that can fit into one bag to be carried. The knapsack problem is a combinatorial optimization of NP (non-deterministic polynomial time) - hard class in terms of computational complexity theory, which means that we do not know any other exact solution techniques that can solve the problem in polynomial time other than a complete enumeration (in the worst case) of the solution space (Garey and Johnson, 1979). There are some techniques to save computations such as branch-and-bound, dynamic programming, and state space relaxation, but they are not very suitable to find global optima in large problems. Genetic algorithms also have shown to be very well suited for solving knapsack problems, so that it was chosen as the method of this study. As stated in the previous sections, GAs are

adaptable for multiobjective problems as well and flexible, which is the other reason why GAs are chosen. Since the problem is multi-objective, NSGA-II, which was introduced in the previous section, was adopted.

The GAs were implemented using a C++ library, PARADISEO (Cahon, Melab*, et al.*, 2004), which provides the backbones of GAs such as traditional crossover, mutation, selection, replacement strategies. However, most of GA routines in the optimization of this study were newly written or modified in order to meet the requirement of the problem. The code and the library were written and compiled by G++ on RedHat Linux platform with Intel-family CPUs.

As mentioned above, a candidate solution contains nodal indices which are integer numbers. In the GAs, a candidate solution should be converted into a genetic form which can go through genetic operations. The converted form of a candidate solution is called an individual, building block, or chromosome. The traditional way of genetic conversion of candidate solutions is to use a binary string, which is a series of zeros and ones. This idea is based on the biological genetics that are coded in only 4 kinds of DNA (Deoxyribonucleic acid). However, to convert integer or real values into a binary string back and forth is cumbersome and often unnecessary. Hence, integer values are directly used as genes in a chromosome in this study. An example of genetic expression using nodal indices instead of coordinates is graphically presented in Figure 5.5.

The sequence of genes in a chromosome is not important because the problem is a combinatorial problem. Since a gene in a chromosome represents a location of water quality monitoring location, it does not need to be repetitive. To prevent genes from

repeating, a post-processing may be necessary after genetic operations. They will be discussed in the genetic operation section as follows.

Finally, individuals construct a population, and the genetic algorithm will put evolutionary pressure on the population through genetic operations in order to obtain optimal solutions.

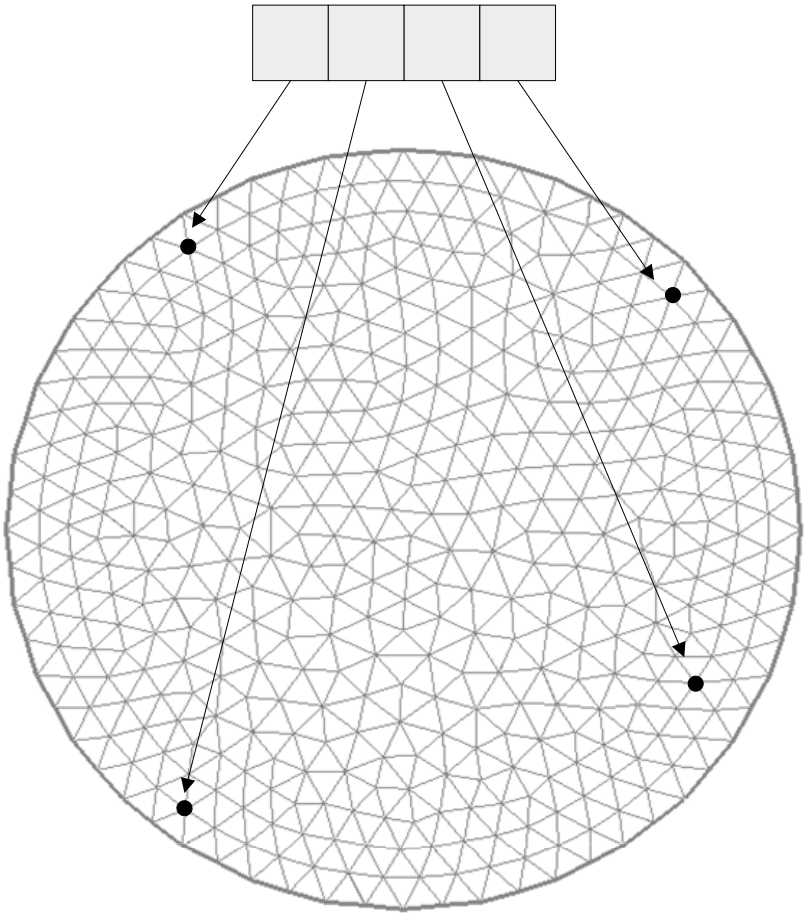

Figure 5.5 Example of genetic expression of a fixed location

5.3.2. Genetic operations for the monitoring locations

The genetic algorithms involve four key operations: selection, crossover, mutation, and replacement. These steps make a population to evolve to global optima as if it happens in the nature.

For selection mechanism, stochastic tournament selection was chosen for this study. Stochastic tournament allows inferior solutions can be selected by some probability. The idea behind the stochastic tournament is adjusting selection pressure so that it prevents a population from premature converging to sub-optimal solutions. By adjusting the rate of the stochastic tournament selection, it can be a deterministic tournament selection as well. The rate of selecting an inferior solution over a superior solution is usually kept very small.

One-point crossover was selected for the crossover operation to exchange information between two individuals. A single point (or often called locus) crossover was selected, and all the data beyond this crossover point in either chromosome are exchanged. The crossover operation can generate infeasible individuals that have multiple identical genes in one individual. There are several ways to handle infeasible individuals generated by genetic operations in the GAs. Infeasible individuals can be completely rejected, repaired, or penalized. For the optimization of monitoring locations, repairing was adopted. Repairing is commonly used combinatorial optimization problems since it is easy to repair an infeasible solution of the integer combinations (Sarker, Mohammadian*, et al.*, 2002). Repairing procedure depends on problems so that it must be designed according to a specific problem. If an individual has infeasible genes, which are

repeated genes in this case, then a repeated gene was slightly mutated not to be repeated. An example of the crossover operation and repairing is shown in Figure 5.6.

A random uniform mutation that picks a random integer number uniformly within a certain mutation range from a current value was selected for the mutation operation. The mutation procedure was designed not to generate repeated or out-of-range genes. Examples of the mutation and repairing procedure are shown in Figure 5.6.

For the replacement strategy to make a new generation from parents and offspring, a modified $\mu + \lambda$ replacement strategies was adopted. The replacement strategy, $\mu + \lambda$ replacement, is a pseudo-elitist strategy, which is generally the part of NSGA-II algorithm. It takes into account both the parent and the offspring population and selects the best μ individuals out of $\mu + \lambda$ candidates as the parents of the next generation (Abraham, Jain*, et al.*, 2005). Since the optimization model of this study is a multi-objective problem, optimal solutions from the algorithm usually do not converge to one optimal solution but form a Pareto-frontier as presented in Figure 5.2. However, if a penalty value is used, a population may converge into a single solution instead of a set of optimal solutions. This may cause a premature convergence easily. To prevent this adverse effect and to increase the diversity of a population, identical individuals to some of parents in offspring are kicked out by mutation operations. This will prevent the algorithm from falling into a premature local optimum.

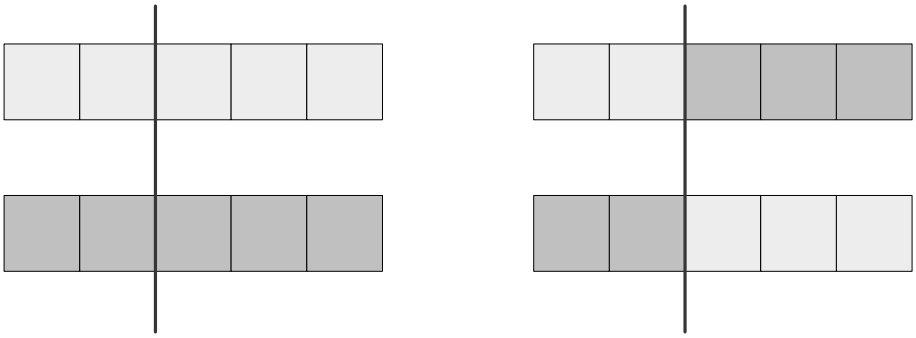

(a)

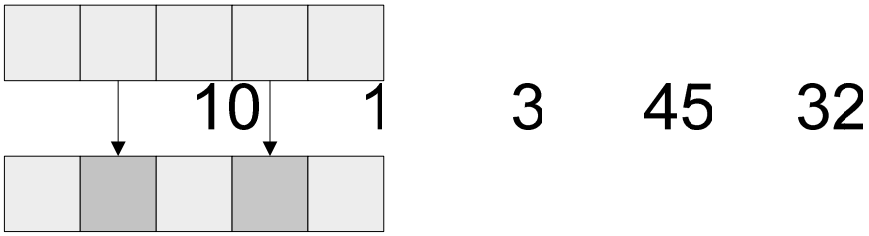

(b)

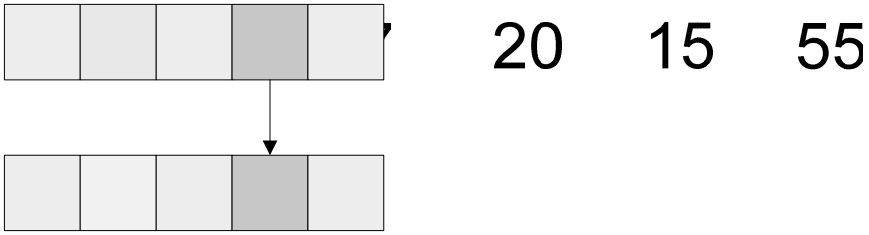

(c)

Figure 5.6 Examples of crossover, mutations and repairing operation for monitoring locations
(a) One-point crossover, (b) Mutation, and (c) Repairing

10 1

5.3.3. Evaluation of fitness for a combination of monitoring locations

The evaluation procedure is basically the arithmetic averaging procedure of detection times and detection likelihood for all possible scenarios as in Eqn (5.3) and (5.4). Figure 5.7 shows the flow of the evaluation process.

A preliminary step of the evaluation is to calculate the earliest arrival times or possible earliest detection time for all nodes in a mesh as described in 5.3.1. Since the configuration of monitoring locations will not affect the contaminant transport or earliest arrival time neither, and since it is assumed that the candidate monitoring locations are nodes in a mesh, it is possible to calculate the earliest arrival times at all nodes before the optimization procedure. Once all the earliest arrival times are calculated and stored, they can be used repeatedly for the evaluations. The amount data of all the concentration snapshots of every time step of every scenario is huge, and they cannot be handled efficiently in the optimization directly. Hence, this preliminary step is essential.

The evaluation routine for the first objective compares the earliest arrival times at all monitoring locations of an individual and picks the minimum one as a detection time of a scenario. If a given combination of monitoring locations cannot detect a contamination within a given detection time limit, it is regarded as a failure and a penalty value is assigned to the detection time. Then, the average of all the detection times for all scenarios is taken. In the averaging process, weights on scenarios are taken into account.

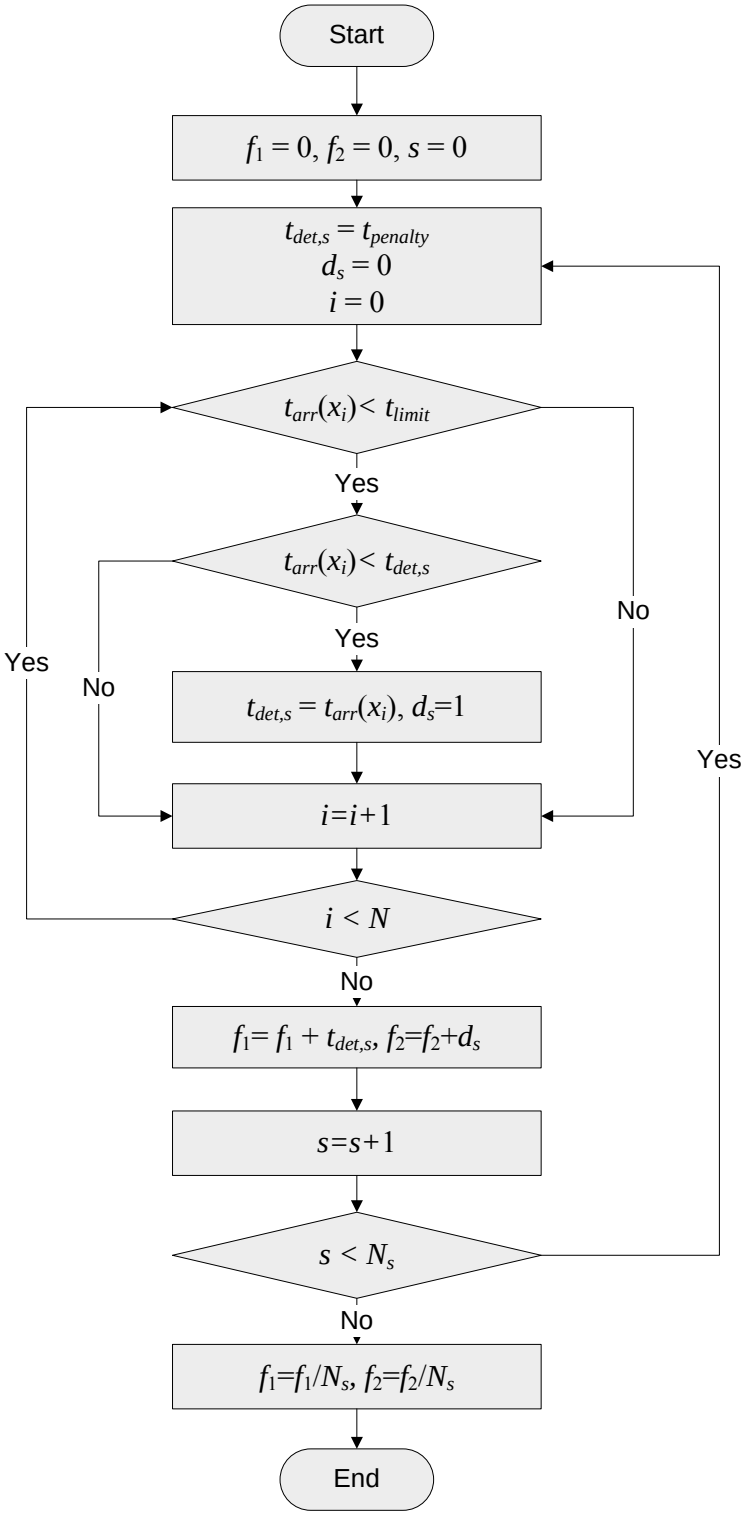

Figure 5.7 Flowchart of Evaluation of fitness for a combination of monitoring locations

Also, the number of failure is counted while calculating the detection time. The number of failure can be converted into a detection rate, which represents the estimation of detection likelihood or reliability. The flowchart of the procedure is presented in Figure 5.7 This evaluation procedure is done for the entire parent and offspring population at every generation.

5.4. Test problems

5.4.1. Circular lake with a variable bathymetry

To test the optimization procedure on a simple representative case, a hypothetical circular lake with parabolic bathymetry was set up. The diameter of the lake is 10 km and the bathymetry has a parabolic corn shape as shown in Figure 5.8. The depth at the center is 5m, and the depth at the shoreline is 1 m. The lake is discretized with 1,230 6-node isoparametric triangular elements. The total number of nodes is 2,589. The size of the elements along the shore is smaller than that of the elements at the center in order to manage the effect from boundary.

5.4.1.1. Constant Wind Case

Hydrodynamics

Only hydrodynamics forcing for this case was a constant wind from east with the speed of 10 m/s. The size of the time step was set as 30 seconds. The coefficient of implicity was 0.67. The eddy viscosity was set as 50 m^2/s. The Manning's *n* was 0.025. The Coriolis effect was not included.

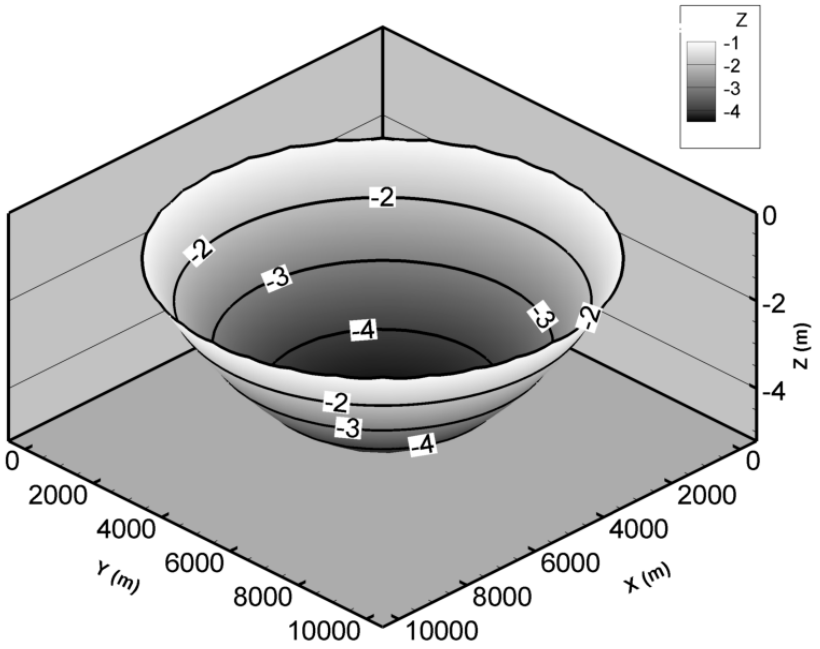

Figure 5.8 Bathymetry of the circular lake

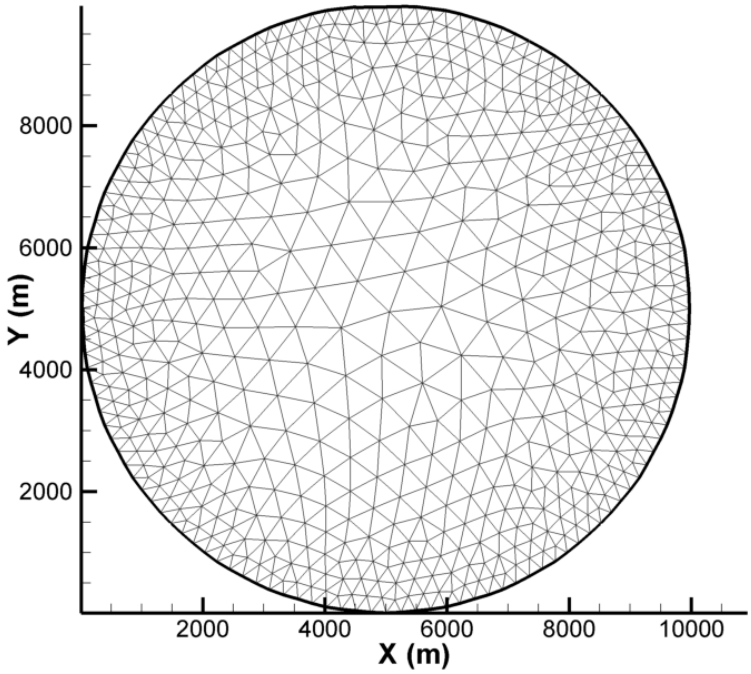

Figure 5.9 The mesh of the circular lake

The simulation started from stagnant water. The hydrodynamics reached to a steady state flow condition in about half a day of simulation time as shown in Figure 5.10. The distinctive two-gyre pattern, which is typical for a wind-driven lake with a round shape, was established well. A return flow was formed at the center against the wind direction. The value of the velocity at the center is about 4.5cm/sec. The surface setup is about 5 cm across the lake.

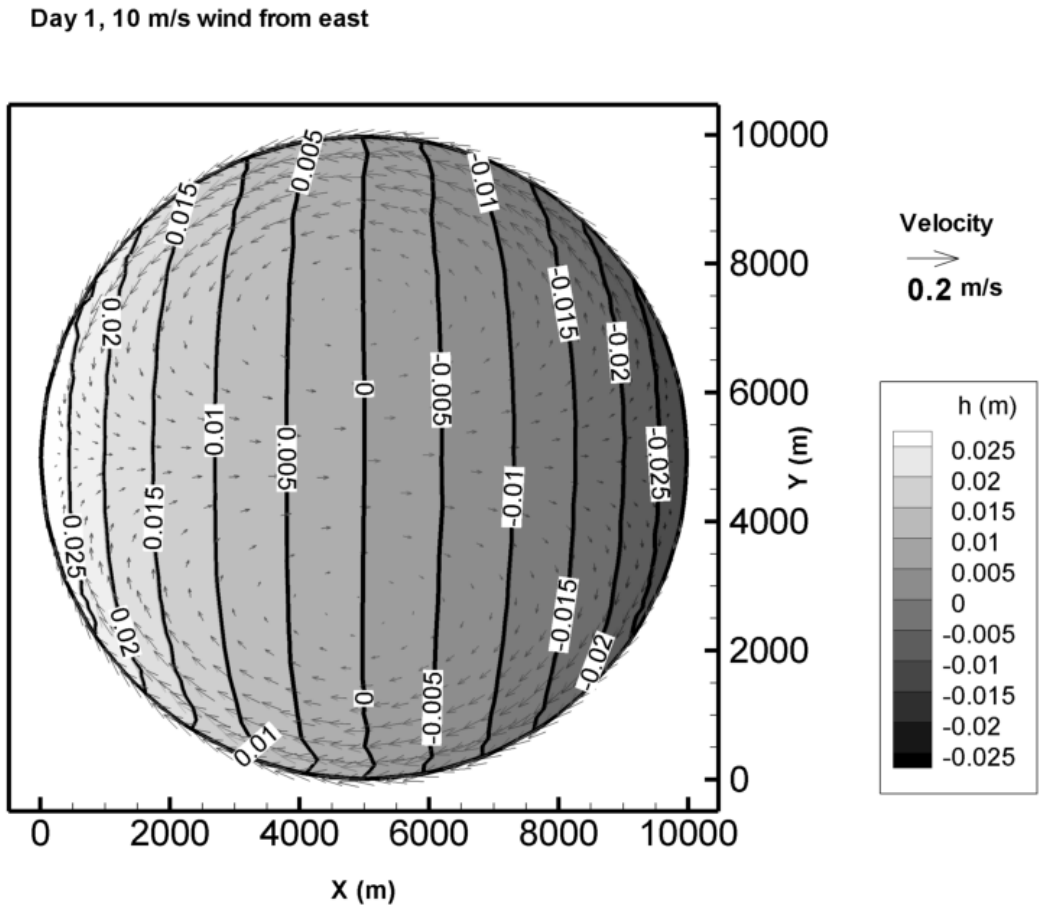

Figure 5.10 Steady state flow of a wind-driven circular lake by a constant wind from east

Contaminant Transport

All the elements on the shore of the lake were selected as possible source locations, which became 128 scenarios. The hydrodynamics of this case was steady so that the time of contaminant spill was not relevant. In other words, whenever the contaminant is released after the steady state is established, the development of a concentration profile will be identical. Hence, the time of spill for every scenario was set at day 1 of the simulation time, and the model was run for a day of the simulation time. The mass of released contaminant was 10^4 kg, and it was released at a constant rate over a time period, 30 minute in this case, to reduce the oscillation by sudden input of mass. The longitudinal and lateral dispersion coefficients were 10 and 5 m^2/s respectively, instead of variable values. The size of the time step was 30 sec as the same as that of hydrodynamics, and the coefficient of implicity was 0.33. All the 128 scenarios were run in the same fashion.

An example of the snap shots of the concentration profile is presented in Figure 5.11. As shown in the figures, the contaminant was transported and dispersed along the shore of the lake and to the center of the lake according to the flow condition that has two circulations. Due to the larger longitudinal dispersion coefficient than the lateral one, the plume was elongated into the direction of the flow. Since there was no reaction or in/outflow either, the total mass could be checked easily. The total mass of the contaminant for the case shown in the figures was checked, and the error is 0.014%. The size of the concentration data for 128 scenarios was about 9.1 Gigabytes in the form of binary single-precision floating-point number files. Even though this was a simple case,

the amount of the data was large, and it showed the difficulty from the huge amount of the data.

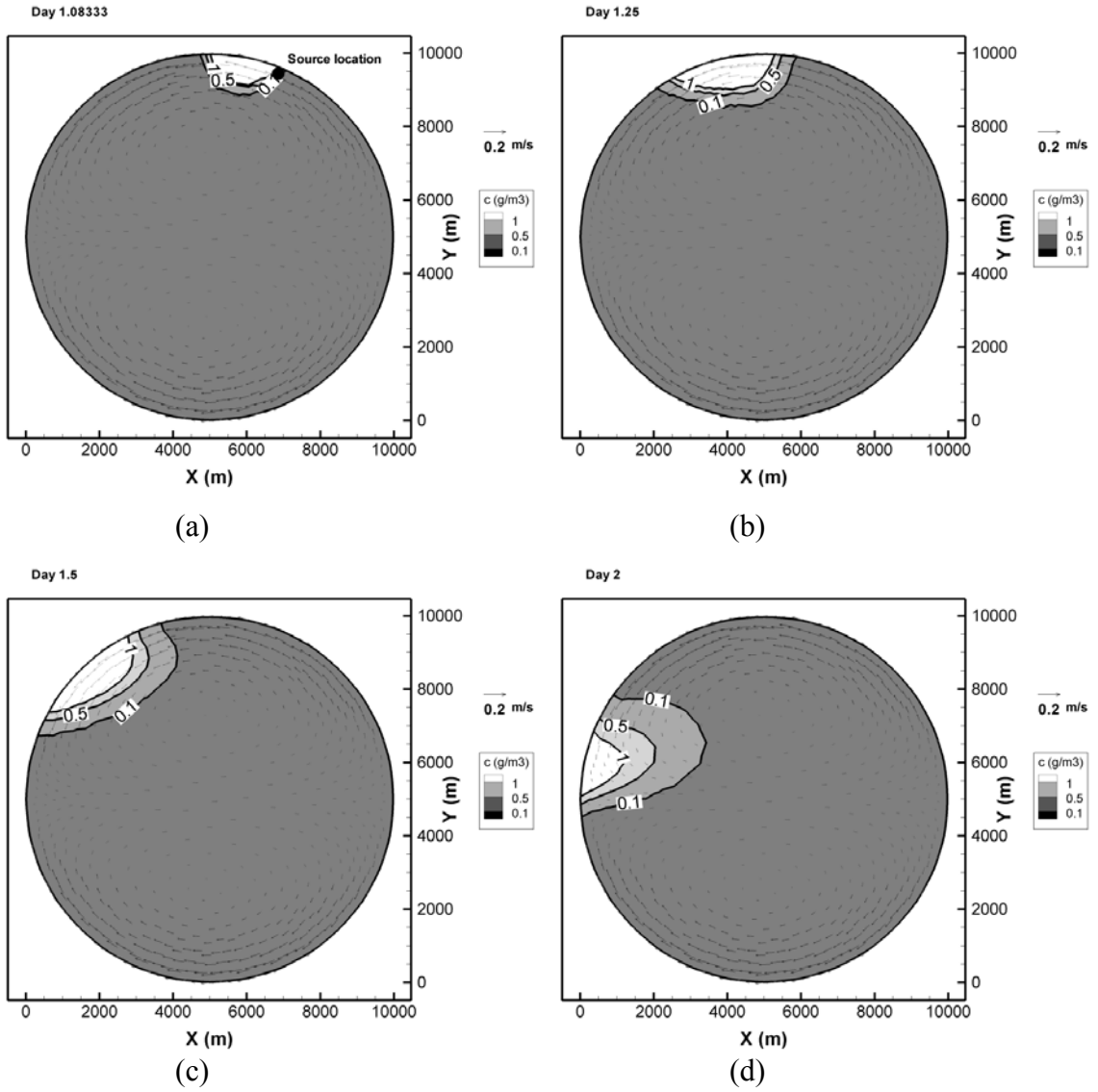

Figure 5.11 Example of concentration profile for one of the scenarios in the wind-driven circular lake
(a) 2 hours after release, (b) 6 hours after release,
(c) 12 hours after release, and (d) 24 hours after release

Optimization of monitoring locations

The optimized monitoring locations under the previously described situation were obtained. The first case was against all 128 scenarios with the same possibility. When three monitoring locations needed to be chosen, the number of all possible combinations of monitoring locations was ${}_{2,589}C_3 = 2.889 \times 10^9$, which was already numerous to search by enumeration. Even though this problem is not extensively complex, obtaining global optima by an exhaustive search may be very hard. As the number of monitoring locations increases, the number of combination increases exponentially

For the genetic algorithm, the maximum generation was 1,000. The detection threshold, which is the minimum concentration to be detected, was set 0.1 g/m^3. The penalty value for a non-detected scenario was the same as detection time limit assuming that late detection close to the detection time limit was considered as a failure.

The parameters for genetic algorithms were: the maximum generation was 500. The population was 50. The mutation rate was adjusted according to the number of monitoring stations to be optimized. Generally, the rate that causes about one mutation in an individual converges to the best solution set quickly.

When the detection time limit was given as 24 hours, only one optimal solution was obtained even though the multi-objective optimization was implemented. The best results with 3 to 6 monitoring locations are shown in Table 5.1 and Figure 5.12. The reason why only one optimal solution with 100 % detection likelihood was obtained was the large value of the penalty used to penalize non-detected scenarios. When the penalty value is large, the estimation of detection time increases greatly even by adding just one penalty value by one failure. This effect rules out any solutions with less than 100 %

detection likelihood out of the optimal set. This also means that the two objectives did not conflict in this case.

As shown in Table 5.1 and Figure 5.13, as the number of monitoring locations increased, the estimation of detection time decreased maintaining 100 % detection likelihood. If the number of monitoring locations is considered as another objective, which may represent the cost of the system, Figure 5.13 becomes a Pareto-frontier line between the estimation of detection time and the number of monitoring locations.

Due to the symmetric flow pattern and contaminant sources distributed evenly around the shore, the monitoring locations tended to be placed along the shoreline evenly and symmetrically. The most selected location was on the west end of the lake where two flows from north and south shores of the lake met. A monitoring location at this location may have more chances to detect spills from the north and south shores of the lake so that it is obviously a good candidate monitoring location.

Table 5.1 Estimation of detection time of the best solutions of monitoring locations in the circular lake driven by a constant wind with 24 hour detection time limit

# of locations	3	4	5	6	7
The estimation of detection time	6.25	4.59	3.27	2.5	1.94

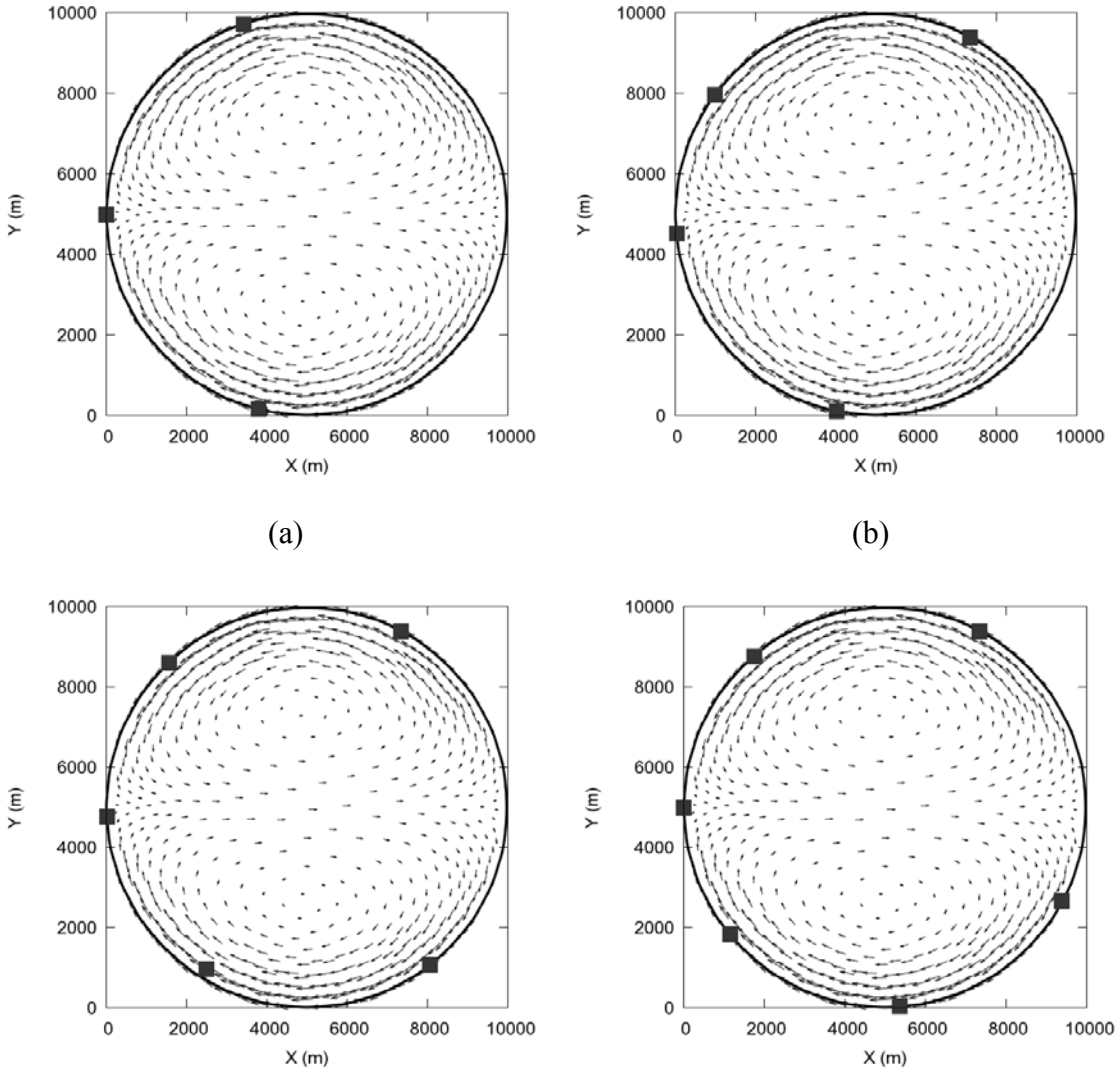

Figure 5.12 The best solutions of monitoring locations in the circular lake driven by a constant wind with 24 hour detection time limit
(a) 3 locations, (b) 4 locations, (c) 5 locations, and (d) 6 locations

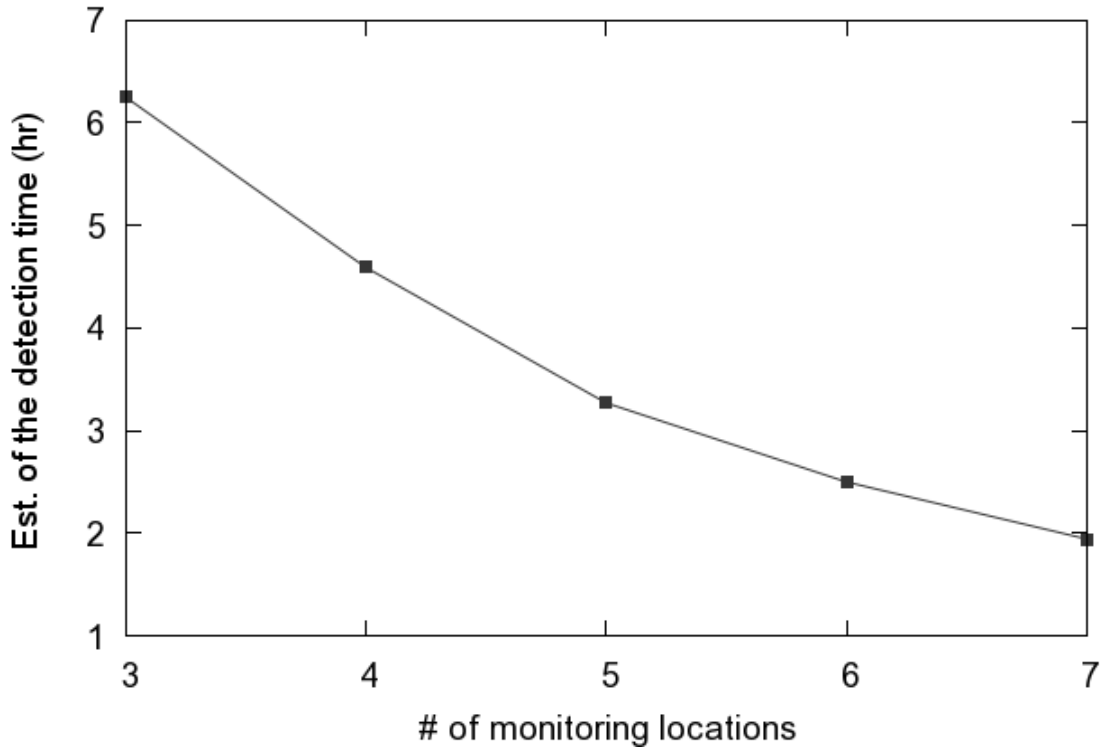

Figure 5.13 Tradeoff between the number of monitoring locations and the estimation of detection time in a circular lake driven by a constant wind with the detection time limit of 24 hours

The detection time limit of one day is quite a loose constraint for an early warning system so that the detection time limit was reduced to 3 hours. The penalty value for a non-detected case was also adjusted to be 3 hours. However, as presented in Figure 5.11, the contaminant did not travel and disperse from the source locations within 3 hours, and it can be easily expected that the detection likelihood by a few monitoring location would not be 100 %. Table 5.2 and Figure 5.14 show some of optimal solutions for various number of monitoring locations. As the number of monitoring locations increased, the detection likelihood increased, and the estimation of the detection time decreased. The first 100 % detection likelihood was achieved with 10 monitoring locations. Unlike the

optimal solutions with 24 hours detection limits, multiple optimal solutions were obtained for 5 to 10 monitoring locations. For 10 monitoring locations, the optimization model obtained 8 optimal solutions so that only two solutions with best detection time and detection likelihood are presented in the table. (From now on, not all optimal solutions will be presented in a table if there are more than 3 optimal solutions.) The number of optimal solutions was small, unlike a typical multi-objective optimization, because of the effect of penalty value.

Table 5.2 Optimal solutions in the circular lake driven by a constant wind with 3 hour detection limit

The number of monitoring locations	Estimation of the detection time with penalty (hr)	Estimation of detection likelihood (%)	Figure
3	2.3488	34.4	Figure 5.14 (a)
4	2.1344	45.3	
5	1.9327	56.3	Figure 5.14 (b)
	1.9304	55.5	
	1.9297	54.7	
10	1.0352	100.0	Figure 5.14 (c)
	⋮	⋮	
	0.9971	94.5	
11	0.8398	100.0	

The distribution of 10 monitoring locations with 100% detection likelihood was again fairly even along the shore of the lake as shown in Figure 5.14. However, the monitoring locations of less than 10 were not distributed evenly.

The flow velocity around the shore in this case was fairly uniform as shown in the hydrodynamics, and it means that some variance of a monitoring location along the shore would not change the estimation of detection time much because the variance will cause roughly the same amount of the gain from the scenarios upstream and loss from the scenarios downstream at the monitoring location. For example, two different optimal solutions for 5 monitoring locations are shown in Figure 5.15. The major difference between two solutions is that one monitoring location at the south shore moved to the north shore. However, the objective values of the two solutions did not differ much. The solution with the maximum reliability in Figure 5.15,(a) detected 2 more scenarios than the solution with the minimum detection time did, and the difference in the estimation of detection time between the two solutions was mere 10 seconds. This tells us that the adjustment of one location from the south shore and to the north cancelled out the loss and gain from the adjustment.

It must be noted that the estimations of detection time and detection likelihood are not absolute indicators because they vary much depending not only the distribution of locations but also on the mass of a spill, the detection threshold, and detection time limit. For example, an optimal solution with 100 % detection likelihood does not mean that it will detect every possible spill regardless of the amount of the spill or detection threshold. Thus, when some of values are adjusted in the optimization model, the optimal solutions may change consequently. However, it can be stated that high detection likelihood with a

certain mass of spill implies a good performance in general. Hence, a care must be given in order not to misunderstand the meaning of the detection time and likelihood from the optimization when the results are interpreted.

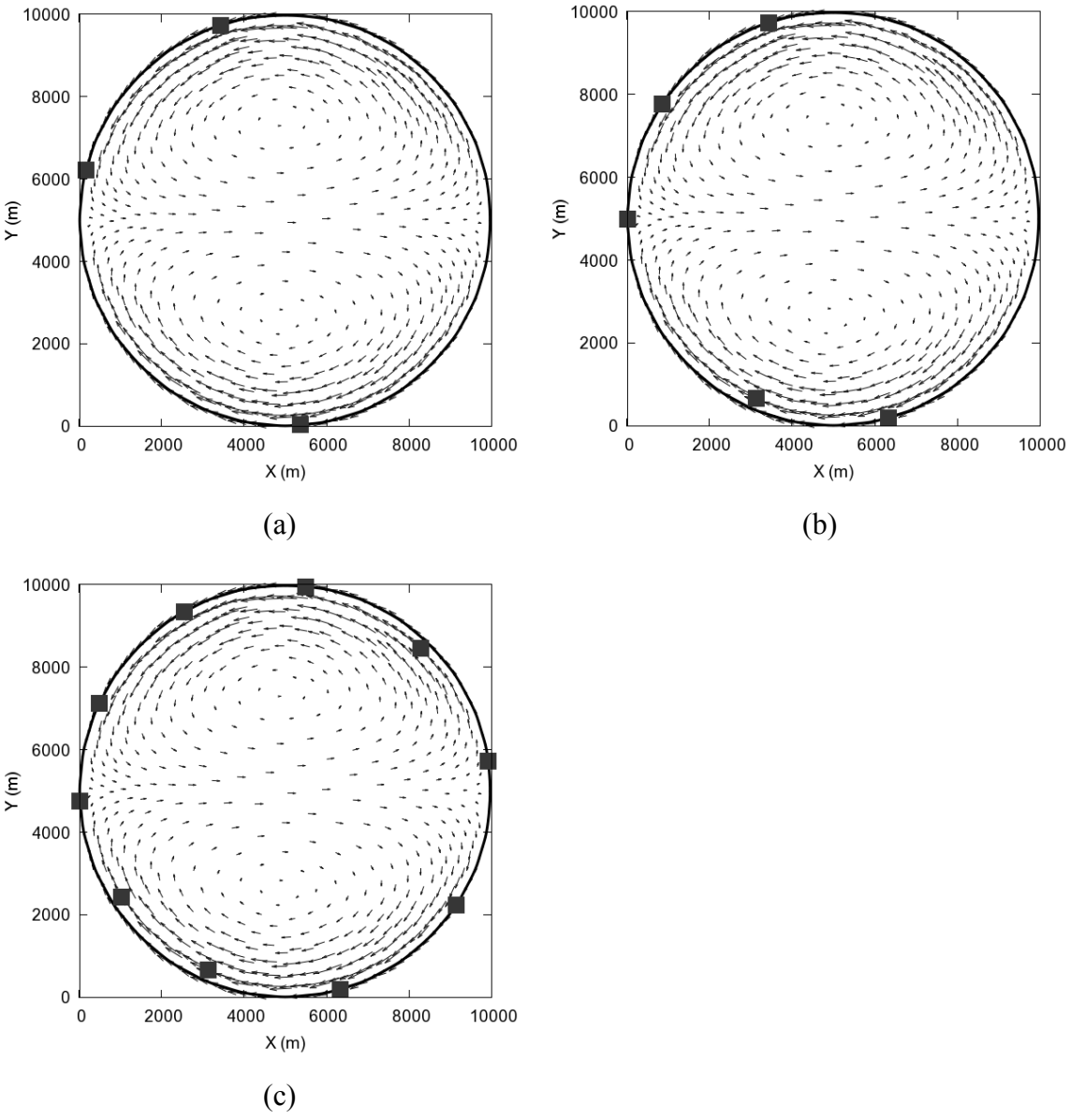

Figure 5.14 The best solutions of monitoring locations in a circular lake driven by a constant wind with 3 hour detection time limit
(a) 3 monitoring locations, (b) 5 monitoring locations (56.4% detection likelihood), and (c) 10 monitoring locations (100% detection likelihood)

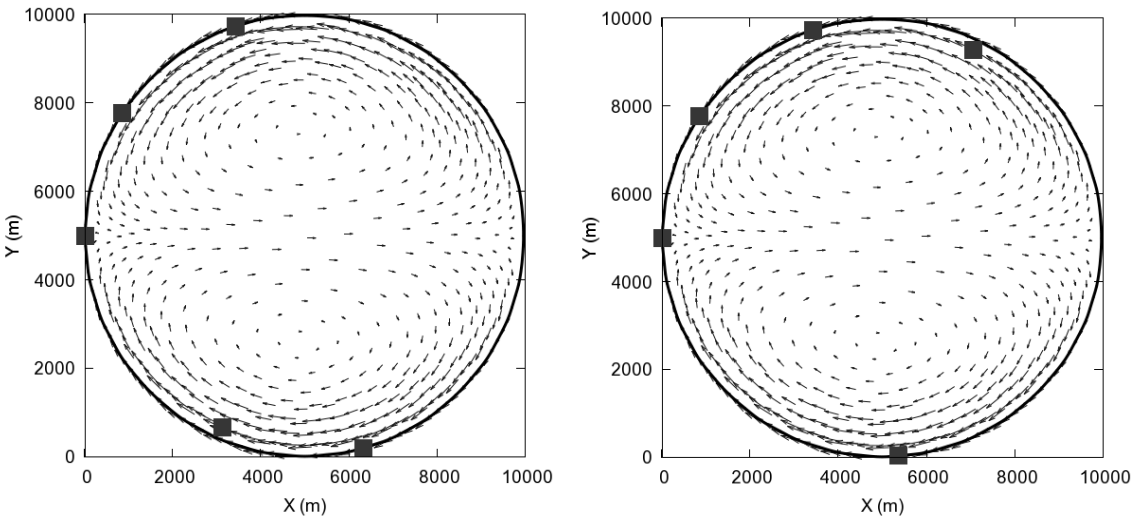

Figure 5.15 Comparison of two optimal solutions of 5 monitoring locations in a circular lake driven by a constant wind with 3 hour detection time limit
(a) maximum detection likelihood and (b) minimum estimation of detection time

`

Effect of the Weights

In the previous case, all the scenarios had the same weight, i.e. every spill had the same chance to happen. However, in a real situation, accidents do not happen with the same degree of chances. To check the effect of the weight of scenarios, one of scenarios was weighted more than other, and the results with 3 monitoring locations are presented in Figure 5.16. The detection time limit was 24 hours. As the weight of one of scenarios increased, one monitoring location that was placed downstream of the spill location of the weighted spill moved closer to the spill location to decrease the weighted estimation of the detection time. In this way, more likely scenario can be detected sooner than others by sacrificing other low-weighted scenarios. Hence, as shown here, if the relative probability of accidents at certain locations are known, one can assign appropriate weight

to each scenario, and an optimization routine may find better solutions that respond better to the reality.

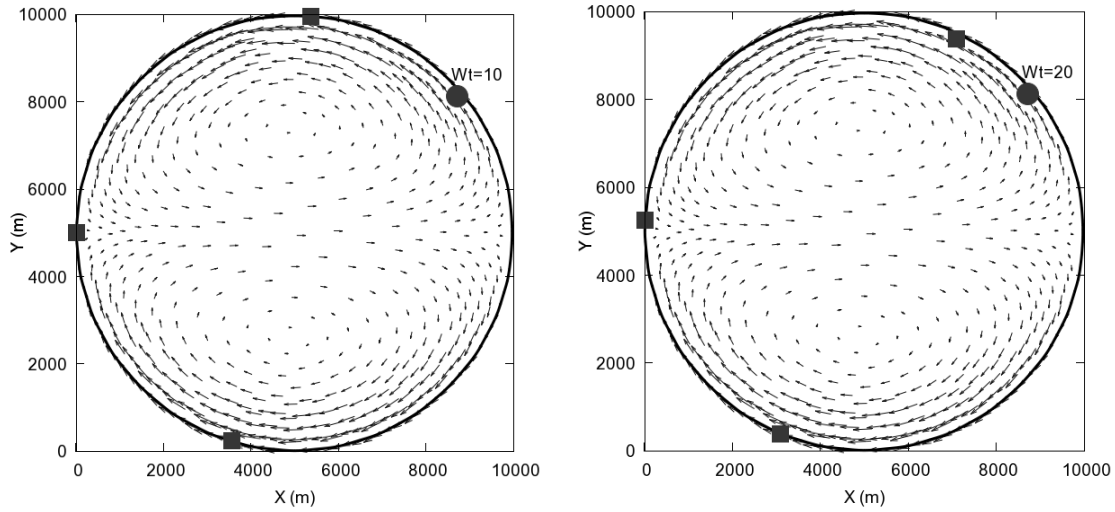

(a) (b)

Figure 5.16 Optimal monitoring locations with weights in a circular lake driven by a constant wind with 24 hour detection time limit
(a) 10 times weight, 3 locations, (b) 20 times weight, 3 locations
(The weight was given a spill at the circular dot)

5.4.2. Circular lake with tide

To test the effect of tidal forcing to the optimal locations, a circular lake with a tidal inlet was set up. The diameter of the lake was 10 km, and the depth was constant as 5 m. The discretized domain is presented in Figure 5.17. The mesh has 5,152 nodes and 2,508 elements. The two hypothetical tides were imposed on the mouth of the east side of the lake as boundary conditions to check the effect of the tidal amplitude, and they had semidiurnal 12 hour period, and 10 and 20 cm amplitude as shown in Figure 5.18. The Manning's roughness, *n*, was 0.020. The Coriolis Effect was ignored.

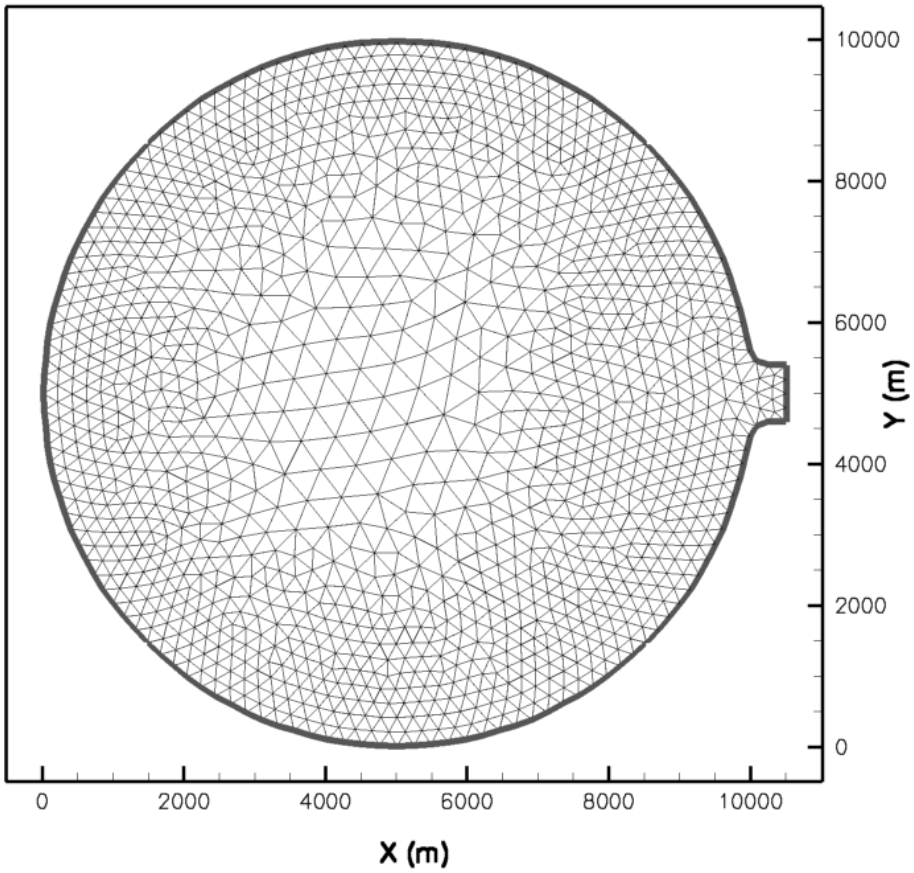

Figure 5.17 Discretized mesh of the circular lake with a tidal inlet

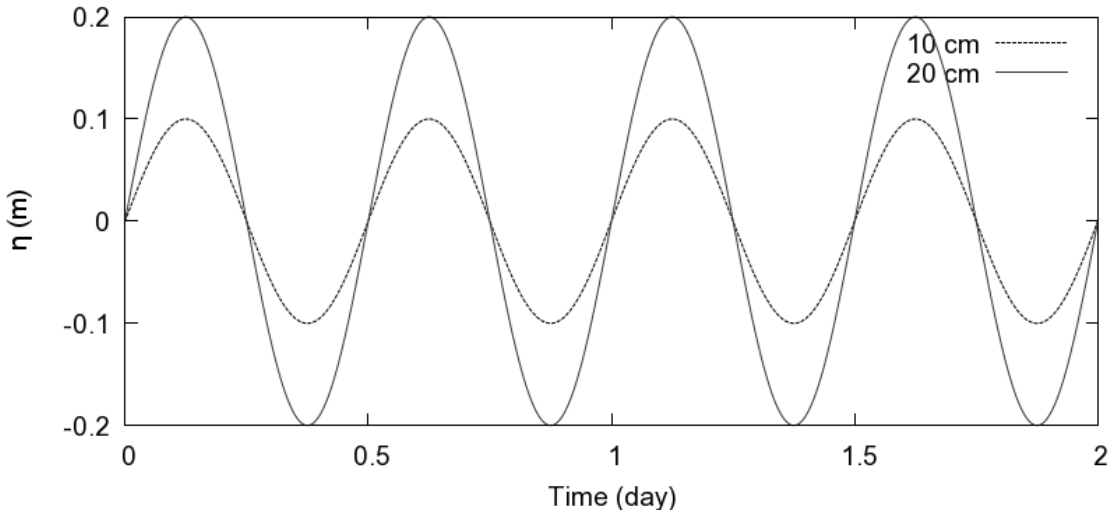

Figure 5.18 Hypothetical tides on the inlet

Hydrodynamics

The simulation started from a stagnant initial condition, and the hydrodynamics by the tides was well established after one tide cycle. The two hydrodynamics snapshots in the middle of a flood tide and ebb tide with 20 cm amplitude are presented in Figure 5.19. The velocity of water flow with 20 cm amplitude tides reached almost 60 cm/sec at the tidal inlet, but it quickly attenuated as the tidal wave proceeded to the center of the lake. The velocity at the center did not reached up to maximum 10 cm/sec, and that at the left end of the lake was very close to zero. Because the scale of the domain was relatively small to the wave length, virtually no surface level slope was observed over the lake except around the inlet. When the tidal amplitude was 10 cm, the velocity at the inlet was around 20 cm/sec, which was about one third of the case with 20 cm tide, but the flow pattern was almost identical to the 20 cm tide case.

Contaminant transport

Unlike the previous wind-driven lake that reached a steady-state flow condition, the lake under the tidal effect had a transient-state flow, i.e. the flow condition changed over time. Under a transient flow condition, even though locations of spills are identical, the contaminant will be transported differently depending on the hydrodynamics condition at and after the time of spills. Hence, separate scenarios were prepared for different times of accidents at each candidate spill locations.

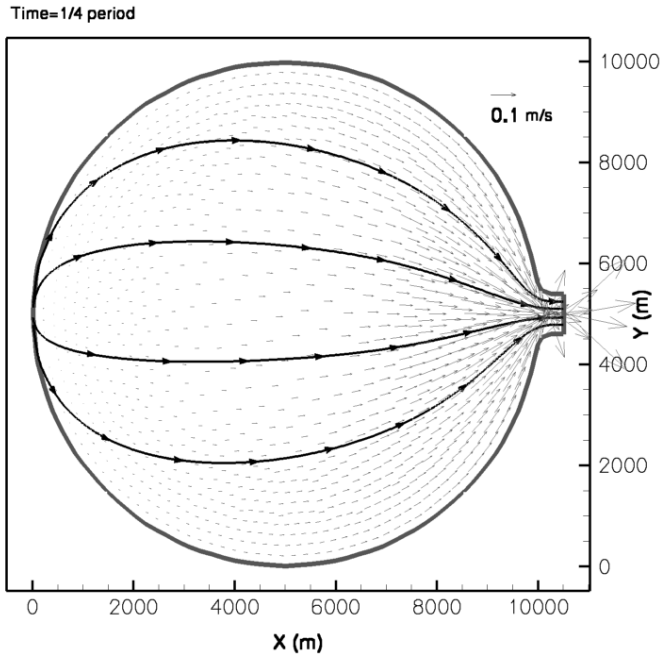

(a)

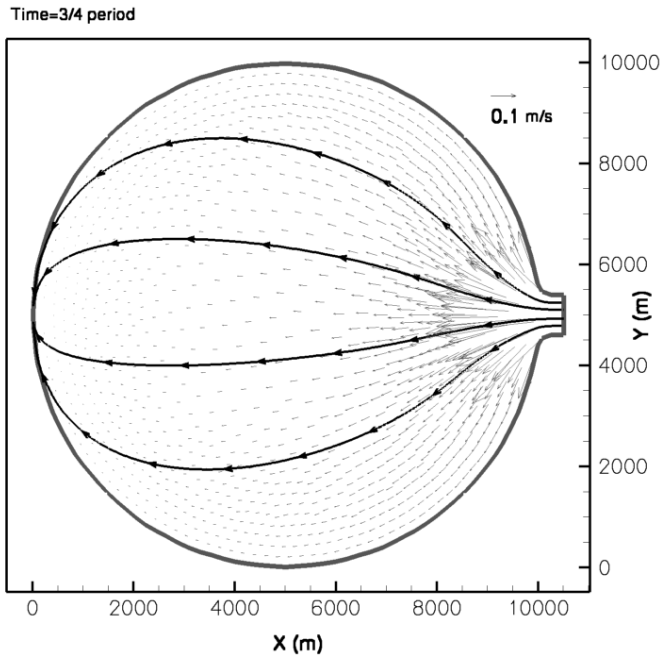

(b)

Figure 5.19 Hydrodynamics snapshots of a circular lake under tidal effects
(a) at 1/4 of the period (1day 6 hours) and (b) at 3/4 of the period (1day 12 hours)

The hydrodynamics of this problem repeated itself every tide cycle so that it is enough to set up a series of spill times within one period of the tide, 12 hours. Theoretically, having as many scenarios as possible with a small amount of time difference for a series of spill is better, but it will increase the number of scenarios quickly. The number of total scenarios will be decided by the number of candidate spill locations times the number of times in a spill time series.

For this problem, 30 locations were picked evenly around the shore as shown in Figure 5.20 in order to reduce the number of scenarios, and the 8 spill times in a tidal period were selected such as 0, 1/8, … , 7/8 of the tide period. Hence, the total number of contaminant scenarios became 240 for one hydrodynamics case. The amount of the spill was 10 tons, and the longitudinal and lateral dispersion coefficients were 10 and 5 m^2/sec.

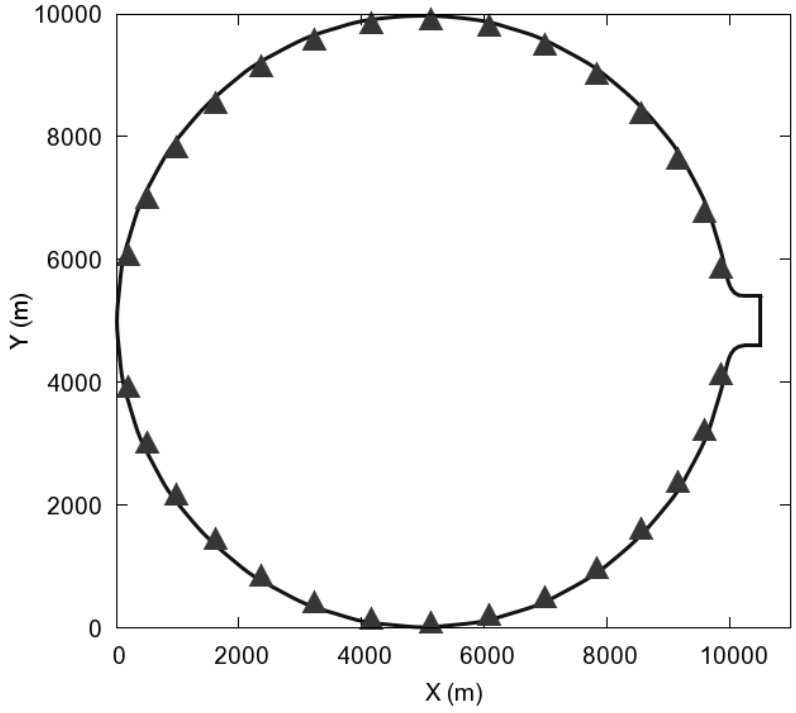

Figure 5.20 Source locations for a lake under tidal effects

Figure 5.21 shows comparisons between two spill cases that occurred at different times but at the same locations on the eastern shore of the lake in 20 cm tide cases. Due to the different hydrodynamics pattern after the spills as shown in the streamlines, the shapes of the contaminant plumes developed into different patterns. Eventually, it may affect the optimal solutions of the monitoring locations. Also, the flow was oscillating back and forth due to the tides so that the mass of the contaminant did not travel far away from the source locations. In result, the tides dispersed the contaminant rather than transported in more than a tidal cycle. A few scenarios that have source locations around the inlet lost the mass of the contaminant during ebb tides. The majority of the spills in the lake were governed by dispersion due to very slow flow velocity.

Optimization of monitoring locations

A set of monitoring locations were optimized against 240 scenarios proposed with 20 cm and 10 cm tides. The detection time limit was set 24 hours. The detection threshold was 0.1 g/m^3. The number of maximum generation was 1,000, and the population was 50.

The results with 5, 6, and 7 monitoring locations were presented in Table 5.3 and Figure 5.23 for the 20 cm tides and Table 5.4 and Figure 5.25 for 10 cm tides. Multiple optimal solutions were obtained for each case, and not all solutions are presented in the tables. Because the flow velocity was very low inside the lake, and the flow direction changed back and forth depending on the tides over time, the contaminant was not transported far away from the source locations as shown in Figure 5.21. In result, many scenarios could not be detected by a few fixed monitoring locations. The detection likelihood was low even with 24 hours detection time limit, and at least 7 locations were necessary to achieve 100 % detection likelihood.

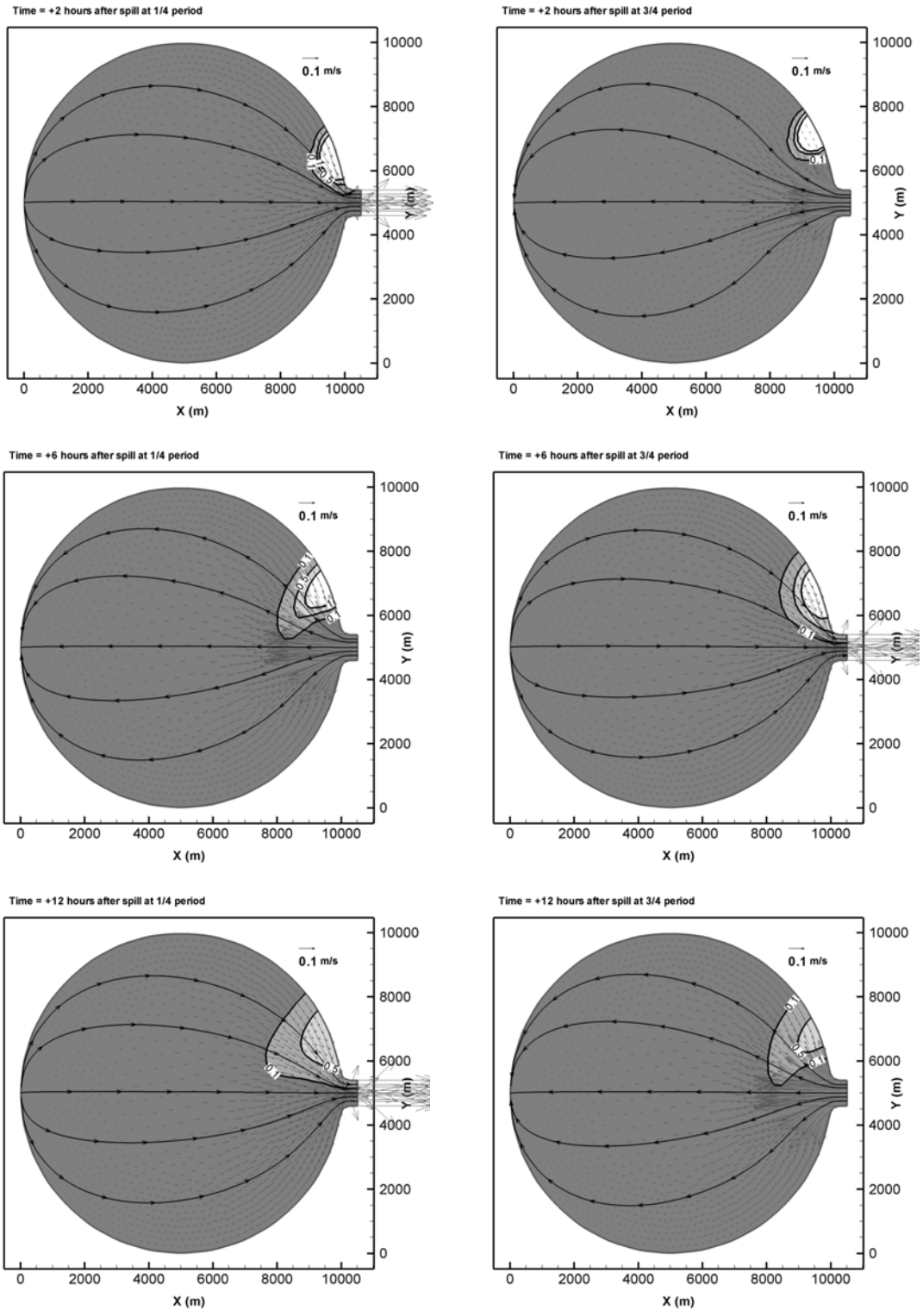

Figure 5.21 Comparisons of two spill cases at the same location at different times (a) spill at 1/4 period (left column) and (b) spill at 3/4 period (right column)

To see the trade-off between the detection time and the detection likelihood, the Pareto frontier of 5 monitoring locations is presented in Figure 5.22, and it showed a significant increase in estimated detection time with a small increase in the estimated detection likelihood. Because the spills that occurred on the left side of the lake traveled very slowly due to low flow velocity in the area, if monitoring locations gives up those cases, the estimation of detection time can be reduced by detecting other spills faster with some sacrifice on the detection likelihood. Figure 5.24 shows this effect. As shown in the figure, the solution with shorter average detection time placed monitoring locations closer to the tidal inlet on the east of the lake.

The distribution of the 7 monitoring locations was fairly symmetric and evenly distributed along the shore, but the distribution of the 5 monitoring locations was not even because the detection likelihood was not 100%.

Table 5.3 Optimal solutions in a circular lake with 20 cm tides

The number of monitoring locations	The number of solutions in the Pareto frontier	The estimation of detection time with penalty (hr)	The estimation of detection likelihood (%)	Figure
5	7	9.9328	82.92	Figure 5.23 (a)
		⋮	⋮	
		8.7819	79.17	Figure 5.1 (b)
6	7	7.0533	96.67	Figure 5.23 (b)
		⋮	⋮	
		6.3733	92.08	
7	8	5.7636	100.00	Figure 5.23 (c)
		⋮	⋮	
		4.8567	95.42	

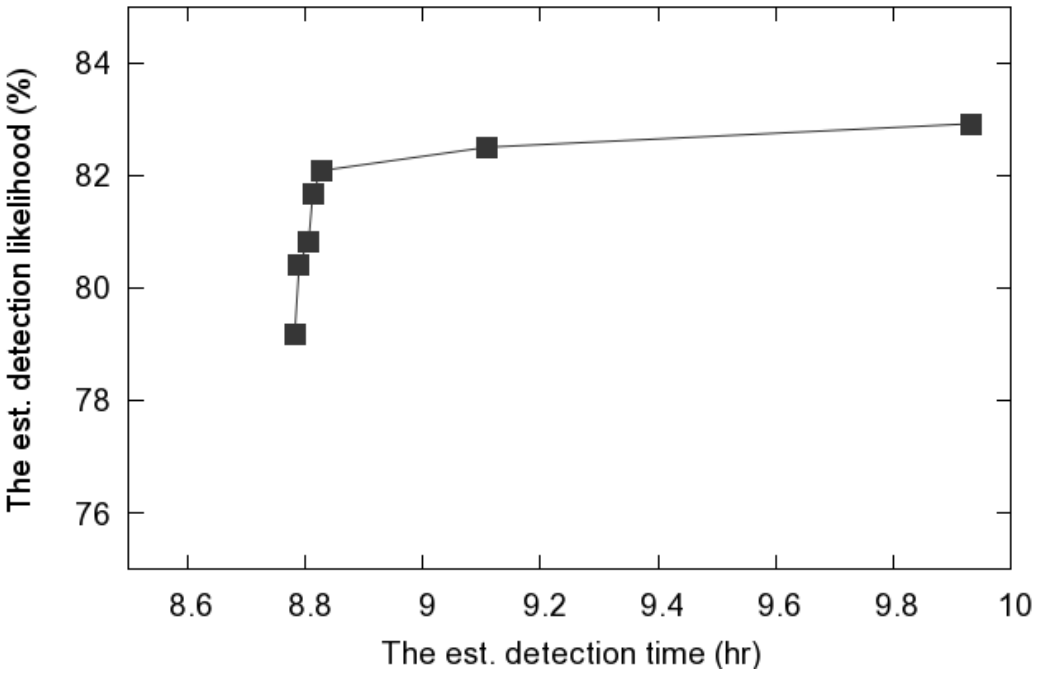

Figure 5.22 Pareto frontier of 5 monitoring locations in a circular lake with 20 cm tides

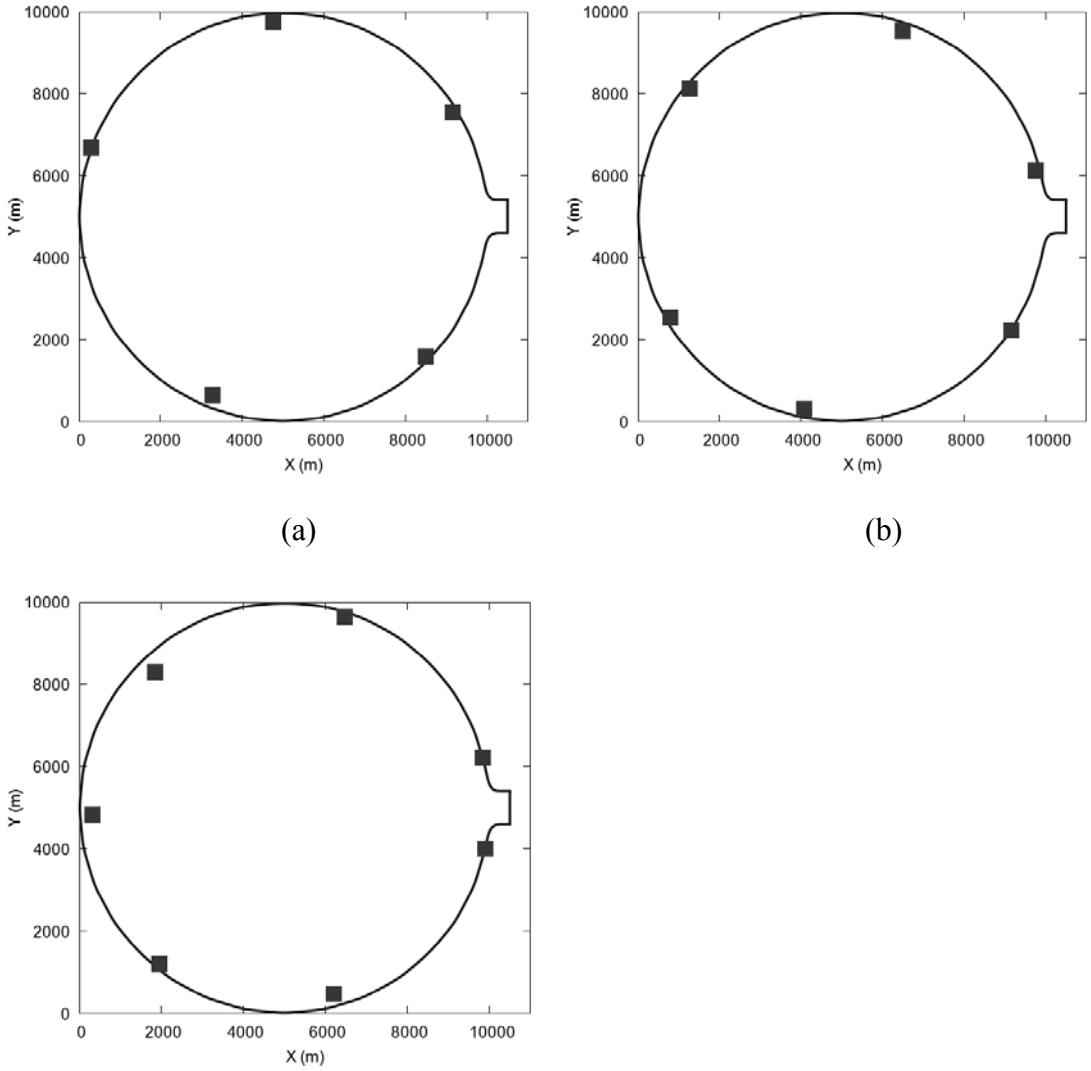

(a) (b)

(c)

Figure 5.23 Optimal monitoring locations with the maximum detection likelihood in a lake with 20 cm tides
(a) 5 monitoring locations, (b) 6 monitoring locations, and (c) 7 monitoring locations

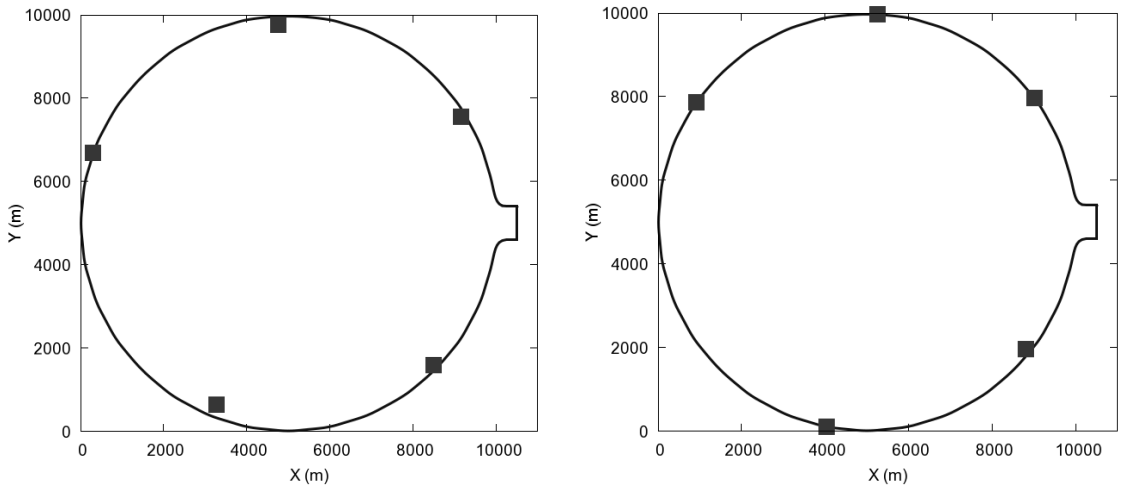

Figure 5.24 Comparison between the solutions with maximum detection likelihood and minimum detection time for 5 monitoring locations in a circular lake with 20 cm tides
(a) a solution with maximum detection likelihood and (b) a solution with minimum detection time

To compare the effect of the tidal amplitude, the same optimization with the tide with 10 cm amplitude was done. The estimation of detection times and detection likelihoods for 5 and 6 monitoring locations with the 10 cm tides were very close to those of the cases with the 20 cm tides. However, the estimation of the detection the distribution of 7 monitoring locations for 10 cm tides has one monitoring location at the inlet, and the corresponding detection time and detection likelihood were much better than those for 20 cm tides. For the case with 20 cm tides, it was not possible for one monitoring location at the center of the inlet to detect spills from the north and south of the inlet at the same time due to the high velocity, but it became possible for the case with 10 cm tides so that it was selected as one of the monitoring locations. In result, the performance of 7 monitoring locations in the case with 10 cm tides was better than the

case with 20 cm. These results show that optimal monitoring locations are sensitive to many factors such as dispersion coefficient and flow speed. In this test problem, constant dispersion coefficients were used, but the results would be different if variable dispersion coefficients were used. Hence, the model parameters need to be selected carefully, and simulations must be approached conservatively.

Table 5.4 Optimal solutions in a circular lake with 10 cm tides

The number of monitoring locations	The number of solutions in the Pareto frontier	The estimation of detection time (hr)	The estimation of detection likelihood (%)	Figure
5	14	9.8704	85.42	Figure 5.25 (a)
		⋮	⋮	
		8.8073	79.17	
6	12	7.2716	97.08	Figure 5.25 (b)
		⋮	⋮	
		6.3830	92.03	
7	4	4.8327	100.0	Figure 5.25 (c)
		⋮	⋮	
		4.793	95.00	

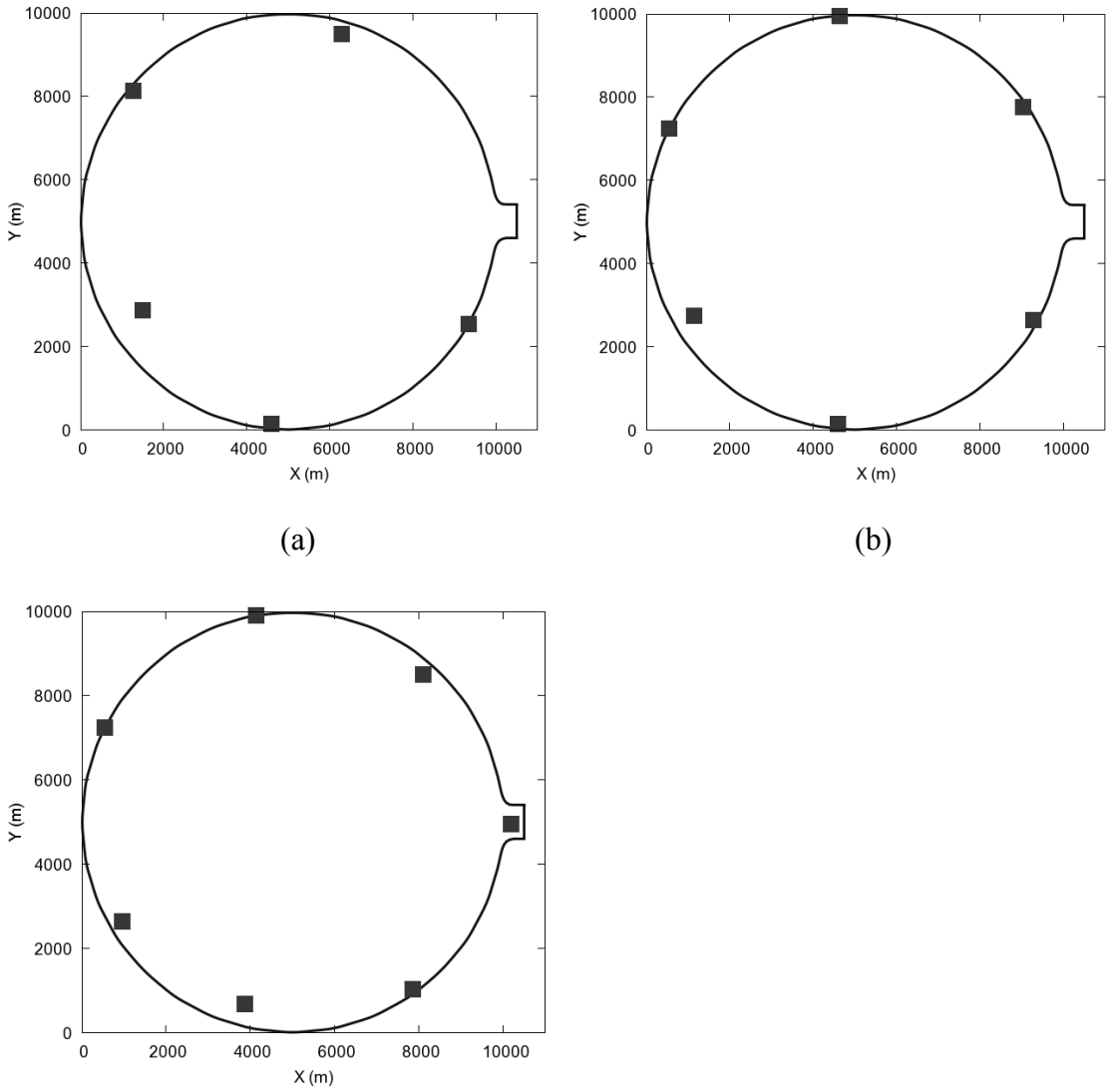

Figure 5.25 Optimal monitoring locations with the maximum detection likelihood in a lake with 10 cm tides
(a) 5 monitoring locations, (b) 6 monitoring locations, and (c) 7 monitoring locations

5.5. Lake Pontchartrain

The optimization of monitoring locations for the Lake Pontchartrain was tried with 20 hypothetical contaminant source locations as shown in Figure 5.26 with the same chance of occurrence. The locations were either river mouths or canals assuming they are

most likely contaminant sources. All other hydrodynamics and contaminant transport simulations had the same parameters used in the previous chapter for the simulations.

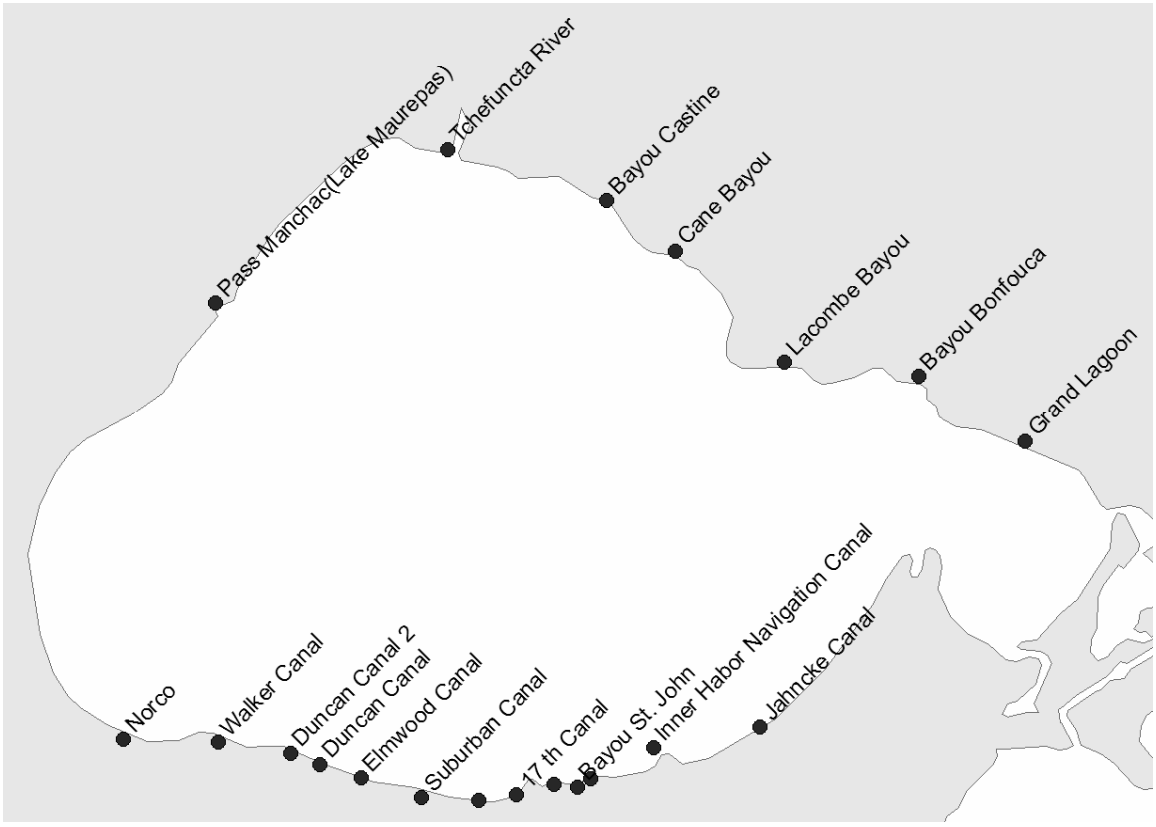

Figure 5.26 Selected source locations for Lake Pontchartrain

5.5.1. Wind-only case

To investigate the effect of the wind on the optimization, a constant wind with 15 m/s speed from southeast was applied for the hydrodynamics. The hydrodynamics reached to a steady state less than one day so that only one spill time was set for all the locations. Hence, the number of scenarios in this case was 20, which is the same as the

number of possible selected spill locations. The mass of the spill was 1 ton, and the detection threshold was 0.1 g/m^3.

The various results of the optimal monitoring locations in Lake Pontchartrain under the constant wind are presented in Table 5.5. Five optimal monitoring locations were obtained with two detection time limits: 12 and 24 hours. Figure 5.27 and Figure 5.28 present the solutions with the best detection likelihood for 12 and 24 detection time limits respectively. Three of the monitoring locations were placed on the New Orleans shoreline because it was assumed that the area had many possible source locations in the optimization. The many of selected monitoring locations were the same as the source locations, and they tend to be ones at the most downstream among source locations as shown in the southwestern side of the lake. When the detection time limit increased, the distance between monitoring locations increased as well in order to improve the detection likelihood.

When the number of monitoring locations increased, the estimation of the detection time decreased, and the detection likelihood increased at the same time. The detection likelihood of 100% was achieved with 10 monitoring locations with the given conditions.

Table 5.5 Optimal monitoring locations in Lake Pontchartrain under the constant wind

The number of monitoring locations	The detection time limit (hr)	The estimation of detection time with penalty (hr)	The estimation of detection likelihood (%)	Figure
5	12	5.778	75	Figure 5.27
		5.695	70	
		5.607	65	
	24	8.776	80	Figure 5.28
		9.609	75	
7	12	4.403	85	
		4.198	80	
	24	7.793	90	
		6.423	85	
9	12	3.481	95	
		3.035	90	
	24	4.173	95	
10	12	3.071	100	Figure 5.29
		2.399	95	
	24	2.974	100	

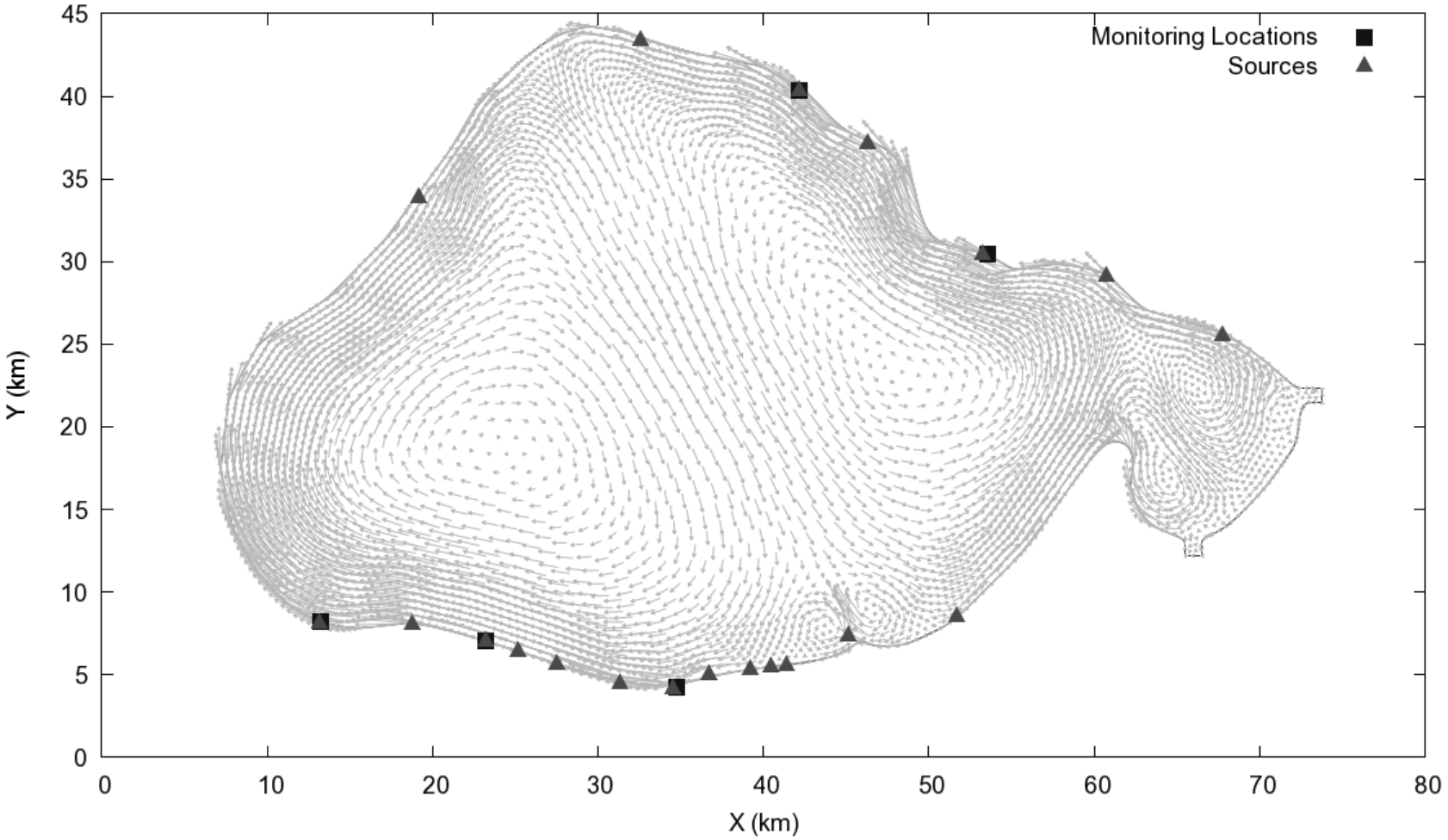

Figure 5.27 Five optimal monitoring locations in Lake Pontchartrain under the constant wind with 12 hours detection limit

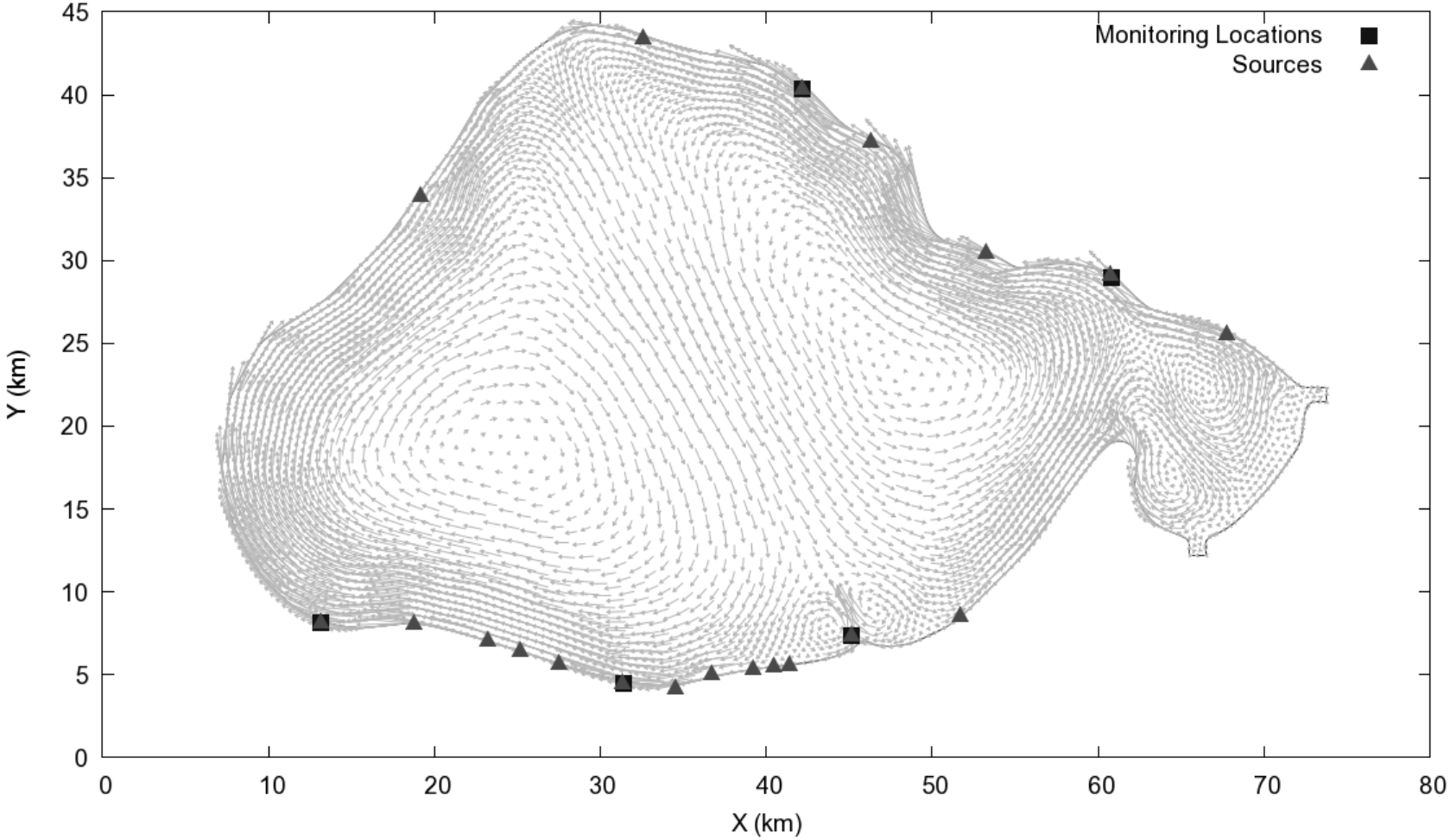

Figure 5.28 Five optimal monitoring locations in Lake Pontchartrain under the constant wind with 24 hours detection limit

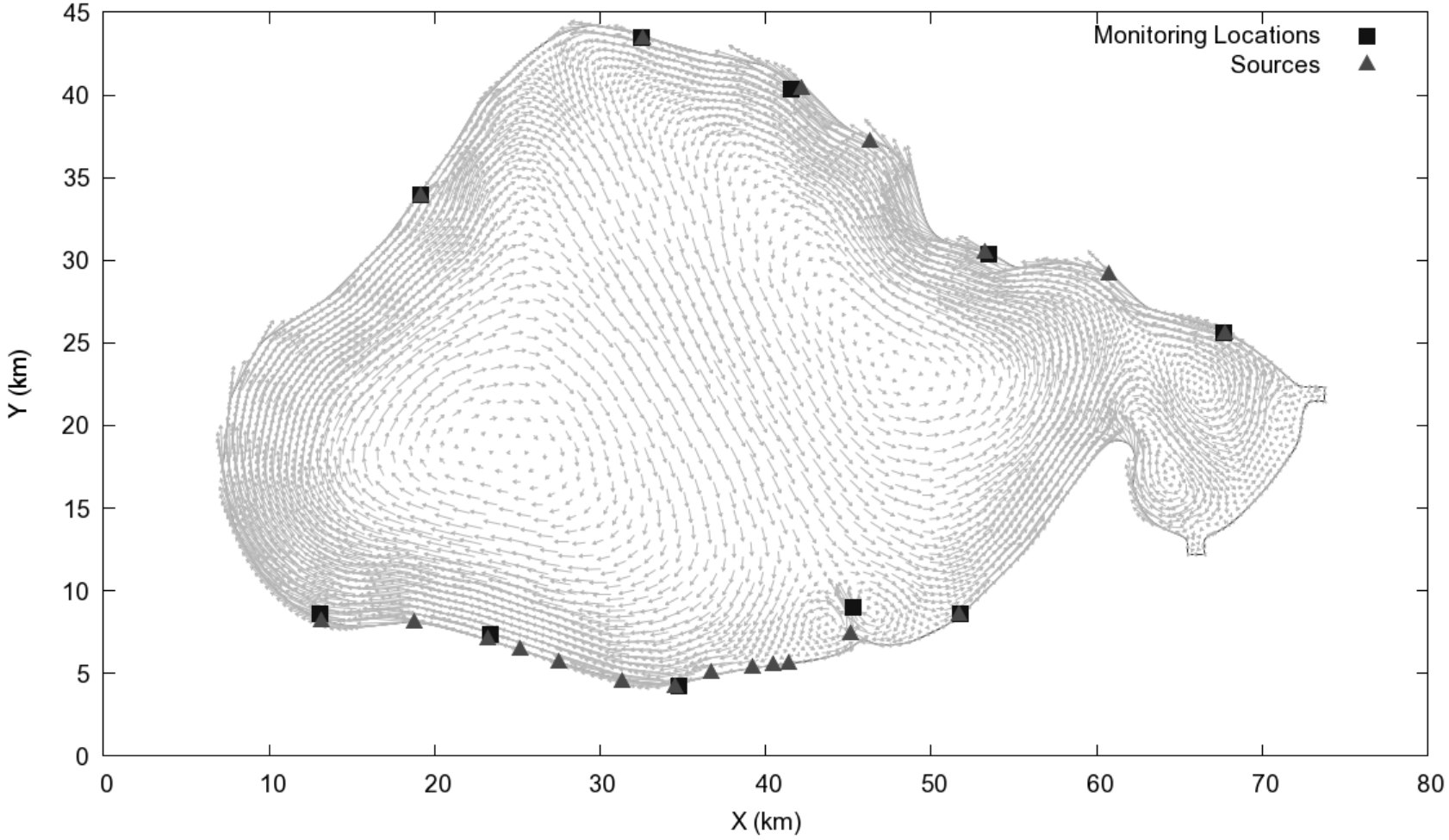

Figure 5.29 Ten optimal monitoring locations in Lake Pontchartrain under the constant wind with 12 hours detection limit

5.5.2. Site specific-wind data and tide case

To investigate the effect of real wind and tide on the optimal monitoring locations, the optimization model was applied to the results with real wind and predicted tide as described in Chapter 4. The selected time period for the optimization was from 12:00 of March 3rd to 00:00 of March 5th because the direction of wind changes from southeast to northwest in this time period. Since the hydrodynamics was not steady, eight different spill times were assumed for each of 20 possible spill locations that were used in the previous section. Thus, total 160 contaminant spill scenarios were set up and simulated. The mass of spill was 1 ton, and the threshold for detection was $0.1 g/m^3$, which are the same as the previous case. The detection time limit was set 12 hours uniformly in this case. Because of many scenarios and possible locations involved, longer generations up to thousand for the genetic algorithms were required to obtain high quality solutions.

The results of the optimization are presented in Table 5.6. Just like previous problems, as the number of monitoring locations increased, the estimation of detection time decreased and the estimation of detection likelihood increased. The performance of the same number of optimal monitoring locations with variable wind and tide dropped, compared with the results for constant wind only case in the previous section, as shown in Table 5.7. First of all, when wind direction changes over time, the flow direction does not maintain over time. Then, the direction of contaminant transport depends on when a contaminant is spilled. Also, a contaminant does not travel into one direction over time. In fact, these effects are reflected into many scenarios. Secondly, even though the selected time period for the optimization was under strong wind as presented in Figure 4.20, the wind speed was around between 10 and 13 m/sec, which was smaller in terms of

average than 15 m/sec constant wind for the previous case. These made complete detection by stationary monitoring locations very hard. To obtain 100 % detection likelihood with the given conditions, 16 monitoring locations were required. This result covered more than three fourths of 20 possible spill locations, and showed the difficulty of the detection again.

The pattern of the optimal solutions also changed according to the degraded performance. Comparing Figure 5.27 and Figure 5.30, a monitoring location on the northeastern shore was abandoned in the result for real wind and tide, and instead a new location on the south shore was selected. The reasons why this happened are the same as described above.

According to the results, it can be deduced that average flow pattern (or direction) and speed over time are the most influential factors of optimal solutions. When wind condition, which is most important forcing in a closed water body, changes over time, the average flow speed and direction may be close to stagnant water. Then, a contaminant will not be transported by advection, and detection of a contaminant will be very difficult eventually. However, because harmful effect from spills under these kinds of hydrodynamic conditions also becomes minimal, finding optimal solutions for these conditions may not be very meaningful either. Hence, it can be recommendable that the optimization of monitoring locations is done not against unrepresentative real conditions which does not have clear average flow pattern, but against representative hydrodynamic conditions which may cause large harmful effect.

Table 5.6 Optimal monitoring locations in Lake Pontchartrain under the real wind and predicted tide

The number of monitoring locations	The estimation of detection time with penalty (hr)	The estimation of detection likelihood (%)	Figure
5	6.815	58.13	Figure 5.30
	6.815	57.50	
	6.790	56.88	
	6.790	56.25	
10	3.803	83.13	Figure 5.31
	3.778	81.88	
	3.776	81.25	
16	0.914	100.00	

Table 5.7 Comparison of performance among optimal solutions for constant wind cases and variable wind and tide cases

The number of monitoring locations	Solution with the best detection time for	The estimation of detection time with penalty (hr)	The estimation of detection likelihood (%)
5	constant wind only	5.778	75
	variable wind and tide	6.815	58.13
10	constant wind only	3.071	100
	variable wind and tide	3.803	83.13

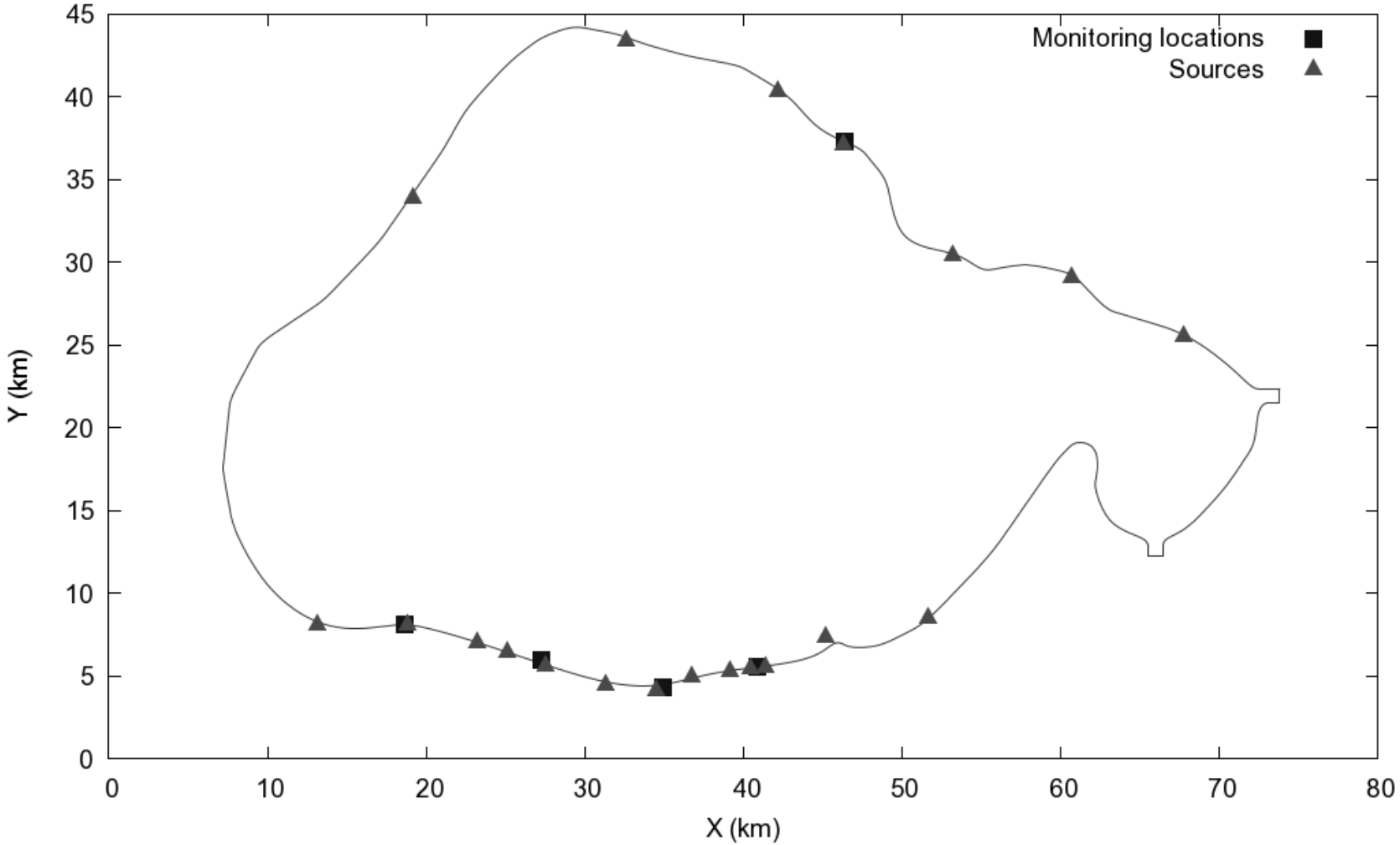

Figure 5.30 Five optimal monitoring locations in Lake Pontchartrain under the real wind and predicted tide with 12 hours detection limit

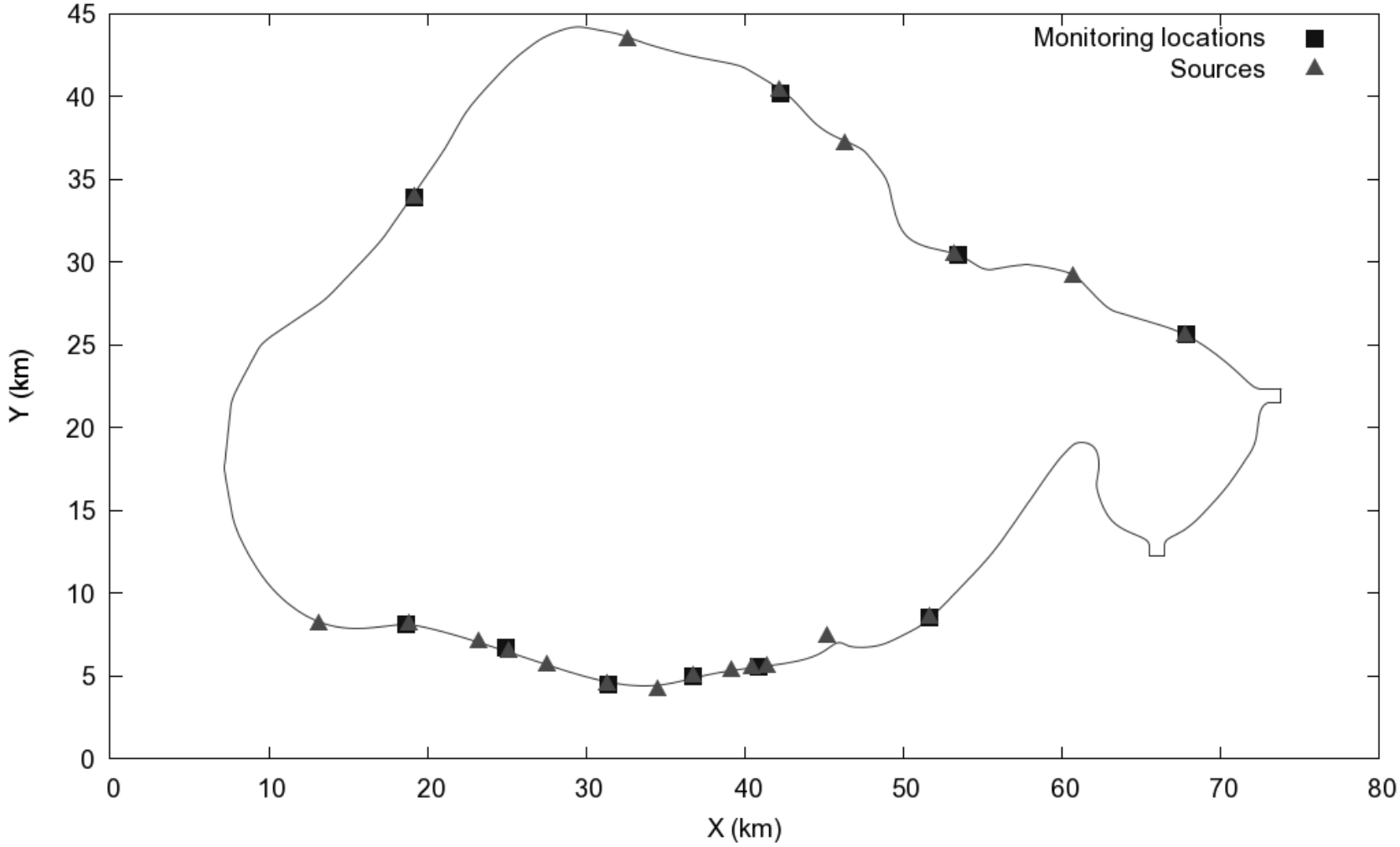

Figure 5.31 Ten optimal monitoring locations in Lake Pontchartrain under the real wind and predicted tide with 12 hours detection limit

5.6. Summary

The use of the genetic algorithm to find the best monitoring network in a lake environment is proposed and tested. Overall, the optimization model found optimal locations that could not be guessed easily due to complex hydrodynamics and many spill scenarios.

In a closed water body such as lakes, wind is a major factor of hydrodynamics and subsequent contaminant transport. Wind generates circulations that have a longshore flow occurring along the shore and a return flow at the center against wind direction. Assuming that most of possible contaminant sources were on the shoreline of a lake such as rivers and urban settings, contaminants were transported along the shore of a water body. Consequently, optimal monitoring locations were placed on the shore. The distribution of monitoring locations on the shore depended mainly on the possible source locations used for the optimization. The weights of spills also affected the distribution. A scenario that has higher weight tends to attract a monitoring location.

Since the flow speed in a lake was generally relatively small, many monitoring locations were necessary to achieve high detection likelihood in a short amount of time. This is especially troublesome when a domain of interest is huge and/or flow is weak. When the detection likelihood was not 100 %, the monitoring locations were selected where more spills could be detected by giving up others. The change of the tidal amplitude in the test case did not change the pattern of the optimal solutions much.

The optimal solutions can be sensitive to parameters such as dispersion coefficients so that conservative parameters need to be used to obtain reliable solutions.

CHAPTER 6

Optimal Design of Straight Monitoring Paths

6.1. Optimal model for a straight water quality monitoring line

A monitoring vessel for surface water quality can take the measurement of water quality constituent while it can move around on a water body. By doing so, a water quality monitoring program may overcome the spatial restriction that a network of stationary monitoring stations has. One major challenge of such a mobile monitoring system is deciding the optimal routes to follow. A route to monitor by a monitoring vessel can take any shape, but the simplest way is following a straight line.

The objectives of a mobile monitoring system can be comprehensive, but two objectives – minimizing detection time and maximizing detection likelihood – were selected assuming we have an early warning system as discussed in the previous chapter for stationary water quality monitoring locations.

6.2. Implementation of the genetic algorithm for a straight monitoring line

The two objectives need to be defined in mathematical formulae for the optimization routines. A straight line segment to monitor water quality can be defined mathematically by two points: one is the start location and the other is the end location of a monitoring path. A path has a direction of motion so that a monitoring vessel travels from a start point to an end point. The velocity of a vessel may change, but it will be assumed constant for simplicity. The objectives of the optimization can be mathematically stated as:

$$\min f_1 = \frac{1}{T_s}\sum_{j=1}^{T_s}\frac{1}{W}\sum_{s=1}^{N_s} w_s t_{d,s,j}(X) \tag{6.1}$$

$$\max f_2 = \frac{1}{T_s}\sum_{j=1}^{T_s}\frac{1}{W}\sum_{s=1}^{N_s} w_s \delta_{s,j}(X) \tag{6.2}$$

such that

$$X = \overrightarrow{\mathbf{x}_s\mathbf{x}_e} \text{ s.t. } \mathbf{x}_s, \mathbf{x}_e \in \Omega, X \bigcap \Gamma = \varnothing \tag{6.3}$$

where

$X = \overrightarrow{\mathbf{x}_s\mathbf{x}_e}$ = a straight monitoring line
$\mathbf{x}_s$ = the cooridnate of the start point of a straight monitoring line
$\mathbf{x}_e$ = the cooridnate of the end point of a straight monitoring line
Ω = the domain, the area to be monitored
Γ = the boundary of the domain
$t_{d,s,j}$ = the detection time of j-th deployment of a scenario s if detected
otherwise a penalty value
$\delta_{s,j}$ = the detection flag of j-th deployment of a scenario s
0 if not detect, 1 if detected
T = the set of the deploying times
$= \{t_1, t_2 = t_1 + \Delta t, \ldots t_j = t_j + (j-1)\Delta t, , \ldots t_{limit}\}, n(T) = T_s$
t_{limit} = the detection time limit
T_s = the number of deploying times per scenario
w_s = the weight of scenario s
$W = \sum_{s=1}^{N_s} w_s$ = the sum of weights
N_s = the number of scenarios.

The difference in the objective functions of a monitoring line, Eqn (6.1) and (6.2), from those for stationary monitoring locations in the previous chapter, Eqn (5.3) and (5.4),

is one more averaging summations with respect to the series of deploying times. What a monitoring vessel does is to move around to find the frontline of a contaminant plume as soon as possible. The time of contaminant release is not known to a monitoring vessel, and a monitoring vessel may start monitoring any time before or after the contaminant release. A plume of a contaminant may be developing differently when a monitoring vessel starts monitoring – this time will be referred to as the deploying time for convenience. Consequently, the detection time may change, or even a vessel may fail to detect a plume depending on the deploying time. For example, as shown in Figure 6.1, even though a vessel travels the same path, it may or may not detect the contamination depending on when the vessel starts to travel. Hence, it is necessary to calculate the average of detection time and detection likelihood considering the relative time difference between the time of release and the deploying time.

Hence, several deploying times are picked, and the average of detection times is taken with respect to different deploying times. For the detection likelihood, the same averaging procedure is necessary. To the contrary to the monitoring line, the monitoring locations discussed in the previous chapter just sit and wait for incoming contaminants all the time so that the relative time difference does not need to be considered.

For the genetic algorithm, a straight monitoring line needs to be converted into a form which can be used first. The genetic coding of a straight monitoring line consists of four real numbers that represent x and y coordinates of the start and the end points of a line segment. An example of the graphical representation for a line segment is shown in Figure 6.2. Unlike the genetic coding of the monitoring locations, the sequence or the

locus of each gene is meaningful. The first two genes are the coordinates of a start point, and the last two genes are those of an end point.

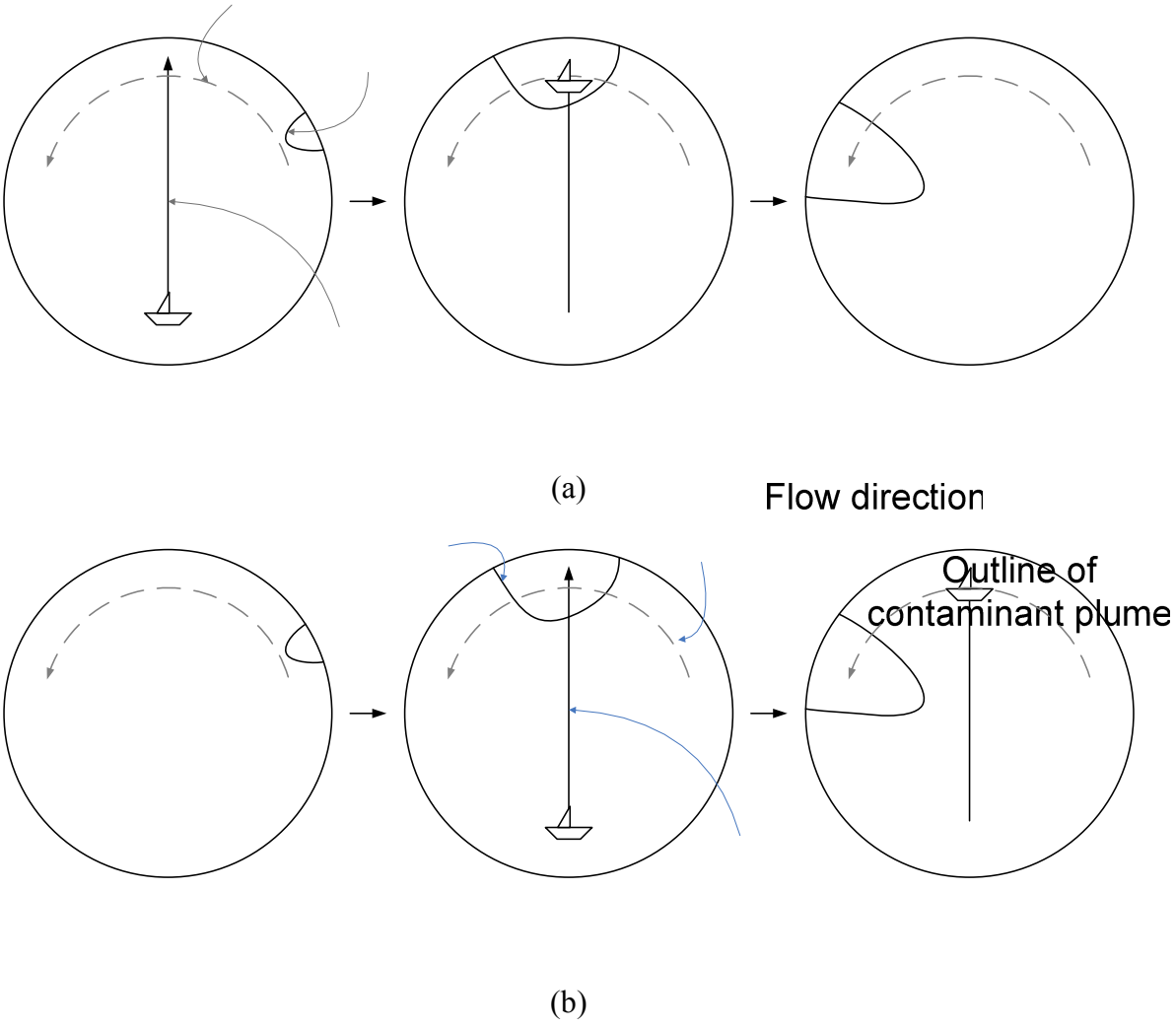

Figure 6.1 The effect of different deploying time for the same scenario and the same straight monitoring path
(a) Successful case (deployment at time t_1) and (b) unsuccessful case (deployment at time t_2)

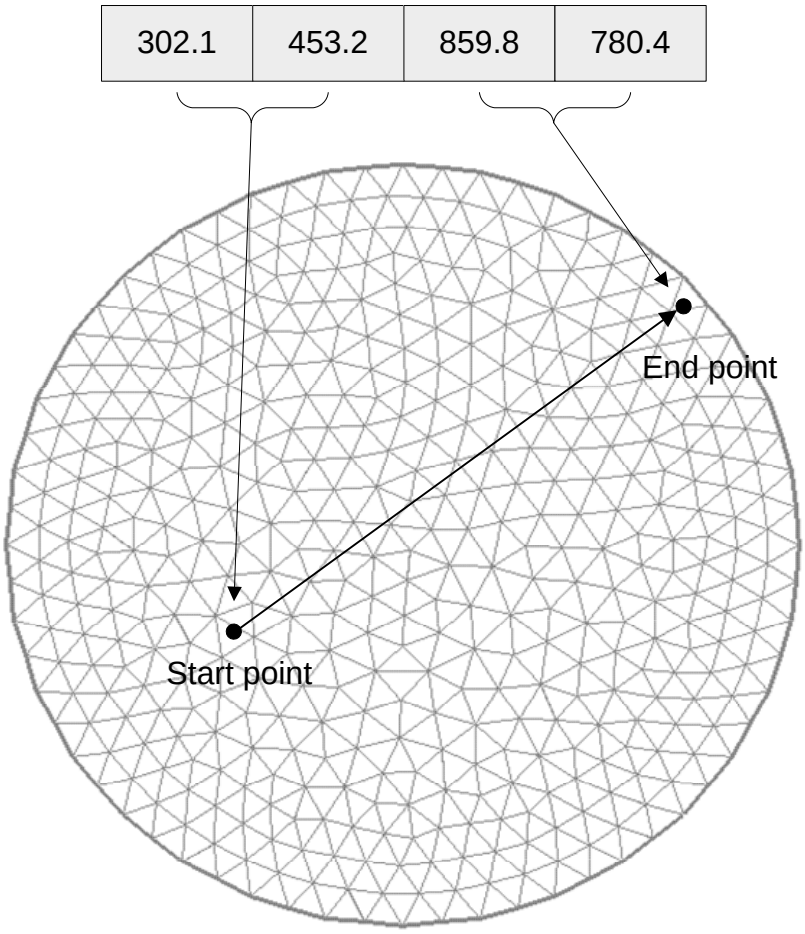

Figure 6.2 An example of a straight monitoring line defined by starting and ending points

6.2.1. Genetic operations of a straight monitoring line

A crossover operation of an individual of a straight monitoring line was designed with a simple one-point crossover. A mutation of an individual was a uniform mutation, which picks a random real numbers within a certain range from a current value. Hence, the mutation will generate a new point in a box that has a current point at the center, as shown in Figure 6.3.

Like the genetic operations of the optimization of the stationary monitoring locations, the crossover and mutations on individuals for a straight monitoring line can

generate infeasible solutions. Firstly, when one of the start and the end points of a monitoring line is outside of a domain, the solution is infeasible. Secondly, even though both of end points of a monitoring line are inside of a domain, the line may intersect with the outline of a domain when the domain is not convex as shown in Figure 6.4. In nature, shapes of water body are hardly 100% convex, and this type of infeasible solutions can happen very often.

For the optimization of straight monitoring lines, infeasible solutions are not repaired because the procedure is not simple. Instead, when they are evaluated, a penalty value is assigned if they are infeasible.

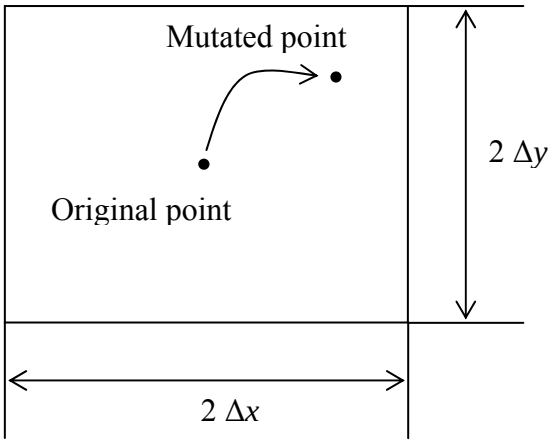

Figure 6.3 Mutation of starting and ending points
(Δx, and Δy are mutation ranges in x and y directions)

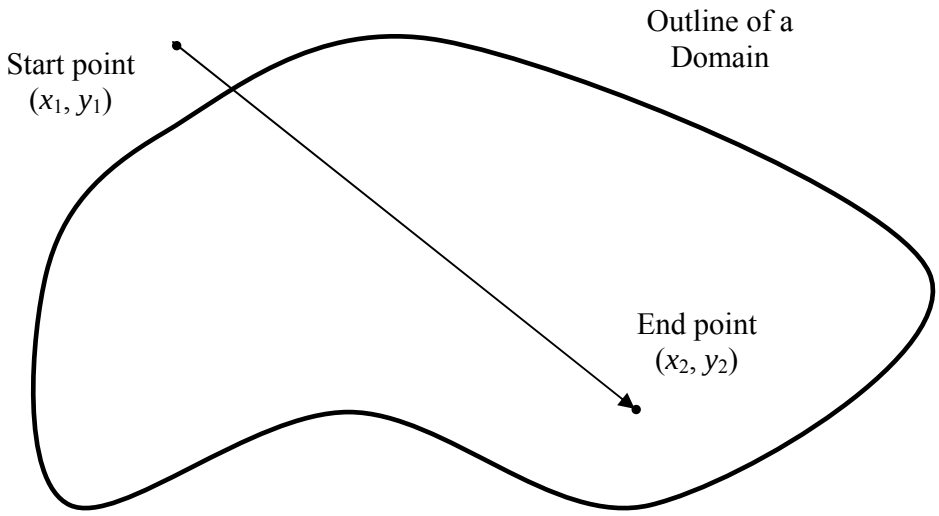

(a)

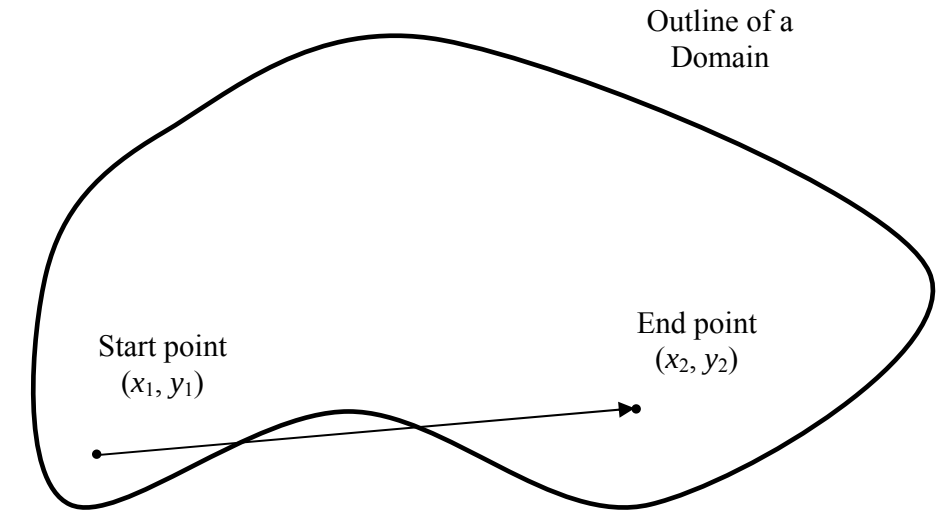

(b)

Figure 6.4 Examples of an infeasible straight monitoring line defined by the start and end points
(a) One of the end points is out of the domain, and
(b) a monitoring line intersects with the domain boundary.

6.2.2. Evaluation of straight monitoring lines

The evaluation of a straight line is similar to that of monitoring locations. The difference for straight monitoring lines is one more loop to take an average over series of deploying times. Also, a new preliminary step is necessary because the earliest arrival time for each node is not enough anymore.

As a preliminary step of the evaluation, the detection time windows at each node of a mesh are calculated instead of the earliest arrival times. The detection time window at a node is the time window when the concentration at the node is over a certain detection threshold as shown in Figure 6.5. Without this preliminary step, it is almost impossible to manage the vast amount of concentration data directly at the evaluation step. Once all the detection time windows are calculated, they can be used repeatedly to evaluate all the monitoring lines in a population.

After the preliminary step described above is finished, all the lines in a population can be evaluated based on the detection time window. First of all, the feasibility of a line is tested because the genetic operations may generate infeasible solutions. If a line is infeasible as described in the previous section, a penalty value is assigned and the evaluation is over.

If a line is feasible, then it is divided into several locations and corresponding times for detection test as shown in Figure 6.6. These discretized points of a monitoring line will be called waypoints later on. The speed of a vessel is assumed constant from the start point to the end point of a line without any interruption for simplicity. This assumption is reasonable because a vessel does not need to stop to measure if the measurement can be taken continuously using a continuous measuring device such as a

sensor. In the next step, the evaluation routine examines each waypoint on a monitoring line from the start point. One issue here is that the discretized waypoints to evaluate a line do not coincide with nodes in a simulation mesh where the concentration is known from the simulations.

Ideally, the concentration value at a waypoint at a certain time can be calculated via an interpolation procedure, but this may be computationally infeasible due to the vast amount of concentration data and geometrical calculation for an interpolation. One way to overcome this difficulty is to choose simplest interpolation, i.e. the nearest-point interpolation as shown in Figure 6.7. By adopting this interpolation, the complex interpolation that requires all the concentration data from the simulations can be avoided, and the detection time windows from the preliminary can be used directly.

Hence, the evaluation routine loops through the waypoints of a monitoring line, finds the nearest node from each waypoint, and check if the corresponding time at the nearest node is in the detection time window. If it is in detection time window, the time becomes a detection time, and the value is added for the average. If a monitoring line does not detect till the end of the line, it is a failure, and a penalty value is assigned for the detection time. The overall flowchart of this evaluation procedure is presented in Figure 6.8.

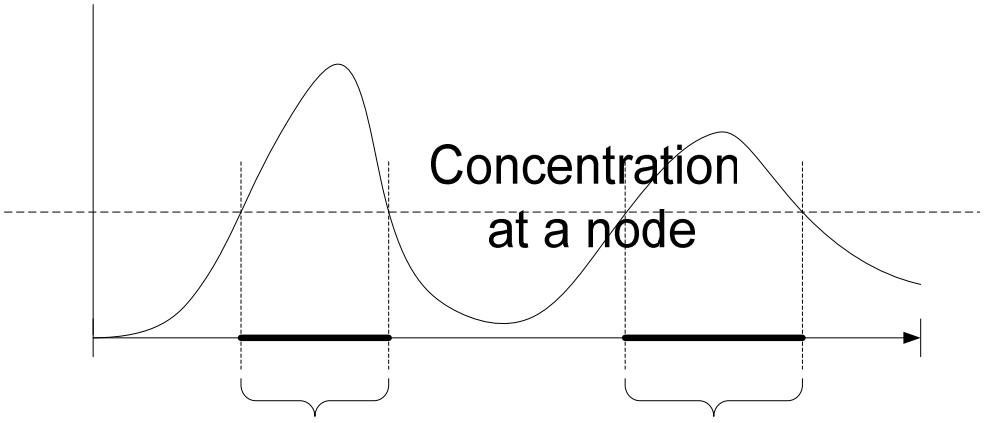

Figure 6.5 Concept of detection time window at a node

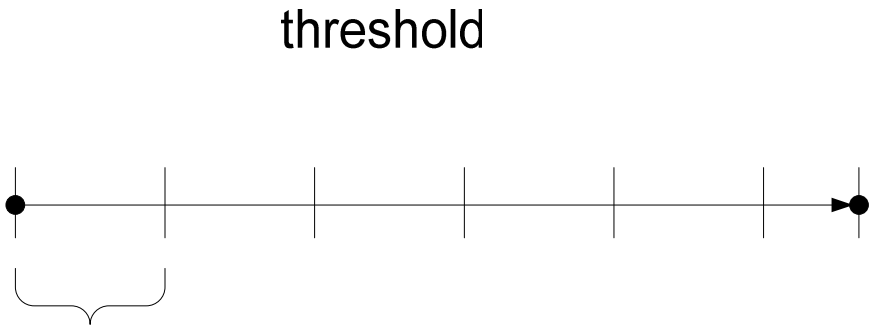

Figure 6.6 Dicretization of a line for the evaluation

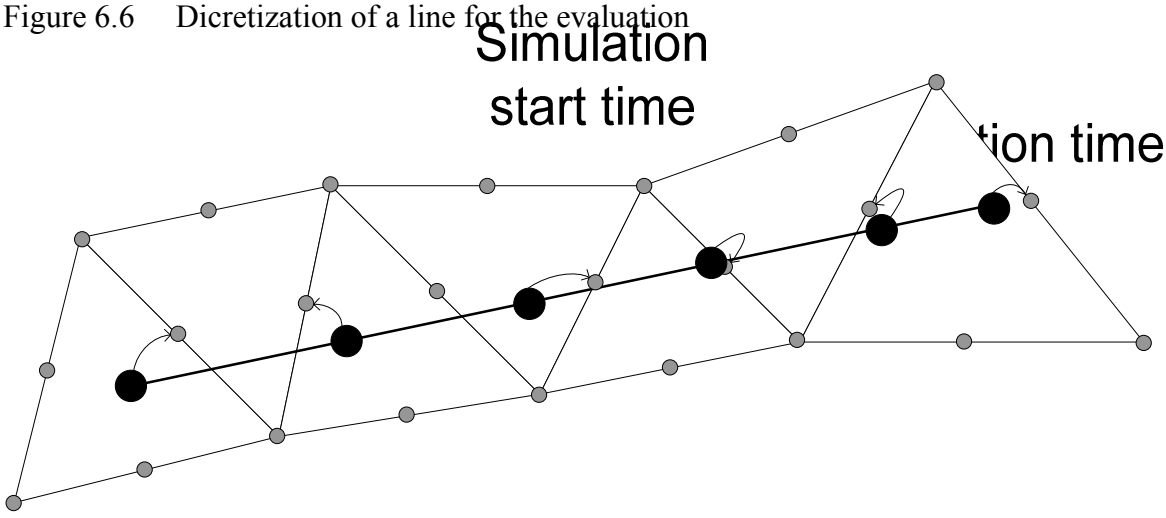

Figure 6.7 Approximation using the nearest-point interpolation

Start point and time

$\mathbf{x}_0, t_0$ $\mathbf{x}_1, t_1$ $\mathbf{x}_2, t_2$

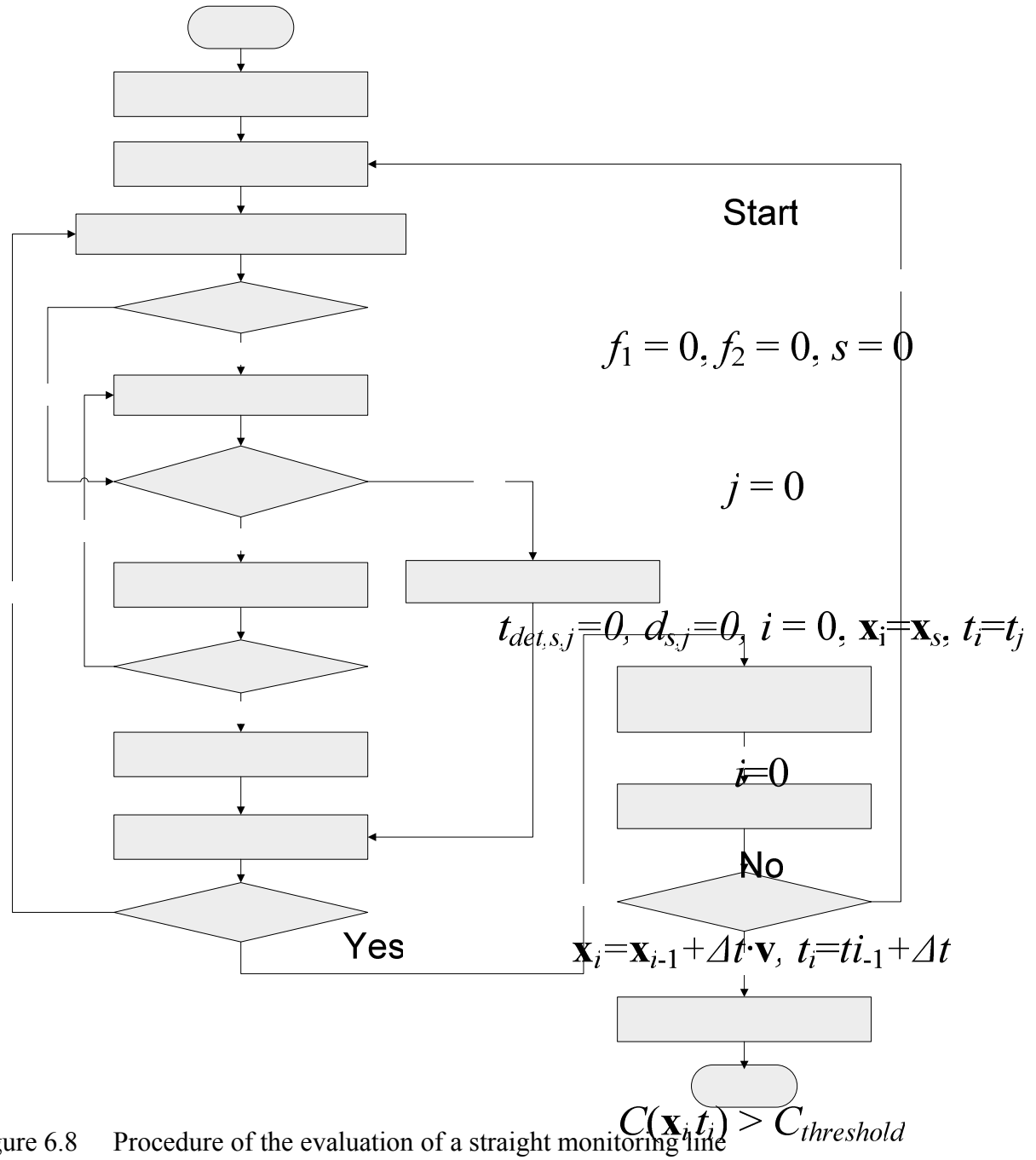

Figure 6.8 Procedure of the evaluation of a straight monitoring line

6.3. Test problems of monitoring lines

6.3.1. Circular lake

The same circular lake driven by a constant wind was adopted for a straight line optimization as well. A constant wind of 10 m/sec from east was imposed over a circular lake, and the flow reached to a steady state with two circulations. Total 128 contaminant spills around the lake were simulated as the whole possible scenarios.

Response to various numbers of scenarios

To investigate the behavior of optimal solutions first, optimizations of monitoring lines for one, two, three, and 128 around-the-shore contaminant scenarios were done. The mass of contaminant spill was 10 ton, and the detection threshold was 0.1 g/m^3, the detection time limit was 12 hours, the penalty for a detection failure was 12 hours, and the speed of the vessel was set 3 m/sec. The population in the genetic algorithm was 50, and the maximum generation was set as 200.

The results are presented in Figure 6.9 and Table 6.1. As shown in the figure, if there was only one possible source location, a monitoring line started downstream from the source location and moved up to the spill location. If there were two candidate spill locations, a monitoring line started from one of the locations and ended at the other. If there were three possible spill locations, a line was formed mainly by two spill location, and it passed where two circulation flows met on the west side of the lake. The detection likelihood dropped to 73 percent by missing one of the spills often. The numbers of obtained optimal solutions for one, two, and three scenarios were one for each.

If 128 spill scenarios around the shore were considered in the optimization, multiple optimal solutions were obtained, but all the solutions and their objectives were

very close. The comparison between the optimal solutions with the maximum detection likelihood and minimum detection time are presented in Figure 6.10. As it can be noticed, two solutions are very similar. Since the flow and possible contaminant spills were symmetric, the direction of the monitoring line was not important.

Table 6.1 Optimal monitoring lines for various numbers of spill scenarios in a wind driven circular lake

The number of scenarios for the optimization	Estimation of detection time with penalty (hr)	Estimation of detection likelihood (%)	Figure
1	5.704	100.0	Figure 6.9 (a)
2	6.066	97.9	Figure 6.9 (b)
3	8.060	73.1	Figure 6.9 (c)
128 around the shore	9.609	49.12	Figure 6.10 (a)
	⋮	⋮	
	9.582	48.489	Figure 6.10 (b)

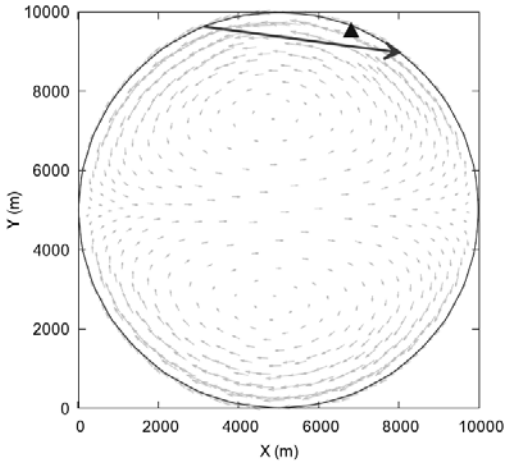

(a)

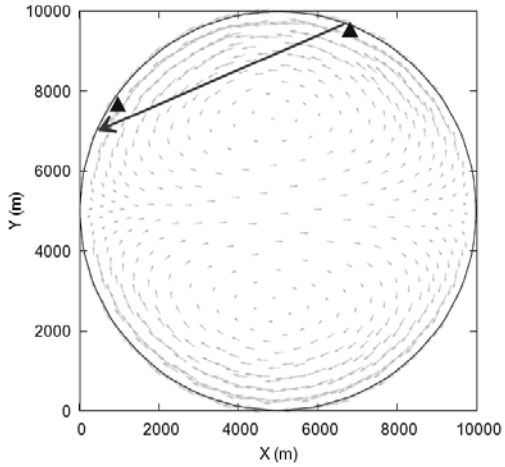

(b)

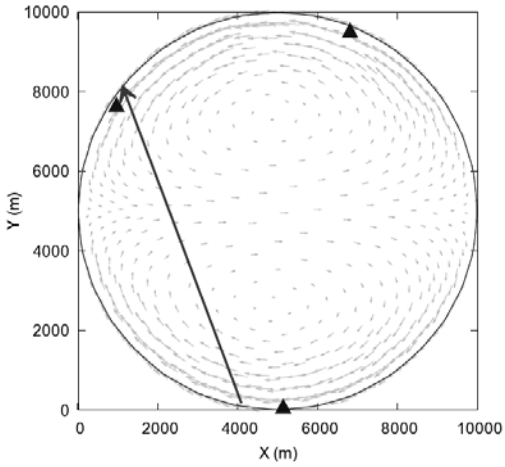

(c)

Figure 6.9 Optimal monitoring lines for various numbers of scenarios in a wind-driven circular lake
(a) one scenario, (b) two scenarios, (c) three scenarios, (Triangles: Sources)

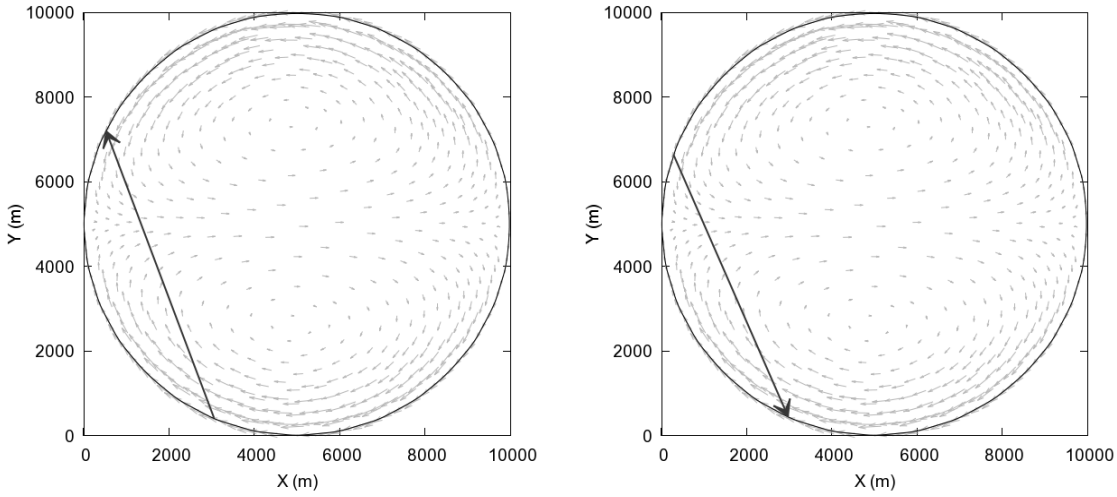

Figure 6.10 Comparison between the solutions with maximum detection likelihood and minimum detection time in a wind-driven circular lake with 128 scenarios around the lake
(a) maximum detection likelihood and (b) minimum detection time

Effect of the detection time limit

To investigate the effect of the detection time limit on the optimal solutions, 6 and 3 hours of the detection time limit were given to the optimization routine with the same other parameters used above. The penalties for detection failure were also adjusted to 6 and 3 hours respectively.

For 3 hour detection time limit, only one optimal solution was obtained. Multiple solutions for 6 and 24 hour detection time limit were obtained as shown Figure 6.1 and Table 6.2., but the objective values of the solutions were very close. In general, if the detection time limit was short, the detection likelihood was degraded quickly. Also, as detection time limit got shorter, an optimal monitoring line became shorter, and the solutions started and ended where a contaminant could be most likely detected, in this

case the west end of the lake. In other words, a monitoring line behaved like a stationary monitoring location. Hence, a very short detection time limit for the optimization of a monitoring line may not be suitable.

Table 6.2 Optimal monitoring lines with respect to different detection time limit in a wind-driven circular lake

Detection time limit (hr)	The estimation of detection time with penalty (hr)	The estimation of detection likelihood (%)	Figure
3	2.648	23.31	Figure 6.11 (e)
6	5.122	33.09	Figure 6.11 (c)
	5.121	32.23	
	5.120	32.05	Figure 6.11 (d)
24	17.17	69.45	Figure 6.11 (a)
	⋮	⋮	
	17.11	69.07	Figure 6.11 (b)

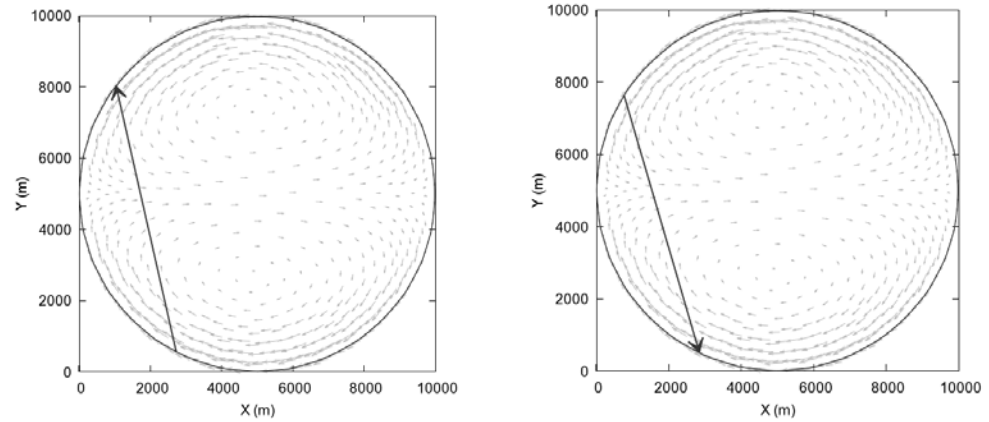

(a) (b)

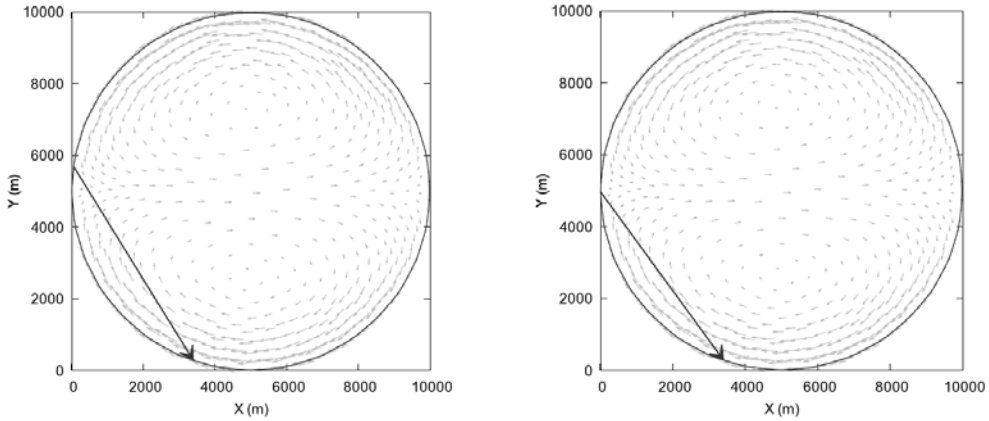

(c) (d)

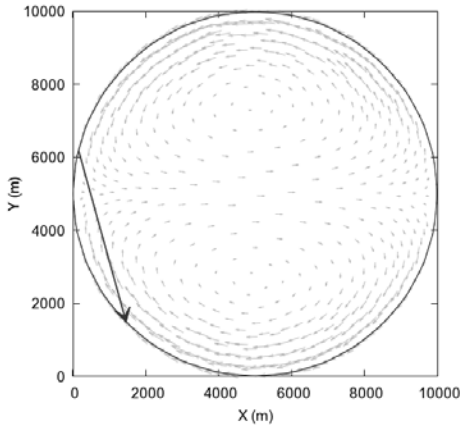

(e)

Figure 6.11 Optimal monitoring lines with respect to different detection time limit in a wind-driven circular lake with 128 scenarios around the lake
(a) detection time limit 24 hrs, maximum detection likelihood,
(b) detection time limit 24 hrs, minimum detection time,
(c) detection time limit 12 hrs, maximum detection likelihood,
(d) detection time limit 12 hrs, minimum detection time, and
(e) detection time limit 3 hrs

The objective values of the optimal monitoring lines can be compared with the stationary monitoring locations in the previous chapter. For example, the optimal solutions of monitoring locations and a monitoring line with the same 128 scenarios are compared and presented in Table 6.3. If a detection time limit was as short as 3 hours, the detection time of the three monitoring locations and the monitoring line were close, but the estimation of detection likelihood of three monitoring location was better by 10 % than that of the monitoring line. However, when the detection limit was 24 hours, the network of monitoring locations performed much better in both of the objectives than the monitoring line did. Hence, it can be stated that a straight monitoring line did not perform very well in this case.

One reason why the monitoring line performed badly was mainly because of the geometrical constraint of a straight line to follow. In this problem, a contaminant was spilled on the shore, and it traveled along the shoreline. This means that a monitoring vessel should travel closely to the shoreline to detect the change of water quality, but it was not possible for a straight monitoring line due to the circular shape of the lake. However, only one monitoring vessel was used in this case, and a monitoring line is flexible so that it should not be underestimated. Furthermore, multiple vessels may be utilized at the same time, and the performance would be comparable to a network of stationary monitoring locations.

Table 6.3 Comparison of the solutions of monitoring locations and monitoring path

	The detection time limit (hr)	The estimation of detection time with penalty (hr)	The estimation of detection likelihood (%)
3 monitoring locations	3	2.349	34.4
	24	6.25	100.0
A monitoring line	3	2.648	23.3
	24	17.17	69.45

Effect of the speed of a vessel

Another design factor for a monitoring line is the speed of a vessel. To investigate the effect of the speed of a monitoring vessel, different speeds were applied for the optimization. The detection time limit was 6 hours. The other parameters were kept the same as the previous cases.

The results are presented in Table 6.4 and Figure 6.12. As shown in the results, as the speed of a vessel increased, the estimation of the detection likelihood increased. When the speed of a vessel is high, the vessel can cover a long distance within a short amount of time, and the detection likelihood increases in result as shown in the table. However, the estimation of the detection time did no change much. Hence, high speed of a vessel is desirable especially in terms of detection likelihood.

The pattern of the optimal lines did not change except when the speed of a vessel is very low. It suggests that the optimal monitoring lines are determined mainly by the

locations of contaminant sources not by the speed of a vessel. The estimation of detection time did not vary much by the different speed of a vessel.

When the speed was very small, the vessel even could not travel enough distance in the given detection time limit and it became a constraint. For example, when the speed of the vessel was 0.1 m/sec, the maximum distance that the vessel could travel in 6 hours was 2.16 km, and this was one fifth of the diameter of the lake. In result, the optimal solutions with the speed of 0.1 m/sec were significantly shorter than the other solutions, and the patterns of them differed from the others as well.

Table 6.4 Optimal monitoring lines with respect to different vessel speed in a wind-driven circular lake

The speed of a vessel (m/sec)	The estimation of detection time with penalty (hr)	The estimation of detection likelihood (%)	Figure
0.1	5.374	14.52	Figure 6.12 (a)
	⋮	⋮	
	5.374	14.46	
1	5.115	28.71	Figure 6.12 (b)
	5.112	28.70	
10	5.158	34.48	Figure 6.12 (c)

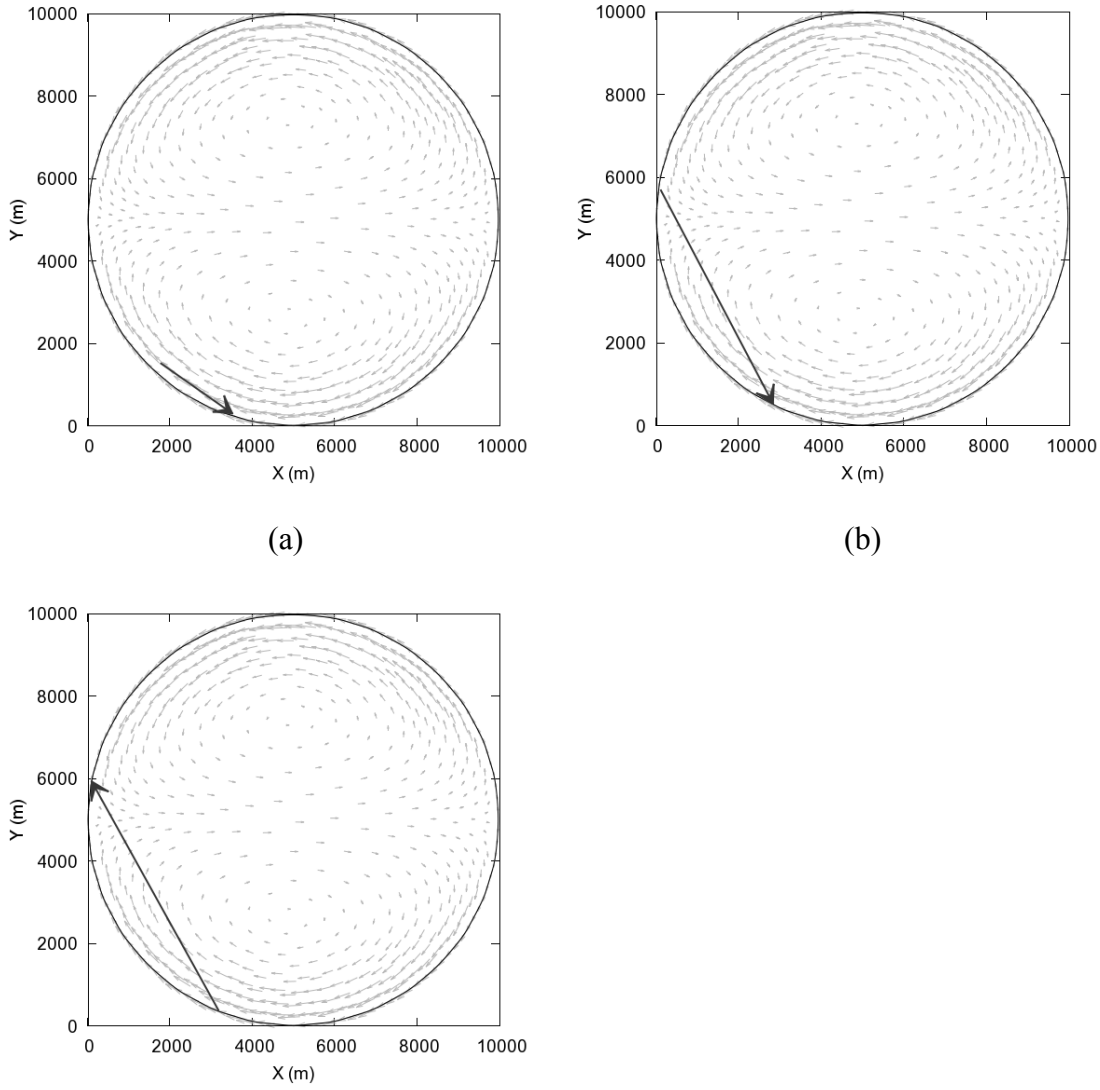

Figure 6.12 Optimal monitoring lines with respect to different vessel speed in a wind-driven circular lake
(a) 0.1 m/sec, (b) 1 m/sec, and (c) 10 m/sec

Effect of the weight

To investigate the effect of the weight of scenarios, one of 128 spill scenarios was given more weight as done in the previous chapter for the optimization of stationary monitoring locations. The location of the weighted spill was on the northwest shore

where was far from the optimal monitoring lines without weight. The detection time limit was 6 hours.

The results are presented in Table 6.5 and Figure 6.13. Five optimal solutions were obtained for the case with 10 times weight, but all the solutions were very similar. Comparing these solutions with the previous case without weight in Table 6.2, no big difference in the locations of the lines was observed, but both of the objective values were slightly degraded due to missing the weighted spill scenario. When the weight was increased to 11, two different types of optimal solutions were observed among 9 optimal solutions. One was close to the solutions without weight, and the other was a new solution that ends at the location of the weighted spill. When the weight was increased to 12, two different types of optimal solutions were observed among seven optimal solutions, but more than half of them were the new type of solutions that end at the location of the weighted spill. When the weight was increased to 20, which means that this spill scenario could happen 20 times more likely than the others, only one optimal solution was obtained, and the line ended around the location of the weighted spill. This solution is similar to the optimal solution for just one spill scenario.

As it shown, the optimal lines changed rather abruptly from the optimal solution without weight to the optimal solution with weight. When a small weight was imposed on a spill, the optimal monitoring lines without weight were maintained. Once the loss in the objectives by missing the weight spill scenario overwhelmed the gain in the objectives by maintaining the old solution without weight, the old solutions were replaced with the new solution.

Table 6.5 Comparison of optimal monitoring line with respect to different weight

Weight	The estimation of detection time with penalty (hr)	The estimation of detection likelihood (%)	Figure
10	5.200	30.83	Figure 6.13 (a)
	⋮	⋮	
	5.157	28.06	
11	5.049	30.56	Figure 6.13 (b)
	⋮	⋮	
	5.136	28.63	Figure 6.13 (c)
12	5.202	30.27	
	⋮	⋮	
	5.121	29.19	
20	4.977	33.66	Figure 6.13 (d)

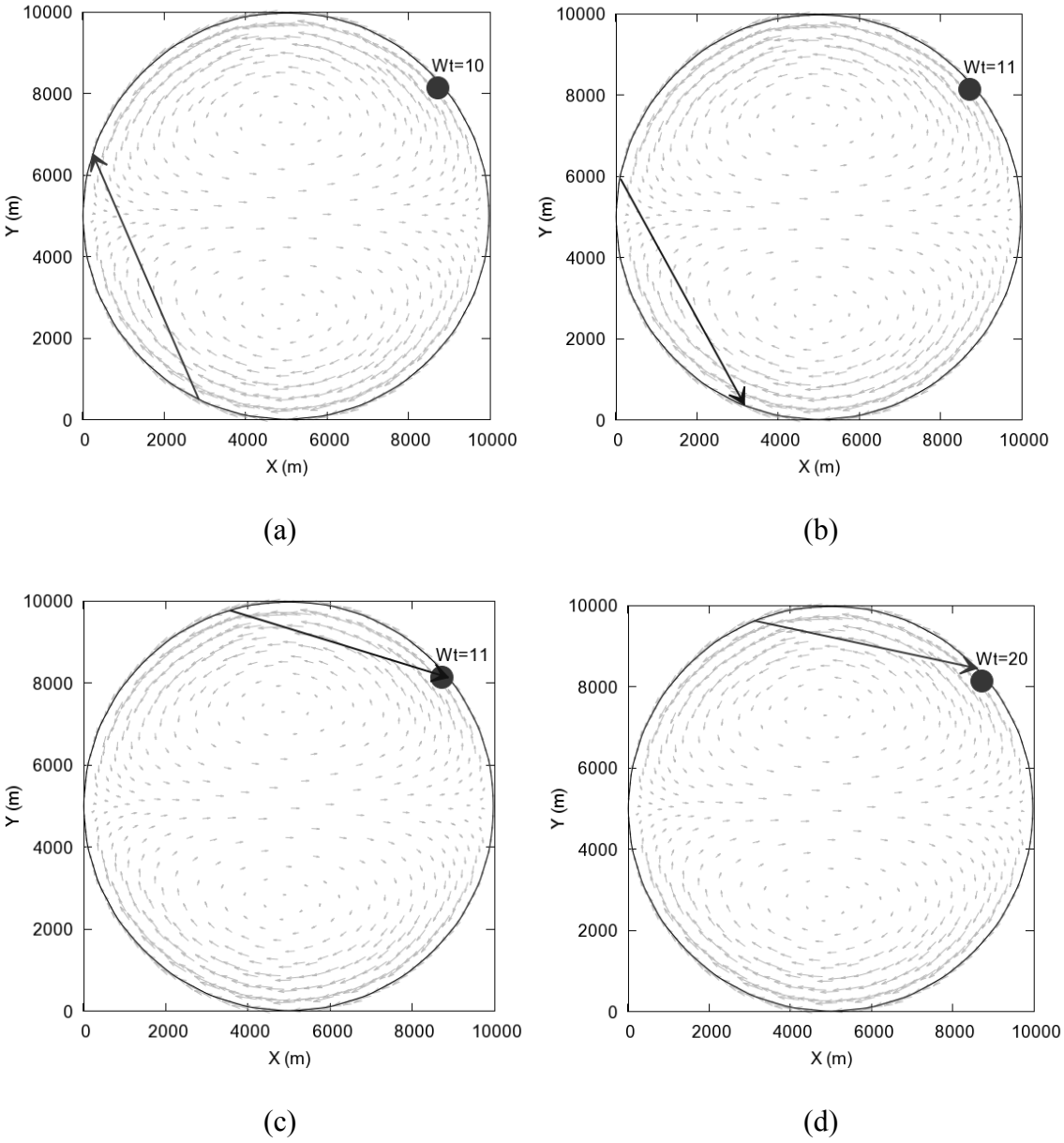

Figure 6.13 Comparison of optimal monitoring line with respect to different weight (a) 10 times weight and (b) 20 times weight on the spill at the dot

Summary

The optimization of a straight monitoring line was done in a wind-driven circular lake with possible spills all around the shore. To investigate the effect of parameters, parameters such as the speed of a vessel were adjusted for each optimization.

An optimal monitoring line tends to start or end where spills can be detected most likely. In this test case, it was the west end of the lake or where a high weight on a spill is given. If there was one spill scenario with high weight, a line was formed from downstream of the spill to the spill. Generally, the faster the speed of a vessel is the better optimal solutions perform because they can cover a wide area in a short amount of time. The weight on spill scenarios tends to change optimal solutions rather abruptly. The performance of a monitoring line was not high mainly due to the geometrical constraints, but it could be comparable with 3 or less monitoring locations when a short detection time limit was required.

6.3.2. Circular lake with tides

To investigate the effect of tides on the optimization of monitoring lines, the flat-bottomed circular lake with tides from the previous chapter was used. Since this case was not steady state case, many different scenarios that had same spill locations but different spill times were assumed as described in the previous chapter. The one hydrodynamics condition with tides of 20 cm amplitude was considered in the optimization. Hence, the number of scenarios used for the optimization was 240. The mass of the spills was 10 ton, and detection threshold was 0.1 g/m^3.

The results with the vessel speed of 3 m/sec were presented in Table 6.6 and Figure 6.14. The detection likelihoods were even lower than those of the previous circular lake under the constant wind because the flow speed in this case was lower than the previous case, and some contaminant was lost through the tidal inlet. The change in the detection time limit did not improve the detection likelihood much either. In some

cases, multiple optimal solutions were obtained, but the differences among them were very small.

To investigate the effect of the velocity of the vessel, the speed of 1 m/sec and 10 m/sec were applied for the optimization. The detection time limit was 6 hours for both cases. The results are presented in Table 6.7 and Figure 6.15. Similarly to the optimization in the wind-driven lake, as the speed of a vessel increased, the detection likelihood increased. Even though multiple optimal solutions were obtained, the differenced were very small. Also, the pattern of the optimal lines was not affected by the speed of a vessel similarly to the previous wind-driven lake case.

Table 6.6 Optimal monitoring lines in the circular lake with tides

The detection time limit (hr)	The estimation of detection time with penalty (hr)	The estimation of detection likelihood (%)	Figure
3	2.707	19.78	Figure 6.14 (a)
6	5.328	24.35	Figure 6.14 (b)
	⋮	⋮	
	5.320	23.51	
12	10.470	28.40	Figure 6.14 (c)
	⋮	⋮	
	10.455	27.84	

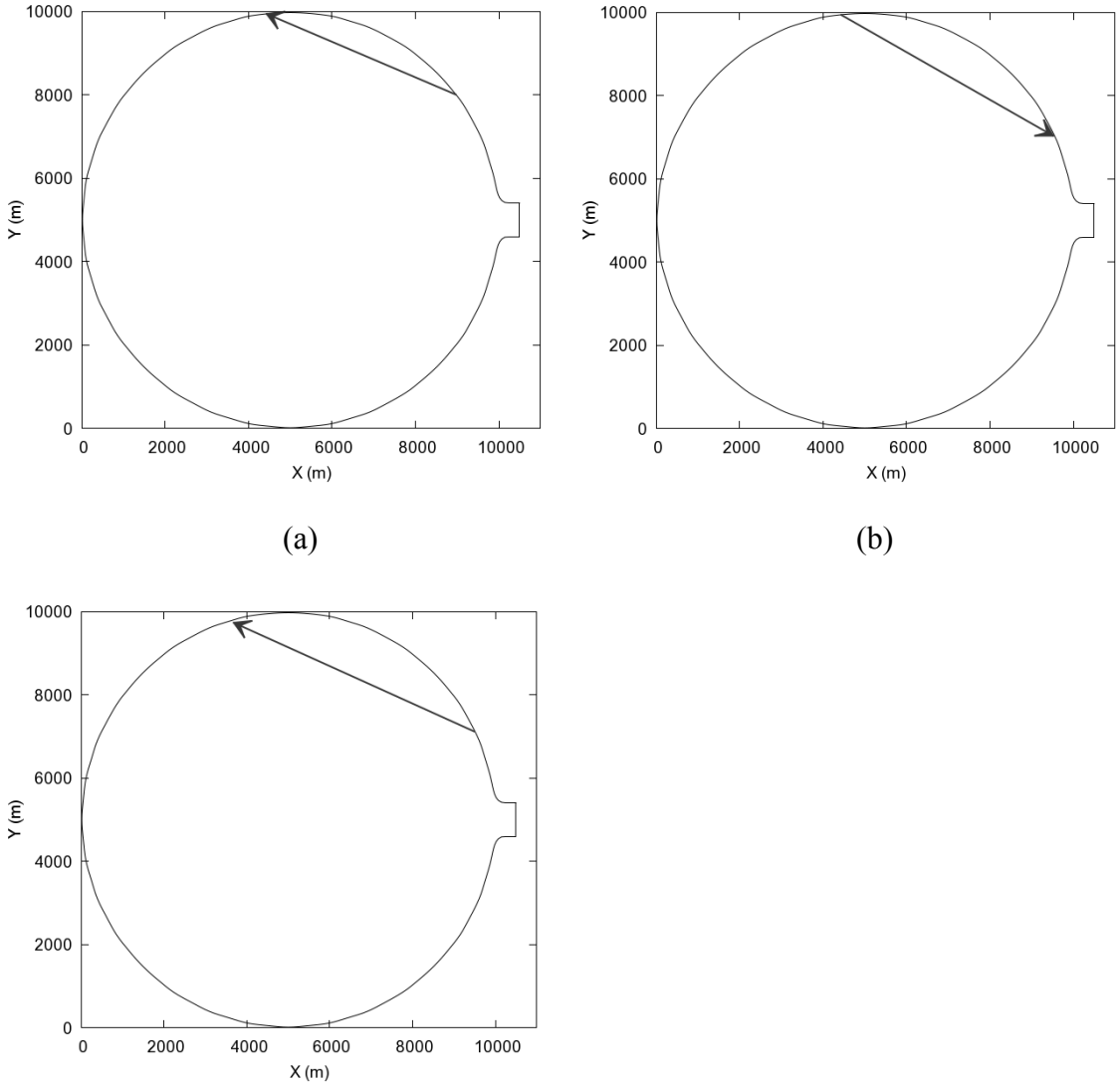

Figure 6.14 Optimal monitoring lines in the circular lake under tidal effect
(a) the best detection likelihood solution with 3 hr detection time limit,
(c) the best detection likelihood solution with 6 hr detection time limit, and
(d) the best detection likelihood solution with 12 hr detection time limit

Table 6.7 Comparison of optimal monitoring lines with respect to the speed of a vessel in the circular lake with tides

The speed of a vessel (m/sec)	The estimation of detection time with penalty (hr)	The estimation of detection likelihood (%)	Figure
1	5.314	22.31	Figure 6.15 (a)
	5.300	21.98	
10	5.367	24.33	Figure 6.15 (b)
	⋮	⋮	
	5.362	24.06	

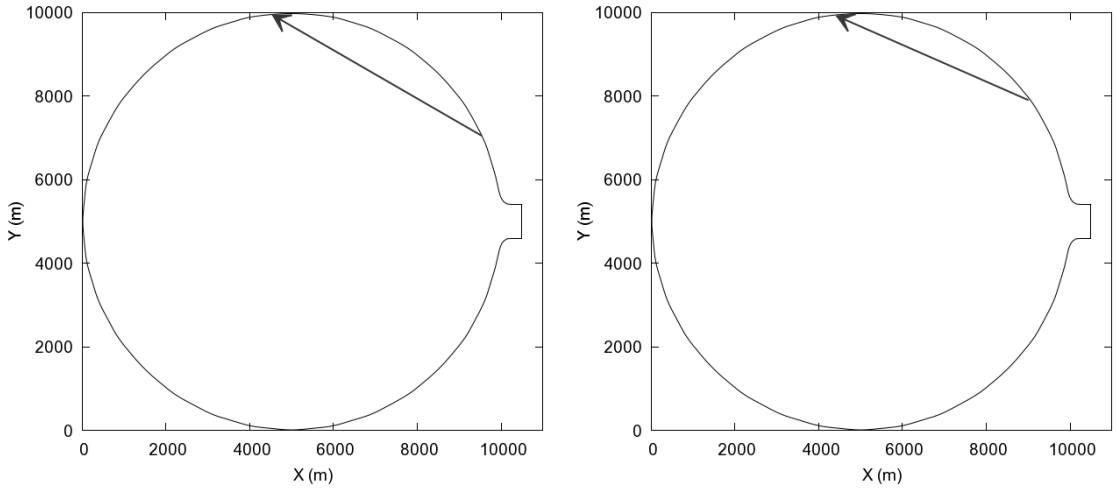

Figure 6.15 Comparison of optimal monitoring lines with respect to the speed of a vessel in the circular lake with tide
(a) the solution by 1 m/sec, and (b) the best detection likelihood solution by 10 m/sec

Because of the shape of the domain, slow transport of contaminant transport, and loss of the contaminant mass through the tidal inlet, the performance of the optimal solutions were low compared to the results of a wind-driven closed circular lake. Generally, optimal monitoring lines were obtained along the shore line near the tidal inlet. The direction of the monitoring was not critical. The detection likelihood increased as the speed of a vessel increased, but the effect was small.

6.4. Lake Pontchartrain

To apply the optimization routine for a real situation, Lake Pontchartrain was used. The same hydrodynamics and contaminant transport simulations described in the previous chapter were reintroduced for the optimization.

6.4.1. Wind-only case

As described in the previous chapter, wind is the major factor of hydrodynamics in Lake Pontchartrain. Hence, the optimization of monitoring lines was done with Lake Pontchartrain under a constant wind. A constant wind of 15 m/sec from southeast was given, and 20 possible source locations were selected as done in the previous chapter for the optimization of monitoring locations.

The mass of the spills was 1 ton, and the detection time limit was 12 hours. Since the scale of Lake Pontchartrain is larger than the hypothetical circular lake, slow vessel speed such as 1 km/hour is not meaningful. Two speeds were selected: 3 m/sec and 10 m/sec. With 10 m/sec, which is 36 km/hour, the optimization obtained one optimal solution with the detection likelihood of 31.60 % as shown in Table 6.8 and Figure 5.27. The line was formed where a straight line could pass near to as many source locations as possible. The direction of the monitoring line was against the flow direction. Even though

a monitoring line could travel from one end of the lake to the other in the given detection time limit, it did not happen. Instead, the optimal monitoring line picked where the most number of sources can be detected, and the length was restricted by the geometry of the lake. The effect of the velocity in this case was not significant as shown in Table 6.8. The pattern of the lines and the objective values were very similar as well.

These results tell that the initial design of possible sources is very important. Straight monitoring lines have geometrical restriction so that they tend to pick a few sources and abandon others. In result, a straight monitoring line is determined by a distribution of possible scenarios. Hence, if possible sources are not correctly proposed, the result can be unreliable.

Table 6.8 Optimal monitoring lines with respect to the speed of a vessel in Lake Pontchartrain under the constant wind

The speed of a vessel (m/sec)	The estimation of detection time with penalty (hr)	The estimation of detection likelihood (%)	Figure
3	9.9851	32.71	Figure 6.16
10	10.091	32.78	Figure 6.17
	10.072	32.50	

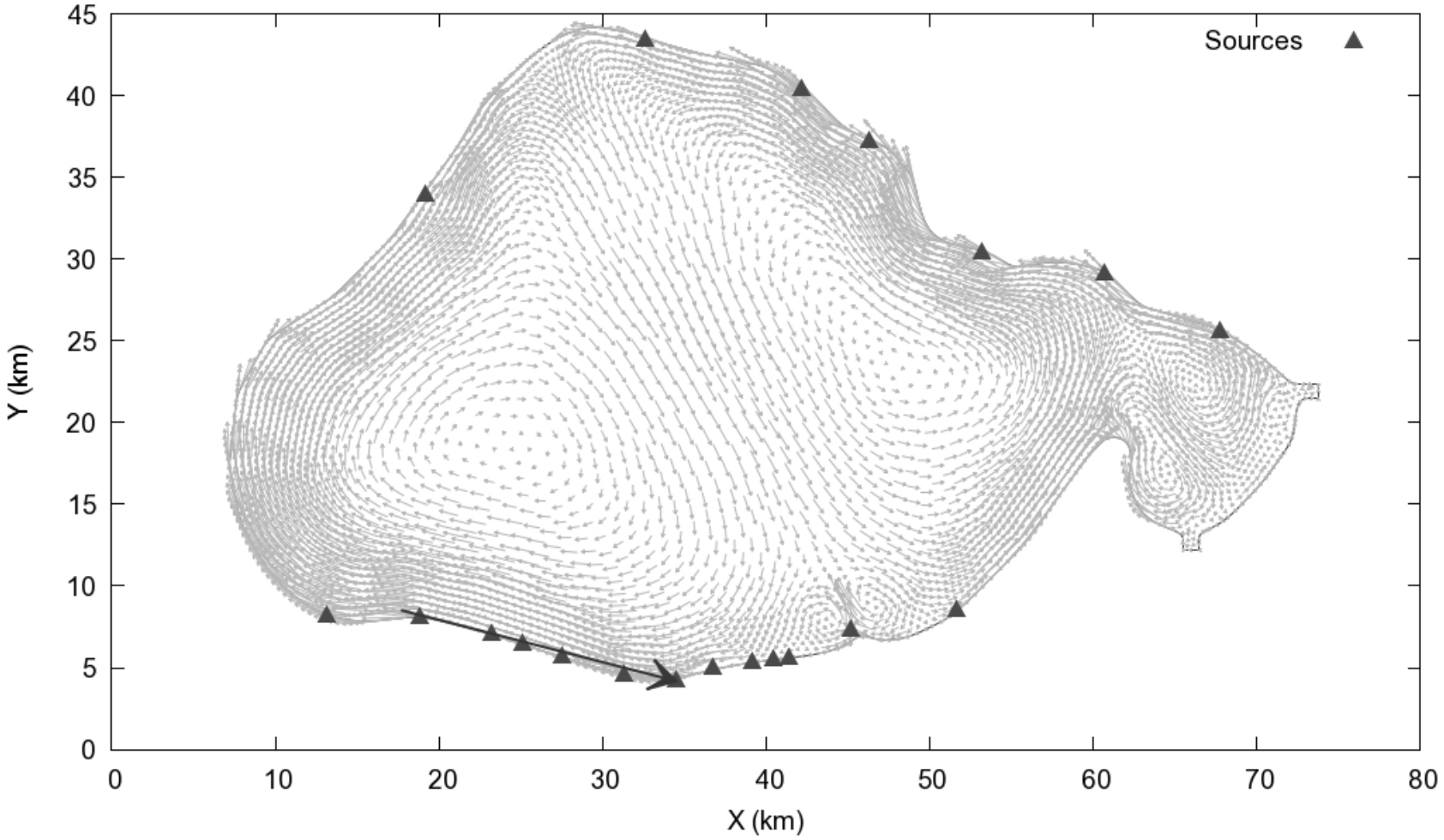

Figure 6.16 Optimal monitoring line in Lake Pontchartrain under the constant wind with the speed of 3 m/sec and detection time limit of 12 hours

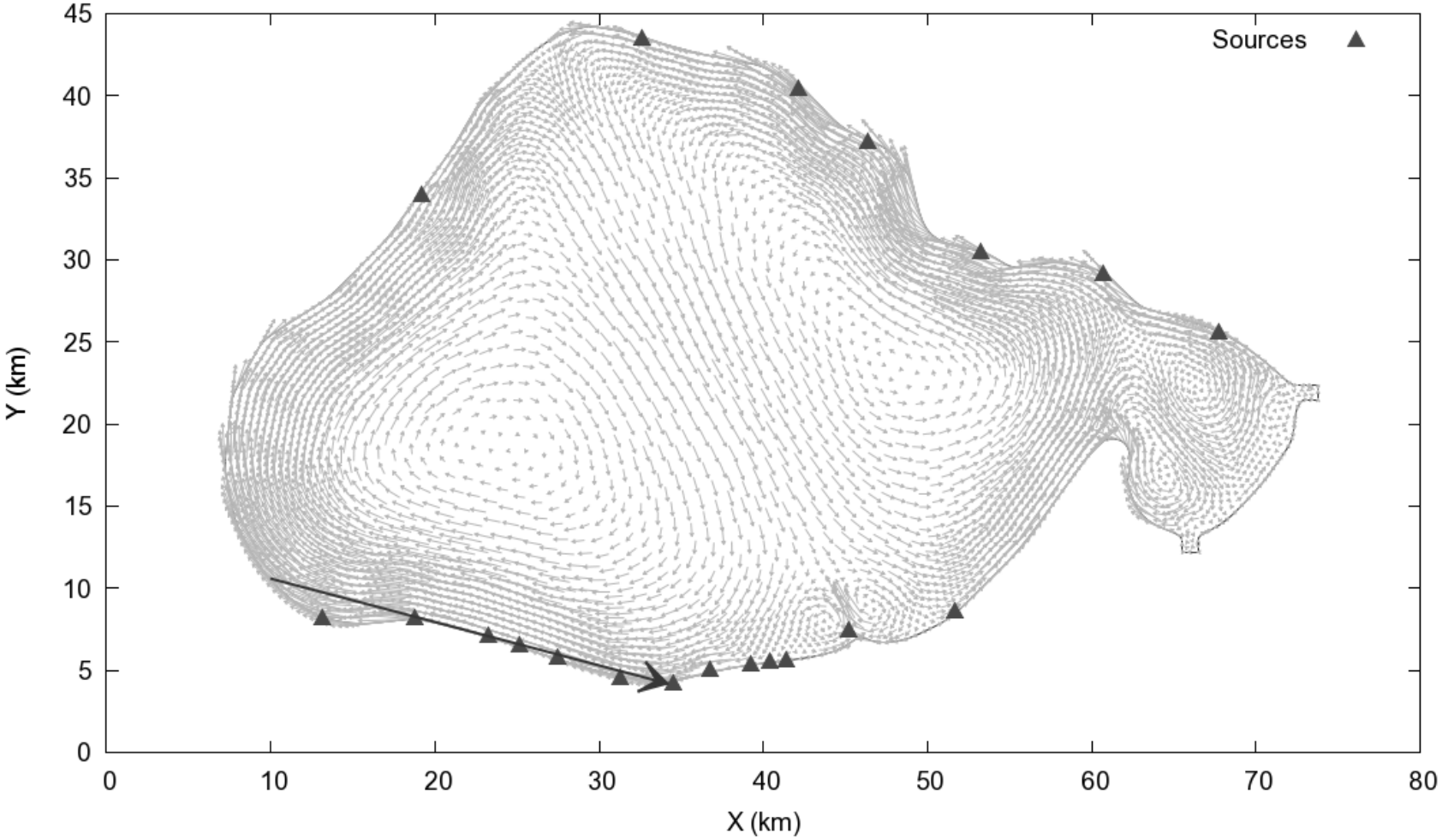

Figure 6.17 Optimal monitoring line in Lake Pontchartrain under the constant wind with the speed of 10 m/sec and detection time limit of 12 hours

6.4.2. Site-specific wind and tide case

The optimization of straight monitoring lines was done for Lake Pontchartrain with real wind and tide. The conditions for hydrodynamics were identical to the real-wind and predicted-tide case in Chapter 4. For contaminant scenarios, the same 20 possible spill locations as in the wind-only case of the previous section were selected. Then, 8 different spill times were selected for each spill locations so that the number of all scenarios was 160. These were the same scenarios used for the optimization of monitoring locations in Lake Pontchartrain in Chapter 5.

The results of the optimizations are presented in Table 6.9, and Figure 6.18. Only one optimal solution for each speed of a vessel was obtained. Similarly to the optimization of monitoring locations for Lake Pontchartrain in the previous chapter, the performance of the optimal monitoring lines with real wind and predicted tide was worse than those with constant wind because of many different scenarios. The optimal monitoring line with vessel speed of 3 m/sec under real wind and predicted tide was almost identical to that with constant wind. When the speed of the vessel increased, the performance maintained, but an optimal solution with different pattern was obtained as in Figure 6.18 (b). The optimization model chose this short line because other solutions had low performance as well.

Overall, the optimal monitoring lines were not very sensitive to the change of flow conditions, and instead it tended to pass through as many source locations as possible. Hence, even though the hydrodynamics varied, the optimal solutions were not affected much by them.

Table 6.9 Optimal monitoring lines with respect to the speed of a vessel in Lake Pontchartrain under the real wind and predicted tide

The speed of a vessel (m/sec)	The estimation of detection time with penalty (hr)	The estimation of detection likelihood (%)	Figure
3	10.371	26.43	Figure 6.18 (a)
10	10.610	26.38	Figure 6.18 (b)

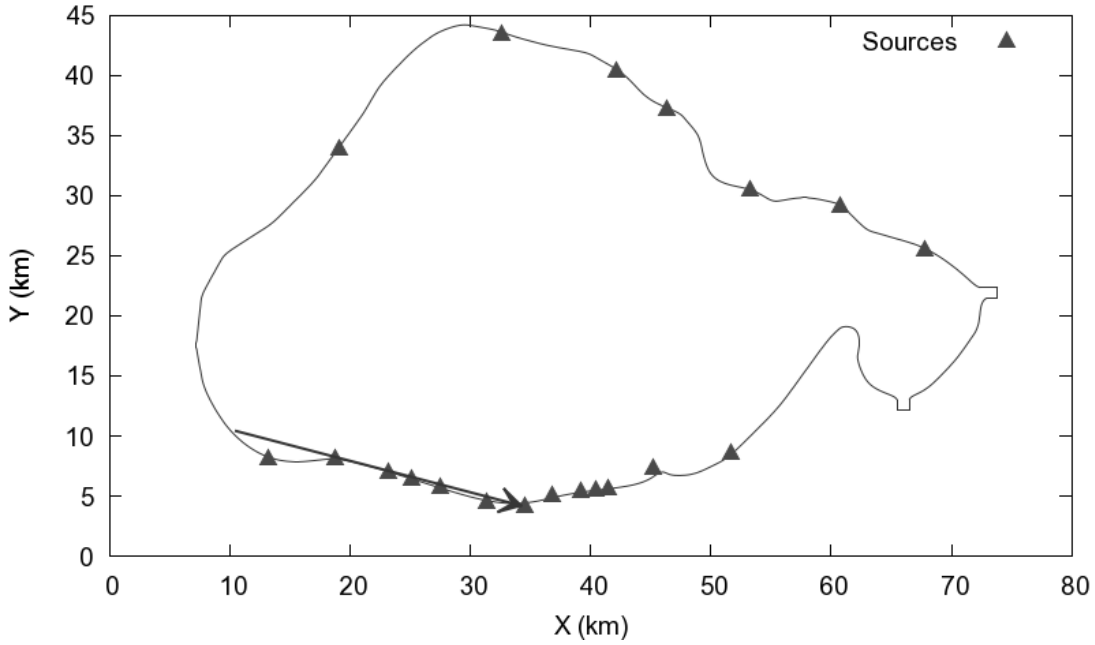

(a)

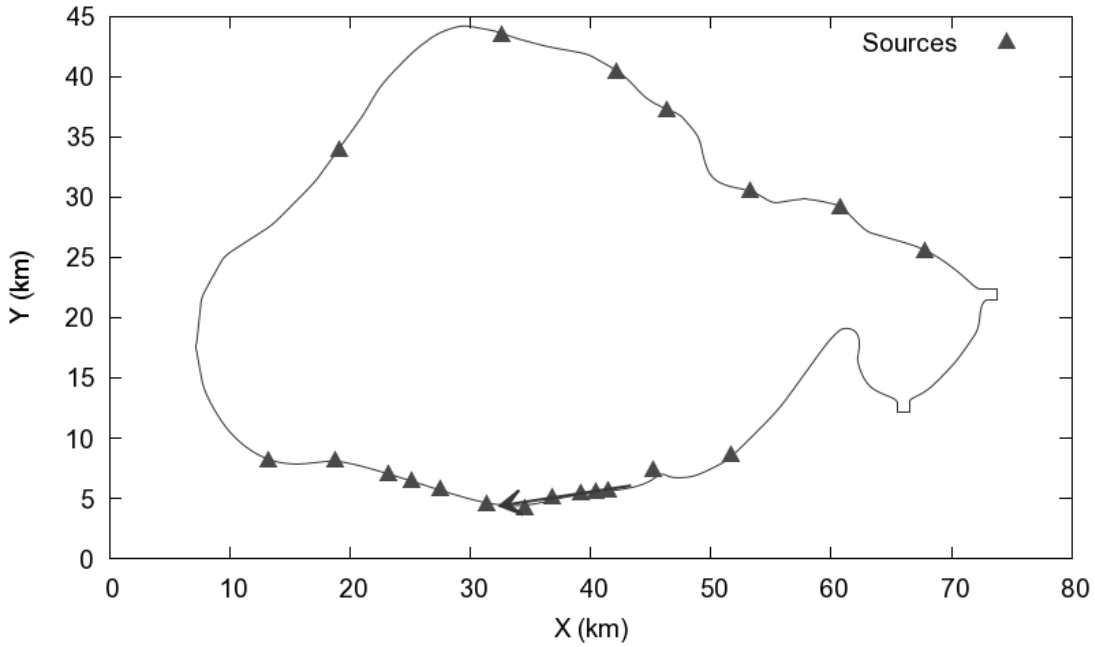

(b)

Figure 6.18 Optimal monitoring line in Lake Pontchartrain under the real wind and predicted tide with detection time limit of 12 hours
(a) vessel speed of 3 m/sec, and (b) vessel speed of 10 m/sec

6.5. Summary

To overcome the spatial restriction of stationary monitoring locations and to utilize advanced mobile monitoring system, an optimization routine to find the best straight monitoring line is proposed and tested.

The optimization model found straight optimal monitoring lines that passed through as many source locations as possible. Due to the geometrical restriction of a straight path, a straight line could not follow irregular shorelines where source locations were located, and the performance of optimal solutions was not high. However, the performance of some results was comparable to that of a few stationary monitoring locations.

The speed of a monitoring vessel was one important factor that affected the performance of optimal solutions in many cases. The higher the speed of a vessel was, the better performance of the solutions was obtained, generally. However, the improvement by increasing vessel speed did not show in Lake Pontchartrain cases. The effect of weights on optimal solutions was not large.

The performance of optimal straight monitoring line was not high, especially for complex real situations, and the optimal solutions were not sensitive to change of parameters.

CHAPTER 7

Optimal Design of Higher Order Monitoring Paths

7.1. Optimization model for a water quality monitoring path

Another type of mobile monitoring system that follows a free path instead of a straight line discussed in the previous section is what we call a higher order path that may be represented by a polynomial higher than a straight line although we are not going to use polynomials in defining these paths. Since a straight monitoring line has geometrical restriction, its performance is low especially when the shape of a domain is complex, and the contaminant is transported following the irregular boundary of the domain. A way to overcome this restriction is adopting a free form of a monitoring path that can follow any shape, thus the definition of a higher order monitoring path.

7.2. Implementation of the genetic algorithm for a monitoring path

The selected objectives of the design of a free monitoring path are: (i) detecting contaminants in a water body as soon as possible in order to minimize the area affected by contamination and to secure ample amount of time for appropriate response; and, (ii) maximizing detection likelihood. These are the same objectives for the previous monitoring location designs and straight monitoring line alternative discussed earlier.

The optimization problem of a monitoring path with these two main objectives can be mathematically stated as:

$$\min f_1 = \frac{1}{T_s}\sum_{j=1}^{T_s}\frac{1}{W}\sum_{s=1}^{N_s} w_s t_{d,s,j}(X) \tag{7.1}$$

$$\max f_2 = \frac{1}{T_s}\sum_{j=0}^{T_s}\frac{1}{W}\sum_{s=1}^{N_s} w_s \delta_{s,j}(X) \tag{7.2}$$

such that

$$\begin{aligned} X &= \overrightarrow{x_1 \ldots x_i \ldots x_n},\ 0 \le x_i \le x_{\max} \\ l_{\min} &\le \left\| \overrightarrow{x_1 \ldots x_i \ldots x_n} \right\| \le l_{\max} \end{aligned} \tag{7.3}$$

where

X = a monitoring path constructed by a sequence of monitoring points
x_i = nodal index as coordinate of a monitoring points
$x_{\max}$ = maximum nodal index number
$l_{\min}, l_{\max}$ = minimum and maximum length of a path
$t_{d,s,j}$ = detection time of j-th deployment of a scenario s if detected
otherwise a penalty value
$\delta_{s,j}$ = detection flag of j-th deployment of a scenario s
0 if not detect, 1 if detected
T = the set of the deploying times
$= \{t_1, t_2 = t_1 + \Delta t, \ldots t_j = t_j + (j-1)\Delta t, , \ldots t_{limit}\}, n(T) = T_s$
T_s = the number of deploying times per scenario
w_s = the weight of scenario s
$W = \sum_{s=1}^{N_s} w_s$ = the sum of weights of all scenarios
N_s = the number of scenarios.

The objective functions given above are identical to those for the straight monitoring line given in the previous chapter, but the decision variable is different. The length of a path is given as a constraint because the length of a path can be infinitely long without such a constraint. This was not a big concern for a straight monitoring line

because a straight monitoring line is always restricted by the geometry of the boundary of a domain.

The decision variable for this case is a free monitoring path defined by a series of integer node indices in a mesh. There are many possible ways to define a free path in a two-dimensional domain, but a free path constructed from a connection of dots are one of the easy ways even though it would not generate a smooth path. The other reason why this representation of a free path was selected is that a discretized mesh used for the simulations already consists of many nodes (or points) where the concentration values are calculated. Hence, using nodes from a mesh directly as possible waypoints and monitoring points of a free monitoring path, which a vessel will follow and take measurement along this path one by one as shown in Figure 7.1, is a computationally efficient way for the optimal solution of this problem. The reason why this is computationally efficient is because it can avoid any interpolation similarly to the straight monitoring line case. Also, this method can allow the pre-calculation of detection time windows in advance of the optimization, which is crucial for computational efficiency.

Then, the problem becomes similar to the famous traveling salesman problem (TSP) but with different objectives. In the case of TSP, the objective is usually travel length or cost of travel. TSP is a discrete or combinatorial optimization problem which is classified as NP-hard (nondeterministic polynomial hard, which means that no polynomial algorithm exists). Due to its complexity, many heuristic algorithms including genetic algorithms have been applied to solve it. The genetic algorithms have been used to solve TSP for a long time and have shown its capability very well (Goldberg, 1989).

The way of the genetic expression for a free monitoring path is based on series of nodal indices, which is similar to that used for the optimization of stationary monitoring locations in Chapter 5. The sequence of the nodes in a chromosome is not important for the optimization of monitoring locations, but it is important for the path optimization because a monitoring vessel will follow the nodes one by one. The number of genes in an individual chromosome can vary as well, and the maximum length constraint will limit the number of genes accordingly. Also, repetitive genes are allowed because a free path may have a loop.

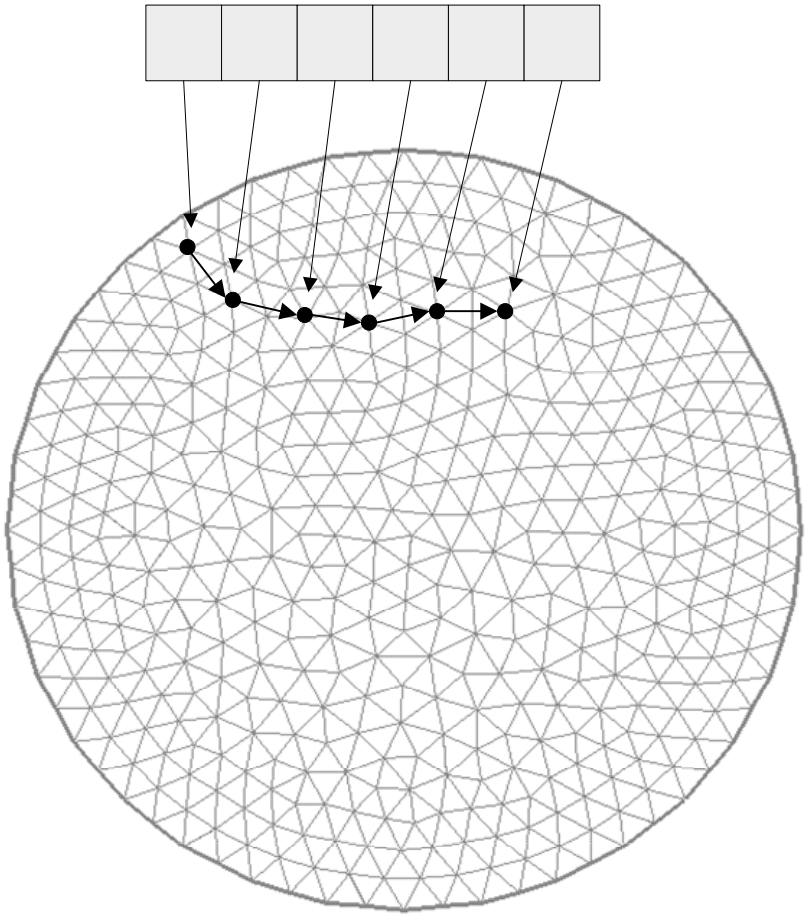

Figure 7.1 Example of a genetic expression of a path

Overall optimization procedure was written in C++ with PARADISEO library (Cahon, Melab, *et al.*, 2004). The code was compiled with G++ on RedHat Linux with Intel-family CPUs as done in the previous chapters.

7.3. Genetic operations for a monitoring path

The idea of the crossover and mutations are exchanging good traits of parents and adding new random information. However, if the traditional one point crossovers and/or random mutations are applied on individuals for paths, the goals of crossover and mutation operations stated above cannot be achieved because they will break paths, and desirable traits will not be preserved. For example, the one-point crossover happens at the same gene location of two individuals, and this may generate sudden jump of waypoints in the middle of paths. These sudden jumps – two waypoints separated by a long distance – are not desirable because an abrupt jump in a path means a long travel between two waypoints without measurement according to the genetic coding. Similar degradation of paths may be caused by the traditional mutation operation as well. Hence, crossover and mutation for paths need to be designed specifically to preserve desirable characteristics of individuals without generating sudden jumps.

The idea of a crossover operation to preserve the path trait is not new. In a routing problem such as the internet packet routing (Ahn and Ramakrishna, 2002), a crossover operation finds common genes of two selected parents first and exchanges information at one of the common gene locations. By selecting a common gene instead of a locus, a crossover operation can exchange information nicely without causing sudden jumps in offspring. In a traditional crossover operation on the other hand, a crossover operation picks random loci (locations in a chromosome) and exchanges information at the picked

loci, which generate abrupt jumps in offspring paths even though the parents do not have any abrupt jumps in themselves. A graphical example of the one-point crossover operation for paths is presented in Figure 7.2. As shown in the figure, the crossover operation may change the length of paths, but it maintains the geometrical traits of two parents well without generating abrupt jumps.

The mutation operation for a free monitoring path also needs to consider the geometrical traits of a path. First, locations for a mutation are selected just like the traditional mutation does. To prevent sudden jumps in offspring, candidate nodes within a given mutation radius from a previous and next waypoints of a mutation location are chosen, and the mutation occurs only among the candidate nodes. If a mutation node is either one of end points, only a previous or next node is used to find candidate nodes. This method guarantees that the distance between any of two consecutive waypoints always stays in the mutation radius. The graphical representation of the mutation process is presented in Figure 7.3.

Initial population is generated based on the same mutation rules described above. Then, all individuals in an initial population do not have sudden jumps. Consequently, as long as the crossover and mutation operations described above are applied on initial and subsequent populations, all generations will keep the same nice traits as well.

The selection and replacement strategies are the same as those for the monitoring locations: Stochastic tournament and $\mu + \lambda$ replacement, which are described in the previous chapter.

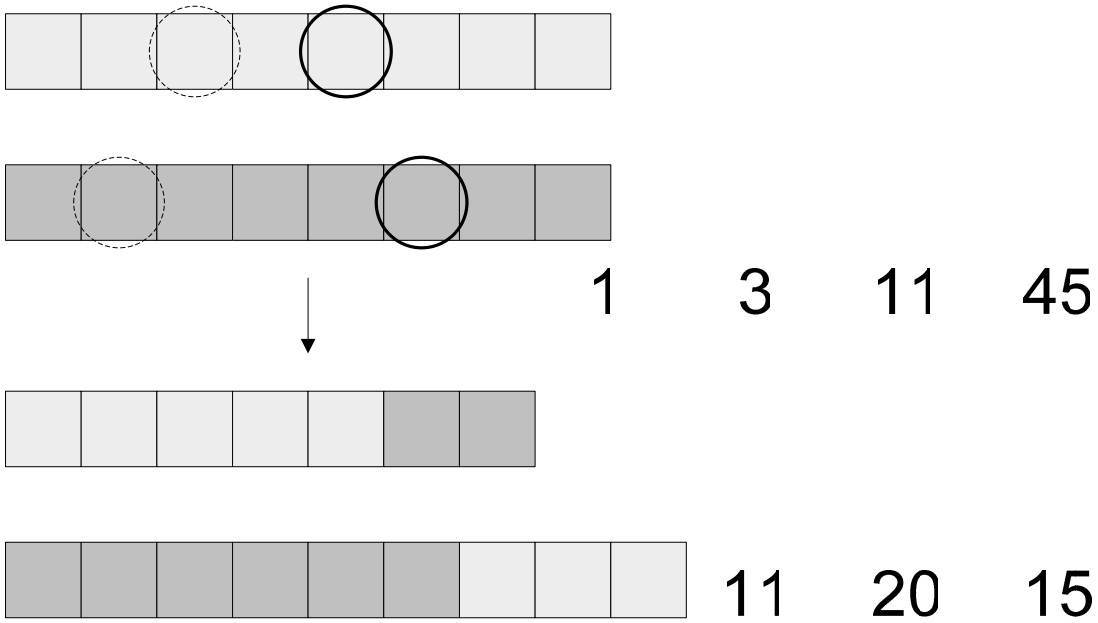

(a)

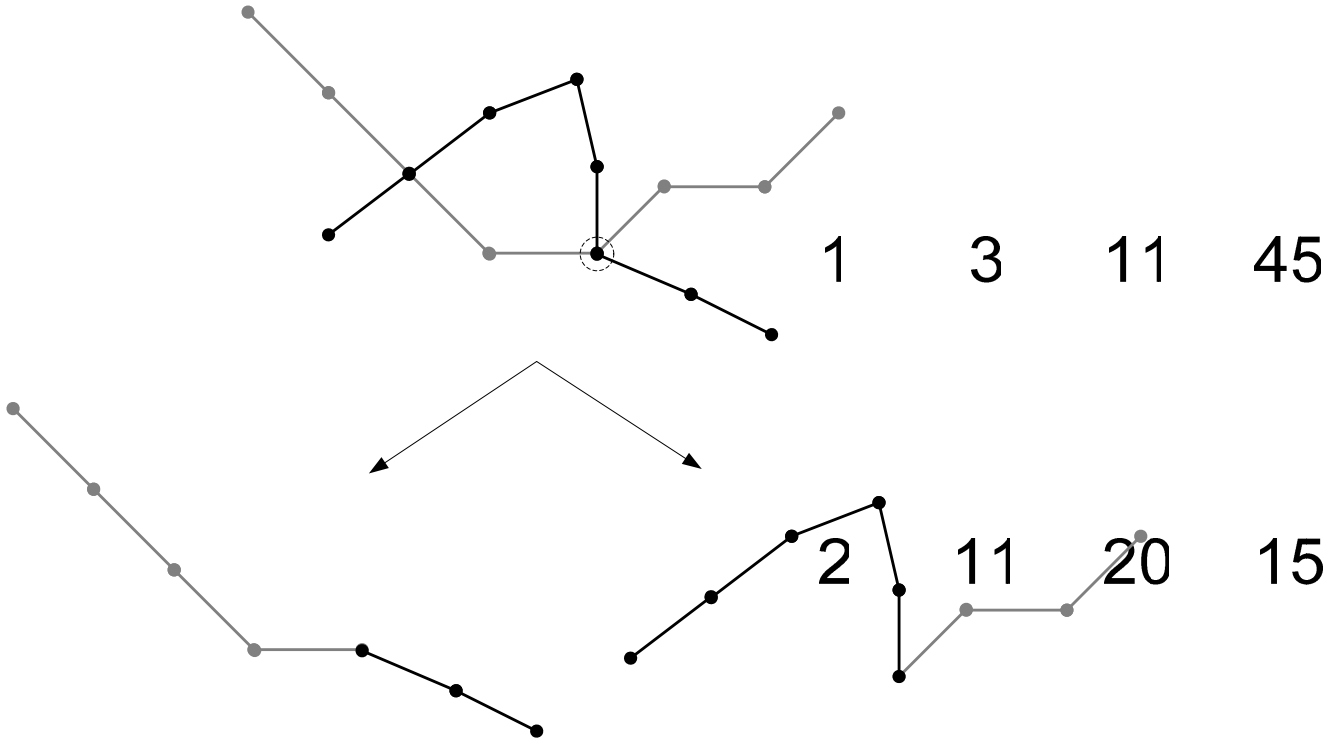

(b)

Figure 7.2 Example of the crossover operation for a path
(a) genetic coding, and (b) corresponding graphical representation

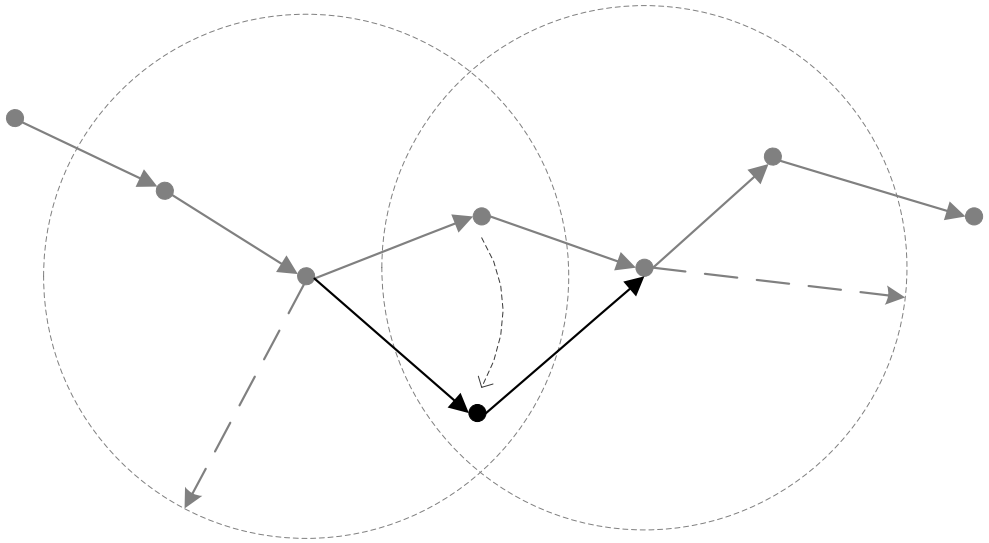

Figure 7.3 Example of the mutation operation for a path
(Gray lines are an old path, Dark lines are a newly mutated path. The mutation radius is r_m.)

7.4. Evaluation of a path

The evaluation procedure of monitoring paths is very similar to that of monitoring lines in the previous chapter. As a preliminary step, all detection time windows at every node are calculated before the optimization. The evaluation routine iterates from the first waypoint to the last waypoint and check if a contaminant can be detected at each r_m waypoint. Waypoints in a free path are given by a chromosome directly so that waypoints do not need to be derived. For the previous optimization for straight monitoring lines, waypoints between start and end points are generated. Corresponding time at each waypoint can be calculated by adding traveling time from one waypoint to a next one sequentially. The velocity of a monitoring vessel is set constant again for simplicity, and the traveling time between two waypoints can be calculated easily with the distance

between two consecutive waypoints and the velocity. The flowchart of the evaluation routine is presented in Figure 7.4

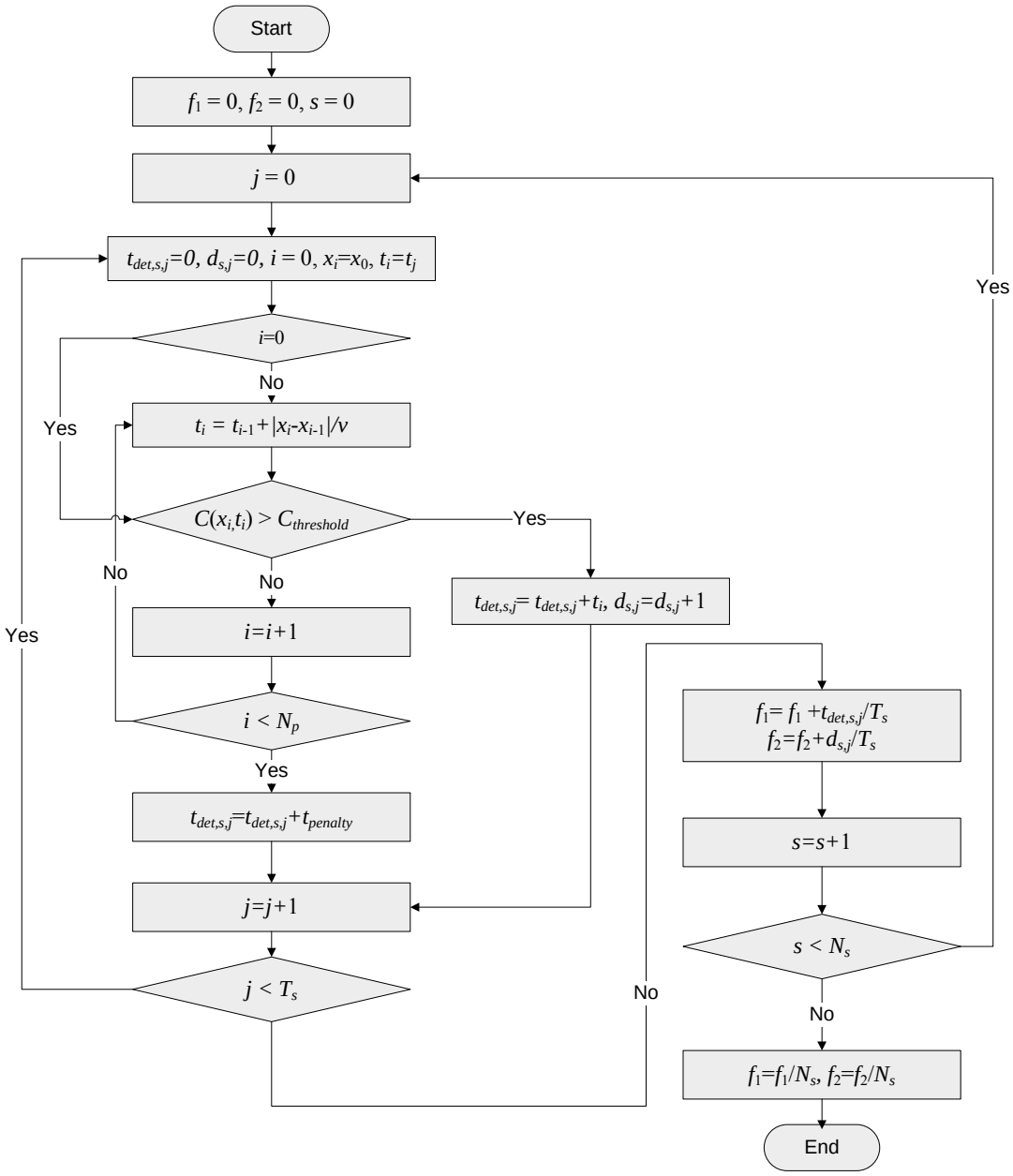

Figure 7.4 Flowchart of evaluation procedure for a monitoring path

7.5. Test problems of monitoring paths

7.5.1. Wind-driven circular lake

The same circular lake case with a constant wind from east used in the previous chapter was adopted again to test the path optimization model. The diameter of the lake was 10 km, and the number of scenarios was 128.

The effect of path length

To investigate the effect of path length, the length constraint was adjusted, and other parameters were fixed. The speed of a monitoring vessel was set 3 m/sec, which is 10.8 km/hr, and the detection time limit was 24 hours. The penalty value for a non-detected scenario was set the same as the detection time limit, 24 hours. The minimum length was zero, and the two maximum lengths of 10.8 km and 21.7 km were selected. The two lengths were derived from the distance that a vessel can travel in one and two hours respectively by 3 m/sec speed. The results are presented in Table 7.1 and Figure 7.5.

It can be easily noticed that the optimal paths followed the shoreline and passed the far left side of the lake, where two flows from north and south met. The optimization model obtained multiple solutions, but the shapes of all the solution paths were very similar, as shown in the figures despite different parameters. The detection likelihood of longer paths was better than that of shorter paths because long paths could cover wider area. Hence, the lengths of optimal paths were very close to the maximum length.

It should be noted that the optimal monitoring paths performed better than the best straight monitoring lines did with similar parameters since a free path does not have a geometrical constraint. However, the optimal paths were not so simple that it may cause some trouble for a vessel to follow.

Table 7.1 Optimal solutions of monitoring paths with respect to different length restriction in the wind-driven circular lake with the detection time limit of 24 hours

Maximum length of the path (km)	The estimation of detection time with penalty (hr)	The estimation of detection likelihood (%)	Figure
10.8	6.434	74.87	Figure 7.5 (a)
	⋮	⋮	
	5.484	66.81	Figure 7.5 (b)
21.6	3.328	89.34	Figure 7.5 (c)
	⋮	⋮	
	3.028	83.51	Figure 7.5 (d)

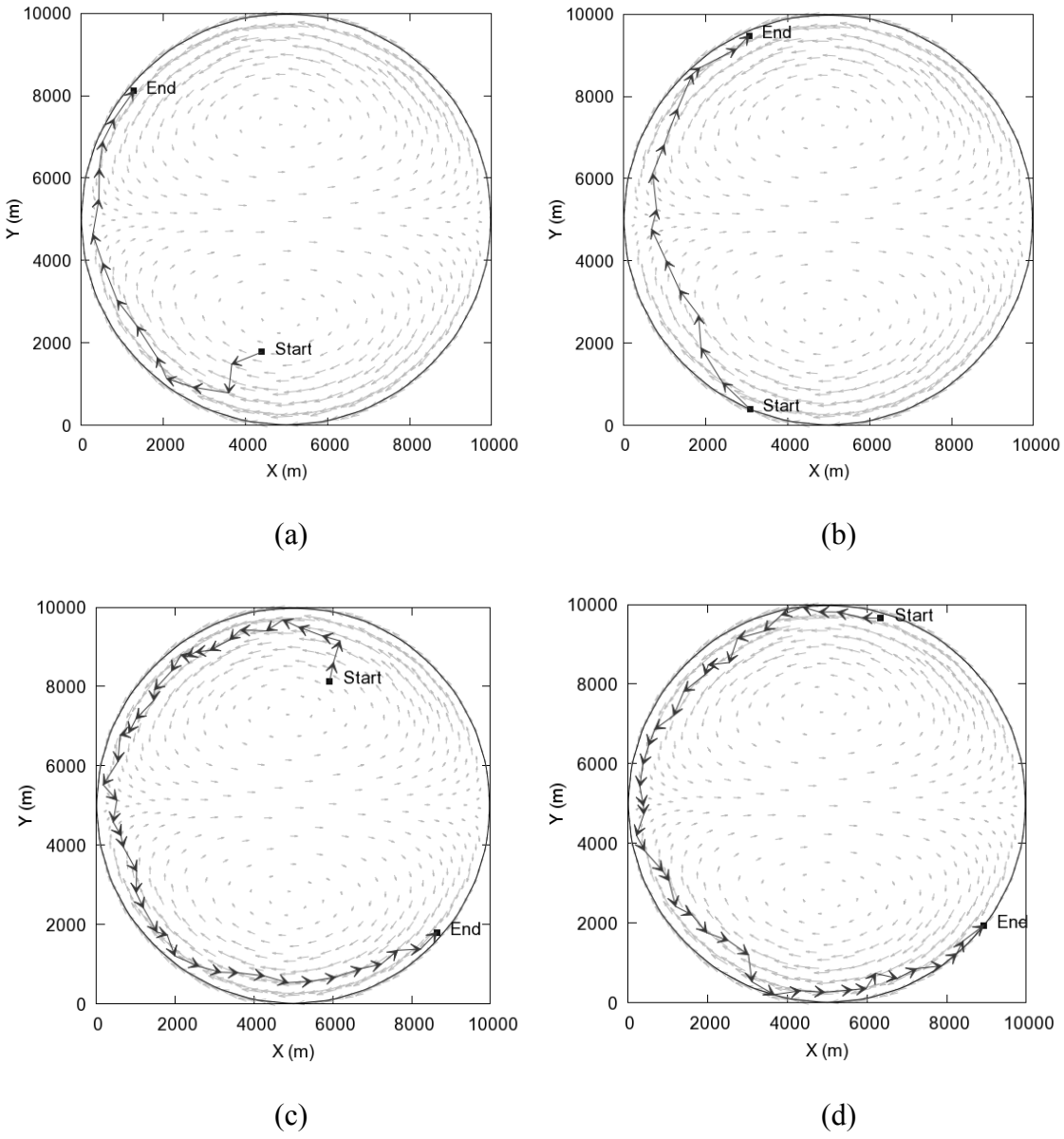

Figure 7.5 Optimal monitoring paths in a circular lake driven under a constant wind with the vessel speed of 3 m/sec and 24 detection time limit with 128 scenarios around the lake
(a) a short path with best detection likelihood,
(b) a short path with shortest detection time
(c) a long path with best detection likelihood, and
(d) a long path with shortest detection time

The effect of detection time limit

To see the effect of detection time limit on the optimal solutions and their performance, the detection time limit was adjusted to 3 hours from 24 hours of the previous case. The penalty value was adjusted to 3 hours as well. The results are presented in Table 7.2 and Figure 7.6. The shapes of the paths were basically the same as the previous results with the detection time limit of 24 hours, but the detection likelihood dropped significantly. Hence, the detection time limit does not affect the shapes of optimal paths necessarily, but the detection likelihood drops with shortening detection time.

Table 7.2 Optimal solutions of monitoring paths with respect to different length restriction in the wind-driven circular lake with detection time limit of 3 hr

Maximum length of the path (km)	The estimation of detection time with penalty (hr)	The estimation of detection likelihood (%)	Figure
10.8	2.043	38.25	Figure 7.6 (a)
	⋮	⋮	
	1.995	35.75	Figure 7.6 (b)
21.6	1.839	61.84	Figure 7.6 (c)
	⋮	⋮	
	1.767	59.02	Figure 7.6 (d)

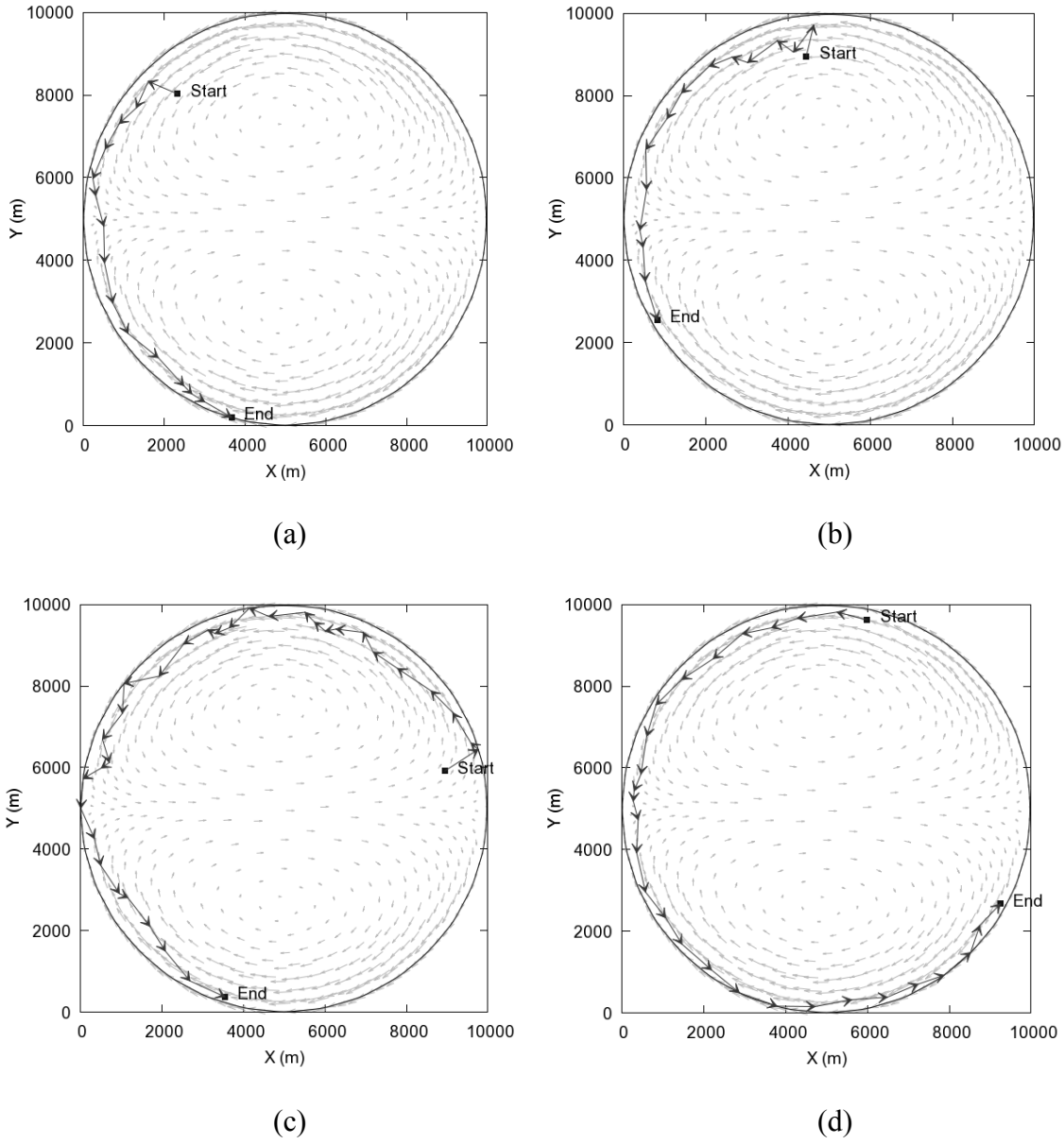

Figure 7.6 Optimal monitoring paths in a circular lake driven under a constant wind with the vessel speed of 3 m/sec, the detection time limit of 3 hours, and 128 scenarios around the lake
(a) a short path with best detection likelihood,
(b) a short path with shortest detection time
(c) a long path with best detection likelihood, and
(d) a long path with shortest detection time

The effect of the speed of a vessel

Another factor in the monitoring path optimization is the speed of a vessel. To investigate the effect of the speed of a vessel, the speed of the vessel increased to 10 m/sec, which is 36 km/h. The detection time limit was 3 hours. The other parameters were kept the same.

The results are presented in Table 7.3 and Figure 7.7. As shown in the figure, a vessel now can travel 36 km per hour, and a vessel can travel more than the circumference of the lake with the diameter of 10 km in an hour. The optimal paths follow the shore of the lake. If a vessel can run two hours, the boat traveled twice around the lake.

The optimal solutions with higher speed (10 m/sec) and shorter detection time limit (3 hours) had better performance than those with slower speed (3m/sec) and longer detection time limit (24 hours) as presented in Table 7.1 and Table 7.3. Hence, speeding up a monitoring vessel is a very good way to increase the performance of an early warning system because wide coverage in a short amount of time is crucial. With the high speed of 10 m/s, the performance of the monitoring system was comparable to a monitoring network with 7 ~ 8 monitoring locations in terms of detection likelihood.

Table 7.3 Optimal solutions of monitoring paths with respect to different length restriction in the wind-driven circular lake with the vessel speed of 10 m/s

Maximum length of the path (km)	The estimation of detection time with penalty (hr)	The estimation of detection likelihood (%)	Figure
36	0.849	86.25	Figure 7.6 (a)
	⋮	⋮	
	0.797	81.66	Figure 7.6 (b)
72	1.065	87.42	Figure 7.6 (c)
	⋮	⋮	
	1.009	82.21	Figure 7.6 (d)

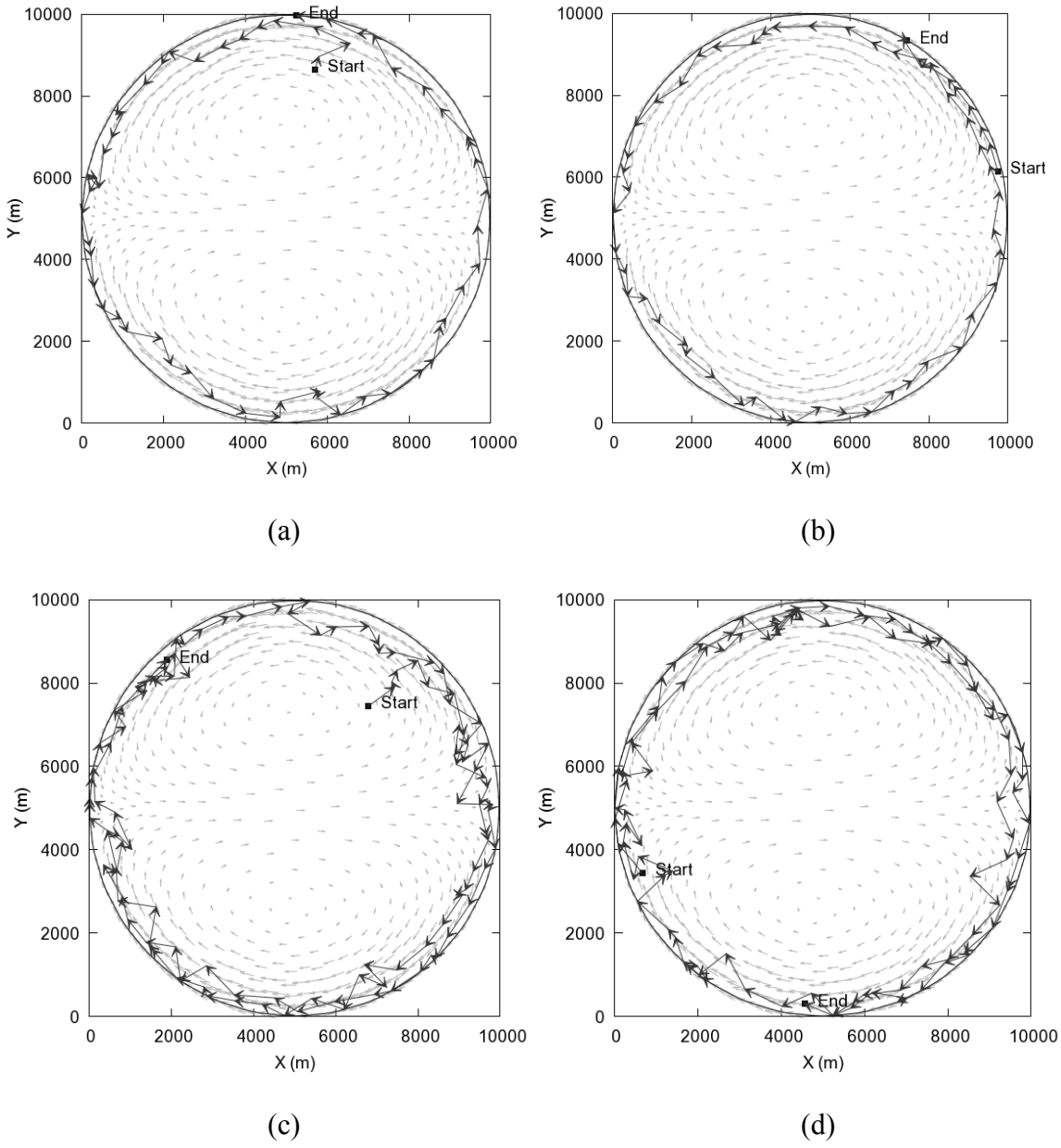

Figure 7.7 Optimal monitoring paths in a circular lake driven under a constant wind with the vessel speed of 10 m/sec and the detection time limit of 3 hours (a) the best detection likelihood solution with the maximum length of 36 km, (b) the shortest detection time solution with the maximum length of 36 km, (c) the best detection likelihood solution with the maximum length of 72 km, and (d) the shortest detection time solution with the maximum length of 72 km

Effect of weight on scenarios

The probability of each contaminant source or spill may be different in a real situation. To investigate the effect of weight, one of the scenarios was selected, and its weight increases to 10 and 50 times of other scenarios. The detection time limit was 3 hours, and the speed of a vessel was 3 m/sec.

The results are presented in Table 7.4 and Figure 7.8. Because of the weight scenario, the locations of the optimal paths moved to the north side of the lake. The major part of the paths was downstream of the weighted source location along the shoreline, where the contaminant was transported. These results show that the weight of scenarios affect the optimal solution greatly. Hence, the probability of contaminant spills in a real situation need to be managed carefully to obtain reliable optimal solutions.

Table 7.4 Optimal solutions of monitoring paths with respect to different weights in the wind-driven circular lake

Weight	The estimation of detection time with penalty (hr)	The estimation of detection likelihood (%)	Figure
10	2.081	37.37	Figure 7.8 (a)
	⋮	⋮	
	2.007	35.27	
50	1.821	50.40	Figure 7.8 (b)
	⋮	⋮	
	1.758	48.43	

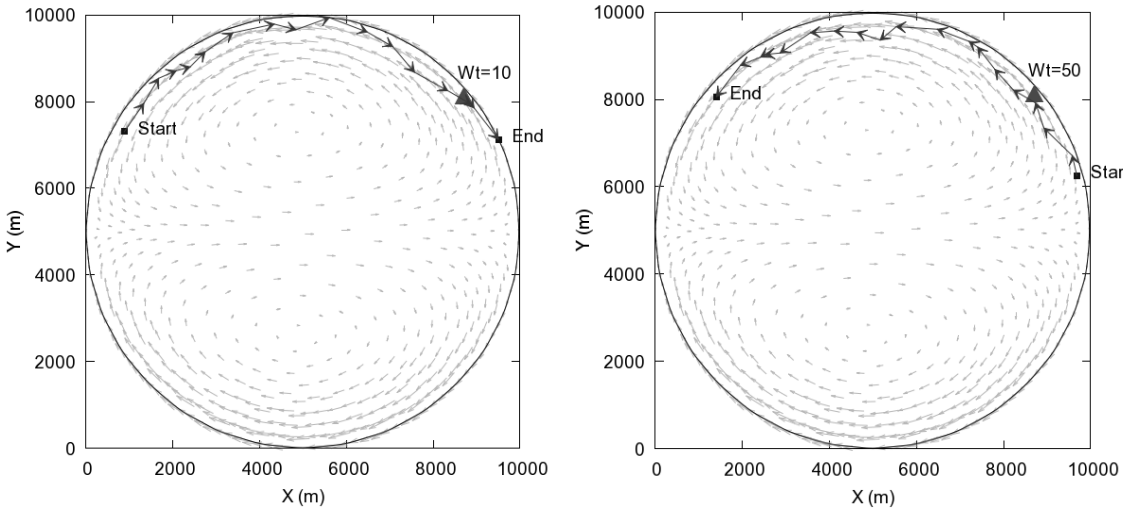

(a) (b)

Figure 7.8 Optimal monitoring paths with respect to different weights
(a) 10 times weight and (b) 50 times weight at a source location (triangle)

7.5.2. Circular lake with tides

To find out optimal paths in a lake under tidal effect, the same circular lake with tides from the previous chapters were adopted. The tidal amplitude was 20 cm at the mouth on the east side of the lake. The number of scenarios was 240. The speed of a vessel was set 3 m/sec, and the maximum length was 10.8 km and 32.4 km respectively. The detection time limit was 3 hours. The mass of the spilled contaminant was 10 tons, and the detection threshold was 0.1 g/m^3.

The results are presented in Table 7.5 and Figure 7.9. Multiple solutions for each case were obtained, but all of them were very similar. The optimal paths followed the shoreline again because the possible source locations were around the lake. When the length of a path was short, it picked one side of the lake and followed the shoreline.

In this case, even the performance with the high speed was not good compared with the previous closed lake cases. The reason of the low detection likelihood of this case was caused by the loss of the contaminant to the tidal lets.

Table 7.5 Optimal solutions of monitoring paths in the circular lake under tidal effect

Maximum length of a path (km)	Estimation of detection time with penalty (hr)	Estimation of detection likelihood (%)	Figure
10.8	2.155	33.68	Figure 7.9 (a)
	⋮	⋮	
	2.088	32.75	
32.4	0.917	83.78	Figure 7.9 (b)
	⋮	⋮	
	0.882	79.22	

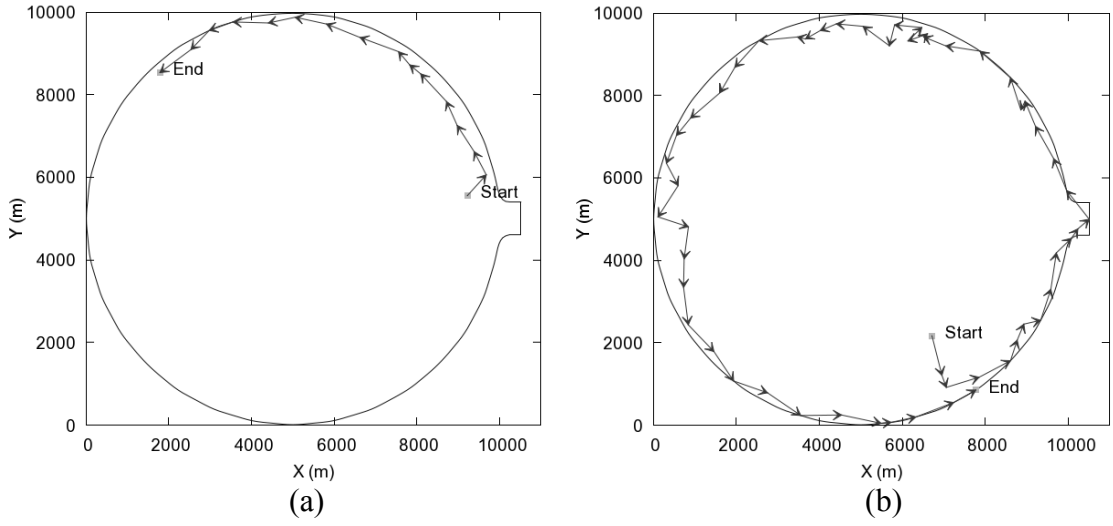

Figure 7.9 Optimal solutions of monitoring paths in the circular lake under tidal effect (a) the best detection likelihood solution with the maximum length of 10.8 km, and (b) the best detection likelihood solution with the maximum length of 21.6 km

7.6. Lake Pontchartrain

To apply the optimization model for a real case, Lake Pontchartrain was tested as done in the previous chapters. The same 20 source locations presented in Figure 5.26 were chosen as possible spill sites. The mass of the contaminant spill was 1 ton, and the detection threshold was 0.1 g/m^3.

7.6.1. Wind-only case

Because of the large scale of the lake, the speed of a vessel was set 10 m/sec. To see the effect of the maximum length of monitoring paths, the length was adjusted. The detection time limit was set 12 hours. The results are presented in Table 7.6 and Figure 7.10 through Figure 7.12.

The optimal paths started the west of the source location on the far southwestern parts of the lake, and traveled along the shore of the lake. Since the area has more than half of source locations mainly from New Orleans, the optimal paths stayed the area without trying to detect other contaminant on the north shore. This was similar results to the straight monitoring lines in the previous chapter. Even when the length of a path was increased up to a distance to travel the whole lake, a vessel did not go to the other side of the lake. Thus, about half of scenarios were missed, and the performance of the optimal solutions was not good. When a monitoring vessel was allowed to move around 3 hours, which is up to 216 km, the vessel wandered and moved back and forth around the southwestern shore. Also, the performance of optimal solutions did not improve much as the length of paths increased.

This shows that the limitation of one vessel in a large domain clearly. When a domain is large, a monitoring vessel cannot cover the whole area. Thus, it chooses an

area where many contaminations are detected especially when sources are not evenly distributed. Hence, multiple monitoring vessels at the same time or combination with stationary monitoring locations need to be considered to improve performance in a large domain.

Table 7.6 Optimal solutions of monitoring paths with respect to different length restriction in Lake Pontchartrain under the constant wind

Maximum length of a path (km)	Estimation of detection time with penalty (hr)	Estimation of detection likelihood (%)	Figure
36	6.692	45.93	Figure 7.10
	6.603	45.74	
72	6.288	52.41	Figure 7.11
	6.288	51.38	
	6.288	50.86	
216	6.878	50.95	Figure 7.12
	6.861	50.68	

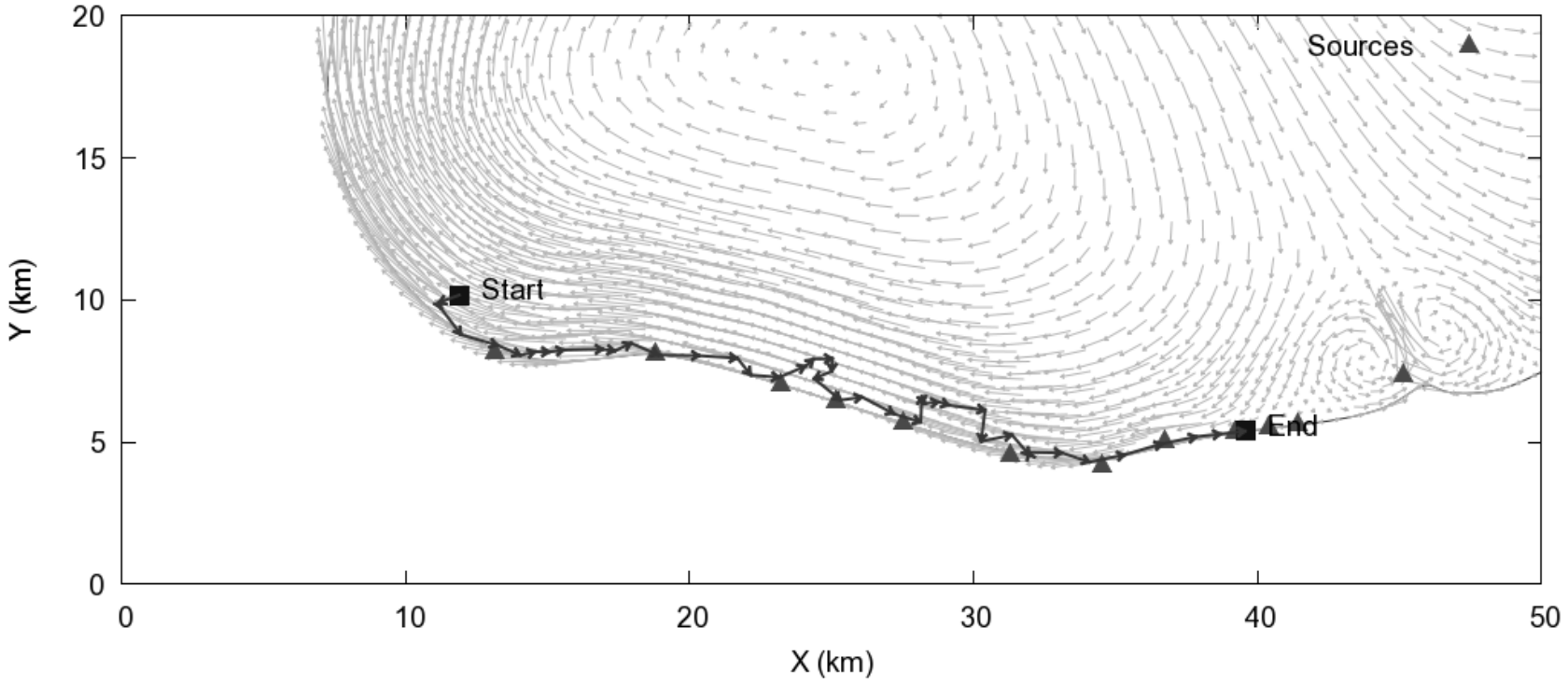

Figure 7.10 Optimal monitoring path in Lake Pontchartrain under the constant wind with the speed of 15 m/sec, maximum length 36 km, and detection time limit of 12 hours

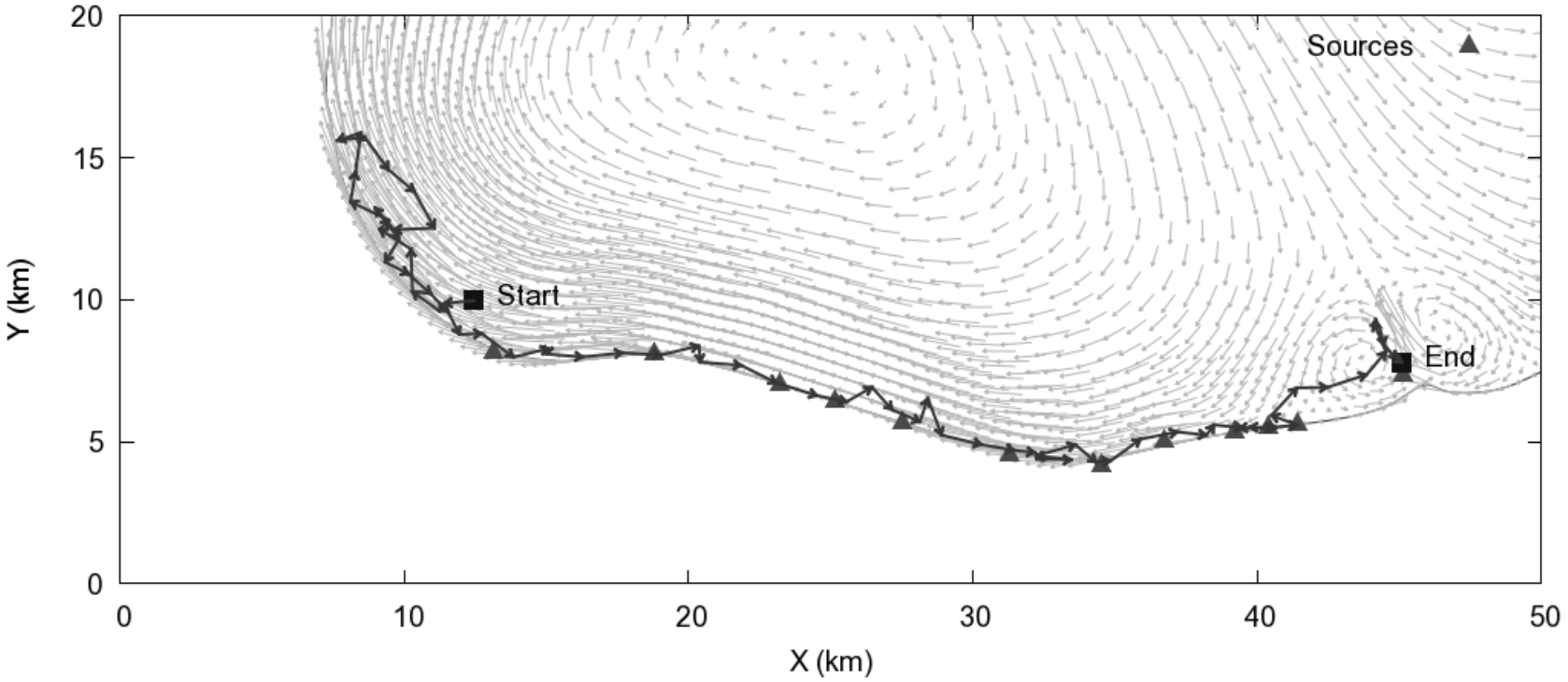

Figure 7.11 Optimal monitoring path in Lake Pontchartrain under the constant wind with the speed of 15 m/sec, maximum length 72 km, and detection time limit of 12 hours

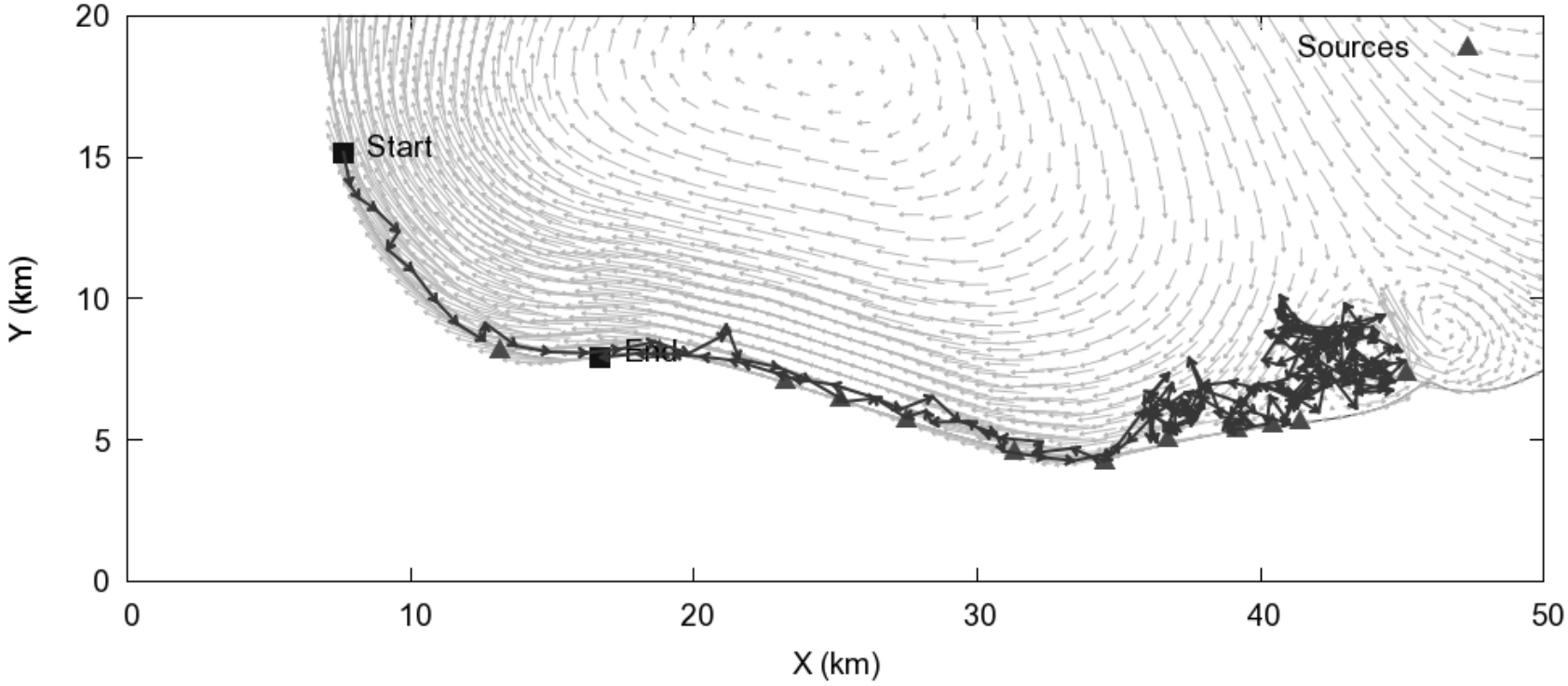

Figure 7.12 Optimal monitoring path in Lake Pontchartrain under the constant wind with the speed of 15 m/sec, maximum length of 216 km, and detection time limit of 12 hours

7.6.2. Site-specific wind and tide case

The optimization of higher order monitoring paths was done for Lake Pontchartrain with real wind and tide. The conditions for hydrodynamics were identical to the real-wind and predicted-tide case in Chapter 4. For contaminant scenarios, the same 20 possible spill locations as in the wind-only case of the previous section were selected. Then, 8 different spill times were selected for each spill locations so that the number of all scenarios was 160. These were the same scenarios used for the optimization of monitoring locations in Lake Pontchartrain in Chapter 5 and 6.

The results are presented in Table 7.7 and Figure 7.13. Compared with the wind-only cases, the results with read wind and predicted tide showed even better performance. The direction of travel in the results of 36 and 72 km length limit was the opposite of that in the previous results with constant wind. However, the locations and patterns of all the optimal solutions were almost identical to those of the results with constant wind in the previous section. The solution with 216 km length limit again did not leave the southern shoreline of the lake. It departed from the southwestern corner of the lake, traveled to the most right possible spill locations on the south shore, wandered around there, and finally came back to where it departed. This solution is almost identical to the solution with 216 km length under constant wind in the previous section.

These results shows that the superiority of higher order monitoring paths clearly. The performance of higher order monitoring paths were twice better than straight monitoring paths for the same cases. Also, higher order monitoring paths did not suffer from performance degradation in the complex real situations where as the straight monitoring lines performed worse against the real situations. When the performance was

compared with the stationary monitoring locations, the performance of higher order monitoring paths was comparable to that of the five optimal stationary monitoring locations in Chapter 5.

Table 7.7 Optimal monitoring paths with respect to the speed of a vessel in Lake Pontchartrain under the real wind and predicted tide

Maximum length of a path (km)	Estimation of detection time with penalty (hr)	Estimation of detection likelihood (%)	Figure
36	6.540	46.81	Figure 7.13 (a)
	⋮	⋮	
	6.506	42.20	
72	5.881	55.78	Figure 7.13 (b)
	⋮	⋮	
	5.855	54.61	
216	6.324	57.89	Figure 7.13 (c)
	6.322	57.33	

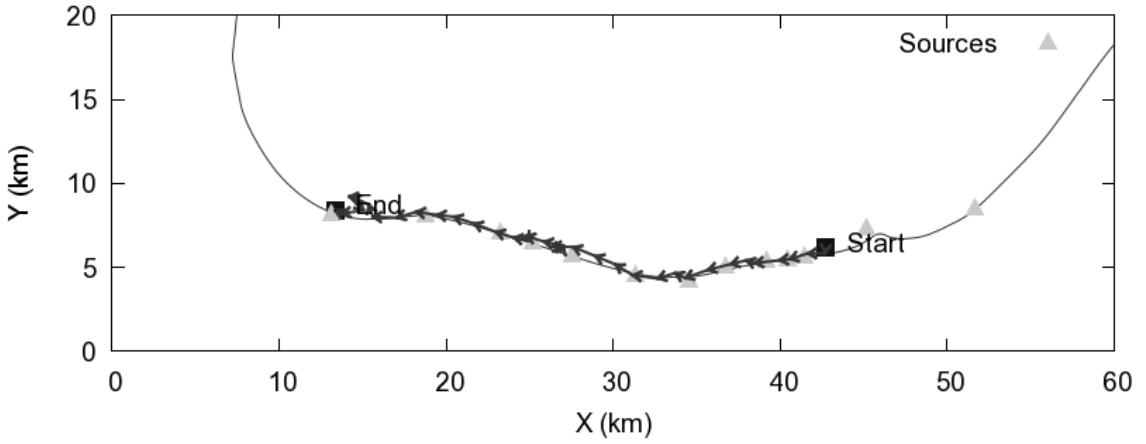

(a)

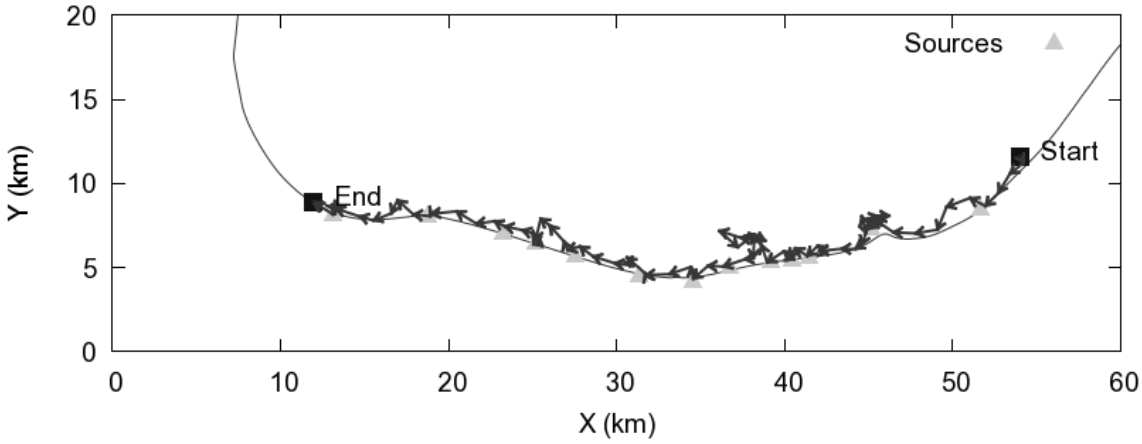

(b)

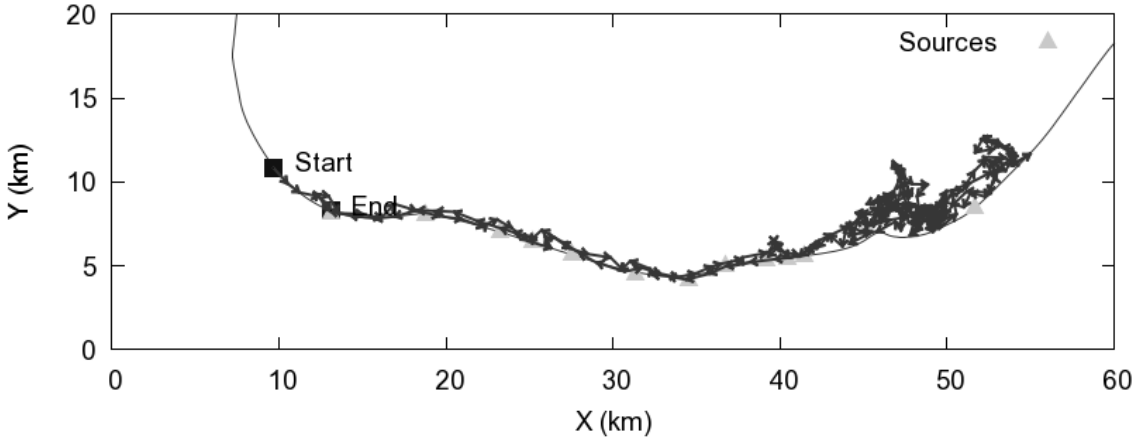

(c)

Figure 7.13 Optimal monitoring paths in Lake Pontchartrain under the real wind and predicted tide with the speed of 10 m/sec and detection time limit of 12 hours
(a) Maximum length of 36 km, (b) Maximum length of 72 km, and (c) Maximum length of 216 km

7.7. Summary

To overcome the geometrical constraint of a straight monitoring line path, an optimization model for a free monitoring path was proposed and applied for various cases. For the optimization model, the appropriate crossover and mutation operations were developed, and they found optimal solutions in relatively short amount of time despite the huge search space.

Higher order monitoring paths showed better performance than straight monitoring lines because free monitoring paths could follow irregular domain boundaries very well. This is particularly important because it is likely that most source locations are located on the shoreline of a domain. The performance of optimal solutions was comparable to many fixed monitoring stations in a closed wind-driven lake especially when the speed of a vessel was high. The direction of travel was often against flow direction. Also, the performance of higher order monitoring paths did not get worse under complex real-wind and tide cases.

When there is an outlet in a domain as shown in the circular lake with tides, a monitoring vessel may miss spills that will exit through the tidal outlet. This lowered the performance of optimal paths. However, missing these cases may not be critical in a practical point of view.

The shapes of the optimal paths were not very smooth in some cases. This is mainly due to the limitation by adopting nodes of a mesh as possible waypoints of a path. Also because the speed of a vessel was set as constant, a monitoring vessel had to go around an area to slow down in some cases. When a path becomes very long like as shown in the Lake Pontchartrain cases, it becomes hard for the optimization model to

find a smooth solution as well. To avoid this problem a variable speed monitoring boat path can also be tested as an extension to this study.

When the scale of a domain is large such as Lake Pontchartrain, one vessel cannot cover the whole area effectively so that a vessel stays where it can detect contamination the most. Hence, two or more monitoring vessels at the same time or combining with stationary monitoring locations may be alternatives to improve the performance of a monitoring system.

CHAPTER 8

CONCLUSIONS

The health risk from the degradation of surface water quality is increasing worldwide, and this problem necessitates public health managers implement water quality monitoring systems to protect public health and the ecosystem. The health risk from direct exposure such as recreational activities is also becoming a health issue as well. Thus, the need for an early warning system against adverse water quality conditions is an increasing concern.

The goals of a water quality monitoring system is the development of a comprehensive monitoring system designed to address several concerns such as early detection, threshold detection, monitoring system design for fixed stations or monitoring system design for unmanned mobile detection devices and the like. Thus, in the design of a water quality monitoring program, many design factors such as what, when, where, and how to take the measurement must be decided within scientific limitations. Among them, where to make the measurement is very critical because inappropriate monitoring places may lead to redundant, incomplete and insufficient information for decision making. The locations for water quality monitoring stations are often decided by expertise rather than by engineering methods.

Furthermore, due to recent advances in robotics and autonomous measuring techniques, autonomous mobile water quality monitoring, which takes measurement automatically while the mobile monitoring vehicle moves from one point to another, is becoming available, and this opens a whole new possibility of water quality monitoring

problems. However, how to design the optimal paths for these mobile water quality monitoring vehicles has not been investigated in detail at this time.

The procedures of designing the monitoring locations or monitoring paths need to consider numerous factors such as uncertainty and different hydrodynamic situations, and they should pursue conflicting goals as well. These make the design problem to employ multi-objective optimizations methods requiring multiple computational steps, multiple objectives and constraints for a multitude of physical considerations.

To consider various cases of hydrodynamics and random contaminant source possibilities into account, many possible scenarios were designed as representative realizations for the first step of the overall optimization procedure proposed in this thesis. The scenarios then were simulated numerically to find their fate, and the numerical simulations which required enormous amount of computational resource. Consequently, the computational time became a major issue. To resolve this issue, parallel simulation codes were developed, and computational time was reduced effectively. Even though a parallel computing was adopted, the computational time for the hydrodynamics and contaminant transport simulations was longer than that for the optimization procedures that utilized them, and they still remain to be a major obstacle for efficient solution of these problems.

To solve the optimization problem using the results obtained from contamination scenarios, the genetic algorithm based on NSGA-II was implemented with specifically designed crossover and mutation operators. The main objectives of the optimizations were: (i) minimization of the detection time; and, (ii) maximization of detection likelihood. These objectives were selected by targeting an early water quality warning

system. To simplify the optimization procedures, the values at nodes in a discretized mesh were directly used. This approach made preliminary calculations of detection times and detection time windows at all the nodes in a mesh possible in advance of the optimization routines.

The proposed methods were tested for a wind-driven lake circulation problem, a lake under tidal influence, and Lake Pontchartrain. It was shown that a closed water body that was affected mainly by the wind and the resulting wind-driven circulation was an important factor in determining the optimal monitoring station locations. This effect eventually was reflected in the contaminant transport and the optimization solutions of monitoring locations and monitoring paths.

The genetic algorithm developed for this purpose solved the optimization problem very effectively. Even for the complex case such as Lake Pontchartrain, an optimization problem could be finished in less than an hour on an Intel-based workstation.

In a closed water body, wind generated circulations that showed longshore flows with a return flow at the center. Assuming that possible source locations were on the shores, contaminants were transported on the longshore flows. Hence, monitoring locations were distributed on the shores. Also, monitoring lines and paths there were found as the optimal paths were located close to the shore of a water body as well.

Even if there was the effect from tides, the circulatory flows were established along the shores so that the optimal solutions were located closely to the shores. However, the performance of monitoring systems dropped due to the loss of contaminant to the open sea for some cases.

Optimal monitoring locations coincided with some of source locations to minimize the estimation of detection time. If the direction of flows were constant, monitoring locations were placed mostly downstream of the sources.

Straight monitoring lines are simple for a monitoring vessel to follow, but due to its geometrical constraint, their performances were generally low. Free forms of monitoring paths achieved higher performance than the straight monitoring lines because it did not have the geometrical restrictions. Optimal monitoring paths were obtained along the shoreline where the contaminant sources were located. In some cases, only one monitoring vessel could achieve comparable performance to several stationary monitoring locations.

The shape of the lines and higher order monitoring paths were not very sensitive to monitoring parameters such as the speed of a vessel or detection time limit. Generally, the performance of the optimal solutions of monitoring lines and higher order monitoring paths increases as the speed of a boat increased. When the solution domain was large, and possible sources were not distributed evenly along the shores, optimal monitoring lines and higher order monitoring paths were formed where most of sources are distributed.

In most of the cases, the locations of sources were the most influential factor, and hydrodynamics was also important. If contaminant spills did not have the same likelihood of occurrence, it affected the optimal solutions as well. Hence, well-designed hydrodynamics and contaminant spill scenarios that reflect real situations is very crucial in solving this problem. Also, the number of scenarios needs to be minimized to reduce computational time but this may affect the random nature of contaminant spill occurrences.

The adaptation of penalty value for non-detected scenarios got rid of practically meaningless solutions and reduced the number of optimal solutions greatly. Sometimes all the optimal solutions converged into one or a few solutions. Most of the optimal solutions had the highest detection likelihood possible because this approach put more weight on reliability of monitoring system.

The proposed methods can overcome this difficulty by engaging complexities with numerical simulations and optimization in an engineered way. Eventually, the optimal solutions with the proposed method will increase the detection likelihood and decrease the detection time of a monitoring program at the same time. These objectives are hard to be achieved just by expertise due to the complexity of the problem. The methodologies developed in this thesis may be extended to other areas with more comprehensive models and more powerful computation devices. For example, the interaction with sediments and application with three-dimensional simulations are the ones among possible improvements. Accordingly, the optimization routines can be expanded to three dimensional spaces. When a domain to be monitored is large, it is found that one vessel may not achieve a high enough rate of detection. In the future, multiple vessel cases can be adopted to increase the efficiency, and an improved optimization routine that can manage multiple vessels will be necessary as well to manage multiple monitoring paths. Also, the same optimization method can be applied in different fields that require optimizing locations and paths such as early detection of attacks in chemical/biological warfare in water and atmosphere. Finally, adopting new objectives such as finding the best places for monitoring programs to achieve better

reconstruction or prediction of some values – data assimilation problems – can be another application of this optimization.

The creatures in the nature always wander around to search a better place to find foods and a safer place to live. The design of monitoring locations and paths is actually solving similar problem to what is happening in the nature, and the genetic algorithm may be understood as one way inspired by them. We may find a better way to solve our problems through deeper understanding of the nature in future studies.

REFERENCES

Beach Environmental Assessment and Coastal Health Act of 2000, Public law 106-284, 114 Stat 874. (2000).

Abraham A, Jain LC, Goldberg R. Evolutionary multiobjective optimization : theoretical advances and applications. New York: Springer; 2005.

Ahn C-W, Ramakrishna RS. A genetic algorithm for shortest path routing problem and the sizing of populations. IEEE Transactions on Evolutionary Computation. 2002;6(6):566-579.

Applegate DL. The traveling salesman problem : a computational study. Princeton, NJ: Princeton University Press; 2007.

Argus Holdings. Ltd. Argus ONE. 1999.

Balay S, Buschelman K, Eijkhout V, Gropp WD, Kaushik D, Knepley MG*, et al.* PETSc Users Manual: Argonne National Laboratory; 2004

Balay S, Buschelman K, Gropp W, Kaushik D, Knepley MG, McInnes LC*, et al.* PETSc Web page. 2001 [updated 2001; cited 2005]; Available from: http://www.mcs.anl.gov/petsc.

Batchelor GK. An introduction to fluid dynamics. 1st pbk. ed. Cambridge ; New York: Cambridge University Press; 1973.

Berry J, Hart WE, Phillips CA, Uber JG, Watson JP. Sensor placement in municipal water networks with temporal integer programming models. Journal of Water Resources Planning and Management-Asce. 2006 Jul-Aug;132(4):218-224.

Berry JW, Fleischer L, Hart WE, Phillips CA, Watson JP. Sensor placement in municipal water networks. Journal of Water Resources Planning and Management-Asce. 2005 May-Jun;131(3):237-243.

Blumberg AF, Mellor GL. A Description of a Three-Dimensional Coastal Ocean Circulation Model. In: Heaps I, Norman S, editors. Three-Dimensional Coastal Ocean Models: American Geophysical Union; 1987. p. 1-16.

Bowie GL, Mills WB, Porcella DB, Campbell CL, Pagenkopf JR, Rupp GL*, et al.* Rates, Constants, and kinetics Formulations in Surface Water Quality Modeling; 1985

Boyd GR, Palmen JM, Zhang S, Grimm DA. Pharmaceuticals and personal care products (PPCPs) and endocrine disrupting chemicals (EDCs) in stormwater canals and Bayou St. John in New Orleans, Louisiana, USA. Science of The Total Environment 2004;333(1-3):137-148.

Cahon S, Melab N, Talbi EG. ParadisEO: A framework for the reusable design of parallel and distributed metaheuristics. J Heuristics. 2004 May;10(3):357-380.

Carr RD, Greenberg HJ, Hart WE, Konjevod G, Lauer E, Lin H, *et al.* Robust optimization of contaminant sensor placement for community water systems. Mathematical Programming. 2006 Jun;107(1-2):337-356.

Carrera J, Usunoff E, Szidarovszky F. A METHOD FOR OPTIMAL OBSERVATION NETWORK DESIGN FOR GROUNDWATER-MANAGEMENT. Journal of Hydrology. 1984;73(1-2):147-163.

Center for Operational Oceanographic Products and Services. NOAA Tides and Currents. National Ocean Service, NOAA; 2007 [updated 2007; cited 2007]; Available from: http://tidesandcurrents.noaa.gov/.

Chow VT. Open-channel hydraulics. New York,: McGraw-Hill; 1959.

Corbett SJ, Rubin GL, Curry GK, Kleinbaum DG. The Health-Effects of Swimming at Sydney Beaches. American Journal of Public Health. 1993 Dec;83(12):1701-1706.

Cozzolino L, Mucherino C, Pianese D, Pirozzi F. Positioning, within water distribution networks, of monitoring stations aiming at an early detection of intentional contamination. Civil Engineering and Environmental Systems. 2006 Sep;23(3):161-174.

Crossett KM, Culliton TJ, Wiley PC, Goodspeed TR. Population Trends Along the Coastal United States:1980-2008: National Oceanic and Atmospheric Administration; 2004

Deb K, Pratap A, Agarwal S, Meyarivan T. A fast and elitist multiobjective genetic algorithm: NSGA-II. IEEE Transactions on Evolutionary Computation. 2002 Apr;6(2):182-197.

Dhar A, Datta B. Multiobjective design of dynamic monitoring networks for detection of groundwater pollution. Journal of Water Resources Planning and Management-ASCE. 2007 Jul-Aug;133(4):329-338.

Dhariwal A, Bin Z, Oberg C, Stauffer B, Requicha A, Caron D*, et al.*, editors. Networked aquatic microbial observing system; 2006; Orlando, FL, USA. IEEE.

Dixon W, Chiswell B. Review of aquatic monitoring program design. Water Research. 1996 Sep;30(9):1935-1948.

Dixon W, Smyth GK, Chiswell B. Optimized selection of river sampling sites. Water Research. 1999 Mar;33(4):971-978.

Drage BE, Upton JE, Purvis M. On-line monitoring of micropollutants in the River Trent (UK) with respect to drinking water abstraction. Water Science and Technology. 1998;38(11):123-130.

Engelman MS, Sani RL, Gresho PM. The Implementation of Normal and or Tangential Boundary-Conditions in Finite-Element Codes for Incompressible Fluid-Flow. Int J Numer Meth Fl. 1982;2(3):225-238.

EPA U. Response to 2005 Hurricanes. 2006 [updated 2006; cited 2007]; Available from: http://www.epa.gov/katrina/.

Fetter CW. Contaminant hydrogeology. Upper Saddle River, NJ: Prentice Hall; 1999.

Fischer HB, List EJ, Koh RCY, Imberger J, Brooks NH. Mixing in inland and coastal waters. New York: Academic Press; 1979.

Fleisher JM, Kay D, Wyer MD, Godfree AF. Estimates of the severity of illnesses associated with bathing in marine recreational waters contaminated with domestic sewage. International Journal of Epidemiology. 1998 Aug;27(4):722-726.

Florida Fish and Wildlife Conservation Commission: Fish and Wildlife Research Institute. Features: Marvin 2005. 2005 [updated 2005; cited 2007]; Available from: http://research.myfwc.com/features/view_article.asp?id=24018.

Fraser A, Burnell DG. Computer models in genetics. New York,: McGraw-Hill; 1970.

Free Software Foundation. GCC, the GNU Compiler Collection. 2006 [updated 2006 2008; cited 2006]; Available from: http://gcc.gnu.org/.

Gara A, Blumrich MA, Chen D, Chiu GL-T, Coteus P, Giampapa ME*, et al.* Overview of the Blue Gene/L system architecture. IBM Journal of Research and Development. 2005;49(2/3):195-212.

Garey MR, Johnson DS. Computers and intractability : a guide to the theory of NP-completeness. San Francisco: W. H. Freeman; 1979.

Garratt JR. Review of Drag Coefficients over Oceans and Continents. Monthly Weather Review. 1977;105(7):915-929.

Glasgow HB, Burkholder JM, Reed RE, Lewitus AJ, Kleinman JE. Real-time remote monitoring of water quality: a review of current applications, and advancements in sensor, telemetry, and computing technologies. Journal of Experimental Marine Biology and Ecology. 2004 Mar;300(1-2):409-448.

Goldberg DE. Genetic algorithms in search, optimization, and machine learning. Reading, Mass.: Addison-Wesley Pub. Co.; 1989.

Government of Canada, United States Environmental Protection Agency. The Great Lakes : an environmental atlas and resource book. 3rd ed. ed. Chicago, Illinois and Toronto, Ontario: Great Lakes National Program Office, U.S. Environmental Protection Agency; Government of Canada; 1995.

Greenwood R, Mills GA, Roig B. Introduction to emerging tools and their use in water monitoring. Trac-Trend Anal Chem. 2007 Apr;26(4):263-267.

Guan JB, Aral MM, Maslia ML, Grayman WM. Identification of contaminant sources in water distribution systems using simulation-optimization method: Case study. Journal of Water Resources Planning and Management-Asce. 2006 Jul-Aug;132(4):252-262.

Gutin G, Punnen AP. The traveling salesman problem and its variations. Dordrecht ; Boston: Kluwer Academic Publishers; 2002.

Hamilton GD, Soileau CW, Stroud AD. Numerical Modeling Study of Lake Pontchartrain. Journal of the Waterway, Port, Coastal and Ocean Division, Proceedings of the American Society of Civil Engineers. 1982;108(WW1):49-64.

Hinrichsen, editor. The Coastal Population Explosion. Trends and future challenges for US national ocean and coastal policy; 1999 Jan 22; Washington, DC, US. National Ocean Service, NOAA.

Holland JH. Adaptation in natural and artificial systems : an introductory analysis with applications to biology, control, and artificial intelligence. Ann Arbor: University of Michigan Press; 1975.

Hughes JP, Lettenmaier DP. DATA REQUIREMENTS FOR KRIGING - ESTIMATION AND NETWORK DESIGN. Water Resour Res. 1981;17(6):1641-1650.

Icaga Y. Genetic algorithm usage in water quality monitoring networks optimization in Gediz (Turkey) river basin. Environ Monit Assess. 2005 Sep;108(1-3):261-277.

Imm P, Knobeloch L, Anderson HA. Fish consumption and advisory awareness in the Great Lakes basin. Environmental Health Perspectives. 2005 Oct;113(10):1325-1329.

Interagency Performance Evaluation Task Force (U.S.), United States. Army. Corps of Engineers. Performance evaluation of the New Orleans and Southeast Louisiana hurricane protection system draft final report of the Interagency Performance Evaluation Task Force. [United States]: US Army Corps of Engineers; 2006 [cited. Available from: https://ipet.wes.army.mil/.

Jakob A, Binderheim-Bankay E, Davis JS. National Long-Term Surveillance of Swiss Rivers. Verh Internat Verein Linmol. 2002 July;28:1101-1106.

Jin G, Englande AJ, Liu A. A preliminary study on coastal water quality monitoring and modeling. Journal of Environmental Science and Health Part a-Toxic/Hazardous Substances & Environmental Engineering. 2003;38(3):493-509.

Johnson KS, Needoba JA, Riser SC, Showers WJ. Chemical sensor networks for the aquatic environment. Chemical Reviews. 2007 Feb;107(2):623-640.

Kessler A, Ostfeld A, Sinai G. Detecting accidental contaminations in municipal water networks. Journal of Water Resources Planning and Management-Asce. 1998 Jul-Aug;124(4):192-198.

King IP, Norton WR, editors. Recent application of RMA's finite element models for two dimensional hydrodynamics and water quality. Finite Elements in Water Resources, FE2; 1978; London. Pentech Press.

Kirk BS, Peterson JW, Stogner RH, Carey GF. libMesh: a C++ library for parallel adaptive mesh refinement/coarsening simulations. Eng Comput-Germany. 2006;22(3-4):237-254.

Kumar A, Kansal ML, Arora G. Detecting accidental contaminations in municipal water networks - Discussion. Journal of Water Resources Planning and Management-Asce. 1999 Sep-Oct;125(5):308-309.

Kunchev V, Jain L, Ivancevic V, Finn A. Path planning and obstacle avoidance for autonomous mobile robots: A review. Knowledge-Based Intelligent Information and Engineering Systems, Pt 2, Proceedings; 2006. p. 537-544.

Lake Pontchartrain Basin Foundation. Water Quality Report. [cited 2007 Mar]; Available from: http://www.saveourlake.org/water_quality.asp.

Lam DCL, Jaquet JM. Computations of Physical Transport and Regeneration of Phosphorus in Lake Erie, Fall 1970. J Fish Res Board Can. 1976;33(3):550-563.

Lawler EL. The Traveling salesman problem : a guided tour of combinatorial optimization. Chichester [West Sussex] ; New York: Wiley; 1985.

Lee BH, Deininger RA. OPTIMAL LOCATIONS OF MONITORING STATIONS IN WATER DISTRIBUTIONS SYSTEM. Journal of Environmental Engineering-Asce. 1992 Jan-Feb;118(1):4-16.

Li C, Weeks E, Inoue M. Using an Unmanned Boat (U-Boat) for Environmental Measurements. The Third International Conference on Environmental Science and Technology 2007; 2007 Aug 6-9, 2007; Houston, Texan, US. 2007.

Li YH, Hilton ABC. Optimal groundwater monitoring design using an ant colony optimization paradigm. Environ Modell Softw. 2007 Jan;22(1):110-116.

Liu L, Phanikumar MS, Molloy SL, Whitman RL, Shively DA, Nevers MB, *et al.* Modeling the transport and inactivation of E-coli and enterococci in the near-shore region of Lake Michigan. Environ Sci Technol. 2006 Aug 15;40(16):5022-5028.

Loaiciga HA. AN OPTIMIZATION APPROACH FOR GROUNDWATER QUALITY MONITORING NETWORK DESIGN. Water Resour Res. 1989 Aug;25(8):1771-1782.

Lynch DR, Gray WG. Analytic Solutions for Computer Flow Model Testing. J Hydr Eng Div-Asce. 1978;104(10):1409-1428.

Mahar PS, Datta B. Optimal monitoring network and ground-water-pollution source identification. Journal of Water Resources Planning and Management-Asce. 1997 Jul-Aug;123(4):199-207.

Manheim FT. Lake Pontchartrain Basin: Bottom Sediments and Regional Scientific and Educational Resources. U.S. Geological Survey; 1998 [updated 1998 Dec 2002; cited 2006 Oct]; Available from: http://pbus.usgs.gov/of/1998/of98-905/.

Manheim FT, Hayes L. Lake Pontchartrain Basin: Bottom Sediments and Related Environmental Resources. 2002 [updated 2002 Nov 2006; cited Oct 2006]; Available from: http://pubs.usgs.gov/prof/p1634/.

McElroy JA, Kanarek MS, Trentham-Dietz A, Robert SA, Hampton JM, Newcomb PA, *et al.* Potential exposure to PCBs, DDT and PBDEs from sport-caught fish consumption in relation to breast cancer risk in Wisconsin. Environmental Health Perspectives. 2004 Feb;112(2):156-162.

McKinney DC, Loucks DP. NETWORK DESIGN FOR PREDICTING GROUNDWATER CONTAMINATION. Water Resour Res. 1992 Jan;28(1):133-147.

Message Passing Interface Forum. MPI-2: Extensions to the Message-Passing Interface; 2003

Meyer PD, Brill ED. A METHOD FOR LOCATING WELLS IN A GROUNDWATER MONITORING NETWORK UNDER CONDITIONS OF UNCERTAINTY. Water Resour Res. 1988 Aug;24(8):1277-1282.

Meyer PD, Valocchi AJ, Eheart JW. MONITORING NETWORK DESIGN TO PROVIDE INITIAL DETECTION OF GROUNDWATER CONTAMINATION. Water Resour Res. 1994 Sep;30(9):2647-2659.

MindSites Group. LLC. GeoCommunity. [cited 2006]; Available from: http://www.geocomm.com/.

National Climate Data Center. NOAA Satellite and Information Service. 2007 [updated 2007; cited 2007]; Available from: http://www/ncdc.noaa.gov/oa/ncdc.html.

National Research Council (U.S.). Oil in the sea III : inputs, fates, and effects. Washington, D.C.: National Academy Press; 2003.

National Research Council (U.S.). Committee on a Systems Assessment of Marine Environmental Monitoring. Managing troubled waters : the role of marine environmental monitoring. Washington, D.C.: National Academy Press; 1990.

National Research Council (U.S.). Committee on the Causes and Management of Coastal Eutrophication. Clean coastal waters : understanding and reducing the effects of nutrient pollution. Washington, D.C.: National Academy Press; 2000.

National Research Council (U.S.). Committee on the Causes and Management of Coastal Eutrophication. Clean coastal waters : understanding and reducing the effects of nutrient pollution. Washington, D.C.: National Academy Press; 2000.

Natural Resources Defense Council (NRDC). Testing the Waters 2006: A Guide to Water Quality at Vacation Beaches; 2006

Ning SK, Chang NB. Multi-objective, decision-based assessment of a water quality monitoring network in a river system. Journal of Environmental Monitoring. 2002 Feb;4(1):121-126.

Ning SK, Chang NB. Optimal expansion of water quality monitoring network by fuzzy optimization approach. Environ Monit Assess. 2004 Feb;91(1-3):145-170.

Ostfeld A, Kessler A, Goldberg I. A contaminant detection system for early warning in water distribution networks. Engineering Optimization. 2004 Oct;36(5):525-538.

Ostfeld A, Salomons E. Securing water distribution systems using online contamination monitoring. Journal of Water Resources Planning and Management-Asce. 2005 Sep-Oct;131(5):402-405.

Panton RL. Incompressible flow. 2nd ed. New York: Wiley; 1996.

Parhami B. Introduction to parallel processing : algorithms and architectures. New York: Plenum Press; 1999.

Park SY, Choi JH, Wang S, Park SS. Design of a water quality monitoring network in a large river system using the genetic algorithm. Ecol Model. 2006 Dec 1;199(3):289-297.

Petres C, Pailhas Y, Patron P, Petillot Y, Evans J, Lane D. Path planning for autonomous underwater vehicles. Ieee Transactions on Robotics. 2007 Apr;23(2):331-341.

Pinder GF, Gray WG. Finite element simulation in surface and subsurface hydrology. New York: Academic Press; 1977.

Pruss A. Review of epidemiological studies on health effects from exposure to recreational water. International Journal of Epidemiology. 1998 Feb;27(1):1-9.

Ramming H-G, Kowalik Z. Numerical modelling of marine hydrodynamics: applications to dynamic physical processes. Amsterdam; New York: Elsevier Scientific Publishing Company: distributed in the USA & Canada by Elsevier/North-Holland;; 1980.

Reddy JN. An introduction to the finite element method. New York: McGraw-Hill; 1984.

Reed P, Minsker B, Valocchi AJ. Cost-effective long-term groundwater monitoring design using a genetic algorithm and global mass interpolation. Water Resour Res. 2000 Dec;36(12):3731-3741.

Robbins IC, Kirkpatrick GJ, Blackwell SM, Hillier J, Knight CA, Moline MA. Improved monitoring of HABs using autonomous underwater vehicles (AUV). Harmful Algae. 2006 Dec;5(6):749-761.

Sarker RA, Mohammadian M, Yao X. Evolutionary optimization. Boston: Kluwer Academic Publishers; 2002.

Schaffer JD. Multiple Objective Optimization with Vector Evaluated Genetic Algorithms. In: Gerefenstette JJ, editor. Proceedings of the First International Conference on Genetic Algorithms; 1985; Pittsburg, PA, USA. Hillsdale, NJ: Lawrence Erlbaum Associates; 1985. p. 93-100.

Schnoor JL. Environmental modeling : fate and transport of pollutants in water, air, and soil. New York: Wiley; 1996.

Schwefel H-P. Numerical optimization of computer models. Chichester ; New York: Wiley; 1981.

Sharp WE. TOPOLOGICALLY OPTIMUM WATER-SAMPLING PLAN FOR RIVERS AND STREAMS. Water Resour Res. 1971;7(6):1641-&.

Shastri Y, Diwekar U. Sensor placement in water networks: A stochastic programming approach. Journal of Water Resources Planning and Management-Asce. 2006 May-Jun;132(3):192-203.

Sikora WB, Kjerfve B. Factors Influencing the Salinity Regime of Lake Pontchartrain, Louisiana, a Shallow Coastal Lagoon - Analysis of a Long-Term Data Set. Estuaries. 1985;8(2A):170-180.

Srinivas N, Deb K. Multiobjective optimization using nondominated sorting in genetic algorithms. Evolutionary Computation. 1994;2(3):221-248.

Strobl RO, Robillard PD, Day RL, Shannon RD, Mcdonnell AJ. A water quality monitoring network design methodology for the selection of critical sampling points: Part II. Environ Monit Assess. 2006 Nov;122(1-3):319-334.

Strobl RO, Robillard PD, Shannon RD, Day RL, McDonnell AJ. A water quality monitoring network design methodology for the selection of critical sampling points: Part I. Environ Monit Assess. 2006 Jan;112(1-3):137-158.

Swenson EM, Chuang WS. Tidal and Subtidal Water Volume Exchange in an Estuarine System. Estuar Coast Shelf S. 1983;16(3):229-240.

Thomas HJ, Sibenac M, Haddock S, Herren CM, Moline M, Blackwell S, *et al.*, editors. AUV surveys of bioluminescence and coastal processes in the Monterey Bay; 2003; San Diego, CA, USA. IEEE.

U.S. Commission on Ocean Policy. An Ocean Blueprint for the 21st century. Washington, DC; 2004.

U.S. Department of Energy. A Report to Congress on Long-Term Stewardship, Volume I - Summary Report. Washington, D.C.: Office of Environmental Management, Office of Long-Term Stewardship; 2001 January

U.S. Geological Survey. Environmental Atlas of the Lake Pontchartrain Basin. 2002 [updated 2002 5-14-2002; cited 2007]; Available from: http://pubs.usgs.gov/of/2002/of02-206/.

United States. Environmental Protection Agency. Office of Water. Technical guidance manual for performing waste load allocations book III estuaries-part 2 application of estuarine waste load allocation models. [Washington, D.C.]: United States Environmental Protection Agency, Office of Water; 1990 [updated 1990; cited]; 154 p.]. Available from: Available online, Government web site, 1990 http://purl.access.gpo.gov/GPO/LPS67680.

The Safe Drinking Water Act (SDWA), 42 U.S.C., Chapter 5A, Subchapter XII. (1974).

USDA Forest Service and the University of Tennessee. National Survey on Recreation and the Environment (NRSE) 2000: The Interagency National Survey Consortium, Coordinated by the USDA Forest Service, Recreation, Wilderness, and Demographics Trends Research Group, Athens, GA and the Human Dimensions Research Laboratory, University of Tennessee, Knoxville, TN.; 2000

USEPA. National Coastal Condition Report: USEPA; 2001

Wade TJ, Calderon RL, Sams E, Beach M, Brenner KP, Williams AH, *et al.* Rapidly measured indicators of recreational water quality are predictive of swimming-associated gastrointestional illness. Environmental Health Perspectives. 2006 Jan;114(1):24-28.

World Resources Institute (WRI). World Resources 2000-2001: People and ecosystems: The fraying web of life. Washington, DC.: WRI; 2000

Yoder JS, Blackburn BG, Craun GF, Hill V, Levy DA, Chen N, *et al.* Surveillance of Waterborne-Disease Outbreaks Associated with Recreational Water - United State, 2001-2002. Morbidity and Mortality Weekly Report. 2004:1-21.

Zienkiewicz OC, Taylor RL. The finite element method. 4th ed. London ; New York: McGraw-Hill; 1989.

VITA

Kijin Nam was born in Seoul, Republic of Korea. He received his Bachelor and Master of Science at Department of Civil Engineering, Urban Engineering major from Seoul National University in 1996 and 1998 respectively. After serving a military service, he worked for Kyonggi Research Institute, Suwon, Republic of Korea in 2000 as a research assistant. He participated in a project on a watershed protection plan. In 2001, He started his Ph.D. degree program as a graduate research assistant in School of Civil and Environmental Engineering at Georgia Institute of Technology and received his Master of Science in Environmental Engineering in December 2003. His research interests are numerical techniques in environmental fluid mechanics and water resources, heuristic optimizations, high performance computing, statistical models, and human health risk assessment.